FACULTÉ DE PHARMACIE

UNIVERSITÉ LIBRE DE BRUXELLES

Evaluation of the combination of a cisplatin-based dry powder inhaler with conventional treatments against lung tumours

Thesis presented by Selma CHRAIBI
with a view to obtaining a PhD Degree in Biomedical and Pharmaceutical Sciences *"Docteure en Sciences Biomédicales et Pharmaceutiques"*

Academic year 2020-2021

Supervisor : Prof. Karim AMIGHI

Co-supervisor : Prof. Nathalie WAUTHOZ

Unit of Pharmaceutics and Biopharmaceutics

Thesis jury :

Prof. David VERMIJLEN (Université libre de Bruxelles, Chair)
Prof. Gilles BERGER (Université libre de Bruxelles, Secretary)
Prof. Joëlle NORTIER (Université libre de Bruxelles, Hôpital Brugmann)
Prof. Nicolas TSAPIS (CNRS, Université Paris-Saclay)
Prof. Thierry BERGHMANS (Institut Jules Bordet)

REMERCIEMENTS

Ce travail est le fruit de nombreuses collaborations que je tiens à remercier chaleureusement. C'est grâce à ces échanges et à l'expertise de chacun que ce travail aussi transdisciplinaire qu'il soit a pu être mené convenablement.

Tout d'abord, je tiens à remercier le Professeur Karim Amighi de la confiance qu'il m'a accordé en me confiant un projet aussi cher au Laboratoire. Monsieur Amighi s'est toujours montré disponible depuis le début de ma thèse pour faire des réunions, me guider, me challenger, relire les différents documents, revoir les présentations, et re-relire les documents corrigés. Monsieur Amighi a toujours eu des commentaires qui me poussaient au bout de mes retranchements et qui m'ont permis de développer mon esprit critique. Je dois avouer que j'ai toujours eu une admiration pour son travail acharné et son assiduité. Durant ces quatre années, j'avais envie de réussir chaque tâche qu'il me confiait en allant toujours chercher plus. Je tiens également à le remercier pour les moyens financiers qu'il a déployés pour la réalisation de ce projet. Je le remercie également de l'opportunité qu'il m'a donné d'aller en formation ou en congrès, et de tous les bons souvenirs que j'en garde. Enfin, j'espère que ces quelques mots puissent lui montrer mon admiration pour son travail, la reconnaissance de la chance que j'ai eue de collaborer avec lui ainsi que de mon estime.

Je tiens également à remercier la Professeure Nathalie Wauthoz pour les différentes relectures et commentaires de mes documents/présentations. Nathalie a toujours poussé ma réflexion, interprétation et analyse le plus possible; ce qui a sans doute forgé mon esprit d'analyse. Malgré que cela n'ait pas été toujours évident, je pense que nous avons réussi à trouver une vitesse de croisière qui nous convenait à toutes les deux.

Je tiens à remercier chaleureusement le Dr. Rémi Rosière (R2O, RR) de tout ce qu'il a pu m'apporter personnellement et professionnellement. En effet, ayant été mon maître de stage lors de mon stage de fin d'études, il m'a transmis la passion de la recherche. Je me rappelle encore de la réunion que nous avons eue à la fin de mon stage pendant laquelle il m'a exposé l'opportunité de faire une thèse au sein du Laboratoire, un grand bouleversement dans mon plan de carrière initiale. Rémi m'a guidée tout au long de la thèse, à chaque étape: de la préparation du FRIA, à la prise en main des différentes techniques *in vitro*, aux manipulations *in vivo* (administrations IV !), planifications d'études, mise en forme des résultats, interprétation, rédaction, … et j'en passe. Cela m'a permis d'apprendre énormément de son savoir-faire et d'acquérir de nouvelles compétences. Mener ce projet avec Rémi au jour le jour était stimulant et m'a beaucoup appris autant sur moi que sur mes envies professionnelles. Merci Rémi !

Je remercie également toute l'équipe Inhatarget pour son aide à la réalisation de ce projet. C'est grâce à cette collaboration et à un tel support que ce projet a également pu être mené à bien. Merci à Fréderic de Coninck pour sa confiance, à Tamara pour le développement du modèle LLC1-*Luc*, et à Ismael Hennia ainsi qu'à Pierre Gérard pour l'énorme travail technique. Merci à toute l'équipe pour les différentes discussions et les bons moments de convivialité passés

ensemble, que ce soit au BARABAR ou pendant les fameux lunchs à Gosselies. Un regret serait finalement de n'avoir pas pu se rendre au RDD 2020 en Californie ensemble !

Je tiens également à remercier le Professeur Francis Vanderbist pour son soutien tout au long de ma thèse, que ce soit lors de son passage au Laboratoire, que lors de nos discussions autour de bons petits plats. Je souris en repensant aux souvenirs du congrès DDL18 à Edinburgh avec Francis, Mr Amighi et Rémi. Merci pour ces bons moments de convivialité !

Je tiens également à remercier l'ensemble des personnes de la faculté qui étaient présentes pour m'entrainer au FRIA. J'en profite pour remercier chaleureusement les membres du comité d'accompagnement qui ont pris le temps de suivre mon projet pendant ces quatre dernières années. Je remercie bien évidemment les membres du Jury d'avoir accepté de lire ce manuscrit et d'évaluer sa qualité.

Je tiens à remercier tous les collaborateurs pour leur expertise et leur disponibilité. Je remercie le Professeur Jean-Michel Kaufmann d'avoir mis à disposition le SAA afin que je puisse réaliser les mesures en début de thèse. Je remercie également la Professeure Véronique Mathieu d'avoir mis à disposition la salle de culture afin que je puisse préparer les cellules pour les greffes.

Je remercie bien évidemment le service de Néphrologie Expérimentale d'Erasme pour leur accueil, soutien et aide précieuse à la réalisation de l'histologie rénale (Professeure Marie-Hélène Antoine), ainsi que les dosages plasmatiques et urinaires des marqueurs d'atteinte rénale (Eric de Prez). Merci à la Professeure Joëlle Nortier pour la mise à disposition de son laboratoire, la confiance qu'elle m'a accordé, son soutien depuis notre première rencontre ainsi que toutes les discussions que nous avons eues ! Je remercie également et particulièrement la Professeure Ingrid Langer de m'avoir formée sur les techniques ELISA, cytospin, et de m'avoir ouvert les portes de l'IRIBHM. Merci également à Maxime pour sa bonne humeur et son aide. Je remercie particulièrement le département de Pathologie et particulièrement la Professeure Myriam Remmelink d'avoir revu toutes les lames des coupes pulmonaires. Merci à ces trois laboratoires pour leur accueil, c'était un réel plaisir de collaborer avec vous.

Je remercie également DiaPath pour la réalisation des lames des coupes pulmonaires. Merci au CMMI et particulièrement à Lionel pour son aide. Je remercie également le CER groupe pour la réalisation des analyses sanguines ainsi que SimulationPlus^{TM} pour la réalisation du travail de simulation préliminaire pour le module pulmonaire.

Je remercie également Ruth Ivory pour la correction de l'anglais, sa patience et sa disponibilité.

Je tiens bien évidemment à remercier les différentes personnes du Laboratoire de Pharmacie Galénique. Tout d'abord je remercie Nancy pour sa sympathie et son aide précieuse pour commander les produits/animaux, tout au long de ma thèse. Je la remercie également pour l'organisation de tous les sorties aux jeux d'hiver, et autres moments conviviaux. Ces moments étaient essentiels au maintien de liens forts au sein de l'équipe. Je remercie également Maxime Paide et Pierre Sacré pour leur aide et sympathie, ainsi que Coralie pour toute l'aide technique

apportée lors des manipulations *in vivo*. Enfin je remercie tous les chercheurs de la faculté, anciens et actuels pour le dynamisme et l'entraide que nous avons pu partager. Merci particulièrement aux chercheurs du Laboratoire de Pharmacie Galénique: Vincent, Romain, Philippe, Laura, Emilie et « petit » Jonathan. Je remercie particulièrement Elena avec qui j'ai commencé ma thèse, pour tous les bons moments passés dans notre bureau, pour le soutien, les rires et les discussions sur nos projets respectifs.

Je remercie également d'anciennes collègues, devenues amies, pour leur soutien je pense notamment à Federica, le petit soleil italien, Audrey, la discrète au tempérament corse et Majda, la bonté sans mesure.

D'un point de vue plus personnel, je tiens à remercier mes amis Zijada, Sophia, Nassim, Cham, Isa, Mélina, Blaz, Omar, Ruth, Antoine, Alia, Zineb, Laure-Xavier, Vincent-Audrey et le petit Romain (mon petit soleil) pour leur soutien, malgré les distances qui peuvent nous séparer. Merci pour les rires et les bons moments de convivialité passés ensemble qui me motivaient et me donnaient de la force pour maintenir le cap. Merci également à mon coach de sport et ami Salam de m'avoir boostée à me dépasser pendant ces quatre années.

Je tiens également à remercier mes beaux-parents ainsi que ma « belle » belle-sœur Astrid pour leur soutien, leur écoute et leur bienveillance. Je tiens bien évidemment à remercier ma famille, et particulièrement mes grands-mères, ma tante Amina, son mari Mahmoud, mes cousins Yasmine et Youssef ainsi que ma petite sœur Meryem.

Je remercie à l'infini et au-delà mes parents : Mama et Babou pour leur soutien sans faille depuis toujours. Ils ont toujours su m'écouter, m'encourager, me soutenir et me motiver. Ils m'ont tous les deux transmis cette passion pour le travail bien fait, une forme de leadership du côté de de mon père et un esprit critique et scientifique du côté de ma mère. Ils m'ont également appris la valeur de l'investissement de soi et la motivation à mettre dans son travail tous les jours; des qualités que j'ai vues en eux depuis mon plus jeune âge. Ils ont toujours su trouver les mots à toute épreuve, ce qui m'a toujours consolée. Ils sont un véritable moteur pour moi au quotidien, et ma mission est de toujours les rendre encore plus fiers. Être loin d'eux est un réel déchirement, et j'espère que cet aboutissement attendrit, ne serait-ce que légèrement, cette douleur.

Je tiens finalement à remercier Emeric pour tout le soutien, la motivation ainsi que l'aide qu'il m'apporte au quotidien. Merci d'avoir supporté mon stress, ma fatigue et merci d'avoir su me relever dans les moments les plus durs. Merci de booster ma confiance en moi, et de m'aider à prendre du recul quotidiennement. Nous sommes inéluctablement complémentaires ; construire notre vie professionnelle et privée à deux est un véritable shot de bonheur quotidien.

Je tiens finalement à dédier ce travail à deux étoiles parties trop tôt et qui veillent sur moi au quotidien. Passidi et Hbibi seraient sûrement très fiers de me savoir là où je suis actuellement. *Je leur dédie ce travail.*

TABLE OF CONTENT

ABBREVIATIONS

AB:	Acute bronchopneumonia	**FBS:**	Foetal bovine serum
AKI:	Acute kidney injury	**FMA:**	Formaldehyde
ALK:	Anaplastic lymphoma kinase	**FPD:**	Fine particle dose
AM:	Alveolar macrophages	**FPF:**	Fine particle fraction
APSD:	Aerodynamic particle size distribution	**FPF_d:**	Fine particle fraction from the delivered dose
AUC:	Area under the curve	**FPF_n:**	Fine particle fraction from the nominal dose
BALF:	Bronchoalveolar lavage fluid	**FSI:**	Fast-screening impactor
BEV:	Bronchiolar epithelial vacuolation	**GRAS**	Generally recognized as safe
BLI:	Bioluminescence imaging	**GSD:**	Geometric standard deviation
Bw:	Body weight	**GSH:**	Glutathione
CARB-PTX	Carboplatin-paclitaxel	**Hb:**	Haemoglobin
CIS-DPI-50:	Cisplatin-based DPI using 50% of excipients	**HCO:**	Hydrogenated castor-oil
CIS-DPI-TS:	Cisplatin-based DPI using tristearin	**HE:**	Haematoxylin-eosin
CIS-IV:	IV cisplatin solution	**HPH:**	High-pressure homogenization
C_{max}:	Maximum concentration	**Ht:**	Haematocrit
COPD:	Chronic obstructive pulmonary disease	**IHC:**	Immunohistochemistry
CT:	Computed tomography	**IP:**	Intraperitoneal
CTLA-4:	Cytotoxic T-lymphocyte-associated antigen-4	**IPA:**	Isopropanol
Ctr1:	Copper transporter 1	**IV:**	Intravenous
Ctr2:	Copper transporter 2	**k_{el}^i:**	Initial elimination rate constant
DAB:	3,3'- diaminobenzidine	**k_{el}^t:**	Terminal elimination constant
DDU:	Delivered dose uniformity	**KIM-1:**	Kidney injury molecule 1
DLT:	Dose-limiting toxicity	**LDH:**	Lactate dehydrogenase
DPI:	Dry powder for inhalation or Dry powder inhalers	**LLC1:**	Lewis lung carcinoma
DPPC:	Dipalmitoyl-phosphatidylcholine	**LLC1-*Luc*:**	Lewis lung carcinoma expressing luciferase
DSC:	Differential scanning calorimetry	**LPS:**	Lipopolysaccharide
EGFR:	Epidermal growth factor receptor	**LYM:**	Lymphocytes
EOS:	Eosinophils	**MCH:**	Mean cell haemoglobin
ESMO:	European Society for Medical Oncology	**MCHC:**	Mean corpuscular haemoglobin concentration
ET:	Endotracheal	**MCV:**	Mean corpuscular volume
ETAAS:	Electrothermal atomic absorption spectrometry	**MMAD:**	Mass median aerodynamic diameter

MON:	Monocytes		**PSD:**	Particle size distribution
MPV:	Mean platelet volume		**RBC:**	Red blood cells
MRP2:	Multi-resistance-associated protein 2		**RDW:**	Red cell distribution width
mSLF:	Modified simulated lung fluid		**REC:**	Recovery
MTD:	Maximum tolerated dose		**RH:**	Relative humidity
MTL:	Metallothionein		**ROS:**	Reactive oxygen species
MW:	Molecular weight		**ROS-1:**	ROS proto-oncogene 1
NCCN:	National Comprehensive Cancer Network		**RPMI:**	Roswell Park Memorial Institute medium
NGAL:	Neutrophil-gelatinase associated lipocalin		**SAR:**	Systemic absorption rate
NGI:	Next-generation impactor		**SBRT:**	Stereotactic body radiation therapy
NK:	Natural killer		**SCLC:**	Small cell lung carcinoma
NSCLC:	Non-small cell lung carcinoma		**SD:**	Standard deviation
NT-GRA:	Neutrophil granulocytes		**SEM:**	Standard error of the mean
OCT:	Organic cation transporter		**SLM:**	Solid-lipid microparticles
PAS:	Periodic acid Schiff		**SP:**	Surfactant Proteins
PBS:	Phosphate buffer saline		$t_{1/2}{}^{i}$**:**	Initial half-life
PD-1:	Programmed cell death-1		$t_{1/2}{}^{t}$**:**	Terminal half-life
PD-L1:	Programmed death-ligand 1		T_a**:**	Targeting advantage
PEG:	Polyethylene glycol		**TKI:**	Tyrosine kinase Inhibitors
PET:	Positron emission tomography		T_{max}**:**	Time to reach the maximum concentration
PK:	Pharmacokinetic		**TNF-α:**	Tumour necrosis factor α
PLT:	Platelets		**TNM:**	Tumour, node, metastases
pMDI:	Pressurised metered-dose inhalers		**TPGS:**	Tocopherol poly(ethylene glycol) 1000 succinate
PP:	Pulmonary permeability		**TS:**	Tristearin
PS:	Performance status		**WBC:**	White blood cells

SUMMARY

Despite recent advances in new therapies and diagnosis, lung cancer remains the most common and deadliest cancer worldwide. Conventional chemotherapy, combining a platinum compound (cisplatin or carboplatin) to another antineoplastic agent is used at nearly all stages. As it is administered using the intravenous (IV) route, it leads to heavy systemic side effects, with dose-limiting toxicities (DLT) such as nephrotoxicity for cisplatin, or myelotoxicity for carboplatin-paclitaxel doublet. Consequently, cytotoxic drugs are administered in well-spaced cycles between which all tissues can recover, including the tumour, which leads to tumour repopulation. Indeed, a significant correlation between platinum concentration in lung tumours and treatment efficacy was established in lung cancer patients. The aim of this work was to evaluate the potential of combining a cisplatin-based dry powder for inhalation (CIS-DPI-50) with conventional IV-chemotherapies to continuously expose the tumour to cytotoxic drugs.

The first experimental part aimed to develop the CIS-DPI-50 formulation. To limit a high cisplatin concentration from being directly solubilized once delivered in the lungs (i.e. lung toxicity) and to ensure enough lung exposure, it was essential to develop appropriate controlled-release and sustained lung-retention dry powder for inhalation (DPI) formulations. This consisted in optimizing a previous solid lipid microparticle-based formulation developed by Levet *et al* (CIS-DPI-TS). CIS-DPI-TS was re-produced to evaluate its efficacy on the M109-HiFR lung carcinoma model (0.5 mg/kg, 3 times per cycle for two cycles) and showed similar survival rates to the ones obtained with CIS-IV (1.5 mg/kg, once a cycle for two cycles). This optimization was done by *(i)* using generally recognised as safe (GRAS) and pharmaceutical grade excipients (49.5% (w/w) of hydrogenated castor-oil (HCO) and 0.5% (w/w) of d-α-Tocopherol polyethylene glycol 1000 succinate (TPGS) following a scalable process, and *(ii)* increasing the burst effect to boost the anti-tumour response. CIS-DPI-50 showed an interesting aerodynamic performance at both high and sub-optimal air flows (i.e. 100 and 40 L/min) with a fraction of fine particle from the delivered dose (FPF_d) of $86 \pm 1\%$ and $74 \pm 1\%$ respectively. These interesting characteristics were reproduced from batch to batch and maintained during 6 months' storage at normal conditions (25°C, RH 60%) with an FPF_d varying from $81.0 \pm 0.6\%$ at T0 to $81 \pm 2\%$ after 6 months. This was certainly related to *(i)* the stabilization of the *β*-form of HCO as well as the crystalline state of cisplatin and *(ii)* the low residual solvent content (< 0.2% w/w). Moreover, it demonstrated a higher burst release than CIS-DPI-TS while

maintaining controlled-release properties *in vitro* as $48 \pm 2\%$ were dissolved within 2h *vs.* $35 \pm 11\%$ for CIS-DPI-TS and $76 \pm 5\%$ for uncoated cisplatin microcrystals. This was confirmed *in vivo* and proved that the change to HCO decreased the time to reach the maximum concentration (C_{max}) (i.e. T_{max}) in blood from 120 min for CIS-DPI-TS to 1 min for CIS-DPI-50 and maintained lung targeting and retention within 4 hours, with an area under the curve (AUC) in the lungs of $4\,611 \pm 932$ ng.min.mg^{-1}(*vs.* $6\,072$ ng.min.mg^{-1} for CIS-DPI-TS). Consequently, CIS-DPI-50 was selected for further investigation in grafted-mice.

The second part of this work aimed first to evaluate the biodistribution of a single administration of CIS-DPI-50 in Lewis lung carcinoma expressing luciferase (LLC1-*Luc*)-grafted mice. Following the single administration of CIS-DPI-50 at 0.5 mg/kg, a more sustained and 10-fold higher exposure in the tumour than in tumour-free lungs was observed (AUC$_{0-\infty}$ in the tumours: $10\,683 \pm 5\,826$ ng.min.mg^{-1} *vs.* $1\,071 \pm 825$ ng.min.mg^{-1} in tumour-free lungs). The second aim was to select the best CIS-DPI-50 monotherapy regimen for combination to IV chemotherapies. CIS-DPI-50 was administered for two cycles either five times per cycle at 0.3, 0.5 or 1 mg/kg, or three times per cycle at 0.5 mg/kg. Following the first cycle treatment, no significant difference in terms of platinum concentration in the tumours or healthy organs was observed between these groups and a single administration of CIS-DPI-50. However, one treatment cycle later, all the platinum concentrations increased in heathy organs, with a significant decrease in tumours. This was correlated to *(i)* a 23-fold increase in tumour size between cycles (533 ± 23 mg *vs.* 23 ± 3 mg) and *(ii)* the degradation of the overall condition of the mice. Moreover, none of the selected regimens showed an increased pulmonary toxicity or efficacy (i.e. similar tumour size, necrosis and apoptosis). This limited efficacy was related to the lack of sensitivity of the LLC1-*Luc* model to cisplatin. Therefore, regimens with the lowest cumulative cisplatin dose (i.e. the group treated at 0.5 mg/kg three times per cycle *vs.* the group treated at 0.3 mg/kg five times per cycle) were selected to be evaluated on M109-HiFR-*Luc2* grafted mice, as they were intended to be combined with IV chemotherapies. Results from this study showed a statistically significant reduced tumour size with both treated groups ($p < 0.0001$) in comparison with the negative control group, which confirmed the responsiveness of this model to cisplatin. However, no significant differences in terms of tumour growth (similar trends), proportion of responders (33% for both groups) or survival (31 days for both treated groups *vs.* 23 days for untreated group) were reported between the treated groups. Consequently, regarding the potential nephrotoxicity, the less-frequent regimen (i.e. 0.5 mg/kg, repeated three times per

cycle) was selected to prevent a probable accumulation of platinum and therefore acute kidney injury (AKI).

The third part aimed to evaluate the tolerance of CIS-DPI-50, CIS-IV and their combinations. Results from the pro-inflammatory cytokines quantification (Tumour necrosis factor α (TNF-α), IL-6 and IL-1β) in bronchoalveolar lavage fluid (BALF) showed a better tolerance for CIS-DPI-50 than CIS-IV. Neutrophil granulocytes (NT-GRA) increased in BALF dose-dependently for all the groups treated with CIS-DPI-50 and were reversible 1 week later only for CIS-DPI-50 monotherapies and for the combination group for which CIS-IV and CIS-DPI-50 administrations were staggered over 24h. Considering both inflammation and cytotoxicity results, the addition of CIS-DPI-50 to CIS-IV at its maximum tolerated dose (MTD) seemed to have a higher impact than if CIS-DPI-50 was added to a 25% reduced IV dose. Results from the AKI investigation showed a significant increase in all AKI biomarkers (Neutrophil-gelatinase associated lipocalin (NGAL), cystatin C and creatinine) in plasma once CIS-DPI-50 and CIS-IV administered at their MTD the same day or 24h later. Consequently, considering the results from both investigations, it was important to reduce CIS-IV MTD by 25% and stagger CIS-DPI-50 administration by 24h to preserve pulmonary and renal tolerance. This regimen was therefore selected to evaluate its efficacy on M109-HiFR-*Luc2*-grafted mice by combining CIS-DPI-50 to the conventional cisplatin-paclitaxel IV chemotherapy. Even if the results were not significantly different from conventional IV chemotherapy alone, interesting efficacy trends in terms of reduced tumour growth, survival (31 days for combination group *vs.* 26 for IV doublet, *vs.* 21 days for untreated group) and proportion of responders (67% for combination group, *vs.* 50% for IV doublet) were reported for the combination group.

The several adaptations probably hindered the potential of the combinations. It was therefore interesting to investigate the combination of CIS-DPI-50 with a less nephrotoxic doublet (i.e. carboplatin-paclitaxel) that would necessitate fewer adjustments. However, the DLT of carboplatin and paclitaxel imposed an evaluation of myelotoxicity in this study. Results showed that the addition of CIS-DPI-50 to carboplatin-paclitaxel IV doublet on the same day at their MTD induced a higher white blood cell (WBC) and BALF cell counts, a higher proportion of NT-GRA in BALF and earlier regenerative anaemia than with the IV doublet alone. All these side effects were reversible within one week. The strategy of reducing the IV dose by 25% and separating CIS-DPI-50 and IV doublet administration by 24h avoided regenerative anaemia and/or WBC increase as well as total cell increase in BALF when compared to their respective IV doublets. Interestingly, all the combination groups induced higher non-reversible

cytotoxicity than the non-treated groups. These combinations were overall better tolerated than those with CIS-IV and should be tested on murine lung cancer models alone or in combination with immunotherapy (e.g. immune checkpoint inhibitors).

This work has demonstrated the feasibility to combine a loco-regional treatment modality with conventional cisplatin and carboplatin-based IV chemotherapies against pulmonary tumours. This was done by optimizing the combinations to avoid cumulative pulmonary, renal and haematological (i.e. for carboplatin-based chemotherapy) toxicities while showing a tendency to efficacy (i.e. cisplatin-paclitaxel doublet) in an aggressive preclinical model. Therefore, these promising results open the door to several other combination possibilities (i.e. localized treatments and immune checkpoint inhibitors) that should be further investigated to select the indications for which this treatment would be the most effective.

RESUME

Malgré les progrès réalisées en matière de traitement et de diagnostic, le cancer du poumon demeure le plus répandu et le plus mortel dans le monde. La chimiothérapie conventionnelle, associant un composé de platine (cisplatine ou carboplatine) à un autre agent antinéoplasique est utilisée à quasiment tous les stades. Comme celle-ci est administrée par voie intraveineuse (IV), elle entraîne des effets secondaires systémiques importants dont certains sont dose-limitant (DLT) comme la néphrotoxicité pour le cisplatine ou la myélotoxicité pour le doublet carboplatine-paclitaxel. Par conséquent, ces agents sont administrés selon des cycles bien espacés pendant lesquels les tissus se rétablissent, et ce incluant la tumeur ; conduisant à une repopulation tumorale. En effet, une corrélation significative a été établie entre la concentration de platine dans les tumeurs pulmonaires et l'efficacité du traitement. Le but de ce travail était d'évaluer le potentiel de combiner une poudre sèche pour inhalation (CIS-DPI-50) avec le traitement de chimiothérapie IV, afin d'exposer la tumeur à l'agent cytotoxique de manière continue.

La première partie de ce travail a permis de développer le CIS-DPI-50. Afin d'éviter qu'une haute concentration en cisplatine ne soit complètement solubilisée une fois dans les poumons, et afin d'assurer une exposition suffisante, il était essentiel de développer des formulations à libération contrôlée et à rétention pulmonaire suffisante. Ceci consistait en l'optimisation d'une formulation à base de microparticules lipidiques solides (CIS-DPI-TS) préalablement développée par Levet *et al*. Cette formulation a été reproduite afin d'évaluer son efficacité chez des souris greffées avec le modèle M109-HiFR (0.5 mg/kg, trois fois par cycle pendant deux cycles) et a démontré une survie similaire au CIS-IV (1.5 mg/kg, une fois par cycle pendant deux cycles). Cela a été effectué en *(i)* utilisant des excipients de grade pharmaceutique, reconnus comme sûrs (GRAS) (49,5 % (w/w) d'HCO et 0,5 % (w/w) de TPGS) selon un processus facilement transposable, et *(ii)* en augmentant la libération initiale afin d'améliorer la réponse antitumorale. Le CIS-DPI-50 a montré une performance aérodynamique prometteuse à des débits d'air différents (100 et 40 L/min) avec une fraction de particules fines par rapport à la dose délivrée (FPF_d) de 86 ± 1 % et de 74 ± 1 %, respectivement. La reproductibilité du procédé a été démontrée sur 3 lots différents et la stabilité maintenue pendant les 6 mois de stockage avec une FPF_d variant de 81,0 ± 0,6 % au T0 à 81 ± 2 % après 6 mois. Ceci était lié à *(i)* la stabilisation de la forme β de HCO et de l'état cristallin du cisplatine, et *(ii)* à la faible

teneur en solvant résiduel (< 0,2 % w/w). De plus, cette formulation était caractérisée par une libération initiale plus marquée qu'avec CIS-DPI-TS ainsi que par des propriétés de libération contrôlée *in vitro* puisque 48 ± 2% ont été dissous en 2 h, *vs.* 35 ± 11 % pour CIS-DPI-TS et 76 ± 5 % pour les microcristaux de cisplatine non enrobés. Cela a été confirmé *in vivo* et a prouvé que le changement vers HCO a diminué le T_{max} dans le sang de 120 min pour CIS-DPI-TS à 1 min pour le CIS-DPI-50. De plus, la rétention pulmonaire a été maintenue pendant 4 heures avec une aire sous la courbe (AUC) dans les poumons de 4 611 ± 932 ng.min.mg^1 *vs.* 6 072 ng.min.mg^{-1} pour CIS-DPI-TS. Par conséquent, cette formulation a été choisie pour la suite des investigations.

La deuxième partie de ce travail visait tout d'abord à évaluer la biodistribution après l'administration de CIS-DPI-50 à 0.5 mg/kg chez des souris greffées avec le modèle LLC1-*Luc*. Suite à cette administration, une exposition plus soutenue et dix fois plus élevée a été retrouvée dans les tumeurs par rapport au tissu sain (AUC$_{0-\infty}$ de 10 683 ± 5 826 ng.min.mg^{-1}, *vs.* 1 071 ± 825 ng.min.mg^{-1}, respectivement). Le deuxième objectif était de sélectionner le schéma d'administration du CIS-DPI-50 le plus adapté à sa combinaison avec la chimiothérapie IV. Le CIS-DPI-50 a été administrée 5 fois par cycle pendant deux cycles à 0,3, 0,5 et 1 mg/kg, ou à 0,5 mg/kg 3 fois par cycle pendant deux cycles. Après le premier cycle de traitement, aucune différence en termes de concentrations en platine n'a été observée dans les tumeurs ou dans les organes sains entre les groupes traités de manière répétée et ceux administrés une seule fois. Cependant, un cycle plus tard, toutes les concentrations en platine ont augmenté dans les organes sains et diminué dans les tumeurs. Ceci était lié à une augmentation de la taille tumorale d'un facteur de 23 entre les deux cycles (533 ± 23 mg *vs.* 23 ± 3 mg), ainsi qu'à la dégradation de l'état général des animaux. De plus, aucun des schémas n'a démontré une toxicité pulmonaire ou une efficacité. Cette efficacité limitée était liée à la faible sensibilité du modèle LLC1-*Luc* au cisplatine. Par conséquent, les schémas caractérisés par la plus faible dose cumulée (0,5 mg/kg trois fois par cycle et 0,3 mg/kg cinq fois par cycle) ont été sélectionnés afin d'évaluer leur efficacité chez des souris greffées avec le modèle M109-HiFR-*Luc2*. Une réduction significative de la taille tumorale dans les groupes traités (*p* < 0,0001) par rapport au groupe non traité a été observée ; confirmant la réponse de ce modèle au cisplatine. Cependant, aucune différence en termes de croissance tumorale (tendances similaires), de proportion de répondeurs (33 % pour les deux groupes) ou de survie (31 jours pour les groupes traités *vs.* 23 jours pour le groupe non traité) n'a été rapportée entre ces deux groupes. Par conséquent, le

schéma le moins fréquent a été choisi pour éviter une éventuelle accumulation de platine et une atteinte rénale aigue (AKI).

La troisième partie de ce travail avait pour but d'étudier la tolérance pulmonaire et rénale du CIS-DPI-50, du CIS-IV et de leurs combinaisons. Les résultats de quantification des cytokines pro-inflammatoires (TNF-α, IL-6, IL-1β) dans le fluide de lavage bronchoalvéolaire (BALF) ont montré une meilleure tolérance pour le CIS-DPI-50 par rapport au CIS-IV. Les neutrophiles granulocytes (NT-GRA) ont augmenté proportionnellement à la dose pour tous les groupes traités avec le CIS-DPI-50. Ces augmentations étaient réversibles une semaine plus tard uniquement pour les monothérapies et le groupe combiné, dont les administrations ont été espacées de 24h. Compte tenu des résultats d'inflammation et de cytotoxicité, l'ajout de CIS-DPI-50 au CIS-IV à sa dose maximale tolérée (MTD) semblait avoir un plus grand impact que si CIS-DPI-50 était ajouté à une dose IV réduite de 25%. Les résultats de quantification des biomarqueurs AKI plasmatiques (NGAL, cystatine C et créatinine) ont augmentés lorsque les deux monothérapies ont été administrées à leur DMT le même jour ou 24 heures plus tard. Par conséquent, la MTD du CIS-IV devait être réduite de 25% et les administrations séparées de 24h pour préserver la tolérance. L'efficacité de ce schéma a été évaluée sur des souris greffées avec le modèle M109-HiFR-*Luc2* en combinant le CIS-DPI-50 au doublet IV cisplatine-paclitaxel. Malgré le fait que ces résultats n'étaient pas significativement différents, des tendances intéressantes en termes de réduction de la croissance tumorale, de survie (31 jours pour le groupe combiné *vs.* 26 pour le doublet IV, *vs.* 21 jours pour le groupe non traité) et de proportion de répondeurs (67 % pour le groupe combiné, *vs.* 50 % pour le doublet IV) ont été observés pour le groupe combiné.

Comme les différentes adaptations ont probablement pu entraver le potentiel des combinaisons, il était intéressant d'étudier l'association de CIS-DPI-50 avec un doublet moins néphrotoxique (carboplatine-paclitaxel), et qui nécessiterait éventuellement moins d'ajustements. Compte tenu de la DLT du carboplatine et du paclitaxel, l'évaluation de la myélotoxicité était incluse dans cette étude. Les résultats ont montré que l'ajout de CIS-DPI-50 au doublet carboplatine-paclitaxel IV le même jour à leur MTD ont induit une augmentation du nombre de globules blancs et de cellules totales dans le BALF, une proportion plus élevée de NT-GRA dans le BALF et une anémie régénérative plus précoce qu'avec le doublet IV. Ces effets étaient réversibles. La stratégie de réduction de la dose IV de 25 % et la séparation des administrations par 24h ont permis d'éviter le développement d'une anémie régénérative et/ou l'augmentation

de globules blancs ou du nombre de cellules totales dans le BALF par rapport aux doublets IV. De plus, toutes les combinaisons ont induit une cytotoxicité non réversible tout en étant mieux tolérées que celles avec le CIS-IV. Leurs efficacités devraient donc être testées sur des modèles de cancer pulmonaire murin seuls ou en combinaison avec l'immunothérapie (inhibiteurs de checkpoint).

Ce travail a démontré la faisabilité de combiner une modalité de traitement locorégionale avec les traitements de chimiothérapie conventionnelle par voie IV à base de cisplatine et de carboplatine contre les tumeurs pulmonaires. Ceci a été effectué en optimisant les combinaisons afin d'éviter des toxicités pulmonaire, rénale et hématologique (pour la chimiothérapie à base de carboplatine) tout en démontrant une tendance vers une efficacité (pour le doublet cisplatine-paclitaxel) dans un modèle préclinique agressif. Par conséquent, ces résultats ouvrent la voie à plusieurs autres possibilités de combinaisons (traitements localisés et inhibiteurs de checkpoint) qui doivent être investiguées afin de sélectionner les indications pour lesquelles ce traitement serait le plus efficace.

INTRODUCTION

1. <u>Lung cancer</u>

In this research work, we aimed to optimize a loco-regional treatment against lung cancers. Therefore, in this first section, the burden of this disease, its major sub-types and the different treatment modalities are introduced.

1.1. Epidemiology and risk factors

Worldwide, lung cancer is the second most common and deadliest cancer, for both sexes with 2.2 million new lung cancer cases (11.4%) and 1.8 million deaths (18.0%) in 2020 **(Figure 1)** [1]. In Belgium, lung cancer is the second most frequent cancer with 9 646 new cases (11.6%). It is still the leading cause of deaths, with the highest mortality rate (22.7%) among all cancer deaths, in 2020 **(Figure 2)** [2]. Worldwide, the differences between the genders is narrowing as incidence rates have tended to increase for females and decrease for males in recent decades [3–5]. This seems to be strongly related to historical differences in tobacco-smoking interruption for males and an increase in smoking prevalence for females [1,5]. Moreover, if current trends are maintained, in 2045 the mortality in females is expected to exceed that observed in males, in the USA [6]. In addition to gender, incidence rates vary depending on several other factors such as race (highest in African-American and lowest in Hispanic women in the USA), age, socioeconomic status (related to access to education) and geographic location [4]. Indeed, significant variations are observed between developed and developing countries, mainly due to the recent increase in smoking in low- or middle-income countries, and to the implementation of smoking cessation campaigns in high income countries [4].
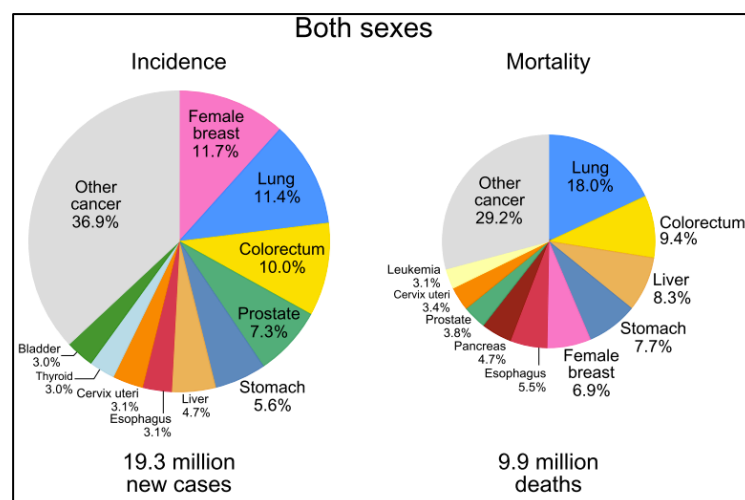
Figure 1: Pie charts representing the distribution of cases and deaths worldwide for the 10 most common cancers in 2020 for both sexes. Source: GLOBOCAN 2020, from *Sung et al., 2021* [1].
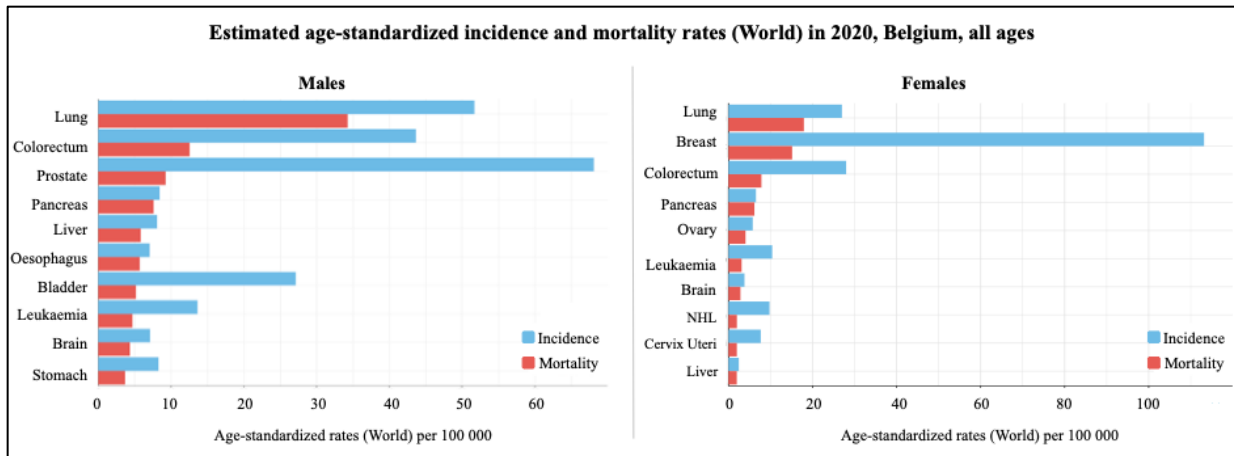
Figure 2: Incidence and mortality rates for the most common cancers in Belgium. NHL stands for non-Hodgkin lymphoma. Source: Globocan 2020 [7].

Tobacco smoking (and second-hand smoke) is still the leading cause of lung cancer as it is responsible for 80% of the total cases [4]. This is related to the 4 000 chemical constituents of cigarette smoke, among which at least 50 carcinogens are identified [4]. However, in these last couple of years, electronic nicotine delivery systems, including E-cigarettes, have been seen as an alternative to tobacco smoking and are increasingly used by teenagers and young adults [8]. These products are controversial as they contain various chemical entities such as carbonyl compounds (acetaldehydes, formaldehydes) that may induce lung tissue damage, and for which the long-term safety has not yet been determined [8]. Except for smoking, other risk of factors have been associated with lung cancer, such as coal burning for heating or cooking, air pollution, and radon and asbestos exposure, as well as chronic lung diseases such as chronic pulmonary disease, idiopathic pulmonary fibrosis and tuberculosis [4,9].

Lung cancer cases (2.2 million in 2020 *vs.* 1.8 million in 2012) and deaths (1.8 million in 2020 *vs.* 1.6 million in 2012) have been increasing worldwide, while the number of smokers has increased between 1980 and 2012 [4]. Since 1991 and up to 2015, a significant decrease in incidence rates was reported in the USA [10], largely due to tobacco cessation campaigns. Indeed, they have played a major role by leading to lower tobacco smoking rates and consequently decreased lung cancer incidence and mortality rates [4,10].

Furthermore, while still low, the 5-year relative survival rates have improved in the USA, from 10.7% in 1973 to 16.0% in 2000, and to 21.7% in 2018 [10,11]. Moreover, these rates were different between females and males, as observed in Belgium between 2013 and 2017 (27.0% for females *vs.* 18.2% for males) [3,4]. This progress was reported to be related to the

improvement of thoracoscopic surgery techniques (surgical rate stable around 25% between 1973 and 2015), to the increased use of a more efficient radiotherapy technique for early stages, and to the extended use of conventional chemotherapy (14.9% in 1973 to 39.2% in 2015), along with the development of more personalized therapies (targeted therapies and immunotherapy) for advanced disease [4,10].

1.2. Clinical manifestations

Lung cancer was the most frequently diagnosed among people in the 65-74 years-old age interval in the USA between 2013 and 2017 [11]. The same trend was observed in Belgium, with a median age for diagnosis of 70 years old for males and 67 years old for females in 2017 [3]. Most of these patients are asymptomatic when diagnosed but they often present nonspecific systemic manifestations such as fatigue, anorexia or body weight (bw) loss [4,12]. Depending on the tumour size and spread, different clinical manifestations are observed [13]. In the case of a primary tumour, cough (75%), dyspnoea (60%), chest discomfort (50%) and haemoptysis (35%) are the most commonly reported manifestations [4,12].

However, in 40% of cases, patients are diagnosed with a tumour that has already spread intrathoracically following tumour size expansion along the lymphatic system [4]. In this case, hoarseness (2-18%), phrenic nerve paralysis, Pancoast's tumour, pleural effusion, superior vena cava obstruction and oesophageal symptoms may be detected [4].

Between 33 and 40% of patients are diagnosed with metastases due to the tumour expanding to metastatic sites such as bones, the liver, the brain, adrenal glands, lymph nodes and the spinal cord [4,14]. In this case, apart from non-specific manifestations such as weakness and weight loss, specific symptoms of bone metastasis (bone fracture and pain) or brain metastasis (headache, nausea, vomiting, confusion, etc.) may be observed [4]. Other manifestations such as paraneoplastic syndromes (10%) can be found [4,12].

1.3. Classification and pathology

Lung cancer is mainly divided into two major histological types: non-small cell lung carcinoma (NSCLC) and small cell lung carcinoma (SCLC). Each category is then divided into different histological sub-units **(Table 1)**, and will be further detailed in later sections.

NSCLC is the most frequent (85% of patients) whereas SCLC is less frequent (15%) [13,15], more aggressive and highly related to cigarette smoking as 90-95% of patients with SCLC are either current or past smokers [15]. It is characterized by rapid growth and metastasis to

extrathoracic organs and is often associated with paraneoplastic syndromes [13,15]. NSCLC and SCLC treatment modalities are different and depend on staging, histological sub-types and genetic alterations. The inter-connection between these parameters will be further detailed in the next sections.

Table 1: 2015 WHO classification of lung tumours, from *Travis et al., 2015* [16].

Histologic Type and Subtypes	ICDO Code	Histologic Type and Subtypes	ICDO Code
Epithelial tumors		Papillomas	
Adenocarcinoma	8140/3	Squamous cell papilloma	8052/0
Lepidic adenocarcinoma[e]	8250/3[d]	Exophytic	8052/0
Acinar adenocarcinoma	8551/3[d]	Inverted	8053/0
Papillary adenocarcinoma	8260/3	Glandular papilloma	8260/0
Micropapillary adenocarcinoma[e]	8265/3	Mixed squamous and glandular papilloma	8560/0
Solid adenocarcinoma	8230/3	Adenomas	
Invasive mucinous adenocarcinoma[e]	8253/3[d]	Sclerosing pneumocytoma[e]	8832/0
Mixed invasive mucinous and		Alveolar adenoma	8251/0
nonmucinous adenocarcinoma	8254/3[d]	Papillary adenoma	8260/0
Colloid adenocarcinoma	8480/3	Mucinous cystadenoma	8470/0
Fetal adenocarcinoma	8333/3	Mucous gland adenoma	8480/0
Enteric adenocarcinoma[e]	8144/3	**Mesenchymal tumors**	
Minimally invasive adenocarcinoma[e]		Pulmonary hamartoma	8992/0[d]
Nonmucinous	8256/3[d]	Chondroma	9220/0
Mucinous	8257/3[d]	PEComatous tumors[e]	
Preinvasive lesions		Lymphangioleiomyomatosis	9174/1
Atypical adenomatous hyperplasia	8250/0[d]	PEComa, benign[e]	8714/0
Adenocarcinoma in situ[e]		Clear cell tumor	8005/0
Nonmucinous	8250/2[d]	PEComa, malignant[e]	8714/3
Mucinous	8253/2[d]	Congenital peribronchial myofibroblastic tumor	8827/1
Squamous cell carcinoma	8070/3	Diffuse pulmonary lymphangiomatosis	
Keratinizing squamous cell carcinoma[e]	8071/3	Inflammatory myofibroblastic tumor	8825/1
Nonkeratinizing squamous cell carcinoma[e]	8072/3	Epithelioid hemangioendothelioma	9133/3
Basaloid squamous cell carcinoma[e]	8083/3	Pleuropulmonary blastoma	8973/3
Preinvasive lesion		Synovial sarcoma	9040/3
Squamous cell carcinoma in situ	8070/2	Pulmonary artery intimal sarcoma	9137/3
Neuroendocrine tumors		Pulmonary myxoid sarcoma with *EWSR1–CREB1* translocation[e]	8842/3[d]
Small cell carcinoma	8041/3	Myoepithelial tumors[e]	
Combined small cell carcinoma	8045/3	Myoepithelioma	8982/0
Large cell neuroendocrine carcinoma	8013/3	Myoepithelial carcinoma	8982/3
Combined large cell neuroendocrine carcinoma	8013/3	**Lymphohistiocytic tumors**	
Carcinoid tumors		Extranodal marginal zone lymphomas of mucosa-associated Lymphoid tissue (MALT lymphoma)	9699/3
Typical carcinoid tumor	8240/3	Diffuse large cell lymphoma	9680/3
Atypical carcinoid tumor	8249/3	Lymphomatoid granulomatosis	9766/1
Preinvasive lesion		Intravascular large B cell lymphoma[e]	9712/3
Diffuse idiopathic pulmonary neuroendocrine cell hyperplasia	8040/0[d]	Pulmonary Langerhans cell histiocytosis	9751/1
Large cell carcinoma	8012/3	Erdheim–Chester disease	9750/1
Adenosquamous carcinoma	8560/3	**Tumors of ectopic origin**	
Sarcomatoid carcinomas		Germ cell tumors	
Pleomorphic carcinoma	8022/3	Teratoma, mature	9080/0
Spindle cell carcinoma	8032/3	Teratoma, immature	9080/1
Giant cell carcinoma	8031/3	Intrapulmonary thymoma	8580/3
Carcinosarcoma	8980/3	Melanoma	8270/3
Pulmonary blastoma	8972/3	Meningioma, NOS	9530/0
Other and Unclassified carcinomas		**Metastatic tumors**	
Lymphoepithelioma-like carcinoma	8082/3		
NUT carcinoma[e]	8023/3[d]		
Salivary gland-type tumors			
Mucoepidermoid carcinoma	8430/3		
Adenoid cystic carcinoma	8200/3		
Epithelial-myoepithelial carcinoma	8562/3		
Pleomorphic adenoma	8940/0		
(Continued)			

[a]The morphology codes are from the ICDO.[2] Behavior is coded /0 for benign tumors, /1 for unspecified, borderline or uncertain behavior, /2 for carcinoma in situ and grade III intraepithelial neoplasia, and /3 for malignant tumors.
[b]The classification is modified from the previous WHO classification[1] taking into account changes in our understanding of these lesions.
[c]This table is reproduced from the 2015 WHO Classification by Travis et al.[1]
[d]These new codes were approved by the International Agency on Cancer Research/ WHO Committee for ICDO.
[e]New terms changed or entities added since 2004 WHO Classification.[3]
LCNEC, large cell neuroendocrine carcinoma, WHO, World Health Organization; ICDO International Classification of Diseases for Oncology.

1.4. Non-small cell lung carcinoma

1.4.1. Screening

Prognosis of NSCLC is strongly related to its stage at diagnosis, which shows the importance of screening. Two randomized clinical trials have demonstrated the benefits of screening by low-dose computed tomography (CT) in terms of reduction of lung cancer deaths in high-risk population [17,18]. The choice of the technique is an important criterion as the benefits of screening using chest X-ray and/or sputum cytology have not been demonstrated [19,20]. However, harms from screening have also been identified, such as false-positive exams and over-diagnosis leading to cost, anxiety and invasive diagnostic procedures. Moreover, radiation exposure for younger people or those with a low risk of developing lung cancer is another limitation to screening [21].

Consequently, in their latest version of screening for lung cancer in 2013, the US Preventive Services Task Force recommended annual screening with low-dose CT in adults aged between 55 and 80 years who have a 30 pack-year smoking history (1 pack-year is equivalent to 1 pack/day for 1 year) or more and are smokers or have quit smoking within the last 15 years. However, screening should be discontinued if the former smoker has not smoked for 15 years or if he develops a health problem that limits his life expectancy or his ability to access lung surgery [22].

Although this screening has demonstrated its beneficial value in terms of mortality, currently, there is no lung cancer screening programmes organised worldwide. Implementation of screening is being discussed throughout Europe among clinicians and policymakers and aims to identify a balance between benefit, harm, cost-efficiency, a shared decision-making process and integration of tobacco cessation [23].

1.4.2. Diagnosis

As mentioned previously, NSCLC is often diagnosed at an advanced stage with non-specific clinical manifestations, laboratory abnormalities or paraneoplastic syndromes [12]. Therefore, the diagnosis must identify histologic specifications (biopsy), tumour extent (staging) and, more recently, the expression of biomarkers to select the most suitable therapeutic option.

The diagnostic strategy needs to be decided in a multidisciplinary team as it depends on the size and location of the tumour, the involvement of nodes, and patient comorbidities [24]. This strategy should include *(i)* an overall investigation (medical history, physical examination,

comorbidity and performance status (PS) assessment), *(ii)* a laboratory check-up (blood-cell counts, renal function, liver enzymes, bone parameters), *(iii)* the determination of the cardio-pulmonary function (e.g. forced expiratory vital capacity, electrocardiogram, forced expiratory volume in 1 second), *(iv)* the use of imaging techniques to determine the tumour size and extent and *(v)* finally, tissue sampling techniques to identify specific abnormalities [25].

The imaging techniques include the use of chest X-ray radiographs, CT and positron emission tomography (PET) scans. Indeed, a Danish randomized study has demonstrated better staging with PET scans combined with CT, in comparison with the traditional invasive staging alone (i.e. mediastinoscopy and mediastinal lymph node biopsy with echo-endoscopy) [12].

The National Comprehensive Cancer Network (NCCN) in the US recommends that patients with a strong clinical suspicion of stage I or II, based on risk factors and radiologic appearance, do not require a biopsy before surgery as biopsy adds time, cost and procedural risk and may not be needed for treatment decisions [24]. Indeed, the European Society for Medical Oncology (ESMO) reported that unlike stage IV, the need for a detailed pre-treatment pathological diagnosis for earlier stages is not yet clear as the consequence of upfront diagnosis is assumed to be less relevant [25]. However, for stage IV, the least invasive biopsy techniques among bronchoscopy, mediastinoscopy, endoscopic ultrasound, endobronchial ultrasound and transthoracic needle aspiration should be selected depending on the tumour mass and location [24]. This is done to identify the histological sub-types, detect molecular abnormalities (epidermal growth factor receptor (EGFR) gene mutations, anaplastic lymphoma kinase (ALK) rearrangements, BRAF mutations; etc.) and checkpoint molecules (programmed death-ligand 1 (PD-L1)) [26]. To do so, various techniques are used such as immunohistochemistry (IHC), real-time polymerase chain reaction (PCR), reverse-transcription PCR (RT-PCR), next-generation sequencing (NGS) and fluorescence in situ hybridization (FISH) [26].

Moreover, the sampling of at least six positive nodes (at least three of them should be mediastinal nodes) during surgery is also recommended to classify the N stage for patients with a suspicion of stages II and IIIA, [12,25]. Finally, the use of brain imaging (magnetic resonance imaging, bone scintigraphy or contrast-enhanced CT) to identify brain metastases remains controversial for early stages as their detection is very low for such patients. However, brain imaging is recommended for patients describing signs or symptoms of brain metastasis with an intent to be cured (i.e. not eligible for palliative treatment) [12,25,27].

1.4.3. Staging

Staging is crucial for the selection of the best therapeutic option: the determination of the stage is in constant change, with improvements in diagnosis techniques tending to describe more precisely the tumour extent [28]. The stage classification is therefore updated by the Union for International Cancer Control (UICC) and the American Joint Committee on Cancer (AJCC) regularly, who published their latest version in January 2017 [28].

Table 2: 8th TNM classification of NSCLC, adapted from *Detterbeck et al.*, 2017 [28].

T/M	Label	N0	N1	N2	N3
T1	T1a ≤1	IA1	IIB	IIIA	IIIB
	T1b >1-2	IA2	IIB	IIIA	IIIB
	T1c >2-3	IA3	IIB	IIIA	IIIB
T2	T2a *Cent, Yisc Pl*	IB	IIB	IIIA	IIIB
	T2a >3-4	IB	IIB	IIIA	IIIB
	T2b >4-5	IIA	IIB	IIIA	IIIB
T3	T3 >5-7	IIB	IIIA	IIIB	IIIC
	T3 *Inv*	IIB	IIIA	IIIB	IIIC
	T3 *Satell*	IIB	IIIA	IIIB	IIIC
T4	T4 >7	IIIA	IIIA	IIIB	IIIC
	T4 *Inv*	IIIA	IIIA	IIIB	IIIC
	T4 *Ipsi Nord*	IIIA	IIIA	IIIB	IIIC
M1	M1a *Contr Nod*	IVA	IVA	IVA	IVA
	M1a *Pl Dissem*	IVA	IVA	IVA	IVA
	M1b *Single*	IVA	IVA	IVA	IVA
	M1c *Multi*	IVB	IVB	IVB	IVB

This classification consists of the tumour, node, metastases (TNM) description of the anatomic extent of the tumour in terms of: **T**, the size of the primary tumour; **N**, the involvement of lymph nodes and their location; and **M**, distant metastases beyond regional lymph nodes. Each one of these components is divided into different groups and their specific combination leads to the determination of the stage [28] **(Table 2)**. Stages I and II with negative nodes are commonly referred as "early-stage disease", while stages II and III with positive nodes are referred as "locally-advanced disease" and stage IV as "advanced or metastatic disease" [24].

The T component is divided into five groups, from T0 (no primary tumour) to T4, depending on the tumour size (T1 for tumour size ≤ 3 cm, T2 for tumour size between 3 and 5 cm, T3 for tumour size between 5 and 7 cm, and T4 for tumour with a greater size than 7 cm). Moreover, these groups can be sub-divided depending on the invasion of adjacent central/mediastinal (*Cent.* In **Table 2**) or peripheral (*Inv.* In **Table 2**) structures [28,29].

The N component is also sub-divided into four groups, from N0 to N3, depending on the location of the nodes involved. As mentioned previously, it is recommended to sample and analyse at least six lymph nodes for accurate staging [28]. The pathological analyses of M0 patients (i.e. patients with no distant metastasis) has demonstrated a correlation between a decreasing 5-year survival rate and the involvement of distant nodes: N1a, 59%; N1b, 50%; N2a1, 54%; N2a2, 43%; and N2b, 38% [29].

The M component is also sub-divided into four groups, from M0 to M1C depending on the localization (intrathoracic for *Contr Nod.* Or extrathoracic for *Pl Dissem.* In **Table 2**) and the number (*Single* for M1b or *Multi* for M1c in **Table 2**) of distant metastasis [28]. Patients with a single extra-thoracic metastasis (M1b) have a better prognosis in terms of mean survival than those with several metastases (M1c) (11.4 months *vs.* 6.3 months) [29].
Stage grouping was also adapted in the last TNM classification and is summarized in **Table 2**. As expected, the more advanced the stage is (from stage I to stage IV), the lower is the 5-year survival rate (from 92% from stage IA1 to 0% for IVB) **(Table 3)** [28,30].

Table 3: 5-year survival rates of NSCLC, adapted from *Detterbeck et al., 2017* [28].

Stages	5-year survival
IA1	92 %
IA2	83 %
IA3	77 %
IB	68 %
IIA	60 %
IIB	53 %
IIIA	36 %
IIIB	26 %
IIIC	13 %
IVA	10 %
IVB	0 %

Considering the importance of the tumour microenvironment in the development and progression of cancer (as will be discussed in *section 1.4.5.2*), several reports indicated that the number, type and location of tumour immune infiltrates in primary tumours were essential prognostic factor for overall survival [31]. As, these are able to influence the risk of relapse, an immune-classification of tumours based on a sample immune score can be interesting. Indeed, this score, quantifying the density and location of immune-cells within the tumour, has a prognostic value that could be superior to the classical UICC/AJCC TNM classification [31].

1.4.4. Histological sub-types

In the previous WHO classifications, the identification of the histopathological sub-types was based on histology using light microscopy and haematoxylin-eosin (HE) staining, and sometimes mucin staining. IHC was introduced in the 1999 WHO classification and has since gained more and more interest. The newest version of the WHO classification was published in 2015 and aims to emphasise on the importance of IHC and genetics in identifying the specifications of the patient's tumour, leading to personalized treatment [16]. This change was related to the discovery of targeted therapies based on specific histologic and genetic alterations, and will be discussed further later in this text [16]. Consequently, lung tumours are divided into many histologic types and even more subtypes, as represented in **Table 1**. Some of these sub-types are illustrated in **Figure 3** and will be discussed hereunder.
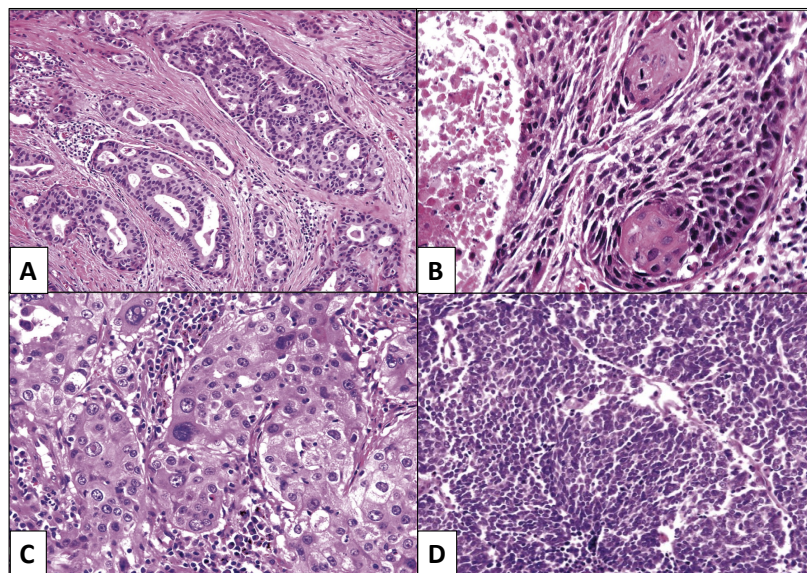
Figure 3: NSCLC sub-types and SCLC. **A:** Adenocarcinoma with acinar pattern. **B:** Invasive squamous cell carcinoma differentiation identified by keratin pearls and prominent keratinization. **C:** Large cell carcinoma with large tumour cells, abundant cytoplasm and large nuclei. **D:** Tumour cells from densely packed SCLC undergoing massive mitoses and apoptosis, from *Zander et al., 2018* [32].

1.4.4.1. Adenocarcinoma

Adenocarcinoma has become the most common sub-type of NSCLC as it represents 40% of patients (smokers and non-smokers). This is explained by the fact that since filters have been added to cigarettes, they have prevented the inhalation of large particles but have induced deeper inhalation of smoke, resulting in more peripheral damages [14]. This sub-type tends to grow relatively slower than other sub-types, increasing the chance of being found before the invasion of extrathoracic organs [12,14]. Adenocarcinoma arises mostly from type II alveolar

cells that normally secrete surfactant in the periphery of the lung and more precisely mostly from the small airway epithelium [14,32] **(Figure 3.A)**. Adenocarcinoma is diagnosed by the presence of pneumocyte markers (TTF-1 and/or napsin A). Its sub-division was completely updated in the 2015 WHO classification to depend on the extent of the invasiveness. Therefore, three major types of adenocarcinomas are identified: pre-invasive (adenocarcinoma in situ), minimally invasive and invasive.

Adenocarcinoma in situ is diagnosed with a tumour size of less than 3 cm describing a pure lepidic growth, which is defined as growth of neoplastic cells along alveolar septa without architectural destruction [33]. No stromal, vascular or pleural invasion is detected in this sub-type, nor are papillary, micropapillary pattern or interalveolar tumour cells [12,16,34].

Minimally invasive adenocarcinomas include tumours with a size no higher than 3 cm and invasion no greater than 5 cm, with a predominant lepidic growth and with less than 0.5 cm of any other invasive component. In this case, the cell type is mostly nonmucinous (i.e. type II pneumocytes or Clara cells) and must not invade lymphatics, blood vessels, air spaces or pleura or contain necrosis [12,34].

Adenocarcinomas with an invasion of 0.5 cm or greater are considered as invasive adenocarcinomas and are divided in five sub-types: lepidic, acinar, papillary, micropapillary and solid. As previously defined, a lepidic growth characterizes the proliferation of tumour cells along the surface of intact alveolar walls, whereas an acinar growth is a gland-forming cancer. The papillary pattern is characterized by papillary structures that replace the underlying lung architecture, while the micropapillary pattern describes papillary tufts that lack a central fibrovascular core. Finally, a solid adenocarcinoma is composed of sheets of polygonal tumour cells [16].

1.4.4.2. Squamous cell carcinoma

Squamous cell carcinomas represent 25-30% of lung cancers, and 90% occur in cigarette smokers [12,13]. The majority of these carcinomas arise in the epithelium cells located centrally in the mainstem, lobar or segmental bronchi. They are diagnosed by the presence of immunohistochemical markers such as CK5, CK6, p40 and desmoglein-3 [12]. Moreover, they show keratinization, pearl formation and/or intercellular bridges [13,32] **(Figure 3.B)**. Recent studies demonstrate mixed results regarding the survival rates between adenocarcinomas and

squamous cell carcinomas [35]. While some studies have shown a significantly better prognosis in terms of the 5-year survival rate for squamous cell carcinomas in comparison with adenocarcinomas [13,35], others have shown the opposite or report no significant difference [35]. Indeed, the comparison between these sub-types is difficult considering the following significant differences: gender (males are more likely to have squamous cell carcinomas), the distribution of the sub-type across stages (adenocarcinomas are more likely to be detected in earlier clinical T and N stage while squamous cell carcinomas patients reveal much more tendency to have clinical M0 stage) and tumour location (adenocarcinomas are detected in the periphery whereas squamous cell carcinomas are retrieved in central locations) [35].

1.4.4.3. Large cell carcinoma

Large cell carcinomas are an undifferentiated NSCLC type that lacks the cytologic and architectures of SCLC and glandular or squamous differentiation. They encompass large cell neuroendocrine carcinoma since the WH0 1999 classification. Large cell carcinoma represent 5-10% of all lung cancers whereas large cell neuroendocrine carcinoma accounts for about 3% of lung cancers. They are both mostly encountered in smokers, but differ from one another by the neuroendocrine features of the latter, that are correlated with a worse prognosis. They are characterized by large cells with abundant cytoplasm and large nucleoli **(Figure 3.C)**. Their numbers are tending to be reduced as newer immunophenotyping techniques improve the classification of poorly differentiated sub-types [12,16].

1.4.4.4. Adenosquamous carcinoma

Adenosquamous carcinoma is a sub-type in which both squamous cell carcinomas and adenocarcinomas are represented, at a minimum of 10% for each [16]. They account for 0.4-4.0% of lung carcinomas and might increase in the case of higher adenocarcinoma incidence [13]. Adenosquamous carcinomas have a poor prognosis and show early metastasis. The tumours are often located in the periphery of the lungs and are highly similar to other NSCLC in terms of presentation and spread [13].

1.4.4.5. Sarcomatoid carcinoma

Sarcomatoid carcinoma is considered as a rare sub-type of NSCLC as it accounts for 0.3-1.3% of all lung malignancies [13]. It is poorly differentiated and contains a component of sarcoma or sarcoma-like tumours and is divided into five subgroups: spindle cell carcinoma, pleomorphic carcinoma, carcinosarcoma, giant cell carcinoma, and pulmonary blastoma [16].

It is majorly related to tobacco smoking (90% of cases are pleomorphic carcinoma) or, at a lower proportion, to asbestos exposure [13]. It emerges from the central or peripheral lung, mostly in the upper lobes [13].

1.4.5. Treatment

The current treatment modalities for NSCLC are divided into two main groups: localized and systemic treatments. The localized treatments include surgery and radiotherapy, and aim to remove the primary tumour. Systemic treatments involve conventional chemotherapy, targeted therapies and immunotherapy and aim to fight tumour invasion from the primary tumour. The combination of these modalities considers the patient intrinsic factors (age, comorbidities, PS and personal choice), the disease characteristics (histology, stage) and the tumour factors (e.g. tumour operability, biomarkers, etc). The management of the treatment could include the option of changing the therapeutic strategy following additional investigations [27].

To increase the chance of success, it is recommended to include a smoking cessation programme as a major part of the management of NSCLC by giving clear and personalized advice as it has been demonstrated that this can improve the treatment outcome. Moreover, smoking is able to interact with systemic therapy, which can interfere with the efficacy of the therapy [27]. However, its direct impact on efficacy remains controversial.

1.4.5.1. Localized treatments

Surgery

Surgery consists of the ablation of a lobe (i.e. lobectomy), in the case of a tumour size greater than 2 cm with a solid appearance, a part of the lung irrespective of its anatomical boundaries (i.e. wedge resection), a segment (i.e. segmentectomy) of the lung containing the tumour, or even of the whole lung (i.e. pneumonectomy). This is the best therapeutic option for NSCLC in the early stages (stages I, II and IIIA) if the tumour is resectable and if the patient cardiopulmonary reserve is compatible with invasive surgery [14,24,30]. As mentioned above and illustrated in **Table 3**, these stages are correlated with the highest 5-year survival rates: 68-92% for stages IB to IA1, 53-60% for stages IIB to IIA and 36% for stage IIIA [28,30].

The tumour operability is assessed using imaging studies, biopsies and patient-intrinsic factors [14]. However, as mentioned previously, NCCN guidelines recommend that patients with a strong suspicion of stages I and II do not require a biopsy before surgery [24]. In contrast, the role of surgery for patients with stage IIIA remains controversial as this population is highly

heterogeneous. Therefore, they must be classified following the recommendations described in the guidelines [24]. Moreover, the high-risk population and also the main part of lung cancer patients are smokers. Indeed, even if smokers have an increased risk of postoperative complications, it is still recommended to consider surgery as it remains the predominant opportunity for prolonged survival [24].

Video-assisted thoracoscopic surgery or minimally invasive surgery (with robotic-assisted approaches), where a small incision is made in the chest and where a thoracoscope is inserted, remains highly recommended [14,24,30]. Indeed, these techniques have shown in large meta-analyses to give a better quality of life and long-term outcomes compared with open lobectomy [30].

Moreover, stage II and IIIA patients who have undergone surgery may receive an adjuvant chemotherapy to kill the remaining cancer cells and reduce the risk of tumour repopulation and cancer relapse [30]. Chemotherapy may also be administered prior to surgery as a neoadjuvant therapy to reduce the tumours and facilitate their shrinkage, as recommended by NCCN guidelines [30]. Indeed, an absolute survival improvement of 5% at 5 years has been reported in patients with clinical stages IB-IIIA [36].

Radiotherapy

Radiotherapy is the use of high-energy X-ray beams to damage DNA within cancer cells and destroy them [30]. Simulation should be assessed using CT scans that were used for the selection of radiotherapy as a treatment. Intravenous (IV) and/or oral contrast are recommended to better target the tumours, especially in the case of central tumours or nodal involvement [24]. Radiotherapy results in a high local tumour control with limited toxicities and has proven its potential in all stages of NSCLC as either definitive or palliative therapy [24]. Indeed, radiation oncology and more precisely stereotactic body radiation therapy (SBRT) is used for early stage NSCLC patients who have a tumour size up to 5 cm without any metastases to nearby lymph nodes (stage I, II N0) and who refused or were not able to support surgery [24,30,36]. It uses an advanced technology (linear accelerator machines, proton beams) to precisely locate the tumour, which ensures the delivery of concentrated and highly focused radiation [30]. This technique has demonstrated good primary tumour control rates and overall survival that are higher than conventionally fractionated radiotherapy, but still lower than surgery [24,30].

The use of radiotherapy is recommended for patients from stage III with residual tumour remaining (either microscopic R1 or macroscopic R2) after surgery as postoperative radiotherapy (PORT) or in combination with adjuvant chemotherapy [36]. Moreover, stage IV

patients are also good candidates for radiotherapy as they may benefit from local palliation or prevention of symptoms (pain, bleeding, obstruction) due to local tumour(s) [24]. For locally advanced NSCLC (stage III), doses of at least 60 Gy should be given in 2 Gy fractions [24]. As radiation therapy can be combined to surgery or to conventional chemotherapy for patients with resectable stage IIIA, doses must be lowered to 45-54 Gy in 1.8-2.0 Gy fractions (6-7 weeks) to avoid complications (stump breakdown, bronchopleural fistula) [24]. In the case of advanced lung cancer patients (stage IV), shorter courses of palliative radiotherapy are preferred (e.g. 17 Gy in 8.5 Gy fractions) [24].

1.4.5.2. Systemic treatments

The use of systemic treatments was initiated with the discovery of the first cytotoxic drug in the 1940s (i.e. alkylating agents, antimetabolites). It is from the introduction of platinum-based chemotherapy in the early 1980s that survival advantages of chemotherapy were reported for NSCLC patients [37]. Different combinations and regimens had been optimized with no additional benefit, leading to the use of platinum drugs combined to another cytotoxic drug as the first-line therapy for approximately 25 years. A general consensus was that a plateau in the development of cytotoxic chemotherapy was reached in the beginning of the 21st century. Interestingly, in parallel, new discoveries in the field of immunology as well as in cell and molecular biology (i.e. cellular pathways in tumour cells) have led to the discovery of targeted therapies. It was not until the beginning of the 21st century, that the benefits of targeted therapies started to be demonstrated, with an improved effectiveness of NSCLC treatments [38], and the first targeted therapy (i.e. gefitinib) approved by the FDA in 2004. Finally in the middle of the 2010s, recent advances in immunotherapy led to the introduction of immune checkpoint inhibitors for the treatment of advanced disease. It is from 2015 that these therapies showed their benefits in NSCLC patients, with the approval of nivolumab by the FDA [37–39].

Therefore, recent advances in targeted therapies and immunotherapy have changed the positioning of conventional chemotherapy for the treatment of NSCLC [38]. Consequently, it is now crucial to investigate specific histologic and genetic alterations, as well as the presence of biomarkers to select the most promising therapeutic option.

Conventional chemotherapy

Conventional chemotherapy is administered using the IV route depending on histology, age, comorbidity and PS [14]. PS is a parameter commonly used by clinicians, who score PS from 0 to 5 (with a PS of 5 corresponding to patient death) to assess the suitability of chemotherapy

for NSCLC patients. Although subjective, it measures functional capacity, the probability of adverse effects, quality of life and survival after treatment [40]. Conventional chemotherapy has proven its effectiveness in comparison with the best supportive care, with a 23% reduction in risk of death, a 1-year survival gain of 9% and a 1.5-month absolute increase in median survival. Moreover, it has improved quality of life irrespective of age, sex, histology and PS [27]. Conventional chemotherapy is used either alone or in combination with localized modalities (i.e. surgery and radiotherapy) for early and locally-advanced diseases, and with immunotherapy for invasive disease [36].
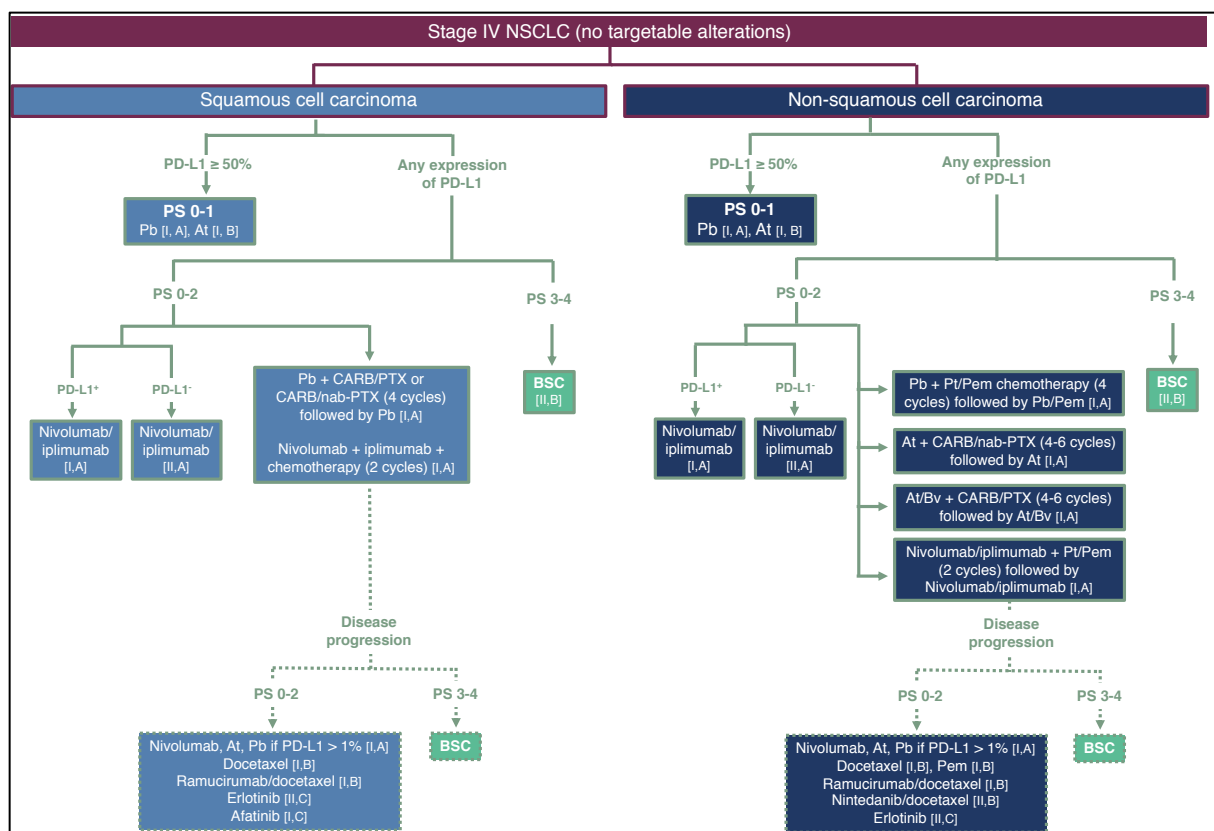
Figure 4: Treatment algorithm for stage IV with no targetable alterations for squamous cell carcinoma and non-squamous-cell carcinoma following ESMO guidelines. Recommendations are classified as strong (I) or moderate (II) based on a high (A) or moderate (B) level of evidence. At stands for atezolizumab, Bv for bevacizumab, BSC for best supportive care, CARB for carboplatin, nab-PTX for nanoparticle albumin-bound paclitaxel, Pem for pemetrexed, Pb for pembrolizumab, Pt for platinum and PTX for paclitaxel, adapted from *Planchard et al., 2020* [36].

It has been stated that 40% of diagnosed patients are stage IV [14]. The treatment for advanced-stage patients with a PS of 0-1 is a platinum-based chemotherapy with a combination of a platinum compound (cisplatin or carboplatin) to paclitaxel, gemcitabine, docetaxel, vinorelbine, irinotecan or pemetrexed [14] **(Figure 4)**. This is explained by the fact that *(i)* two-

drug based chemotherapies have demonstrated a survival benefit over one-drug chemotherapy regimens, *(ii)* a three-drug based chemotherapy combination did not demonstrate any higher survival, and finally that *(iii)* platinum-based doublets have shown a statistically significant reduction in the risk of death at 1 year with a similar toxicity profile to that of non-platinum doublets [27]. Moreover, none of cisplatin and gemcitabine, cisplatin and docetaxel or carboplatin and paclitaxel have demonstrated a significant advantage over the others, and have resulted in similar median overall survivals ranging between 8-10 months [42]. Therefore, the selection of the cytotoxic combination should be personalized to each patient based on the toxicity profile. However, depending on the histologic sub-type, (i.e. squamous or non-squamous), some chemotherapy drugs seem to be preferred over others [27,36] **(Figure 4)**. Indeed in non-squamous NSCLC, a pemetrexed-based doublet (pemetrexed-cisplatin or pemetrexed-carboplatin) is administered either alone or in combination with bevacizumab if there are no contraindications [14,36]. Moreover, in squamous NSCLC, the use of taxanes in platinum-based doublets (e.g. paclitaxel-carboplatin) have demonstrated greater benefit than in non-squamous NSCLC, proving the role of histology in selecting the most promising treatment [43].

Platinum-based chemotherapies are administered over four-six well-spaced cycles (i.e. every 3-4 weeks) due to their toxicities [24]. This range in terms of number of cycles was selected based on the fact that six-cycle treatments did not demonstrate overall-survival benefits over treatments with fewer cycles [27]. The platinum compound is administered the first day of each cycle (50-100 mg/m^2 for cisplatin and AUC 5-6 mg/mL x min for carboplatin) while the other cytotoxic drug may be administered more frequently (1-3 times more a cycle) [24]. Typically, docetaxel (75 mg/m^2), paclitaxel (200 mg/m^2) and pemetrexed (500 mg/m^2) are also administered on the first day of each cycle, while gemcitabine (100-1250 mg/m^2) is administered 2 times per cycle, etoposide (50-100 mg/m^2) 3 times per cycle and vinorelbine (30 mg/m^2) up to 4 times per cycle [24].

For patients with a PS of 2, despite an increased toxicity (mainly haematological), a higher response rate and survival has been demonstrated for platinum-based chemotherapy versus single-agent chemotherapy [27]. Moreover, the superiority of carboplatin in terms of survival has been demonstrated in comparison with single therapy over two phase-III clinical trials [44,45]. Therefore, it is suggested to administer platinum-based chemotherapy (carboplatin, as first choice) in eligible PS 2 patients and to switch to only one-agent chemotherapy (gemcitabine, vinorelbine, docetaxel, or pemetrexed) in the case of high toxicities [27,36]

(Figure 4). Moreover, the chemotherapy drug can be changed if there are serious adverse effects and even stopped in the case of lack of tumours shrinking [14]. Until now, insufficient data are available on the use of checkpoint inhibitors for these patients, but this treatment remains an option [27].

Patients with a PS of 3 are more likely to suffer from systemic toxicities related to cytotoxic drugs than benefit from their efficacy [14]. Consequently, the best supportive care as palliative treatment is the best option for these patients **(Figure 4)** [14]. This kind of treatment aims to anticipate, prevent and reduce suffering and support the best possible quality of life for patients [46].

Targeted therapies

Personalized medicine for NSCLC treatment has gained major interest recently as in 2003, high remission rates were found in some NSCLC patients using tyrosine kinase inhibitors (TKI) [47]. By 2009, the use of TKI had demonstrated an improved overall survival for stage IV patients compared to conventional chemotherapy regimens **(Figure 5)**. However, this improvement was not demonstrated for EGFR of ALK targeted therapies in phase III [24,48].
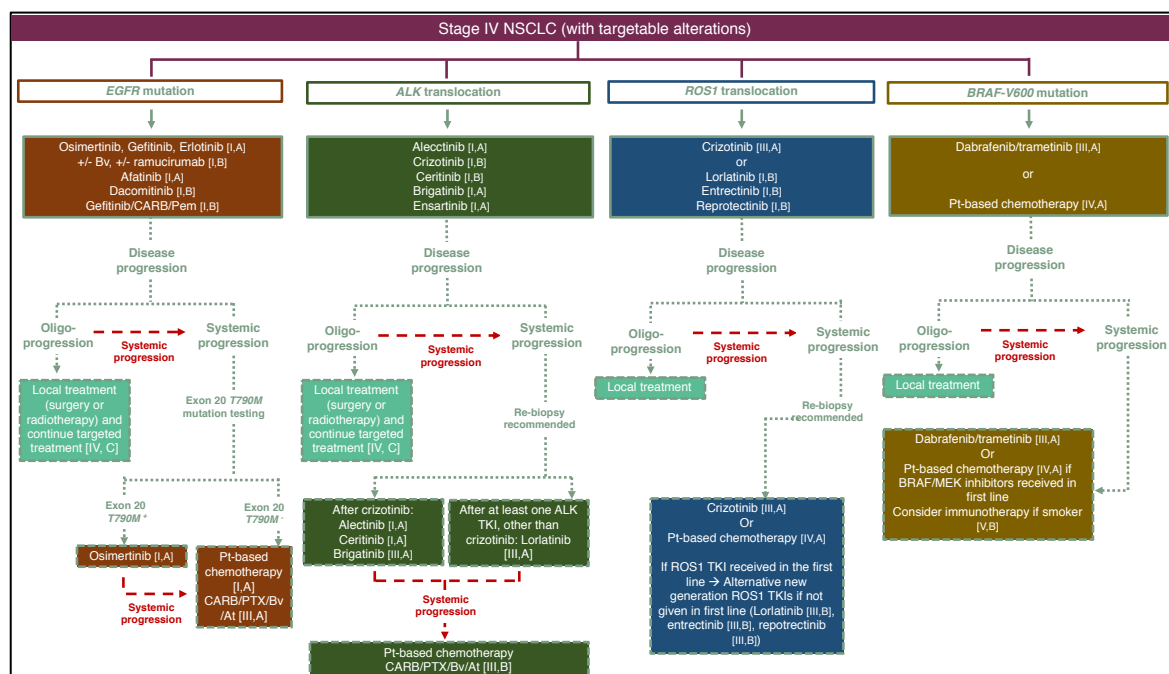

Figure 5: Treatment algorithm for stage IV with targetable alterations following ESMO guidelines. Recommendations are classified as strong (I), moderate (II) or with no benefit (III), based on a high (A) or moderate (B) level of evidence. At stands for atezolizumab, Bv for bevacizumab, CARB for carboplatin, Pt for platinum and PTX for paclitaxel, adapted from *Planchard et al., 2020* [36].

Targeted therapies were developed to trigger specific genomic alterations using predictive and prognostic biomarkers [24]. Some authors estimated that up to 69% of stage IV NSCLC patients could have potential molecular targets, the most frequent among these patients being young patients with adenocarcinoma and who have never smoked; but this seems optimistic for Caucasian populations [24,30].

EGFR gene mutations

EGFR gene mutations are the most commonly detected abnormality for NSCLC patients [24]. They represent 10-20% of Caucasian patients among adenocarcinomas patients and a much higher percentage for those of Asian descent, with never-smoker females predominating [14,30,41]. Testing for EGFR mutations is mandatory in the majority of European countries [27]. This gene codes for a cell surface EGFR that is associated with the activation of several pathways involved in cell growth and proliferation [14]. Therefore, the mutation of EGFR gene is characterized by abnormal cell division as it is constantly activated [14]. This mutation appears in exons 18-21, and is specifically targeted by TKI such as gefitinib, erlotinib and afatinib [14,24,36] **(Figure 5)**. These drugs demonstrated superior progression-free survival, response rates and quality of life than platinum-based conventional chemotherapy [24,36]. A higher overall survival was only observed for afatinib, a second-generation TKI but one that was also associated with higher toxicities (e.g. interstitial lung disease) than first-generation TKI [30,36]. Nowadays, osimertinib is considered as first-line therapy in case of del19/L858R and second-line therapy in case of resistance to TKI for patients with exon 20 790M mutation **(Figure 5)** [49]. Unfortunately, it was reported that most patients treated with erlotinib, gefitinib or afatinib become resistant to treatment in about 9.7-13 months [24]. The treatment after progressive disease should be adapted depending on the patient's failure pattern. In the case of local or slow progression (i.e. oligoprogression), continuation of EGFR TKI therapy is recommended. However, in the case of rapid systemic progression, switching to platinum-based chemotherapy remains the standard of care [30].

ALK rearrangements

ALK rearrangements, also known as ALK fusions, represent 3-7% of NSCLC patients [14,24]. These patients are often around 50 years old at diagnosis, mostly never or light smokers with adenocarcinomas and are more frequently Asian men (50-60%) [14,24,30]. Therefore, the NCCN NSCLC Panel and ESMO recommend testing for ALK fusions in all patients with metastatic non-squamous NSCLC [24]. Rearrangement in EML-4-ALK is the most common

type in NSCLC patients. These patients cannot benefit from EGFR TKI therapy and so specific ALK TKI have been developed and are considered as the backbone of treatment: alectinib, crizotinib, ceritinib, brigatinib and ensartinib **(Figure 5)**. Crizotinib and ceritinib have demonstrated higher progression-free survival than conventional chemotherapy for these specific NSCLC patients in phase III trials [36]. Moreover, alectinib and brigatinib have shown better progression-free survival than crizotinib and are therefore recommended as first-line therapy [24,36]. In the case of the development of resistance, lorlatinib has been reported as having an interesting activity in patients treated with ALK TKI other than crizotinib. However, platinum-based chemotherapy remains the standard of care up to now in case of systemic progression [36]. More recently, in March 2021, lorlatinib was approved by the FDA as a first-line therapy for ALK-positive metastatic NSCLC patients [50].

BRAF mutations

BRAF mutations, and mostly BRAF V600E (50% of cases), are detected in 3-5% of lung cancers, mainly in current or former smokers bearing adenocarcinomas (1-2%), unlike EGFR or ALK patients [24,30]. BRAF is a proto-oncogene able to promote cell proliferation and survival and is non-overlapping with other oncogenic mutations of NSCLC. The NCCN NSCLC Panel and ESMO recommend testing for BRAF mutations in patients with metastatic non-squamous NSCLC. Moreover, testing became required in many countries after the approval of BRAF and MEK inhibitors [27]. The combination of dabrafenib and trametinib is recommended as first-line therapy for patients with BRAF-V600E mutation **(Figure 5)**. In the case of severe toxicities, single-agent therapy with dabrafenib or vemurafenib is the treatment of choice [24,36].

ROS-1 rearrangement

Chromosomal rearrangement in ROS proto-oncogene 1 (ROS-1) is observed in 1-4% of NSCLC patients, mostly those diagnosed with adenocarcinoma and negative to EGFR, KRAS and ALK gene arrangements [24,30]. The NCCN NSCLC Panel and ESMO recommend testing for ROS-1 in non-squamous NSCLC and in metastatic squamous cell NSCLC if small biopsy specimens are already available for the latter [24,27]. Crizotinib seems to be highly effective with ROS-1 patients as it has demonstrated an interesting response rate of up to 80% **(Figure 5)** [24,36].

KRAS oncogene

V-Ki-ras2 Kirsten rat sarcoma (KRAS) is a common mutated oncogene that codes for a G-protein with GTPase activity, as it is detected in approximately 10-25% of patients with adenocarcinoma, mostly Caucasian smokers [14,30]. KRAS oncogene is a prognostic biomarker as no targeted therapy is available and as it indicates poor survival and lack of benefit from EGFR TKI therapy [24]. However, immune checkpoint inhibitors appear to be effective and MEK inhibitors are under investigation for the treatment of KRAS mutations in clinical trials [24].

NTRK gene fusion

Neurotrophic tropomyosin-related kinase (NTRK) gene fusions encode for tropomyosin receptor kinase fusion proteins, which are oncogenic drivers for NSCLC (0.2%) and other cancers (gland, thyroid). It does not over-lap with EGFR, ALK, or ROS-1. The NCCN NSCLC Panel recommends testing in patients with metastatic NSCLC based on encouraging clinical outcomes from larotrectinib and entrectinib [24].

Others

Other emerging genetic alterations have been detected and specific targeted agents are now under investigation, such as rearranged-during-transfection (RET) gene rearrangements (cabozantinib, vandetanib), human epidermal growth factor receptor-2 (HER-2) mutations (ado-trastuzumab emtansine). The FDA approved capmatinib, and tepotinib for the treatment of high-level mesenchymal-epithelial transition (MET) MET exon 14, in May 2020 and February 2021 respectively [24,51,52].

Immunotherapy

Apart from genomic alterations and molecular properties of cancer cells, the interaction with the tumour microenvironment (including the immune system) plays a crucial role in cancer development [53,54]. The tumour microenvironment refers to a cellular environment in which tumours and/or cancer stem cells co-exist with other cells. These are non-malignant cells, blood vessels, lymphoid organs or lymph nodes, nerves, extracellular matrix, cancer-associated fibroblasts, intercellular components (e.g. cytokines and chemokines) and surrounding immune cells **(Figure 6)** [53,54]. It encompasses T and B lymphocytes (LYM), natural killer (NK) cells,

tumour-associated macrophages, myeloid-derived suppressor cells, mast cells, granulocytes, dendritic cells and tumour-associated neutrophils [54].

This tumour microenvironment is trained and shaped by cancer cells to assist the development of cancer hallmarks, respond to stress, stimulation and treatment and finally to assist their survival and migration [54]. Its two main hallmarks are hypoxia and immunosuppression, and are both able to reprogram cancer biology. They are therefore potential target for cancer therapy [54].
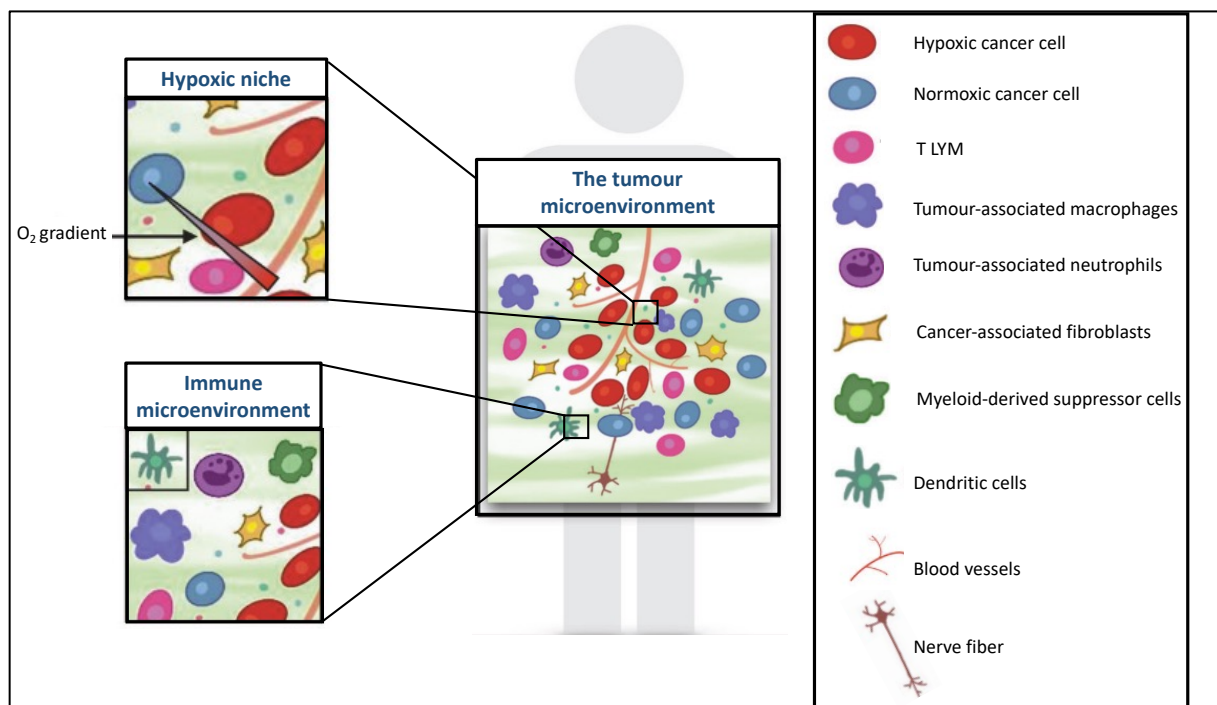
Figure 6: The tumour microenvironment and its two main hallmarks, adapted from *Jin et al, 2020* [54].

Indeed, the first attempts to modulate the immune system aimed to develop vaccines for NSCLC therapy and did not seem to be effective [30]. Nowadays, new immunotherapy approaches mostly target different ligands and receptors that are involved in the immune-modulating pathways. These immune checkpoints are normally used by the immune system to protect the tissues from external damage. However, they can be dysregulated in the case of cancer by tumour resistance mechanisms [14]. The two main check-point inhibitors are described in this part.

Cytotoxic T-lymphocyte-associated antigen-4 (CTLA-4) is an inhibitory receptor that plays a major role in down-regulating T-cell activation by dendritic cells in lymph nodes as well as their proliferation [14,30]. The anti-CTLA-4 therapy, ipilimumab, aims to target this receptor to induce T-cell activation against lung tumours [14,24].

Another interesting target is programmed cell death 1 (PD-1) receptor and its ligand PD-L1, which were the first targets to be approved for the treatment of NSCLC. Indeed, these checkpoints are involved in down-regulating the immune system, thus reducing self-immunity. Their inactivation would therefore boost the immune system and potentialize its involvement in the control of the tumour extent by improving the anti-tumour immunity. Nivolumab and pembrolizumab, both approved by the FDA in 2015, target PD-1 receptors whereas atezolizumab, durvalumab and cemiplimab, approved in 2016, 2018 and 2021 respectively, inhibit PD-L1 [24,55]. Other immune checkpoint inhibitors such as tumour mutation burden (TMB) are under investigation as potential immunotherapy biomarkers [56].

IHC testing for PD-L1 expression is recommended to be performed systematically for all metastatic NSCLC patients [24,27]. The FDA approved the tumour proportion score as a method for evaluating PD-L1 expression. This score represents the percentage of viable tumour cells showing PD-L1 staining [24]. For a PD-L1 expression of 50% or higher, pembrolizumab is recommended as monotherapy in first-line therapy **(Figure 4)** [27]. The recommended dose is either 200 mg every 3 weeks or 400 mg every 6 weeks administered over 30 minutes of infusion. More recently, in May 2020, atezolizumab administered at 840 mg every two weeks or 1 680 mg every four weeks was also approved as first-line monotherapy for advanced NSCLC [57,58]. Furthermore, if PD-L1 expression is lower than 50% (1-49%), pembrolizumab is also recommended to be administered in combination with platinum-based chemotherapy **(Figure 4)**. In this case, pembrolizumab is administered at 200 mg every 3 weeks as an infusion over 30 minutes [59]. However, more recently, the FDA approved pembrolizumab as first-line therapy with an expression higher than 1%, although this was controversial [60]. It should be mentioned that the immunotherapy-based schemes of administration have the specificity of being administered until disease progression, the appearance of unacceptable toxicity or up to 2 years without disease progression.

Regarding these encouraging results, clinical trials on locally-advanced NSLC were conducted and durvalumab demonstrated a higher progression-free and overall survival rate when administered after concomitant chemo-radiotherapy. Durvalumab is now the first immunotherapy validated for stage III NSCLC [61]. However, it did not show an improvement in terms of overall survival over conventional chemotherapy when combined with tremelimumab (an anti-CTLA-4) for metastatic NSCLC patients [62]. In May 2020, the FDA

approved the combination of nivolumab (anti-PD-1) at 360 mg every 3 weeks, ipilimumab (anti-CTLA-4) at 1 mg/kg, every 6 weeks and two cycles of platinum-doublet chemotherapy every 3 weeks as a first-line therapy for patients with advanced or recurrent NSCLC with no specific ALK or EGFR alterations [63]. For PD-L1 expression of 1% or more with specific genomic alterations, targeted therapies are preferred over immunotherapy as they demonstrated higher response rates and better toxicity profiles [24,64].

As demonstrated with the recent approvals by the FDA, the use of immunotherapy is booming and is continuously shifting the position of the standard of care against NSCLC, thus opening up to new treatment perspectives.

1.5. Small cell lung carcinoma

1.5.1. Screening, diagnosis, symptoms and histology

Currently, no effective screening test has been able to detect early-stage SCLC. This disease is typically diagnosed when patients present symptoms indicative of advanced stages. Although low-dose CT is able to detect early-stage NSCLC, this does not seem to be useful for early-stage SCLC. This is certainly related to the aggressiveness of the disease leading to the appearance of metastases between the annual check-ups [65]. As SCLC presents a large hilar mass and bulky mediastinal lymphadenopathy, cough and dyspnoea are often diagnosed. Moreover, other symptoms have also been described such as hoarseness, vocal cord paralysis and paraneoplastic symptoms [13]. Other manifestations reflect the presence of disseminated metastases in the bone marrow or the liver. Metastases in the brain are rare at the time of primary diagnosis but tend to develop during the disease [13].

SCLC is a high-grade neuroendocrine carcinoma with an epithelial tumour characterized by small, oval, round and spindle-shaped cells and by a small cytoplasm [13]. These cells undergo extensive necrosis and high mitotic activities [13] **(Figure 3.D)**. This sub-type arises centrally and spreads locoregionally and can also be combined to another cell type from NSCLC sub-types [13]. SCLC is grouped with carcinoid tumours and large cell neuroendocrine carcinoma as neuroendocrine tumours in the 2015 WHO classification [16].

1.5.2. Staging and prognosis

SCLC is described either as limited-stage or extensive-stage and follows the TNM classification **(Table 4)**. On the one hand, the limited stage includes all patients without metastases and on the other hand, extensive-stage SCLC includes stage IV with metastases [15].

Table 4: 8th TNM classification of SCLC, adapted from *NCCN, 2016* [65].

T/M	Label	N0	N1	N2	N3
	T in situ	0			
	T1mi	IA1			
T1	T1a	IA1	IIB	IIIA	IIIB
	T1b	IA2	IIB	IIIA	IIIB
	T1c	IA3	IIB	IIIA	IIIB
T2	T2a	IB	IIB	IIIA	IIIB
	T2b	IIA	IIB	IIIA	IIIB
T3	T3	IIB	IIIA	IIIB	IIIC
T4	T4	IIIA	IIIA	IIIB	IIIC
M1	M1a	IVA	IVA	IVA	IVA
	M1b	IVA	IVA	IVA	IVA
	M1c	IVB	IVB	IVB	IVB

The 5-year survival rates of SCLC are relatively lower than those observed with NSCLC, demonstrating its higher aggressiveness. These rates range between 40% for stages IA-IIA to 1% for stages IVB **(Table 5)**.

Table 5: 5-year survival rates of SCLC stages, adapted from *NCCN, 2016* [24].

Stages	5-year survival
IA	40 %
IB	40 %
IIA	40 %
IIB	20 %
IIIA	15 %
IIIB	10 %
IIIC	13%
IVA	10 %
IVB	1 %

As conventional chemotherapy is recommended for all SCLC patients, the determination of the stage is useful for the addition of radiotherapy for limited-stage patients [65]. This must be

performed using a history and physical examination with CT scans of the chest/abdomen with IV contrast product and brain imaging magnetic resonance imaging (MRI, preferred over CT scan). Unilateral bone marrow biopsy may be indicated in some patients with haematological abnormalities but remains rare (5% of patients). If a limited-stage tumour is detected, a PET scan is preferred to assess the presence of distant metastases [65]. Moreover, PET scans seemed to be well-adapted to SCLC staging as SCLC is a highly metabolic disease. However, this must be completed with pathologic confirmation.

Therefore, mediastinal staging is required for stage I-IIA patients who are candidates for surgery. This can be performed by minimally invasive techniques such as video-assisted thoracoscopic surgery. Another technique is thoracentesis with cytologic analysis, which is recommended in case of pleural effusion [65]. Poor PS (3-4) associated with extensive-stage disease and weight loss markers of excessive bulk of disease (e.g. serum lactate dehydrogenase, LDH) are the worst prognostic factors, whereas female gender, a younger age than 70 years, normal LDH and stage I disease offer a better prognosis [65].

1.5.3. Treatment

Systemic conventional chemotherapy is the backbone of care in all patients with SCLC. The combination of cisplatin or carboplatin with etoposide is the recommended and most commonly used treatment [15,65]. Even though the use of carboplatin is less common than cisplatin for SCLC patients, four randomized studies have demonstrated similar efficacy of both drugs in terms of response rate, progression-free survival and overall survival, but with different toxicity profiles [66].

Adjuvant chemotherapy is recommended for patients who have undergone surgical resection or SBRT for early-stage cancer. Indeed, SBRT seems to be useful for patients with clinical stage I to IIA tumours who are inoperable or refuse surgery, but this is not clearly established in clinical practice. For limited-stage cancer, concurrent thoracic radiotherapy combined to chemotherapy is recommended. Thoracic radiotherapy has demonstrated an improvement in terms of local control of (25-30%) and survival (5-7% in 2-year survival) in limited-stage patients. However, the combination of chemotherapy and radiation has induced risks of esophagitis, pulmonary and hematologic toxicity [15,65].

For extensive-stage patients, systemic therapy is the first-line treatment and radiotherapy may be considered as a palliative option to reduce the symptoms [15,65]. Finally, a recent study has

demonstrated the benefit of adding immunotherapy (atezolizumab) to chemotherapy as first-line treatment for extensive-stage SCLC and resulted in significantly longer overall survival and progression-free survival than chemotherapy alone [11,65]. More recently, durvalumab was approved by the FDA in combination with etoposide and either carboplatin or cisplatin as first-line treatment for patients with extensive-stage patients [67].

1.6. Reasons for treatment failure

Despite recent advances in lung cancer treatment, the overall 5-year survival of all stages remains low at 21.7% (USA, 2011-2017) [10]. Moreover, the aforementioned treatment strategies have various limitations that may explain their limited effectiveness.

First, as cytotoxic drugs used in conventional chemotherapy act on tissues undergoing rapid mitosis such as cancerous cells but not only these tissues, they do not selectively discriminate cancerous cells from healthy tissues. Therefore, they induce severe toxicities in bone marrow, gastro-intestinal mucosa and skin, which lead to myelotoxicity, gastro-intestinal discomfort and alopecia [68]. These severe toxicities could limit the role of the immune system in controlling the disease [69]. Moreover, as all cytotoxic drugs for conventional chemotherapy (as well as targeted therapies and immunotherapy) are administered using the systemic route (mainly IV), systemic toxicities are more likely to occur as the drugs are distributed in the whole body. Consequently, the administered dose is often reduced and the administration cycles are spaced to limit cumulative toxicities between cycles and to allow healthy tissues to recover [68]. In the meantime, the surviving cancer cells are no longer exposed to cytotoxic treatment, which allows them to proliferate and to invade the lungs and other tissues (i.e. lymph nodes or distant organs), which could lead to tumour relapse.

Moreover, to be efficient, the drug must reach and penetrate the tumour and enter its cells at an effective concentration that is high enough to exert its therapeutic action. This is challenging as tumours often proliferate rapidly, with a poorly-organized vascular architecture. This architecture leads to irregular blood flow and compression of blood and lymphatic vessels by cancer cells and therefore to heterogenous concentration of drugs into the tumour. Consequently, the access of drugs to the cancer cells far from blood vessels (i.e. often in the periphery) remains very challenging, especially when administered using the IV route [70]. Moreover, in zones far from blood vessels, there is a limited access to oxygen and nutriments and higher products of metabolization that lead to a hypoxic environment, a major hallmark of

the tumour microenvironment [54,70]. These hypoxic zones exposed to lower drug concentrations also change the phenotype of the cells, which become progressively more resistant to the treatment and more invasive [70]. Apart from poor drug penetration in solid tumours, resistance is also acquired following tumour proliferation and their ability to increase their survival by acquiring mutations during their development and in exposure to therapies. In addition to highly mutant cells, cancer stem cells are also retrieved in the tumours, which indicates the high level of intratumour heterogeneity [71]. These mutant and cancer stem cells require much higher drug concentrations to be affected and are therefore responsible for tumour repopulation. This has been described for EGFR and ALK TKI for NSCLC treatment to which resistance was acquired due to the perpetual change of cell clones over mutations. Consequently, repeated biopsies are needed to evaluate the constant change in cells clones when they are in relapse to better adapt therapies [71].

Even specific and effective, targeted therapies are only suitable for a minority of patients and have been associated with severe toxicities including diarrhoea, skin rush, anorexia, cachexia, sarcopenia and leukopenia [72,73]. Immunotherapy is also gaining much interest, but it is important to keep in mind that severe toxicities associated to deaths were also observed. Of these deaths, 35%, 22% and 15% were due to pneumonitis, hepatitis and neurotoxic effects, respectively, for anti-PD1/PD-L1 treatment, and 70% due to colitis for anti-CTLA4. The combination of anti-PD1 and anti-CTLA4 has led to severe toxicity associated to death, with 37% and 25% of deaths due to colitis and myocarditis, respectively [74].

1.7. Strategies and new perspectives

One of the most successful strategies to limit the side effects related to the administration of cytotoxic drugs has been the development of nanomedicines. For lung-cancer therapy, nanoparticle albumin-bound paclitaxel (nab-paclitaxel, Abraxane®) is the only nanomedicine accepted by the FDA that has demonstrated an advantageous pharmacokinetic (PK) profile associated with an accumulation in the tumour environment while limiting systemic toxicities [75]. Abraxane® benefits from receptor-mediated transcytosis and from the enhanced permeation and retention (EPR) effect to reach the tumour microenvironment. This effect is related to the leaky vessels in the tumours due to their anarchic development [75]. Moreover, an albumin-based formulation by itself has been well-tolerated, due to its high biocompatibility, whereas a surfactant/solvent-based formulation used by the conventional Taxol® showed hypersensitive reactions (i.e. mild hypotension, dyspnoea with bronchospasm, erythematous

rashes, urticaria, abdominal and extremity pain, angioedema and diaphoresis [76,77]). A change to the albumin-based formulation led to an increase in the administered dose commonly used with Taxol®, which improved its efficacy in NSCLC patients. This effect may be used for the development of other nanomedicines to improve the therapeutic ratios of other cytotoxic drugs.

Despite these advantages, the development of nanomedicines faces major challenges that limit their further development in clinics [78]. The first challenge is related to the formulation development, including often low drug-loading efficiency (i.e. promoting the use of high amounts of excipients), which leads to difficulty in producing large nanopharmaceutical batches with robust characteristics [78]. Moreover, due to their high specific surface, nanomedicines are able to interact with the biological environment, raising concerns regarding their safety. Finally, there is a need to establish clear guidelines by regulatory authorities to define the requirements needed in terms of quality and safety for inhaled nanomedicines to reach the clinical stage [78].

Even if targeting single abnormalities or cancer pathways has shown interesting clinical outcomes, limited improvement in terms of overall survival has been demonstrated [71]. Zugazagoitia *et al.,* insist that it may be interesting to use more multiple drug combinations against several abnormalities and/or targets to improve lung cancer treatment, as done for human immunodeficiency viruses (HIV) [71]. Anti-PD-1/PD-L1 may therefore be combined together or with anti-CTLA4 and conventional chemotherapy to increase the oncogene targeting and improve the treatment efficacy, as recently accepted by the FDA (nivolumab, iplimumab and platinum-doublet chemotherapy). However, the major limitation in this case would be overall cumulative toxicities. The investigation of other regimens, doses and drugs should be investigated to evaluate their clinical outcomes and survival.

Regarding the reasons for treatment failure, and more precisely the need to stagger treatment cycles during conventional chemotherapy, it could be interesting to administer cytotoxic drugs directly in the lungs during these off-cycles. This would lead to increased tumour exposure to cytotoxic drugs while limiting systemic exposure, and would offer the possibility to deliver high-systemic-toxicity drugs by improving their therapeutic ratio, as long as the pulmonary tolerance remained acceptable. Consequently, the access to the site of action would be enhanced (improving the penetration in the tumour site), intensifying the treatment efficacy. The advantage of this loco-regional treatment is that high cytotoxic drug doses would arrive directly

into the lungs and diffuse progressively into the blood and to the lymph, following the same ducts as cancer cells would follow during tumour spread. Inhaled chemotherapy, as a loco-regional modality would therefore fill the gap between localized (surgery, radiotherapy) and systemic treatments (conventional chemotherapy, targeted therapy and immunotherapy) against lung cancers. Interesting results from a phase I/II trial of inhaled carboplatin in combination with IV carboplatin and docetaxel have demonstrated an improvement in terms of survival over IV carboplatin/docetaxel group. This seems to be related to a higher concentration of the chemotherapy in the tumour site, lymph nodes and systemic circulation [79,80]. This strategy will be further discussed in the next sections.

2. <u>Cisplatin, Carboplatin and Paclitaxel</u>

As mentioned in the previous section, platinum-based drugs are the backbone of conventional chemotherapy used against lung cancers. These drugs are often combined to other cytotoxic drugs, including paclitaxel, which was also selected in this work. Therefore the key characteristics of cisplatin, carboplatin and paclitaxel are set out in this section.

2.1. Cisplatin and carboplatin

2.1.1. Generalities and clinical use

Cisplatin was discovered in 1844 by Michele Peyrone and its chemical structure was revealed in 1893 by Alfred Warner **(Figure 7)**. But it was in 1965 that it gained interest when *Rosenberg et al.,* identified by chance its inhibition activity in *Escherichia coli* and hypothesized on its role in cancer treatment. It was only by the end of the 1970s that it had demonstrated its cytotoxic activity for various cancer types, and it was approved by the FDA in 1978 for the treatment of metastatic testicular or ovarian cancer [81,82]. Nowadays, cisplatin is used for the treatment of many types of cancers such as germ-cell tumours, sarcomas, lymphomas and carcinomas, and more specifically in the treatment of lung, bladder and head and neck cancers [83].
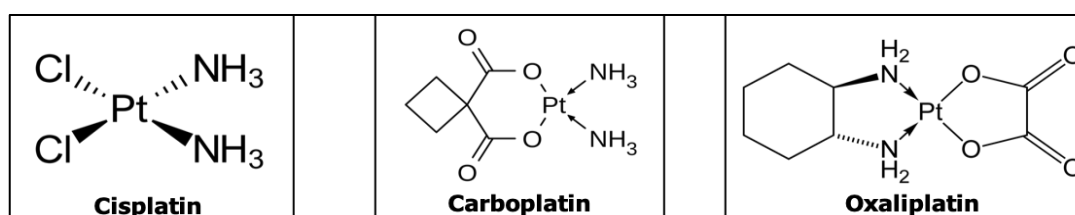

Figure 7: Chemical structure of cisplatin, carboplatin and oxaliplatin, adapted from *Spreckelmeyer et al., 2014* [84].

Proportionally to its advantages, cisplatin is also a highly toxic drug with life-threatening side effects (nephrotoxicity, ototoxicity, and neurotoxicity), which has led to the development of several thousand analogues to improve its therapeutic index. Moreover, since the discovery of cisplatin, wide interest regarding the use of platinum compounds for cancer treatment has begun [81]. Thus, this development was also investigated to overcome cisplatin-resistance mechanisms. Among the platinum compounds investigated, 13 were tested in clinical trials. However, only carboplatin and oxaliplatin were approved by the FDA, in 1989 and 2002 respectively [81] **(Figure 7)**. As illustrated in **Figure 7**, unlike cisplatin and carboplatin, oxaliplatin has an oxalate leaving group and a carrier ligand that are both responsible of its unique properties [85]. Indeed, they are responsible of an increased cellular uptake and different conformation of DNA adduct formation. Therefore, oxaliplatin can overcome the resistance encountered with cisplatin and is used against colon cancer [86]. Unlike oxaliplatin, carboplatin is also used for the treatment of lung cancers [87]. Based on a Cochrane review, carboplatin and cisplatin have a similar efficacy against NSCLC in terms of overall survival, one-year survival and response rates. However, higher rates of nausea and vomiting were described for cisplatin and more thrombocytopenia was reported by carboplatin-treated patients [88].

2.1.2. Cell penetration and efflux

Cisplatin or cis-diamminedichloroplatinum (II) – cis-[PtCl$_2$(NH$_3$)$_2$] – is a small non-charged molecule with a molecular weight (MW) of 300.05 g/mol. Carboplatin or cis-diammine cyclobutanedicarboxylatoplatinum (II) – cis-[PtC$_6$H$_6$0$_4$(NH$_3$)$_2$] – is considered as a second-generation platinum complex and is also a small molecule, with a MW of 371.25 g/mol. It differs from cisplatin in that it has a bidentate dicarboxylate ligand in place of the two chloride ligands **(Figure 7)** [81]. Their structure makes them candidates for passive diffusion (log P of -2.19 for cisplatin and of -2.30 for carboplatin [89,90]) as they have a small size and no net charge [91]. However, their specific toxicities related to their preference to concentrate in some specific cells (especially cisplatin in proximal tubule cells for example) has driven the hypothesis that their cell uptake mechanisms involves other possibilities such as transport proteins **(Figure 8)** [82].

Copper transporter 1 (Ctr1) has been identified in intestinal cells of the mouse, rat and pig and also in the basolateral side of the proximal tubule cells. Moreover, it has also been found in the mouse cochlea and identified in dorsal root ganglia. Ctr1 seems to control the cellular accumulation of cisplatin and carboplatin at both low and high concentrations [82,92].

Moreover, this transporter expression in tumour cells of ovarian-cancer patients has been related to cell sensitivity to carboplatin and cisplatin. However, as it is not specifically overexpressed in particular organs, it does not seem to be the decisive transporter for specific platinum-drug toxicities [93].
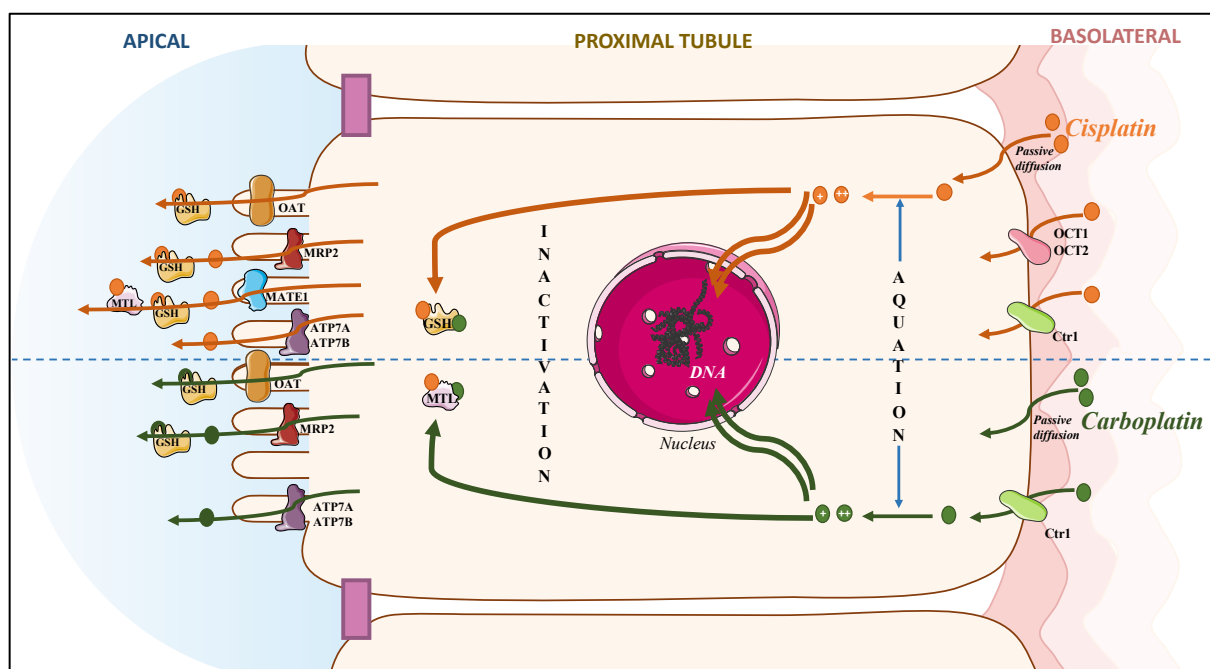

Figure 8: Traffic of cisplatin and carboplatin across the cell membrane. Cisplatin and carboplatin enter the cell by passive diffusion or using transporters such as OCT1/OCT2 for cisplatin and Ctr1 for cisplatin and carboplatin. Once in the cells they are submitted to aquation, leading to the generation of highly reactive species that attack the negatively charged DNA. These species are inactivated by GSH and MTL. Their efflux can be assessed either by transport of the reactive species out of the cell or from their complexes with GSH/MTL using ATP7A, ATP7B, OAT, MRP2 and also MATE1 for cisplatin. This figure was created from information retrieved from the following references [82,93,94].

Copper transporter 2 (Ctr2) is a transport protein with structural homology to Ctr1 and that seems to ensure copper efflux. Ctr2 has also been associated with low sensitivity and consequently to resistance to carboplatin and cisplatin, with higher expression of Ctr2 correlating to lower observed sensitivity to carboplatin or cisplatin [82,93] **(Figure 8)**.

Organic cation transporters (OCT) have demonstrated a specific interaction with cisplatin. Moreover, they have a specific organ distribution with a preference for excretory organs such as the liver (OCT1), kidneys and cochlea (OCT2) [82,93]. In humans, these transporters are expressed in the basolateral membrane (blood-faced part of plasma membrane) of hepatocytes and renal proximal tubule cells and are therefore involved in cisplatin uptake in these cells. It might be useful to mention that in mice, OCT1 expression is higher in renal proximal tubules

than OCT2. In humans, cisplatin seems to interact preferentially with OCT2, suggesting that this transport is critical for cisplatin renal uptake resulting in nephrotoxicity, its main dose-limiting toxicity (DLT). Even if cisplatin has similar affinities to OCT2 and Ctr1 transporters, it has been underlined that Ctr1 is an equilibrative transporter whereas OCTs are electrical and concentration-gradient dependent. The latter is therefore responsible for cisplatin accumulation in the cells presenting these transporters (i.e. kidney, liver and cochlea) [82,93] **(Figure 8)**.

Other transporters expressed in the apical cell membrane (lumen-faced part of plasma membrane), are retrieved in cancer cells and are involved in cisplatin secretion into the urine such as the P-type copper-transporting ATPases ATP7A and ATP7B. They both seem to be involved in transport of carboplatin and cisplatin out of the cells or into specific subcellular compartments as they interact with copper [82,92,93]. Moreover, multidrug and toxin-extrusion protein 1 (MATE1), another transporter that is highly expressed in the kidneys, adrenal gland, liver and other tissues, is involved in cisplatin induced nephrotoxicity as it mediates the secretion of cisplatin into the urine [82,93]. Furthermore, copper-transporting proteins with glutathione (GSH) and metallothionein (MTL) may also influence cisplatin and carboplatin efflux. Cisplatin and carboplatin are able to form a complex with GSH that is refluxed from cells using multi-resistance-associated protein 2 MRP2 (ABCC2) and organic anion transporter (OAT) [92,95] **(Figure 8).**

2.1.3. Mode of action

Once cisplatin and carboplatin are injected in the bloodstream, their neutral forms are conserved as the concentration of chloride ions in plasma is high (100 mM) [92,96]. However, once in the cell, they are able to form highly reactive positively charged metabolites that are able to interact with numerous cytoplasmic substrates (e.g. GSH, MTL and other proteins through their cysteine residues), including DNA (nuclear and mitochondrial) and induce apoptosis [83,97–99].

Indeed, due to the low intracellular concentration of chloride (about 20 mM), cisplatin loses one and/or two chloride ligands for aqua, leading to monoaquacisplatin $[Pt(NH_3)_2Cl(OH_2)]^+$ and diaquacisplatin $[Pt(NH_3)_2(OH_2)_2]^{2+}$ **(Figure 9)**. Moreover, carboplatin loses its 1,1 cyclo-butanedicarboxylate leading to positively charged diaquacisplatin **(Figure 10)** [92,100].
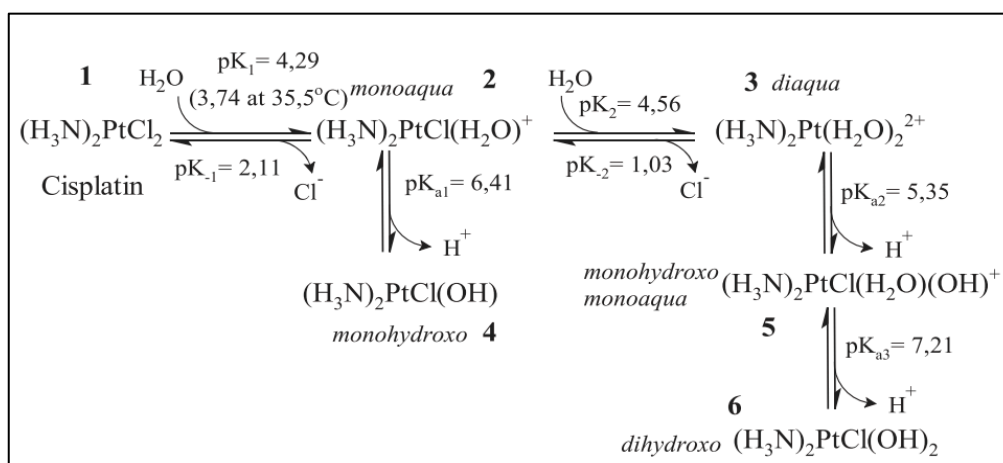
Figure 9: Cisplatin aquation once in the cell *(Makovec et al., 2019)* [85] .
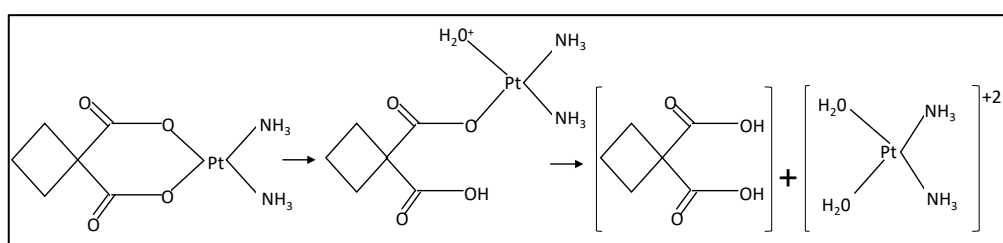
Figure 10: Carboplatin aquation once in the cell *(Oliveira et al., 2018)* [88].

These metabolites interact with nucleophilic molecules in the cell such as DNA and, more precisely, with the N7 position of purine bases leading to the formation of adducts of platinum, called "platination". Most of these adducts (90%) are formed using 1,2-intrastrand cross-link purine bases, leading to cell cycle arrest in G2/M phase and the activation of apoptosis [83,92,96,98]. This results in the activation of various pathways leading to the digestion of the damaged cells through the activation of caspases. Once the caspases are activated, they target nuclear and cytoplasmic factors involved in the maintenance of architecture of the cell [83].

The major difference between cisplatin and carboplatin regarding their activity and therefore their toxicity profiles is probably due to the low reactivity of carboplatin with nucleophiles, as 1,1-cyclobutanedicarboxylate is a poorer leaving group than chloride [92].

Moreover, except from its immunosuppressive effect, cisplatin is also able to trigger immunomodulatory effects that are also important mechanisms of tumour cytotoxicity [98]. Indeed, recent studies have demonstrated that cisplatin can modulate its immune activity by regulating major histocompatibility complex class I, cytotoxic effectors and

immunosuppressive cells in tumour microenvironment [99,101,102]. Unlike oxaliplatin, cisplatin is not able to induce an immunogenic cell death. Indeed, cisplatin was not able to expose calreticulin on the plasma membrane of tumour cells but was associated with an increased level of ATP and high mobility group protein-1 (HMGB-1) [99,101,102]. On the one hand, ATP *(i)* acts as a powerful chemotactic signal; thus recruiting dendritic cells and macrophages to the tumour site, and *(ii)* stimulates the maturation of dendritic cells. On the other hand, once HMGB-1 released from the nucleus, it binds to Toll-like receptors (TLR4) on dendritic cells thus improving the cross-presentation and increasing pro-inflammatory cytokine secretion [101]. Finally, cisplatin was also corelated with tumour cell sensitization to cytotoxic T LYM lysis and downregulation of PD-Ls [101].

2.1.4. Resistance mechanisms

Despite the wide use of platinum drugs in various types of cancers, these drugs have also been associated with relapse and resistance [83,92]. Resistance is described to be related to a failure to induce apoptosis of tumour cells undergoing apoptosis at the right therapeutic concentrations of the drug [83]. This resistance can be either intrinsic to the tumours (most NSCLC patients) or acquired following/during treatment cycles (most SCLC patients) [103]. Three main mechanisms seem to be responsible for this resistance.

The first is a reduction in the accumulation of the drug intracellularly, which is involved in 70-90% of the total incidence of resistance. However, researchers are still divided between those that believe that 20-70% reduction in cisplatin intracellular accumulation could lead to resistance by a factor of 3 to 40, respectively, and those arguing that there is no link between intracellular accumulation and resistance [83]. Moreover, overexpression of ATP7A and ATP7B, which are responsible for drug efflux from the cells, has been demonstrated to be strongly related to the resistance to platinum compounds [92,93].

The second mechanism related to drug efflux is the inactivation of cisplatin and carboplatin. Indeed, they form complexes with GSH and/or MTL leading to their efflux using the MRP2 **(Figure 8)**, as described previously. Moreover, overexpression of MTL in 70% of patients with oesophageal cancer has been correlated with resistance to cisplatin treatment. [92,95]

The third mechanism that may be responsible for resistance is increased repair of DNA damage. Indeed, nucleotide excision repair (NER) is considered as the main pathway for platinum DNA

adduct repair, leading to the inhibition of the cytotoxicity of the drug and therefore of the tumour cell apoptosis [83,92].

More recently, the interference of cisplatin with the tumour microenvironment seems also responsible of drug resistance. The components responsible of this interaction are either physical (i.e. high cell density, fluidic shear stress and extracellular matrix) or biological related to tumour growth (e.g. hypoxia) or to non-cancerous cells (e.g. stroma cells, tumour-associated fibroblasts and immune cells) [98].

2.2. Paclitaxel

2.2.1. Generalities and clinical use

Paclitaxel **(Figure 11)** was discovered in the 1970s in the extract from the bark of the Pacific yew tree *Taxus brevifolia* and was identified in 1971 by Wani *et al.,* [104]. However, its development was suspended for over a decade due to the challenges regarding its formulation (it is practically insoluble in water) [104–106]. Once the hemi-synthesis protocol of paclitaxel was optimized, and polyoxyl 35 castor oil (Cremophor® EL) selected as an appropriate excipient for parenteral administration, the evaluation of its clinical activity against various cancers was initiated [104,106]. Nowadays, paclitaxel is formulated with Cremophor® EL and absolute ethanol (50:50 v/v; Taxol®) and has been approved for the treatment of a wide range of solid tumours such as breast, ovarian, prostate, gastric, NSCLC, and head and neck cancers [104]. However, the amount of Cremophor EL® per administration is relatively high leading to hypersensitivity reactions and neurotoxicity, and has altered the paclitaxel PK [106]. The alteration of the PK seems to be related to the fact that when administered as Taxol®, paclitaxel becomes sequestered in Cremophor® EL micelles, prolonging its circulation time and therefore decreasing systemic clearance [106].
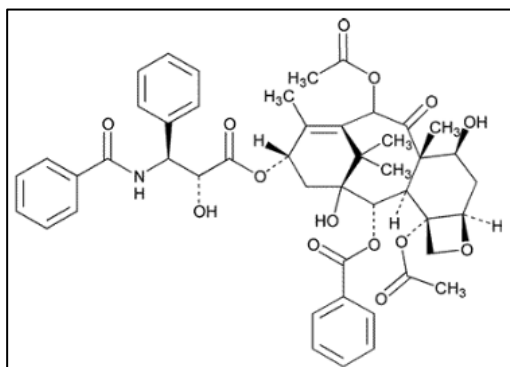

Figure 11: Chemical structure of paclitaxel, adapted from *De Weger et al., 2014* [104].

2.2.2. Cell penetration and efflux

Regarding its highly hydrophobic structure **(Figure 11)**, paclitaxel mostly enters the cell via passive diffusion [105,107]. This phenomenon is non-saturable and is dependent on the extracellular drug concentration and on the duration of exposure [105]. As P-glycoprotein has been associated with resistance to paclitaxel treatment, it has been demonstrated that paclitaxel interacts with a specific binding site on the P-glycoprotein leading to its expulsion from the cell [105]. Moreover, this protein is also located in the blood-brain barrier, preventing paclitaxel from accumulating in the central nervous system by rapidly exporting it to the vascular lumen, back to the blood [108].

2.2.3. Mode of action and resistance mechanisms

Paclitaxel is an anti-mitotic drug, able to bind to the microtubules, leading to the formation of stable assemblies. This leads to the disruption of normal assembly and disassembly of microtubules, preventing their polymerization. Consequently, cell proliferation is inhibited by stopping the cell cycle between metaphase and anaphase, inducing apoptosis [104,107].

Acquired resistance to paclitaxel is related to various mechanisms identified *in vitro*. These mechanisms include *(i)* overexpression of P-glycoprotein, *(ii)* alterations in tubulin, thus reducing the stability of the microtubule network, and *(iii)* inefficient transduction pathways and/or cell death. However, their real contribution *in vivo* remains unclear and seems to depend on the extent of dysregulation of normal cellular integrity in cancer cells [109].

2.3. Cisplatin, carboplatin and paclitaxel related toxicities

Dose delays and dose reductions are often used during conventional chemotherapy to overcome the systemic toxicities (i.e. DLT) encountered with cytotoxic drugs, which could limit their potential. However, up to now, no report has indicated a significant correlation between maintenance of the dose intensity and survival in lung cancer patients [110–112]. The specific toxicities of the most common cytotoxic drugs used in lung cancer treatment and selected in this work are represented in **Figure 12**.

Indeed, cisplatin induces mainly nephrotoxicity (DLT as 47% of patients were reported to have a grade $\geq$ 2, with a fall in creatinine clearance of 40% encountered in 35% of patients [113,114]), ototoxicity (4-90%, [115]), myelosuppression (100% of patients diagnosed with a grade $\leq$ 2, [114]), neurotoxicity (30-40% with a grade 0-1, [83,114,115]) and gastrointestinal

toxicity (i.e. nausea and or emesis 72%, among them 6% were diagnosed with a grade ≥ 3 [66,116]).

On the other hand, carboplatin has a different toxicity profile as it induces myelosuppression (DLT as 73% of patients were reported with a grade ≥ 3 neutropenia, 34% with a grade ≥ 3 leucopenia, 25% with a grade ≥ 3 anemia and 42% with a grade ≥ 3 thrombocytopenia [66]), nephrotoxicity (with 10% of patients diagnosed, among them 5% reported with a grade ≥ 3) and gastrointestinal toxicity (63-65% among them 3% were diagnosed with a grade ≥ 3, [66,116]), but to a lesser extent than cisplatin.

Finally, paclitaxel mainly induces neutropenia (DLT as 22% of patients were diagnosed either with grade 3- 4, [117]), neurotoxicity (57-83%, among them 32% were diagnosed with a grade 3, [76,117–119]), cardiotoxicity (29%, [76]), gastrointestinal toxicity (50%, [120]) and high hypersensitive reactions (**Figure 12)**.

Overall, the toxicities reported with the highest grades in several studies were nephrotoxicity for cisplatin, myelosuppression for carboplatin and neutropenia for paclitaxel [66,76,88,117–119,121,122].
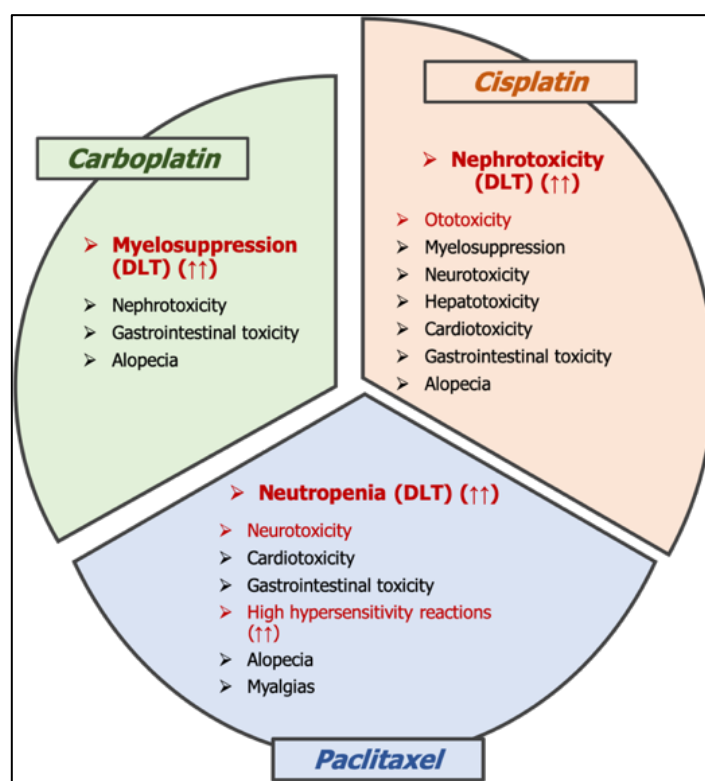
Figure 12: Cisplatin, carboplatin and paclitaxel toxicity profiles. The DLT and the most significant toxicities are coloured in red. Cisplatin induces nephrotoxicity, which is its DLT, and ototoxicity, one of its most significant toxicities. Carboplatin induces myelosuppression (DLT), and paclitaxel induces neutropenia (DLT), neurotoxicity and high hypersensitivity reactions. This figure was created from information retrieved from the following references [115,118,123].

Considering that this work focused on the DLTs of these drugs, only nephrotoxicity and myelosuppression (including neutropenia) were discussed in this section. Moreover, as we also evaluated lung toxicities, the pulmonary toxicity profile of these drugs is also investigated.

2.3.1. Nephrotoxicity

2.3.1.1. Physiopathology

Nephrotoxicity is the cisplatin DLT as it is the main reason for treatment discontinuation for cancer patients treated with cisplatin (**Figure 12)** [115]. The severity of this toxicity leads to dose adjustment, which could limit the treatment efficacy [124]. The exact mechanism during which cisplatin induces nephrotoxicity is not yet fully elucidated [125].

The first consideration of cisplatin nephrotoxicity is its uptake in proximal tubular cells. Indeed, kidney excretion is the main route of excretion for cisplatin as 80% of unbound cisplatin is filtered in 24 hours [126]. The cisplatin concentration in proximal tubular epithelial cells is about 5-fold higher than in plasma, mainly due to peritubular uptake [126,127]. This concentration is mainly due to two transporters: Ctr1 and OCT2, as described previously **(Figure 8)** [128]. Once cisplatin enters the tubular cell, it can interact with GSH leading to the formation of a cisplatin-GSH complex which is able to be metabolised by g-glutamyl transpeptidase (GGT) and cysteine-S-conjugate b-lyase resulting in the formation of a reactive thiol that is reported to be a more potent nephrotoxin [125,127–129]. However, it is still unclear whether all the cytotoxic effects are assessed by the activated metabolites or by cisplatin itself [125].

The different mechanisms related to cisplatin nephrotoxicity, are summarized in **Figure 13**, and will be discussed hereunder.

The first mechanism is DNA damage due to the highly reactive monoaqua and diaqua-cisplatin species that prevent cell replication. This induces activation of the tumour-suppressor protein p53, which can trigger apoptosis leading to the activation of reactive oxygen species (ROS). ROS can also be increased directly by these metabolites as they *(i)* react with GSH, leading to depletion of the cell of antioxidants such as GSH, and *(ii)* interact with the mitochondrial respiratory chain and *(iii)* cytochrome p450 in the microsome [125]. Consequently, ROS *(i)* lead to the initiation of inflammation and *(ii)* contribute to the mitochondrial pathway resulting in cell apoptosis [125,128].
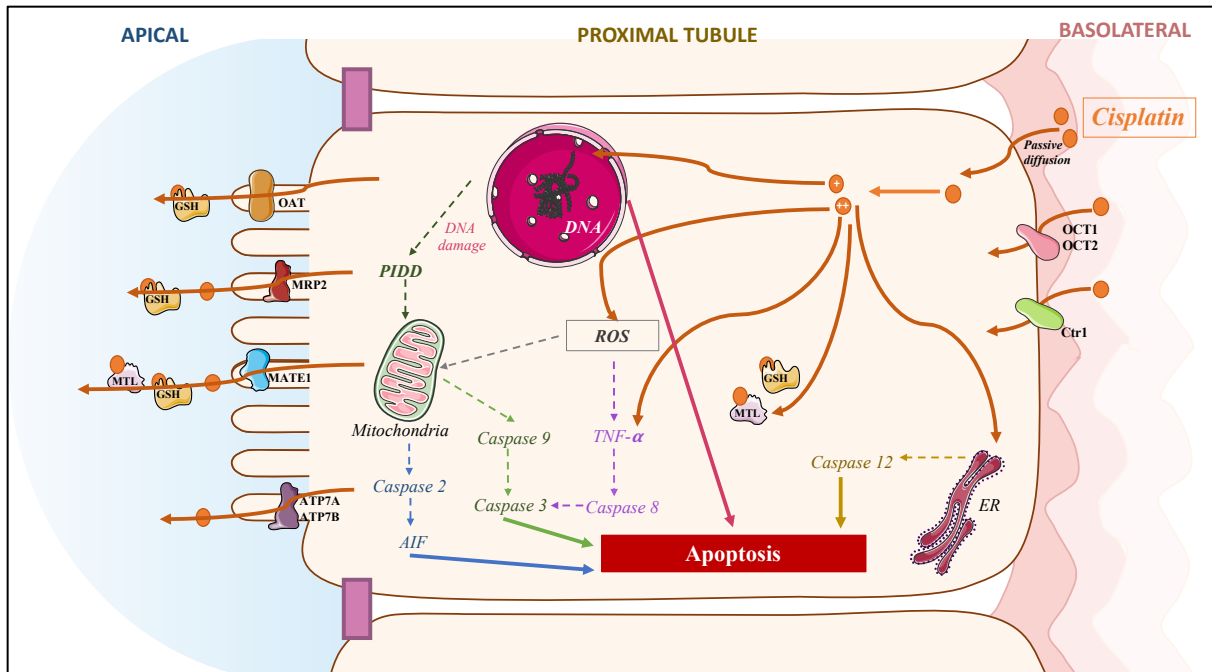
Figure 13: Summary of main apoptosis pathways responsible for cisplatin nephrotoxicity. Cisplatin enters the tubular cells using passive diffusion, OCT1/OCT2 or Ctr1 transporters. Once in the cells, it converts into highly reactive species that trigger various targets to induce apoptosis: DNA damage, mitochondria, ROS release and endoplasmic reticulum (ER). The activation of mitochondria, ROS and ER leads to the release of various caspases and to apoptosis. The reactive species can also bind to GSH and MTL, leading to a depletion of antioxidants. This figure was created from information retrieved from the following references [125,128].

Endoplasmic reticulum and mitochondria also play a major role in cisplatin nephrotoxicity by initiating various caspase activations. Indeed, caspase-12, which is localized in the endoplasmic reticulum, seems to be up-regulated to ensure apoptosis. Moreover, the positively charged metabolites attack the negatively charged mitochondrial DNA leading to its damage [125]. Consequently, the cell switches to a "starvation" mode as it is not able to synthetise ATP, leading to the release of caspase-9 mediators to initiate caspase-meditated apoptosis. Caspase-9 is also secreted by mitochondria following its stimulation by p53-induced protein with a death domain (PIDD). Moreover, mitochondria activation through this pathway has also led to increased caspase 2, inducing the release of apoptosis-inducing factor (AIF) and lead to apoptosis [125,128]. Interestingly, sensitivity to cisplatin seemed to be related to mitochondrial density. This is particularly interesting as proximal tubules, the main renal section damaged by cisplatin, are known to highly concentrate mitochondria [125].

Last but not least, cisplatin is able to induce inflammation in the kidneys by releasing damage-associated molecular pattern molecules (DAMPs), which act on TLR4, and are able to activate a nuclear factor-kappa B (NF-κB) pathway leading to the release of chemokines and cytokines

such as tumour necrosis factor α (TNF-α). These cytokines act on intercellular adhesion molecules (ICAM-1) to attract pro-inflammatory cells to initiate inflammation [125]. Moreover, TNF-α is also known to activate caspase-8, which triggers caspase-3 leading to apoptosis [128].

This damage seems to occur in the tubule-interstitial compartment with minimal glomerular changes. Indeed, a gradual involvement of the tubules is described, with the proximal tubules predominating. Cisplatin has not been correlated with interstitial nephritis; however, its chronic use has led to tubular atrophy and interstitial fibrosis [125]. Indeed, when acute kidney injury (AKI) occurs, and as long as it is early detected early, normal regeneration processes are usually able to restore kidney function [130]. These are mainly related to the resolution of inflammation with tubular regeneration and matrix remodelling [131]. However, in case of defects in these processes mainly through increased release of cytokines, infiltration of inflammatory cells, epithelial mesenchymal transformation and/or fibroblast activation, renal fibrosis and atrophy are encountered. Consequently, a fibrotic scarring tissue is produced and switches the kidney injury from acute to chronic [131,132].

It is important to mention that carboplatin is less toxic to the kidneys than cisplatin as it has slower rates of aquation, reduced generation of ROS and is not recognized by OCT2 [92,128]. However, it induces other type of toxicities, as represented in **Figure 12**.

2.3.1.2.   Clinical manifestations

Nephrotoxicity depends on the dose, the duration, the frequency and the number of chemotherapy cycles [115,125]. Nephrotoxicity is defined as a damage to kidneys related to filtration, reabsorption and excretion that manifests itself as one of the 12 clinical manifestations related to nephrotoxicity, as summarized in **Table 6**.

The two main manifestations are AKI and hypomagnesemia. As mentioned above, cisplatin accumulates in proximal tubular cells leading to their death, resulting in transient and not fully reversible loss of structure and function, called AKI, in 20-30% of cisplatin-treated patients [125,132]. This leads to a dysregulation of the intrarenal haemodynamic, which impairs the glomerular filtration rate [132]. Moreover, the impairment during the regeneration processes can lead to tubular atrophy and to the development of fibrotic scarring tissue, which switches the kidney injury from acute to chronic renal failure [132]. This is increasingly observed as

patients are surviving longer after their cancer treatment and must deal with chronic renal failure in their older age [125]. However, a Cochrane systematic review has demonstrated a non-significant trend toward chronic renal failure associated significantly with transient proteinuria following cisplatin treatment, showing the heterogeneity of the data [125].

Table 6: The common clinical manifestations associated with cisplatin nephrotoxicity, adapted from *Oun et al.,2018* [115] and *Manohar et al., 2017* [125].

Nephrotoxicity side effect	Definition
Acute kidney injury	Sudden onset of kidney damage or failure resulting in a build-up of waste products in blood serum and difficulty in maintaining correct fluid balance
Hypomagnesemia	Low levels of serum magnesium, possibly related to distal tubular injury
Fanconi-like syndrome	Excess levels of potassium, uric acid, phosphates, bicarbonate, glucose, and select amino acids in urine, related to proximal tubular injury
Distal renal tubular acidosis	A defect in the kidneys that causes acid to build up in blood serum, from tubular injury
Hypocalcaemia	Lower than average levels of serum calcium
Renal salt wasting (cerebral salt wasting)	Extracellular volume depletion due to a renal sodium transport abnormality with or without high urinary sodium concentration, presence of hyponatremia or cerebral disease with normal adrenal and thyroid function
Renal concentrating defect	Decreased ability of the kidneys to concentrate solutes for excretion in urine
Hyperuricemia	Excess serum levels of uric acid
Transient proteinuria	Temporary increase in the level of proteins excreted in the urine (>150 mg day−1)
Erythropoietin deficiency	Low levels of erythropoietin, a hormone produced by the kidneys that promotes red blood cell formation
Thrombotic microangiopathy	Damage of the capillaries in the vital organs, especially the kidneys
Chronic renal failure	The gradual loss of kidney function over time

Hypomagnesemia is related to the inability of the injured proximal tubular cells to reabsorb magnesium, with a prevalence estimated to occur between 40 and 100% [115,125,127]. Moreover, it has been reported that hypomagnesemia was also able to increase cisplatin nephrotoxicity [127]. Consequently, magnesium supplementation is recommended after cisplatin administration [127].

Other manifestations related to the damage of kidney reabsorption have been reported, such as Fanconi-like syndrome (depletion of potassium, uric acid, phosphate and others in plasma, **Table 6**), hypocalcaemia, renal salt wasting, renal concentrating defect, hyperuricemia and transient proteinuria. Other symptoms were related to the functional role of the kidney, such as distal renal tubular acidosis, erythropoietin deficiency, thrombotic microangiopathy and chronic renal failure **(Table 6)** [115,125].

2.3.1.3. Risk factors

As mentioned above, cisplatin nephrotoxicity is dose-, frequency- and duration-dependent. Indeed, higher plasma maximum concentrations (C_{max}) and a higher cumulative dose (i.e. area

under the curve (AUC)) both seemed to be correlated to a higher nephrotoxic injury [125]. Except for these risk factors related to the administration of the drug, other risk factors related to intrinsic factors of the patients have been reported and are summarized in **Table 7**.

Indeed, female gender, history of smoking, poor PS, older age, malnutrition/dehydration, alcohol ingestion, electronic disturbance, chronic disturbance and the co-administration of other nephrotoxic drugs increase the risk of nephrotoxicity [115,125,128]. Moreover, patients with lower albumin are subjected to higher nephrotoxicity from cisplatin as a higher active fraction is available in plasma to exert its non-selective cytotoxic action [125]. Moreover, one of the most challenging risk factors to manage is advanced age with pre-existing chronic renal failure, in which case a single injection of cisplatin can induce a transient episode of AKI [132].

Table 7: Risk factors for cisplatin nephrotoxicity, adapted from *Manohar et al., 2017* [125].

Patients factors	Cisplatin related factors
• Female gender • History of smoking • Poor performance status • Older age • Malnutrition and dehydration • Alcohol ingestion • Electronic disturbance (hypomagnesemia) • Chronic comorbidities (diabetes, liver disfunction, chronic kidney injury) • Concurrent nephrotoxic drugs (iodinated contrast, non-steroidal anti-inflammatory drugs, gemcitabine)	• Dose (> 50mg/m^2) • Frequency and duration of administration • Hydration protocols

2.3.1.4. Prevention

The most challenging part in the prevention of cisplatin nephrotoxicity is to not alter its efficacy [125]. Indeed, different strategies for preventing or reducing cisplatin nephrotoxicity will be summarised hereafter.

The first strategy was to target cell entry, and more precisely to use OCT2 and Ctr1 inhibitors to reduce the entry of cisplatin into the tubular cells. This was not successful as cimetidine (OCT2 inhibitor) was needed in high doses in humans, and copper (Ctr1 inhibitor) seemed to alter the efficacy of cisplatin. The inhibition of the activation of nephrotoxin using g-glutamyl transpeptidase (GGT) and GSH transferase inhibitors, high dose of GSH or thiol agents was not successful except for the use of amifostine. This is because amifostine forms complexes with cisplatin, preventing its binding to GSH and therefore its activation in nephrotoxin. Indeed, it

is the only drug approved by the FDA for reducing cisplatin nephrotoxicity in ovarian cancer and NSCLC [125,128].

The use of anti-inflammatory agents (Anti-TNF-α, anti-TLR4, salicylates, etc.) has also been investigated and showed limited and mitigated results except for IL-10, which seemed to protect against cisplatin-associated injury *in vitro* and in rodents [125,128]. Moreover, the use of antioxidant to prevent oxidative stress (natural antioxidants, selenium, magnesium, vitamin E, vitamin C, spirulina, etc.) or anti-apoptotic agents did not demonstrate any benefit in humans and was even associated with cisplatin resistance in the case of P53 inhibitor. However, the use of enalapril as an inhibitor of poly-ADP ribose polymerase demonstrated a reduction in renal injury in rodents, associated with a down-regulation of ROS pathways [125]. Last but not least, tetrahydrocurcumin was also reported as a promising drug to combat ROS generation in rodents [115].

However, the use of hyperhydration protocols is the accepted standard of care for preventing cisplatin nephrotoxicity without impairing its efficacy. Before the application of this standard of care of hyperhydration and diuresis, 100% of patients were diagnosed with AKI [125,127]. Hyperhydration involves the IV administration of a saline solution (NaCl 0.9%) at a rate of 100-200 mL/hour for between 2 and 12 hours before treatment and between 6 hours and up to three days after cisplatin treatment administration [115]. Although this can be associated with nephroprotective agents (mannitol), the use of other diuretics remains controversial as their benefit has not yet been proven and they have possible irreversible side effects [115]. Hyperhydration is performed not only to avoid cisplatin accumulation in tubular cells but also to provide a high concentration of chloride ions that may reduce the formation of mono- and diaqua-cisplatin. However, it has been demonstrated that saline solution does not alter cisplatin accumulation but triggers the release of a stress response that renders the cell less sensitive to cisplatin [127]. In addition to this, the use of antiemetics to prevent vomiting and fluid loss is often recommended.

2.3.1.5.   Evaluation of nephrotoxicity using biomarkers

The early detection of kidney lesions using early biomarkers is valuable to allow clinicians to adjust the dosage in order to preserve the kidneys and to reduce the risk of side effects related to the excretion impairment of other drugs [132]. A biomarker can be defined as *"a characteristic that is objectively measured and evaluated as an indicator of normal biological*

process, pathogenic processes, or pharmacologic responses to a therapeutic intervention" [133]. An optimal biomarker must meet a number of requirements: it has *(i)* to be low in the absence of injury, *(ii)* to show rapid and intense changes in its concentration (thus increased sensitivity) in accessible fluids when the injury appears, *(iii)* to disappear after its release to indicate the kinetics of recovery, and *(iv)* to be easily applicable between different models (cells and animals to humans) [134,135]. Biomarkers must therefore be quantified following their kinetics. Moreover, plasma biomarkers should have a MW large enough (higher than 60 kDa) to be poorly affected by the glomerular filtration rate, unless glomerular filtration is desired (e.g. cystatin C in AKI evaluation) [134].

Recommendations from a 23-expert panel in 2020 suggested combining damage and functional biomarkers to assess early AKI [136]. Different functional (cystatin C, microalbumin, β2 and α1- microglobulin, etc.) and damage (alanine aminopeptidase, alkaline phosphatase, N-acetyl-b glucosamine, neutrophil-gelatinase associated lipocalin (NGAL), kidney injury molecule-1 (KIM-1), etc.) biomarkers have been intensively investigated and have proven their sensitivity for early AKI assessment in both clinical and preclinical studies [137–139]. They demonstrated their ability to detect minor tubule and glomeruli injuries, even when creatinine levels remain in normal ranges [140]. Among these AKI biomarker candidates, specific proximal tubule markers (i.e. the cisplatin-preferred site of injury) will be described, with cystatin C and creatinine as functional biomarkers and NGAL and KIM-1 as damage biomarkers **(Figure 14)**.

Creatinine is a 113 Da molecule produced by the muscle creatine catabolism, thus reflecting the constant breakdown of skeletal muscles. It is eliminated from plasma at a constant rate following free filtration by the glomerulus, which makes it possible to estimate the glomerular filtration rate using plasma creatinine. Plasma creatinine is by far the most frequently used marker of renal function and injury, and is still a gold standard in clinical practice [141]. However, as active tubular secretion has been reported for creatinine clearance, the determination of the glomerular filtration rate using plasma creatinine is slightly overestimated [141]. Other biases have been reported, such as muscle mass in the body composition, age and gender, leading to the calculation of the glomerular filtration rate including these factors in formulas such as the Cockcroft-Gault [141]. Moreover, unlike early AKI biomarkers, it is not possible to use plasma creatinine to detect minor and early injuries.
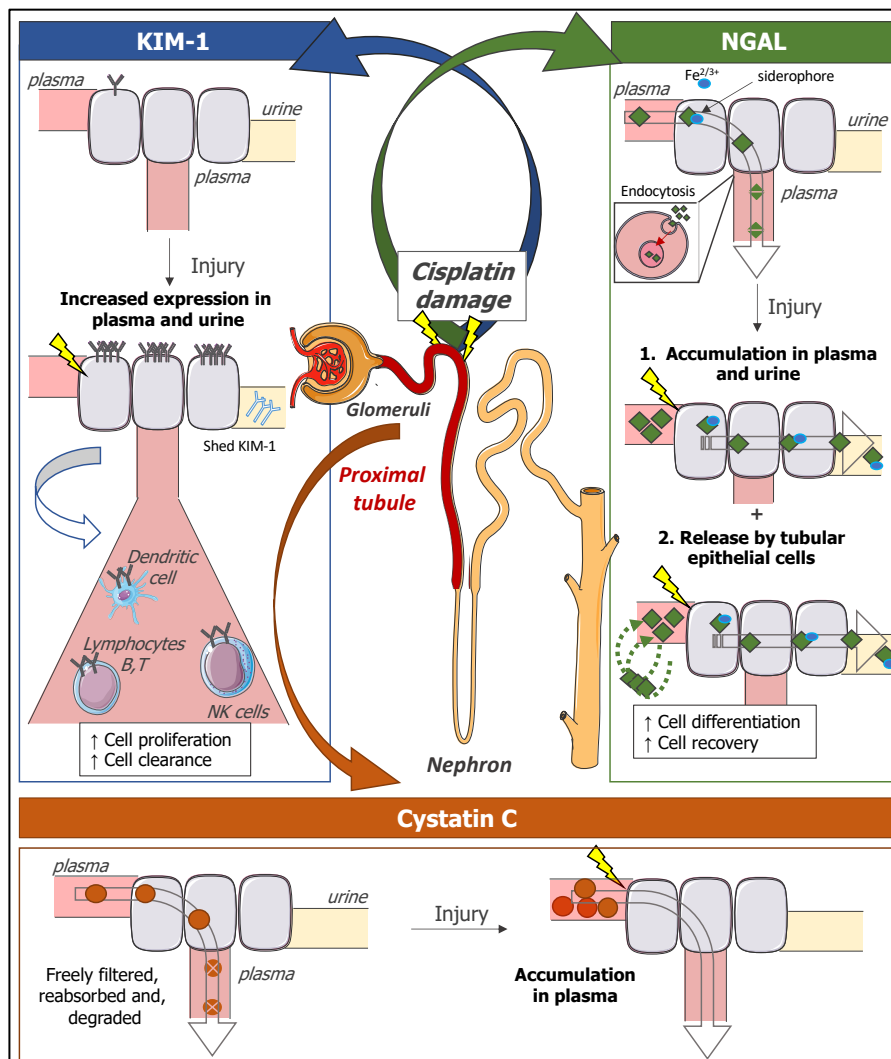
Figure 14: Summary of KIM-1, NGAL, and cystatin C pathways in normal condition and in the case of injury. In the case of injury, KIM-1 is upregulated and shed in plasma and urine, while NGAL is able to scavenge iron, accumulate in plasma and urine and be released by tubular epithelial cells to promote cell differentiation and recovery. Finally, upon injury, cystatin C accumulates in plasma due to the inefficient filtration by the glomerulus. This figure was created from information retrieved from the following references [137,139,142,143].

Cystatin C is a 13-kDa protein that is synthetized constantly in all nucleated cells and is not bound to plasma [137,142,143]. Plasma concentrations seem to be independent of sex, age and muscle mass [137,142]. It is freely filtered by the glomerulus and reabsorbed and degraded in the renal proximal tubule [137,142]. Unlike creatinine, it is not secreted in the urine by the tubule. Thus its increase in plasma reflects a filtration defect whereas its accumulation in urine shows a filtration and a reabsorption impairment by the glomerulus and proximal tubules, respectively **(Figure 14)** [137]. Its sensitivity as a plasma biomarker of the glomerular filtration rate [142,143] over creatinine has been clearly established [73].

NGAL, also known as siderocalin or lipocalin-2, is a novel 25-kDa protein associated with gelatinase in human neutrophil granulocytes (NT-GRA) and is produced by injured epithelial tubular cells [137,139]. Its levels are very low in the steady state and are regulated by renal clearance since it undergoes glomerular filtration because of its low MW [137]. Once filtered, NGAL is reabsorbed, mainly through endocytosis by the proximal tubules, where it is degraded by lysosomes into a 14-kDa protein, if the tubules are intact **(Figure 14)** [137–139]. This makes NGAL a good marker for renal tubular damage [138]. Moreover, its release from tubular cells in response to injury and tubulointerstitial damage may have also a self-defensive action based on the activation of specific iron pathways that are also involved in kidney repair [144]. Indeed, it interacts with the mechanism of iron transfer to the proximal tubule by forming an iron-NGAL complex (siderophore) [135,138]. Moreover, it has been reported to induce the differentiation of kidney progenitors into renal epithelia and to contribute to the recovery of tubular epithelia after injury. All these observations make NGAL a good damage biomarker of AKI [138]. An interest in NGAL as an AKI clinical biomarker was assessed after it was found that it is upregulated in mouse models of ischemia-reperfusion and cisplatin [137]. Indeed, it has been demonstrated that NGAL was up-regulated more than ten-fold within the first hours of renal injury [142]. It is now considered as one of the most promising AKI biomarkers in both urine and plasma [138,139].

KIM-1, also known as T cell immunoglobulin and mucin (TIM-1), is a 38.7-kDa type I cell membrane glycoprotein containing an immunoglobulin-like domain and a mucin domain in its extracellular region that is retrieved in tubular epithelial cells [137,142]. KIM-1 mRNA levels increase more than those of any other gene after kidney injury [137,142]. Indeed, the increase in KIM-1 was found at very high levels on the apical membrane of proximal tubule cells after nephrotoxic injury [144]. KIM-1 is also expressed in immune cells to induce the differentiation of T and B LYM and to activate dendritic cells and NK cells [137]. It has been demonstrated that KIM-1 is involved in generating proximal tubules at it seemed to be responsible for phagocytosis. This shows its ability to facilitate remodelling of injured renal epithelia [137]. It is considered as a promotor of apoptotic and necrotic cell clearance, and is upregulated and shed in urine and extracellular space in the case of AKI [135,137]. It has been approved by the FDA as an AKI biomarker for preclinical drug development [135,137].

As demonstrated in **Figure 14**, these biomarkers can be detected in both urine and plasma. On the one hand, urine has the advantages to be more likely to contain biomarkers originating from

kidneys; thus increasing specificity while being more useful to proteomic screening because of the limited number of protein retrieved. However, urine samples are more susceptible to protein degradation and biomarker concentrations change due to the variability in urine flow rates [145]. On the other hand, plasma biomarkers are easily available even in anuric patients and are correlated with higher stability. However, they may lack of specificity and reflect a systemic response to a disease rather than a specific organ injury. Moreover, the presence of large number of proteins (e.g. albumin and immunoglobulin) may render proteomic approaches challenging [145].

2.3.2. Myelotoxicity

Myelotoxicity is a haematological side effect common to most cytotoxic drugs, including platinum drugs and paclitaxel, that directly impair haematopoiesis in the bone marrow **(Figure 12)** [146,147].

Neutropenia (reduced levels of NT-GRA) is one of the most common side effects observed in clinical trials, with the NT-GRA nadir (the lowest value that NT-GRA will reach during a cycle of chemotherapy) occurring 10-14 days following the treatment initiation and with a complete recovery by day 21-28 [146].

On the other hand, anaemia can either be related to a direct effect of cytotoxic drugs on red blood cells (RBC), as explained above, or can be secondary to renal impairment and its inability to produce erythropoietin, in the case of platinum drugs [76]. Indeed, carboplatin has been associated with the destruction of RBC through three main mechanisms, leading to acquired haemolytic anaemias [148–150]. Following this phenomenon, an increase in the reticulocyte count describes regenerative anaemia [149–151]. Finally, thrombocytopenia potentially requires subsequent dosage adaptation or therapy delays, with an increasing risk of life-threatening spontaneous haemorrhage. The prevention and the management of this side effect remain unsolved, even with platelet transfusions. Moreover, thrombopoietin receptor agonists are still under investigation [146].

These side effects alter the patient general condition so that he feels dizzy, tired, lethargic and is more susceptible to infections in the case of neutropenia and leukopenia [115]. Treatments involve the use of blood transfusions, administration of antibiotics and even the use of granulocyte-stimulating factors [115]. These manifestations have also been encountered more in patients with several risk factors such as kidney function, age and race [115].

Cisplatin, and especially carboplatin and paclitaxel, are known to induce myelotoxicity. Myelosuppression remains the carboplatin DLT and neutropenia remains the paclitaxel DLT [115,119]. Indeed, it has been reported that carboplatin induces a greater risk of bone marrow suppression than cisplatin, with reduced non-hematologic toxicity [152]. Moreover, myelotoxicity in the case of platinum drugs seem to be dose-dependent and occurs in more than 20% of patients, depending on the other combination cytotoxic drug [115]. Neutropenia, in the case of paclitaxel, is reported to be dose- and frequency-dependent, and occurs in up to 52% of patients treated with this drug (135-300 mg/m^2, over 24h) [119]. Indeed longer paclitaxel infusion (24h) has been correlated with a higher risk of myelotoxicity than shorter courses (3h) [76]. Paclitaxel can also induce thrombocytopenia and anaemia but at a less severe level than neutropenia. Indeed only 10% and 78% of patients were reported with thrombocytopenia and anaemia, respectively, in a phase III study [76].

It is still a matter of concern to combine two highly myelotoxic drugs as the co-administration of carboplatin and paclitaxel has induced grade IV neutropenia in more than 50% of patients in several phase II or III studies [119,153,154]. To minimize cumulative side effects, doses and regimen were optimized to find the best balance between efficacy and tolerance. Indeed, the infusion time for paclitaxel administration was reduced and the carboplatin dose was calculated using the Calvert formula as myelosuppression seems to be more precisely forecast using the patient's renal function, age and AUC than body surface area [155]. Consequently, carboplatin (AUC 6 mg/mL x min) and paclitaxel (200 mg/m^2) are recommended to be administered over a 5-hour infusion following spaced-out cycles (the first day of each cycle of 21 days for four cycles) [24]. Moreover, the use of growth factors and a reduction in the regimen adaptions have reduced the occurrence of grade III-IV neutropenia [76].

2.3.3. Pulmonary toxicity

Platinum-based drugs and paclitaxel administered using the IV route have an overall well-tolerated pulmonary toxicity profile. Indeed, except for some hypersensitivity reactions and in some rare cases bronchospasm, cisplatin and carboplatin are relatively well-tolerated by the lungs [77,156,157]. Moreover, in one case report, cisplatin was associated with eosinophilic pneumonia, but this seemed very rare as it was reported for only one patient [158,159].

On the other hand, paclitaxel has also been associated with pulmonary hypersensitive reactions *(discussed in section 1.7)*, and interstitial pneumonitis in 1% of patients [77]. Pulmonary hypersensitive reaction often describes non-specific symptoms such as dry cough, dyspnoea

and hypoxemia and is associated with interstitial inflammation, with hypersensitive pathogenesis (eosinophils (EOS) in bronchoalveolar lavage fluid (BALF) and blood) [77].

3. <u>Inhaled therapy as a loco-regional treatment against lung cancers</u>

In proposing inhaled therapy as a new modality against lung cancer, it is important to consider the anatomy and physiology of the lungs as well the pulmonary delivery of drugs.

3.1. The lungs

3.1.1. Structure and function

The lungs have two essential functions: the first is ventilation-perfusion and aims to deliver oxygen to the body and remove carbon dioxide from it (**Figure 15,** [160]). The second is host defence against foreign particles. The lungs are also responsible for homeostasis and therefore have secondary functions such as surfactant synthesis, and neuroendocrine signalling (synthesis and secretion of molecules such as serotonin or calcitonin) [161].
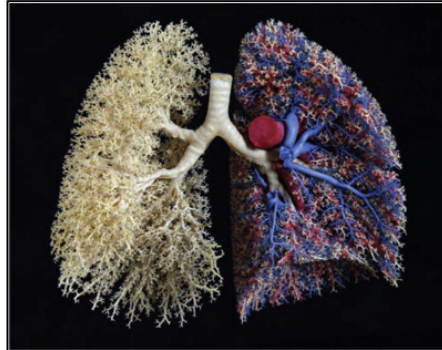
Figure 15: Cast of bronchial tree with airways (yellow), pulmonary arteries (red) and veins (blue), from *Hsia et al., 2016* [160].

The pulmonary tract is divided into two main regions: the upper (nasopharynx, oropharynx, laryngopharynx and the larynx) and the lower respiratory system (trachea, bronchus and the lungs). The left lung is divided into two lobes and the right lung into three lobes [161]. The anatomy of the airways is strongly related to their function. Indeed, they consist of a sequence of branching tubes that become narrower, shorter and more numerous as it goes deeper in the lung down to the terminal bronchi. This area is described as the conducting zone, and aims to channel the inspired gas to the gas exchanging regions of the lungs [161]. The trachea and

bronchi are cartilaginous and do not change shape significantly with ventilation as they do not participate in gas exchange. However, the bronchioles, which have a maximum diameter of 1 mm, have no cartilage and are numerous and short [161]. Each terminal bronchiole divides into a respiratory bronchiole, which transition to the alveolar ducts. Each duct is lined with alveoli, which represent the respiratory region [161].

A dichotomous model of the human airways **(Figure 16)** was established by Weibel in 1965 that extrapolates the length, diameter and number of airways and their branching angles. This dichotomous model is mainly divided into two zones: the conducting zone from generations 0 (lower region of the trachea) to 16, and the translational and respiratory zone from generations 17 to 23. In the first area, the trachea is divided into two primary bronchi. Each bronchus is then divided into two secondary bronchi, and each secondary bronchus is again divided into two segmental bronchi. These become, after few generations, bronchioles and afterwards terminal bronchioles. From generation 17, three generations of alveolar ducts and one generation of alveolar sacs are retrieved, which constitutes the respiratory zone **(Figure 16)** [161]. The alveolar surface area in the adult human is estimated to be 100-150 m^2 [161].
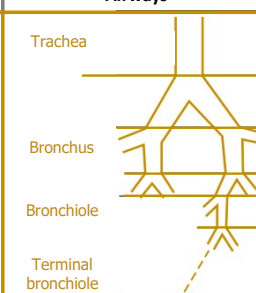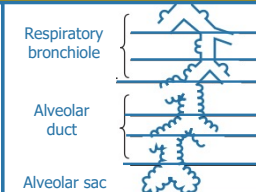
Figure 16: Subdivision of the conducting and the respiratory zones according to Weibel model, adapted from *Broaddus et al., 2016* [161].

3.1.2. Cell types

3.1.2.1. Conducting zone

The cellular composition of the airways is complex. The bronchial mucosa consists of columnar pseudostratified epithelium. Nearly half of the epithelial cells are ciliated at all airway generations down to the bronchioles. Cilia move rhythmically and propel liquid, mucus, cells

and debris towards the pharynx from the deep lung [161]. The tight junctions between airway epithelial cells play two major roles: the first is the limitation of absorption by passive diffusion and the second is polarization of cellular functions between the apical and basolateral membrane [161].

Mucus is secreted by submucosal glands and by goblet cells. The glands are retrieved in the submucosa of the bronchi, and are able to secrete water, electrolytes and mucins into the lumen. Moreover, goblet cells are retrieved at most levels, and diminish peripherally until disappearing at terminal bronchioles (also able to secrete mucin). The mucus is a complex mixture of proteins (glycoprotein and proteoglycan), water (95%) and electrolytes. It plays an important role in innate immunity, by preventing the intrusion of foreign particles into lung tissue, and in preventing airway dehydration [161]. However, its hypersecretion is associated with chronic inflammatory airway diseases such as asthma, chronic obstructive pulmonary disease (COPD), and cystic fibrosis [161].

Clara cells are non-ciliated cuboidal cells retrieved among the ciliated epithelial cells in the terminal airways. Now known as "club cells", they are characterized by large apical granules and play major roles in the lungs. They serve as progenitor cells for themselves and for ciliated epithelial cells and are a source of surfactant proteins (SPs), such as SP-A, SP-B and SP-D, lipids and proteins. Finally, they have a function in liquid balance by influencing ion channels [161].

3.1.2.2. Respiratory zone

To ensure the gas exchange between the air and the blood compartments, the alveolar-capillary barrier is formed by cytoplasmic extension of alveolar type I cells and capillary endothelial cells, separated by a common fused basement membrane [161]. The most common cell types are the alveolar macrophages (AM) (80%, in steady state), which are retrieved in the internal surface of the alveoli and play an important role in innate immunity [161].

The type I cells comprise approximately 10% of the cells in this zone and cover more than 95% of the internal alveolar surface area. These type I pneumocytes are attached to one another at their lateral membrane by different complexes such as tight, adherent and gap junctions [161]. These are large squamous cells with thin cytoplasm and are able to produce pro-inflammatory cytokines (TNF-α, IL-6, IL-1β), following an initiation with lipopolysaccharide (LPS). They

seem to be more susceptible to acute lung injury than type II cells and have important roles in resolving inflammation.

The type II cells comprise approximately 18% of the cells and cover 5% of the internal alveolar surface area. They are identified by the presence of lamellar bodies, the intracellular form of pulmonary surfactant. They are the only source of surfactant and of the SP-C. As Clara cells, they also express SP-A, SP-B and SP-D. They therefore play an important role in innate immunity. Their turnover in steady state is extremely low but in the case of lung injury is accelerated to restore the epithelium. Moreover, they are involved in the transport of sodium and chloride to balance the alveolar fluid volume [161].

The surfactant is composed of 85% phospholipids, and more precisely 76% phosphatidylcholine (47% dipalmitoyl-phosphatidylcholine (DPPC) and 29% unsaturated phosphatidylcholine), 12% phosphatidylglycerol, 4% phosphatidylinositol and 3% phosphatidylethanolamine. It is also composed of neutral lipids (5% cholesterol, free fatty acids) and 10% proteins (mostly SP-A, but also SP-B, SP-C and SP-D). It plays an important role in lowering the surface tension (mainly due to DPPC) by decreasing the effort of breathing, preventing alveolar collapse and atelectasis, and allows alveoli of different sizes to be stable.

3.1.3. Innate immunity cell types

As mentioned previously, the lung epithelium is one of the largest epithelial surfaces in the body. Indeed, with an average respiratory rate of 10-12 breaths/min and an average tidal volume of 600 mL, the lungs are exposed to more than 10 000 L of air per day. Their defences against pathogens and foreign particles are therefore crucial to protect not only them but also the entire organism. In addition to the epithelial type I and II cells, different cell types are involved in innate immunity and are discussed hereunder.

3.1.3.1. Polymorphonuclear cells

NT-GRA are the cells that first migrate to the site of lung injury and defend it using phagocytosis, degranulation and generation of ROS, or by releasing webs of chromatin via neutrophil extracellular traps (NETs) to trap and kill microorganisms. They account for 70% of circulating human blood leukocytes with a survival time of up to 7-10h [162]. However, in the case of inflammation they can survive more than 48h. These cells are able to switch from a pro-inflammatory to an anti-inflammatory phenotype by stopping the release of pro-inflammatory mediators (e.g. leukotriene B4, platelet-activating factor) and starting the release of pro-

resolving mediators (e.g. pro-resolving bioactive lipids, lipoxins). This switch occurs when the secretion of pro-inflammatory chemokines and cytokines (TNF-α, IL-6, IL-1β) is inhibited and the secretion of more anti-inflammatory pro-resolving mediators is increased (lipoxins, resolvins, protectins and maresins). Once they have fulfilled their function, they undergo apoptosis [162].

EOS represent less than 5% of circulating blood, can survive up to one week if necessary and are mostly involved in allergic airway inflammation [162]. When they arrive at the site of injury, they undergo degranulation, which is essential to the removal of the inflammatory stimuli, and are able to contribute to host defence by releasing extracellular traps. Therefore, they release different components such as eosinophilic cationic protein, major basic protein, eosinophil peroxidase and eosinophil-derived neurotoxin, which are cytotoxic to airway epithelial cells. Moreover, they can undergo transformation into both anti-inflammatory and pro-inflammatory phenotypes, as well as phagocytosis once their function is achieved [162].

Last but not least, basophils are the rarest circulating human granulocytes. These are able to migrate to the site of injury and release their contents (e.g. histamine, heparin, serotonin and others) in the case of inflammation to exaggerate inflammation [162].

3.1.3.2. Monocytes and macrophages

Monocytes (MON) are retrieved in bone marrow and blood in steady state. They rapidly migrate to the site of injury upon inflammation and differentiate into large tissue-resident phagocytic macrophages [162]. Their phenotype depends on their environment as they can have either a pro-inflammatory phenotype (M1) or anti-inflammatory phenotype (M2). The M1 phenotype is induced by LPS, IFN-γ and TNF-α, and able to secrete pro-inflammatory cytokines (TNF-α, IL-6, IL-1β, IFN-γ) to emphasize inflammation and to secrete nitric oxide to help in killing microorganisms [162,163]. On the other hand, the M2 phenotype is induced by various parasites, immune complexes, apoptotic cells and soluble mediators such as macrophage-colony stimulating factor (M-CSF) to stop the release of pro-inflammatory stimuli and release pro-repair mediators instead [162].

3.1.3.3. Others

Dendritic cells are an important group of phagocytic and antigen-representing cells. They act as a bridge between innate and adaptive immune systems as once they encounter a microbe,

they leave the epithelium and traffic into regional lymph nodes to interact with naïve T cells [161].

Mast cells are retrieved in mucosal/connective tissues and are involved in healing and repair as they are able to secrete inflammatory mediators such as histamine, proteases, chemotactic factors and arachidonic acid. They are mostly involved in allergy-related inflammation, as with eicosanoids and EOS [162].

NK cells are cytotoxic LYM that represent 10-15% of interstitial LYM and are able to recognize and kill tumour cells and virus-infected cells. They are an important source of cytokines released early in the immune response [161,162].

3.2. Drug delivery to the lungs

To efficiently deliver drugs to the lungs, several parameters related to the delivery devices as well as to the formulations should be considered and are detailed in this section.

3.2.1. Pulmonary delivery devices

There are four types of inhalers: nebulizers, soft mist inhalers, pressurised metered-dose inhalers (pMDIs) and dry powder inhalers (DPIs). The advantages and drawbacks of each inhaler type are summarized in **Table 8**.

Table 8: Advantages and drawbacks of each inhaler type, adapted from *Lavorini et al., 2019* [164].

Device	Advantages	Drawbacks	Additional drawbacks related to the administration of cytotoxic drugs
- Nebulizers	- No specific inhalation required - Vibrating mesh is portable and do not require to be connected to an outside energy source (battery-operated devices) - High lung deposition (vibrating mesh : up to 50%)	- Jet and ultrasonic nebulisers require outside energy source - Treatments time are often long (5mL/15 min) - Performance varies between nebulisers - Risk of bacterial contamination	- Not adapted for lyophilic drugs, (i.e. limited solubility in water) - Not adapted for drugs that need to be delivered in high quantity (e.g. cytotoxic drugs) - Low deposited fraction in the lungs (10-15%) - Environmental contamination
- Soft mist inhaler	- Compact and portable - High lung deposition - Multidose devices - No propellants	- Not breath actuated - Requires some coordination of actuation and inhalation	- Limited solubility for some cytotoxic (i.e. lipophilic) drugs - Environmental contamination
- Pressurized Metered-Dose Inhalers (pMDI)	- Compact and portable - Dose consistency - Multidose devices	- Propellant required - Requires good coordination of actuation and inhalation - High oropharyngeal deposition	- Deposited mass in μg range unsuitable for the delivery of cytotoxic drugs in the lungs
- Dry-Powder inhalers (DPI)	- Unexpensive - Compact and portable - Unidose and multidose - No propellants - Breath actuated (no coordination needed)	- Sensitive to humidity - Requires a more challenging development of drug formulation than nebulizers or pMDI. - Require an inspiratory airflow high enough to overcome interparticulate forces	-

3.2.1.1. Nebulisers

Nebulisers are devices able to convert a liquid as a solution or dispersion into small inhaled droplets. The solutions or dispersions are composed of a drug dissolved or dispersed in a liquid carrier. These nebulizers are mainly divided into three types: jet nebulisers, ultrasonic nebulisers and, most recently vibrating mesh nebuliser and are illustrated in **Figure 17** [164].

Jet nebulisers, also known as pneumatic nebulizers, are the most common type of nebulisers **(Figure 17.A** [165]**)**. These devices use compressed gas, usually air or oxygen, that draws a liquid from a side feed tube into the nozzle as a consequence of aspiration resulting from the expansion of the jet at the nozzle orifice [164,165]. Consequently, the aerosol is generated as it arises from the feed tubes (also called the venturi effect). Particles with a higher particle size are entrapped by the baffles and are returned into the reservoir while smaller particles are either inhaled or may land on internal walls, returning to the reservoir until re-nebulisation [164,165].
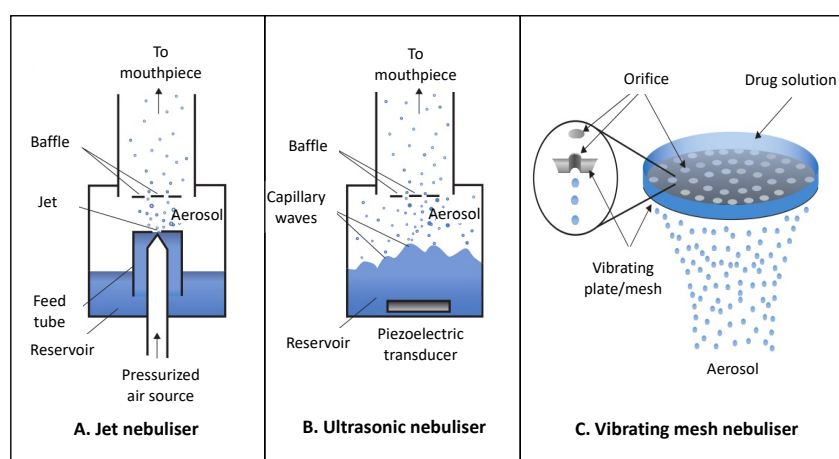
Figure 17: Schematic illustration of jet nebuliser (A), ultrasonic nebuliser (B) and vibrating mesh nebuliser (C), from *Yeo et al., 2010* [165].

Ultrasonic nebulisers induce an aerosol by applying an alternating electric field to a piezoelectric transducer, which leads to the generation of a mechanical vibration in contact with the reservoir **(Figure 17.B)** [165]. Consequently, sound waves are generated and propagate to the entire reservoir, leading to the generation of an aerosol from the droplets that break free from the top of the waves [164,165]. These nebulisers are able to generate solutions more quickly than jet nebulisers but are not suitable for dispersions and heat-sensitive drugs [164,165].

The third nebulizer type is vibrating mesh nebulisers, which were developed to overcome some limitations encountered with conventional nebulisers, related to the long treatment time and inefficient use of drug **(Figure 17.C)** [165]. These nebulisers use the same piezoelectric element and are equipped with a vibrating mesh/plate that allows the passage of droplets with the desired size. Their main advantage is that they are able to deliver a narrower particle size distribution (PSD) than conventional devices **(Table 8)** [164,165].

Although nebulizers have the advantage of not requiring an inhalation technique, treatment administration using these nebulisers is often long, with a high risk of bacterial contamination **(Table 8)**. Moreover, conventional nebulizers (jet, ultrasonic and vibrating mesh) require an outside energy source to generate the aerosol, and precision cleaning and maintenance following administration. Finally, in the case of highly toxic drugs, the risk of environmental contamination and exposure of medical staff is high [164,166].

3.2.1.2. Pressurised metered-dose inhalers

Unlike conventional nebulisers, pMDIs are portable multidose devices that consist of an aluminium canister, lodged in a plastic support, containing a pressurised liquid propellant solubilizing or dispersing the drug particles. The key component of these devices is the metering valve, which is able to deliver a precise volume of propellant containing the micronized drug at each actuation **(Figure 18)** [166]. Actuating the canister causes decompression of the formulation expelled from the metering valve, leading to the generation of an aerosol. This aerosol is composed of droplets containing the drug particles in a shell of propellant. The propellant evaporates rapidly with time and distance, leading to a reduced size of droplets [164,166]. Since their development, these devices have evolved by replacing chlorofluorocarbon (CFC) with hydrofluorocarbon (HFC), which is described as being more environmental-friendly [164,166].
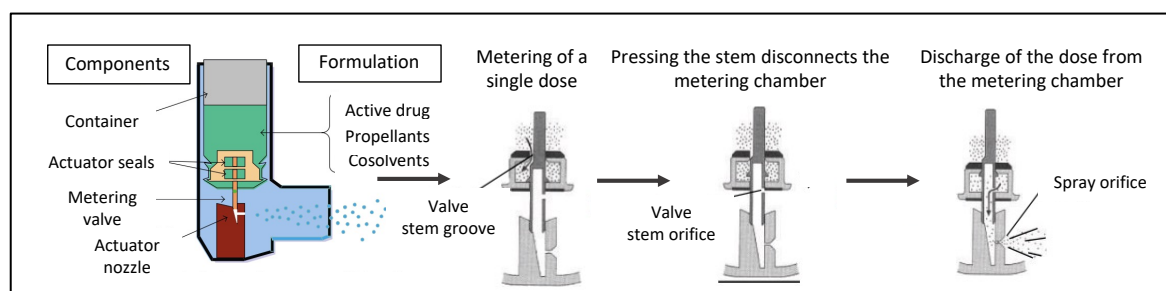
Figure 18: Schematic illustration of the pMDI components and the steps to deliver the aerosol, adapted from *Lavorini et al., 2013* [166].

pMDIs have numerous advantages as they are compact, portable and inexpensive while containing at least 200 metered doses ready to be used **(Table 8)**. However, they contain propellants and are not actuated by breathing. Therefore, they necessitate a coordination between the device actuation and inhalation, which is not easy for most patients, who are not able to use them correctly [164,166]. Indeed, patients must actuate the device while breathing deeply and slowly and continuing to inhale, even when they feel the impact of the aerosol to their throat, which is called the hand-lung coordination. Finally, they should hold their breath (for particle sedimentation) before exhalation [164,166]. Moreover, these devices can deliver masses in the micrograms and are correlated with high oropharyngeal deposition, which is not suitable for the delivery of highly toxic drugs.

The soft mist inhalers have been developed to overcome the limitations encountered with both the previous devices. Indeed, unlike conventional nebulizers, they are portable and multidose devices, and unlike pMDIs, they have limited oropharyngeal deposition and do not necessitate hand-lung coordination. The only such device on the market is Respimat® [164].

3.2.1.3.   Dry powder inhalers

DPIs were first introduced in 1970 as single-dose devices (such as the RS.01 device, **Figure 19**), [167], containing the powder formulation in a capsule that is loaded into the device by the patient in advance. Multidose DPIs have been available since the late 1980s (Diskhaler, Diskus, Turbohaler) [161,164,166].
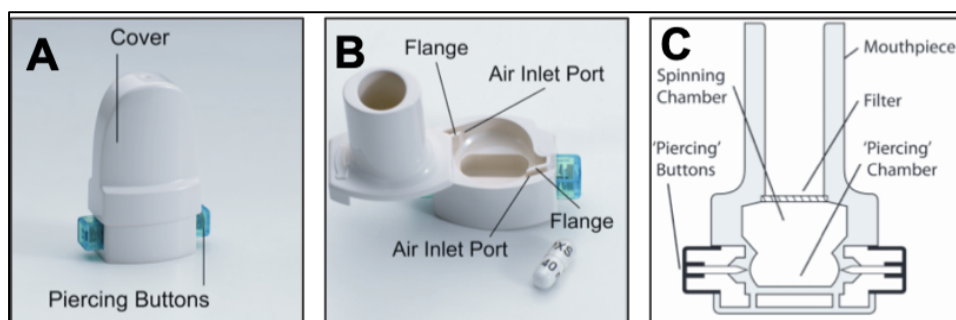
Figure 19: Images of the DPI RS.01 closed (A), and opened (B). Representative illustration of the RS.01 (C) device, adapted from *Elkins et al., 2014* [167].

DPIs contain a powder-based formulation that has been previously micronized to the appropriate particle size range to deposit efficiently in the lungs. They allow the powder to be deagglomerated by the patient's own inspiratory flow and consequently do not require coordination of inhaler actuation with inhalation, which is one of the main drawbacks of pMDIs

(Table 8) [164,166]. Moreover, these devices are designed with an internal resistance that should be overcome to generate a turbulent flow that is able to deagglomerate particles and generate an aerosol [164,166]. They have the advantages of being inexpensive, portable, compact, not using propellants and having increased stability as they are formulated in their dry form **(Table 8)** [164,166]. Moreover, as represented in **Figure 20.A**, DPIs provide a better deposition in the lungs than pMDIs [161]. Indeed, with pMDIs, most of the inhaled dose is deposited in the oropharyngeal area, swallowed and retrieved in the stomach **(Figure 20.B)**. However, DPIs require a minimum inspiratory flow and are sensitive to relative humidity (RH) [164,166].
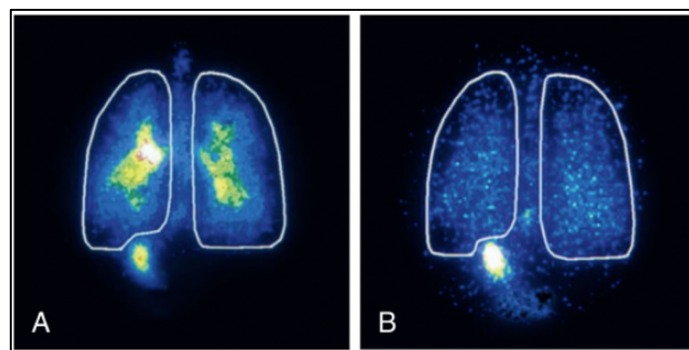
Figure 20: Deposition images following inhalation of radiolabelled aerosols following the use of a DPI (A) and a pMDI (B), from *Broaddus et al., 2016* [161].

3.2.2. Development of DPI formulations

Considering that this work aimed to optimize a DPI formulation, this part will focus on development of such a formulation instead of formulations for the other types of device. It will especially discuss the factors influencing the performance of DPI devices as well as the fate of the particles once deposited in the lungs.

3.2.2.1. Aerodynamic performance and lung deposition

As mentioned above, the lungs have the role of ensuring ventilation-perfusion and protecting the organism against foreign particles, including pathogens. Indeed, except for mucociliary clearance and phagocytosis (discussed in *section 3.2.2.4*), the lungs have a serial branching of the airways that hinder the ability of the particles to deposit in the deeper sections [161]. However, the lungs are not able to discriminate pathogens from therapeutic drugs. Therefore, it is important to adapt the drug formulation to optimally deposit the drug in the desired areas.

The principle of inhalation therapy depends on the ability to generate a population of liquid/solid particles, carried along with the patient inspiratory airflow, that deposit in the different lung sections depending on the aerodynamic diameter (d_{ae}) [168]. The d_{ae} is defined by the following equation:

$$d_{ae} = d_{geo} \sqrt{\frac{\rho_{particle}}{\rho_O \cdot \chi}}$$

Equation 1: Aerodynamic diameter formula [169].

Where d_{geo} is the geometric diameter, $\rho_{particle}$ the density of the particle, ρ_O the particle unit density (1 g/cm^3 sphere) and χ, the dynamic shape factor (measuring the deviation from sphericity).

As this equation demonstrates, d_{ae} considers the particle size, density and shape and therefore characterizes the particle's aerodynamic behaviour in an airflow [168]. In general, the probability of the particle to deposit in a specific lung region is an interaction between the physical characteristics of the particle, the airflow and the airway anatomy [161]. Practically, the greater the mass, the faster the velocity and higher the airflow, and the more a particle is likely to deposit by inertial impaction [161]. Indeed, the air turbulence initiated by the mouth passages and the cartilaginous segmentation of the trachea ensure that the particles with a larger d_{ae} than 5 μm deposit preferentially on the mucus surfaces of the upper respiratory tract [161]. Particles between 1-5 μm are mainly deposited in the lower respiratory tract, which comprises the bronchial tree and alveoli [168]. To specifically target the alveoli, particles must have a d_{ae} ranging between 1 and 3 μm [168]. These particles mainly deposit by gravitational sedimentation, which is described as the process by which a particle accelerates, under gravity, until reaching a terminal velocity. Therefore, sedimentation is closely related to the patient's breathing technique. Indeed, holding the breath before exhalation is encouraged to give to the particles enough time to sediment. Otherwise, these particles are exhaled rather than deposited. Finally, particles with d_{ae} lower than 0.5 μm are subject to Brownian motion, and are mostly exhaled. Indeed they are too small to deposit efficiently by sedimentation and too large to deposit efficiently by Brownian diffusion [161,168].

The evaluation of the fluidisation efficacy of the formulation is performed by determining the delivered dose, defined as the quantity of drug particles able to be delivered from the device. Considering the d_{ae} characteristics, the evaluation of the aerodynamic behaviour of a formulation is performed by characterizing the mass of drug particles with a $d_{ae} < 5$ μm in terms

of fine particle dose (FPD) or fine particle fraction (FPF) from the nominal dose (FPF_n), which corresponds to the dose fraction able to deposit in the deepest part of the lungs following the patient inspiratory airflow [168]. The FPF can also be expressed as a fraction of the delivered dose (FPF_d) [168]. FPF (whatever its expression) and FPD describe the ability of the formulation to be fluidised and deagglomerate before its deposition in the desired areas [168]. To characterize the aerodynamic behaviour of a formulation, different parameters are evaluated such as *(i)* the delivered dose, *(ii)* the delivered dose uniformity (DDU), *(iii)* the FPD, *(iv)* the FPF, *(v)* the mass median aerodynamic diameter (MMAD), which corresponds to the diameter that divides the aerodynamic PSD (APSD) into two equal halves, and *(vi)* the geometric standard deviation (GSD), which indicates the variability around the particle diameter [161,168]. It is commonly accepted that a GSD higher than 1.2 describes a polydisperse PSD, while a GSD lower than 1.2 characterizes a monodisperse PSD [164,168]. The determination of the FPD, FPF, MMAD and GSD is performed using impactors such as a fast-screening impactor (FSI) or next-generation impactor (NGI), as described in the European Pharmacopeia 10.

3.2.2.2.   Interparticulate forces

Interparticulate forces are dictated mostly by Van der Waals forces, but also by capillary forces, electrostatic charges and mechanical interlocking. The intensity of these forces depends on the particle size, shape and surface properties, the hardness of the adhering particle, surface roughness, the intensity of the press-on forces during mixing and the RH. These parameters are therefore able to influence the aerodynamic performance [168].

Van der Waals forces are the most common in dry-powder formulations, especially for particles with a size below 10 μm and an inter-particle distance under 100 nm [168]. They are weak forces that attract neutral molecules to one another. When the neutral particles reach within a threshold distance, electrons from one particle are pulled towards the nucleus of the other particle. This cause a transient polarization with two domains: electron-rich domain and electron-deficient domain. The domain of each particle attracts the oppositely charged side of the other particle [170]. They depend on the structure of the excipients in the formulation and decrease in the case of surface roughness, as the inter-particulate distance is increased [168].

Capillary forces arise from the formation of a liquid bridge between two particles onto the particle surfaces. When this bridge is formed, a narrow slit is created around the surface of

contact. If the gap is sufficiently close and if the two surfaces are lyophilic, some water vapour will condense and form a meniscus. These forces are increased by the shape, size, roughness and chemical properties of the surface but mostly by the powder residual water content and the environmental RH [168,169].

Electrostatic charges arise following contact between a donor and a receptor, and therefore a charge transfer, resulting into oppositely charged surfaces [168]. This short contact is called "triboelectrification" and can be secondary to the manufacturing process (mixing, handling, filling), leading to an increased adhesive-cohesive forces and therefore to a limited aerosol performance [168]. Triboelectrification can also arise at the moment of the fluidisation of the dry powder through the inhaler, and can be used to enhance lung deposition [168].

Finally, mechanical interlocking is a result of the interaction of surface features and is related to the diameter of pores between particles and interfacial tension due to the hydrogen bonding of water, preventing particle dispersion [169].

3.2.2.3. Dispersion force and the generation of the aerosol

As mentioned above, the efficacy of DPI formulations is related to their ability to deposit in the deeper lung areas. The generation of the aerosol is dependent on the ability of a powder to overcome the inter-particulate forces and to be conducted by the patient's inspiratory flow to achieve deep deposition in the lungs [168].

To do so, four main parameters are able to influence lung deposition. The first is related to the properties of the drug formulation, as the stress generated by the inspiratory flow must be great enough to deagglomerate the particles [168]. The second and third parameters are related to the performance of the inhaler device. Indeed, the patient inspiratory flow intensity and the device resistance must be considered together. In general, high-resistance devices are able to generate high air turbulence leading to higher aerosol generation and therefore to higher FPF. However, these devices necessitate high inspiratory effort from the patient, which is often difficult to achieve for patients with respiratory problems. Therefore, a balance between resistance and turbulence is required, and the use of a low-resistance device is often preferred for patients with limited respiratory function [168]. The fourth parameter is a relationship between the correct inhalation technique for deposition in the lungs, with an appropriate breathing hold before exhalation and a high enough inspiratory flow rate of the patient, as mentioned above [168].

3.2.2.4. Fate of deposited particles

Once deposited in the lungs, drug particles are directly in contact with either the thick mucus layer (10-30 μm in the trachea or 2-5 μm in the bronchia), if deposited in the conducting zone, or with the lung surfactant (0.1-0.2 μm) if deposited in the respiratory zone, depending on their d_{ae}, as represented in **Figure 21** [171].

In either case, the dissolution of these particles in the lung fluid (mucus or surfactant) is determined by the Noyes-Whitney equation [171]:

$$\frac{dM}{dt} = \frac{A.D.(C_s - C_i)}{h}$$

Equation 2: Noyes-Whitney equation

where dM/dt is the dissolution rate, A is the surface area of the drug in contact with the fluid, D is the diffusion coefficient of the drug, h is the diffusion layer thickness, and C_s and C_i are the drug saturation solubility at the drug surface and the dissolved drug concentration in the fluid, respectively at a determined time t.

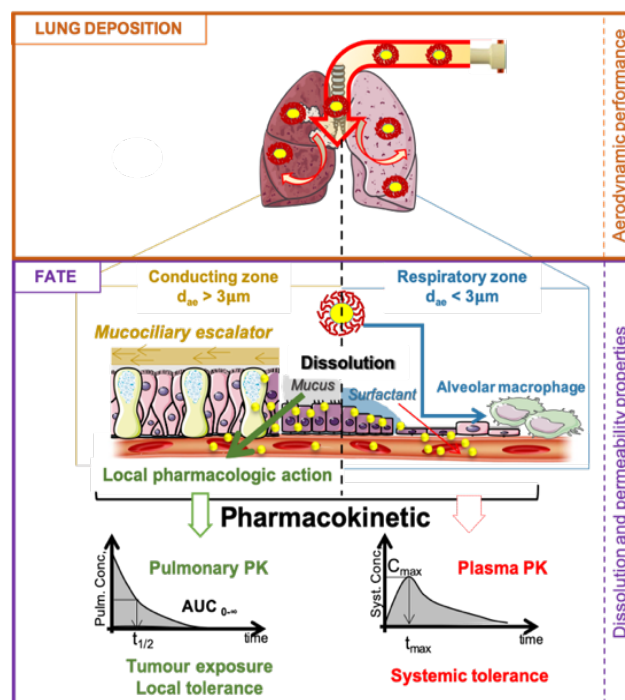Figure 21: Schematic illustration of the fate of particles once deposited in the conducting ($d_{ae} > 3\mu$m) or respiratory ($d_{ae} < 3\mu$m) zone of the lower respiratory airways, adapted from *Wauthoz et al., 2015* [171].

It should be mentioned that despite the small volume of the lung surfactant, the drug is usually dispersed over a large surface area in the respiratory zone, unlike in the conducting zone (100-

120 m^2 *vs.* 2-3 m^2) [171]. Moreover, the surfactant has tensioactive properties that can increase the drug dissolution of the particles deposited in the respiratory zone [171].

Once dissolved, the drug can exert its pharmacological action locally, in the case of local therapies, or can be absorbed into the blood through the lung epithelium at a rate and extent that is strongly dependent on its absorption mechanism and affinity with lung environment. This occurs either by passive diffusion or by saturable active transport [171]. Small molecules (100-1000 Da) with a log P < 0 are lipid-insoluble and are generally assumed to be absorbed paracellularly via aqueous pores in the intracellular tight junctions. In contrast, molecules with a log P > 0 are more lipid soluble and are more likely to be absorbed transcellularly [171].

Moreover, the dissolved drug can also be metabolized locally, but to a lesser extent than orally administered drugs [171]. Consequently these absorptive mechanisms are responsible for the PK patterns from the lungs to the blood, and are directly related to their toxicity profile [171] **(Figure 21)**.

Undissolved drugs can either be submitted to mucociliary clearance or phagocytosis depending on their deposition area, as represented in **Figure 21** [171].

Mucociliary clearance

The particles that are deposited in the ciliated airways (conducting zone) are trapped into the mucus. This mucus is transported proximally by the rhythmic beating of cilia to the pharynx, where it is swallowed or expectorated, which is called "mucociliary clearance" [161,171].

As mentioned above, the ciliated cells are most numerous in the trachea and the bronchi, and decrease in the deeper lungs. Consequently, the mucociliary escalator is less rapid in the peripheral lung. Nevertheless, this effective organisation leads to a complete mucociliary clearance within 24h after deposition [161,172].

Mucociliary clearance can be impaired either by intrinsic defects in ciliary function that can be congenital or induced by external factors such as influenza or tobacco smoking. In addition, impairment can be due to the quantity and composition of airway secretions (chronic bronchitis, cystic fibrosis). In this case, secretions are cleared most often by coughing. If both mechanisms (mucociliary clearance and coughing) are altered, the secretions are retained and obstruct the airways lumen [161].

Phagocytosis

The particles that arrive in the respiratory zone can be phagocytosed by AM, after which they migrate to lymph nodes, a mechanism that is called "the macrophage phagocytosis system".

Indeed, there are almost 10 macrophages per alveolus, which are ready to attack any foreign particles using phagocytic receptors or through specific and non-specific opsonisation [161]. Maximum phagocytosis has been observed for undissolved particles that have a d_{ae} ranging between 1-2 μm, with a maximum intake 1h after incubation [161,172].

In addition to phagocytosis and mucociliary clearance, which are non-absorptive mechanisms, the dissolved drug can be absorbed. This is considered as an absorptive clearance, as the drugs are cleared from the lungs [171], as discussed in the previous section.

3.3. Pulmonary route for lung cancer treatment

As mentioned in the first section of this work, lung cancer treatment modalities are either localized (surgery, radiotherapy) or systemic (conventional chemotherapy, targeted therapies, immunotherapy). The pulmonary delivery of cytotoxic drugs could be a new modality with a loco-regional treatment that would fill the gap between the localized and systemic treatments by offering a local administration of these drugs with a diffusion from the lungs to the systemic compartment. The advantages and limitations as well as the possible strategies are summarized in **Figure 22**.
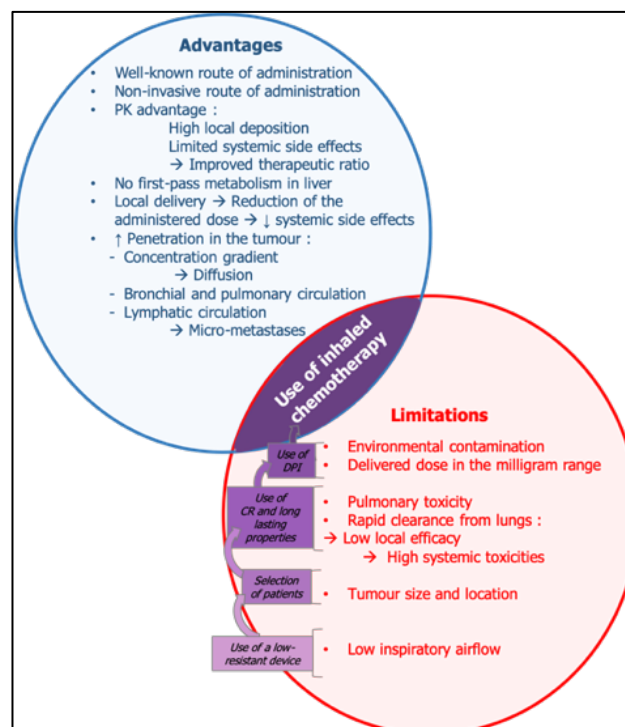

Figure 22: Main advantages (blue) and limitations (red) to the use of inhaled chemotherapy for lung cancer treatment, as well as the strategies (purple) to overcome these limitations. This figure was created from information retrieved from the following references [68,173]. CR stands for controlled release.

3.3.1. Advantages

Nowadays, the use of the pulmonary route is well-established for many pulmonary diseases such as not only COPD and asthma but also for pulmonary hypertension and cystic fibrosis [174]. Indeed, this can be explained by the various advantages of this local route and the limitations related to the systemic routes (oral and IV routes) **(Figure 22)**. This non-invasive route of administration allows the delivery of a high drug concentration locally while reducing systemic exposure, thus improving the therapeutic ratio for pulmonary diseases. In addition to this PK advantage, this allows a rapid onset of action of a lower dose than doses used with systemic therapies, which could lead to reduced side effects [174].

These advantages are mostly needed for cytotoxic drugs [174,175]. In addition, delivering a cytotoxic drug locally close to the tumour would increase the drug concentration gradient and therefore its diffusion inside the tumour **(Figure 22)** [173]. The inhaled cytotoxic drug can also reach the tumour site either by topical penetration from bronchial circulation for tumours located in the conducting zone, or by pulmonary circulation for tumours located away from the airways in the respiratory zone [173,175]. In addition to these advantages, the pulmonary delivery of cytotoxic drugs allows them to reach the lymphatic circulation and therefore access the lymphatic tissue, which is one of the first invaded sites [176], and which could increase the treatment efficacy. Moreover, the absorbed drug can follow the same pattern as cancer cells, which is interesting for the treatment of micro-metastases [176].

Considering these advantages, several cytotoxic drugs have been administered using the pulmonary route to patients with lung tumours in phase I to I/II clinical trials **(Table 9)**. These drugs were either administered alone (cisplatin, doxorubicin) [177–180], or in combination with other cytotoxic drugs administered using the IV route [79,179]. Indeed, a more recent phase I/II study of inhaled carboplatin has demonstrated the added value in terms of survival and progress of the disease of the combination of a carboplatin dose fractionated between the pulmonary route (1/3) and the IV route (2/3) with a total dose of docetaxel, when compared to an IV carboplatin and docetaxel doublet [79]. This can be explained by a longer exposure of the tumour site, lymph nodes and systemic circulation to a therapeutic carboplatin concentration when compared to the IV doublet group [79]. This last interesting result opens the possibilities of investigating promising strategies for new treatment combinations. However, for the group where the total carboplatin dose was administered using the pulmonary route and was combined to IV docetaxel, lower neutropenia was observed than for the two other groups. This was also related to a lower efficacy as a higher but a non-significant median of survival was observed in

comparison with the IV group [79]. This observation also shows the importance of finding the best compromise between efficacy and tolerance.

3.3.1. Limitations: Reports from clinical trials

To develop promising strategies for inhaled chemotherapy, it is mandatory to understand the clinical and technological limitations observed during clinical trials. These trials are summarized in **Table 9**.

Table 9: Description of the clinical trials of inhaled chemotherapy, adapted from *Rosière et al., 2018* [68] and *Wauthoz et al., 2020* [173].

Drug Phase Patients	Device Dose Scheme	Deposition in the lungs	Adverse effects	Efficacy
- 5-Fluorouracil - Pilot study - Untreated lung cancer patients eligible for surgery (9), and with lung metastases (10)	- Ultrasonic nebulizer -2.5 mg/kg -2 x/day for 2-3x/week -10-15 min/nebulization	-Tumour concentration > (5-15) Lung concentration -Concentration in lymph node	No local or systemic side effect	-Complete response (2/10) -Partial response (4/10) -No change (4/10)
- 9-Nitrocampothecin - Phase I - Patients with lung cancer and metastases (25), with no response to other treatment	- Jet nebulizer (liposome) - 6.7 to 26.6 $\mu g/kg/d$, 5x/w up to 6 w - 13.3 $\mu g/kg/d$, 5x/w for 8 w	- BALF concentration > (4.2-10.6) serum concentration	***DLT = 26.6 $\mu g/kg/d$*** - Grade 3: pharyngitis **At 13.3 $\mu g/kg/j$** - Grade 2: cough, bronchial irritation - Grade 2: nausea, vomiting, fatigue, anaemia, neutropenia	- Partial remission (3/25) - Stable disease (3/25)
- Cisplatin - Phase I - Untreated advanced NSCLC (16), SCLC (1) patients	- Jet nebulizer - 1.5-60 mg/m² -1-4 consecutive days in 1-3 weeks for 1-8 cycles - 20 min/nebulization up to 3 consecutive nebulizations	- Deposition in the lungs of 10-15% (radiolabelled solution)	***DLT not reached*** - Grade 3: bronchitis, decreased FEV₁, dyspnea - Grade 4: thrombosis - Grade 3: fatigue	- Stable disease (12/18) - Progressive disease (4/18)
- Cisplatin - Phase Ib/IIa - Osteosarcoma with lung metastases only (>1cm), previously treated with platinum-based chemotherapy	- Jet nebulizer - 24 or 36 mg/m²/2 weeks - Up to 3 sessions/day (2-3h between sessions)	-	- Grade 2: hoarseness - Grade 3: nausea, vomiting	- Complete response (3/19) - Partial response (1/19) - Stable disease (7/19) - Progressive disease (8/19)
-Doxorubicin - Phase I - Lung metastases	- Nebulizer - 0.4-9.4 mg/m², each 3w	Homogenous deposition in the lungs	***DLT : 9.4 mg/m²*** - Grade 4: respiratory distress - Grade 3: hypoxia - Grade 2: cough, dyspnea	- Partial response (1) - Stable disease (8) - Progressive disease (2)
- Doxorubicin (ET) + CIS + Docetaxel (DOC) (IV) - Untreated advanced NSCLC	- 6.0 – 7.5 mg/m² , 1-3h before 75 kg/kg CIS + DOC, each 3 weeks for 24 weeks	-	***DLT : 7.5 mg/m²*** - Decrease of > 20% pulmonary function test - Grade 3-4: cough (**6 mg/m²**). - IV doublet → constipation, hyponatraemia, neutropenia	- Complete response (1/24) - Partial response (6/24) - Stable response (13/24) - Progressive disease (4/24)
- Gemcitabine - Phase I - NSCLC stage IIIb (4) or IV (7), with no response to chemotherapy	- Vibrating mesh Nebulizer - 1 – 4 mg/kg , 1 day/week for 9 weeks	Homogenous deposition in the lungs (42 ± 16%)	***DLT : 4 mg/kg*** - Grade 3-2: cough - Grade 4: bronchospasm - Grade 3: fatigue, vomiting	- Minor response (1) - Stable disease (4) - Progressive disease (4)
- CARB + DOC - Phase I/II - Untreated stage IV NSCLC patients (Tumour 3-5 cm)	- Jet nebulizer - CARB (ET): 160-230 mg/d - CARB (IV): 550– 700 mg - DOC (IV): 100 mg/m² A : IV CARB + DOC B : CARB (ET 1/3+ IV 2/3) + IV DOC C : CARB ET + IV DOC	Deposition of radiolabelled aerosol in the lung parenchyma	A: grade 2 irritative cough Grade 3: fatigue, alopecia, rash, anorexia, anaemia, neutropenia B: grade 3 productive cough Fatigue, rigors, alopecia, anaemia, neutropenia, anorexia (4) C: grade 3 dyspnoea, hoarseness, voice change, irritative + productive cough Grade 3: fatigue, alopecia, mucositis, nausea, pharyngitis, anorexia (4), dysgeusia (4) Less Neutropenia in C than A or B	- Survival (d): B vs A : 275 ± 13 vs 211 ± 13 (p<0.001) C vs A : 250 ± 7 vs 211 ± 13 (p>0.05) - Complete response: A:0, B:2, C:1 - Partial response: 1:5, B:6, C:4 - Stable disease: A:8, B:3, C:5 - Progressive disease: A:7, B:9, C:10

3.3.1.1. Pulmonary toxicity

The first cytotoxic drug ever administered using the pulmonary route for lung cancer patients was 5-Fluorouracil in 1993 [181]. Since then, other cytotoxic drugs have been tested: 9-nitrocampothecin [182], cisplatin [177,178], doxorubicin [179,180], gemcitabine [183] and carboplatin [79], as illustrated in **Table 9**. Although they have limited systemic toxicities with interesting lung targeting (5-flururoacil, 9-nitrocampothecin), they nearly all presented different levels of pulmonary toxicities **(Table 9),** as reported by Sardeli *et al.*, who has

classified these drugs going to the safest locally: taxanes < doxorubicin < gemcitabine < cisplatin-carboplatin < 5-fluorouracil < 9-nitrocampothecin [184]. Indeed, while 9-nitrocampothecin and 5-fluoruracil have induced limited pulmonary effects, platinum drugs have induced irritative and productive cough, bronchitis, dyspnoea and hoarseness **(Table 9)** [181–183]. Doxorubicin seemed to be less tolerated by the lungs as it has induced grade 4 respiratory distress, grade 3 hypoxia, and even decreased the pulmonary function by more than 20% when combined to docetaxel **(Table 9)** [179,180]. Different strategies have been used to limit these toxicities such as the use of bronchodilators and steroids, as well as appropriate cleaning of the face and mouth [182,184].

3.3.1.2. Limitations related to the device

In addition to pulmonary toxicity, the selected formulations (solution, suspension) as well as the chosen device did not seem to be well-adapted to this use. Indeed, the DLT was not reached following the administration of cisplatin at 60 mg/m^2 after 6h of administration over 3 days. Moreover, only 10-15% of the administered dose was retrieved in the lungs [178].

These administrations were performed using jet, ultrasonic, or vibrating mesh nebulizers, which raises an important point regarding the solubility of the drugs and their rapid clearance in the case of lipophilic drug (non-absorptive clearance) [173]. Depending on the drug concentration, the administration time can be long, as observed for liposomal dispersion of 1 mg/mL of cisplatin (20 min per nebulization, up to 3 times per session and up to 3 sessions per day, with a rest of 2-3h between sessions) [177,178]. In addition, nebulizers necessitate heavy infrastructure to avoid environmental contamination.

3.3.1.3. Limitations related to the formulation

In the case of asthma or COPD, the administered doses are commonly in the microgram range. However, in the case of lung cancer and pulmonary delivery of cytotoxic drugs, the delivered dose are in the milligram range (1-80 mg), as demonstrated during a phase I study of inhaled cisplatin **(Table 9)** [178]. Nonetheless, with only 10-15% retrieved in the lung, the targeted cisplatin dose into the lungs seems to be ranged between 0.15 and 12 mg. Moreover, as mentioned in the previous section, cytotoxic drugs have often a limited solubility in water, and their formulation as a solution for nebulization is inappropriate for administration over a reasonable time and without air contamination [68]. Therefore, the use of particulate engineering is often needed to develop more suitable formulations.

The deposition of high doses of cytotoxic drug is a promising strategy in terms of efficacy, but caution should be also paid to pulmonary tolerance. Recent studies have demonstrated that depending on the shape, size, pH and surface chemistry of the inhaled particles, the lung toxicity profile can be different [185].

Moreover, two additional limitations related to the fate of deposited particles can be addressed: *(i)* the dissolved fraction from deposited particles can rapidly be retrieved in plasma (absorptive mechanism), and *(ii)* the undissolved fraction can be cleared through non-absorptive mechanisms. This leads to *(i)* a reduced exposure of the tumour and thus to a potentially reduced efficacy, and to *(ii)* increased systemic side effects.

Both pulmonary tolerance and the fate of deposited particles are more problematic with an immediate-release formulation. Indeed, the total delivered dose is immediately dissolved, which results in high active fraction C_{max} *(i)* in the lungs, leading to limited pulmonary tolerance, and *(ii)* in plasma, leading to systemic side effects.

3.3.1.4.   Environmental contamination

As mentioned previously, another major point to consider is environmental contamination **(Figure 22)**. The aerosol generated during an inhalation session should be confined and the environmental contamination must be controlled to protect medical staff. Full protective equipment is therefore used in terms of clothing (gown, glasses, face mask, gloves, cap and sleeves) and infrastructure (a negative pressure room with depressurized 'tents' or 'cabins' equipped with an air extractor linked to high-efficiency particulate absorbing (HEPA) filters), which imposes heavy procedures for treatment administration and cleaning of the infrastructure/device [173]. Moreover, the patient's exhaled air can also contain a large dose fraction. Consequently, this technique renders the administration of cytotoxic drugs non-patient-friendly, with major compliance issues and logistical costs [186].

3.3.1.5.   Patient intrinsic factors

In the case of lung cancer, the airways can be modified by tumours, which can be responsible for a modified aerosol deposition profile **(Figure 22)**. Indeed, the airways can be partly obstructed by the tumours, leading to a turbulent (not laminar) airflow in these areas and to higher impaction. In the case of total airway obstruction, the airflow will be deviated and the cytotoxic drug will not be deposited in the obstructed areas, which can impair the treatment efficacy [68], as these are the areas that most need the therapy [80]. However, previous clinical

studies have published that patients with tumours characterized by a median diameter higher than 3-5 cm upon diagnosis can be excluded from trials [80].

Moreover, as lung cancer patients often have impaired lung function following the use of tobacco and/or the presence of COPD, they often have a lower respiratory function resulting in a lower respiratory airflow than healthy patients. Consequently, they may not be able to generate an airflow high enough for some DPI to overcome the powder interparticulate forces, leading to low deagglomeration and deposition. In addition, these patients can be more subject to developing severe local side effects due to their weakened lung tissue [186].

3.3.2. Strategies: Lessons learned from clinical studies

As part of the development of inhaled chemotherapies, the strategies developed hereunder included the selection of the most suitable device and formulation. Indeed, the limitations that were disclosed in the previous section could be overcome with different technologies, as represented in **Figure 23**. Different preclinical studies have investigated promising strategies to achieve a safer profile with a reasonable time of administration, sufficient time for tumour exposure, and reduced environmental contamination [186].

First, to ensure high delivered doses in the lungs and to avoid contamination, the use of DPIs is a promising strategy [187–189]. Unlike nebulizers, these devices offer the possibility to deliver high drug doses within a short period of time with limited environmental contamination [173,186]. Indeed, DPIs are able to deposit high drug doses following the use of an aerosol that is transported to the lungs through the patient's inspiratory flow, with a negligible exhalation fraction (e.g. 0.2% of the nominal dose of tobramycin in healthy subjects [190]). Moreover, as discussed above, because lung cancer patients may have an impaired lung function, it is essential to design formulations that are suitable to be used with low-resistance device. These devices minimize the impact of airflow on aerosolization, deagglomeration and lung deposition [173,186].

As discussed previously, although the deposition of high doses of cytotoxic drug is a promising strategy in terms of efficacy, special concerns regarding pulmonary tolerance and the fate of deposited particles should be considered, as represented in **Figure 23**. The development of controlled-drug-release formulations with lung retention properties is the most promising strategy to overcome these limitations. Indeed, this type of formulation is suitable as they can

flatten the C_{max} of the active fraction in the lungs and avert pulmonary toxicity. Moreover, as the cytotoxic drug is released gradually from the controlled-release particles, the AUC in the lungs is increased, leading to an increased lung/tumour exposure to the cytotoxic drug. In addition, the decreased C_{max} in the lungs will be correlated to a decreased C_{max} in plasma and to an improvement of the systemic tolerance. Moreover these particles can also escape the fast elimination of the cytotoxic drug from the lungs, leading to a better systemic tolerance and to an increased lung/tumour ratio [186,191].
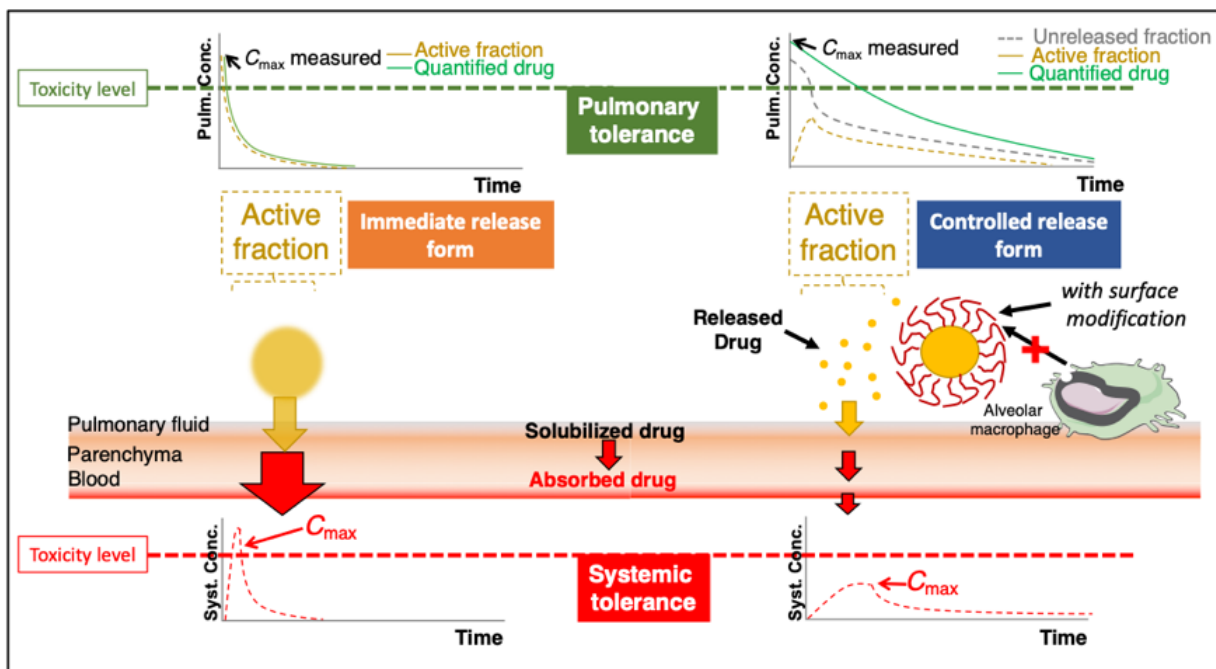
Figure 23: Immediate- *vs.* controlled-release DPI formulations and their related pulmonary and systemic profiles. On the one hand, following the administration of an immediate-release formulation, the delivered dose is immediately dissolved leading to a high C_{max} from the active fraction in the lungs and in plasma. This can impair both pulmonary and systemic tolerance. On the other hand, the development of a controlled-release formulation flattens the C_{max} of the active fraction resulting from a progressive release of the drug from the particles. This improves both pulmonary and renal tolerance. It should be mentioned that following the administration of the controlled-release formulation, the measured C_{max} in the lungs would include the total drug delivered from both the active and the unreleased fractions. This figure was created from information retrieved from the following references [186,191].

To decrease the clearance mechanisms of non-solubilized particles, developing particles with d_{ae} between 1.8 and 2.8 μm (to avoid mucociliary clearance) and with stealth properties using excipients with polyethylene glycol (PEG) (to avoid AM clearance) is a promising strategy [173]. Other strategies, such as muco-adhesion and modification of the particle size or shape, can also be considered [173]. However, considering the objectives of the thesis, the formulation strategies as well as the different types of controlled-release particles were not discussed in detail. Only the most promising cytotoxic drug-based formulations are presented. Indeed,

different particulate engineering techniques have led to the development of formulations in the nano-range such as liposomes (9-nitrocamptothecin, paclitaxel), micelles (paclitaxel), human serum albumin nanoparticles (doxorubicin), polystyrene nanoparticles (losartan, telmisartan), solid-lipid nanoparticles (paclitaxel), nanostructured lipid carriers (celecoxib), hybrid lipid-polymer nanoparticles (5-fluorouracil, paclitaxel), lipid nanocapsules (paclitaxel), inorganic nanocarriers and others [188,191–202]. These formulations have interesting advantages in terms of passive and active targeting of tumour tissues [186]. Cisplatin-based PEGylated solid-lipid microparticles (SLM) have been developed with this aim and have avoided lung clearance, while maintaining high concentration in the lungs over 8h with encouraging preliminary pulmonary tolerance and efficacy results, as reported by Levet *et al.,* [187,203].

SCIENTIFIC STRATEGY AND MAIN OBJECTIVES

Worldwide, the numbers of lung-cancer new cases and deaths are increasing [11]. There is an urgent need to increase treatment effectiveness by developing new drugs or combinations of drugs or by repurposing current therapies as the 5-year relative survival remains low at 21.7% (USA, 2011-2017) [11]. To treat NSCLC and SCLC, conventional platinum-based chemotherapy remains the backbone of care as it is used at nearly all stages. Indeed, cisplatin or carboplatin are often combined either with paclitaxel, gemcitabine or pemetrexed for the treatment of NSCLC, or with etoposide for the treatment of SCLC [15,42,65]. These platinum-based therapies present a dose-dependent efficacy as a significant correlation has been observed between the tumour platinum concentration and the treatment effectiveness in terms of tumour-size reduction, survival and recurrence of the disease for NSCLC patients [204].

Although these systemic chemotherapy treatments are effective, they remain highly toxic as they do not discriminate between healthy tissues and tumours. Indeed, cisplatin, one of the most effective cytotoxic drugs, is highly nephrotoxic (DLT) and induces various other toxicities (e.g. ototoxicity, myelosuppression), requiring well-spaced cycles between its administrations. Heavy hydration protocols are prescribed to avoid its accumulation in proximal tubules. Moreover, other severe toxicities such as myelosuppression, neurotoxicity or gastrointestinal toxicity are increased when combined to another cytotoxic drug (i.e. platinum-based doublets), leading to delay of treatment cycles and to dose reductions. These adaptations are made to help the patient recover from the toxicities induced by chemotherapy. However, they are also responsible for either not exposing or reduced exposure of the tumour to cytotoxic drugs, which could limit their potential.

Considering the advantages of the pulmonary route, delivering cisplatin directly into the lungs of lung cancer patients is an interesting modality (i.e. loco-regional treatment) for combination to IV systemic treatments. Indeed, this would allow a high dose to deposit directly in the lungs (i.e. the tumour site), improve the therapeutic ratio and potentialize its efficacy. In addition, it has been reported that the pulmonary delivery of cytotoxic drugs allows them to reach the lymphatic circulation and therefore access lymphatic tissue [176], which could increase the treatment efficacy.

The use of the pulmonary route to deliver cisplatin has been investigated in clinical trials against NSCLC, SCLC and osteosarcoma with lung metastases and shown the limitations of the use of nebulizers [177,178]. Consequently, an alternative to these devices is the use of small, compact

devices such as single-dose DPIs as cytotoxic drugs must be delivered in the milligram range [178]. Indeed, these devices offer the possibility to deliver high drug doses in a short period of time using portable devices able to trigger the formulation aerosolization following the patient's inspiratory air flow, thus limiting environmental contamination concerns. In addition, as they can be used as disposable devices, they do not require cleaning procedures, as required for nebulizers.

Considering the clearance mechanisms in the lungs, the cisplatin-based DPI should be developed to have a controlled drug release and long-lasting properties. The controlled-release formulation is selected to avoid direct pharmacological action and absorption of the dissolved drug. This leads to lower C_{max} peaks in lungs and plasma, thus preventing toxicities and increasing the tumour exposure. The long-lasting properties are developed to avoid the drug particles being recognized by AM and therefore eliminated.

Regarding all these parameters, Levet *et al.,* developed a promising controlled-release cisplatin-based DPI formulation with an interesting lung deposition profile *in vitro* and with controlled-release properties *in vivo* using PEGylated SLM [187,205]. This formulation allowed *(i)* the maximum tolerated dose (MTD) to be increased and *(ii)* its efficacy to be improved when administered to M109-HiFR carcinoma model-grafted mice ($p < 0.01$, log-rank test, respectively) in comparison with an immediate-release formulation. However, its efficacy was lower than the efficacy obtained with cisplatin delivered by IV at 1 mg/kg in comparison with the untreated group ($p < 0.01$ and $p < 0.001$, log-rank test, respectively). The hypothesis made after this study was that the high metastatic rate of the model led the mice treated with cisplatin inhaled formulation to die from secondary metastases and the mice treated with IV cisplatin solution (CIS-IV) to die from pulmonary metastases. Consequently, it seemed interesting to investigate the combination of both of these routes of administration to intensify cisplatin efficacy.

From a clinical perspective, our strategy would be to deliver cisplatin using the pulmonary route during the off-cycles encountered with conventional systemic chemotherapy. Indeed, the addition of localized delivery to the systemic route could allow a therapeutic intensification due to a loco-regional diffusion of the drug close to the tumour, while fighting invasive and diffuse cancerous cells by systemic chemotherapy [173,206,207]. Indeed, Zarogoulidis *et al.* demonstrated in phase I/II clinical trials on NSCLC patients with tumours of 3-5 cm that there

was no significant difference between the IV control group (i.e. 3/3 carboplatin and docetaxel) and the locally treated group (3/3 carboplatin by inhalation and IV docetaxel). In contrast, they reported a significant increase in survival for the combined group (i.e. 1/3 of carboplatin dose by the pulmonary route and 2/3 of carboplatin by the IV route with docetaxel on day 1) when compared to the IV control group [79]. This can certainly be related to a longer exposure of the tumour site, lymph nodes and systemic circulation to a therapeutic carboplatin concentration when compared to the control group, as observed with the reported PK data [79]. Moreover, a significant difference in terms of tolerance was reported between these groups and demonstrates the need to investigate the tolerance. Indeed, this promising strategy can only be successful if pulmonary and renal tolerance are both preserved.

Considering these statements, the main objectives of this work were:

(i)   the optimization of a cisplatin-based DPI formulation and the evaluation of its *in vitro* (optimal lung deposition adapted for lung cancer patients) and *in vivo* (biodistribution and tumour retention) properties

(ii)   the selection of the most appropriate combinations with cisplatin-based IV chemotherapy based on pulmonary and tolerance evaluation

(iii)   the evaluation of the added-value of the selected combination on an aggressive lung carcinoma model

(iv)   the investigation of the pulmonary, renal and haematological tolerance once combined with carboplatin-based IV chemotherapy

To do so, the main objectives of this research work are divided into four main parts. As aforementioned, the first objective was to optimize the controlled-release DPI formulation with long-lasting properties, with generally recognized as safe (GRAS) and pharmaceutical excipients, using scalable and reproducible processes. Moreover considering the similar efficacy obtained with CIS-IV on grafted mice, it was interesting to increase the burst effect to improve the efficacy outcomes while maintaining a good local tolerance. Therefore, this formulation was expected to *(i)* have an interesting deposition profile *in vitro*, *(ii)* be able to release cisplatin continuously *in vitro* but with a higher burst effect than before and *(iii)* maintain good stability over time. Moreover, this controlled release would have to be demonstrated *in vivo* with a PK advantage in terms of lung targeting, in comparison to the IV route.

The second part consisted of the selection of the best cisplatin-based DPI regimen to be combined to the conventional IV chemotherapy treatment. This selection should consider both their efficacy (i.e. platinum concentration inside the tumour, caspase-3 immunostaining, tumour size and survival) and their tolerance (i.e. platinum accumulation in tumour-free organs, histology of the tumour-free lungs). These evaluations were crucial to select the regimen with the highest efficacy and the lowest accumulation in tumour-free lungs, kidneys and blood.

The third part aimed to *(i)* investigate the *in vivo* pulmonary and renal tolerance following the addition of the selected cisplatin-based DPI regimen to CIS-IV, *(ii)* optimize the delay between the administration of the selected cisplatin-based DPI monotherapy regimen and CIS-IV, and *(iii)* adapt the administered doses of the locoregional and the systemic therapies. This was done to select the regimen with the highest cumulative dose (i.e. highest efficacy) while limiting pulmonary and renal toxicities. The efficacy of the combination regimen was therefore evaluated on an orthotopically M109-HiFR-*Luc2* lung carcinoma murine model.

Last but not least, the fourth part consisted of the evaluation of pulmonary, renal and haematological tolerance following the co-administration of the cisplatin-based DPI monotherapy with another conventional platinum-based doublet (i.e. carboplatin-paclitaxel). Indeed, considering that carboplatin has a better toxicity profile than cisplatin in terms of nephrotoxicity, the combination of the IV doublet with the cisplatin-based DPI formulation was hypothesized to be less harmful in terms of renal injury and to necessitate fewer adjustments. This would therefore potentially increase the treatment efficacy. Moreover, as myelosuppression is a carboplatin and paclitaxel DLT and as platinum drugs are also able to induce pulmonary hypersensitive reactions, it was crucial to consider the whole IV doublet (i.e. not carboplatin alone) for the tolerance evaluation. This also aimed to be closer to clinical practice as the use of a doublet is the backbone of conventional chemotherapy.

EXPERIMENTAL PART

Part I: Optimization of cisplatin-based DPI formulation with controlled-release and lung-retention properties
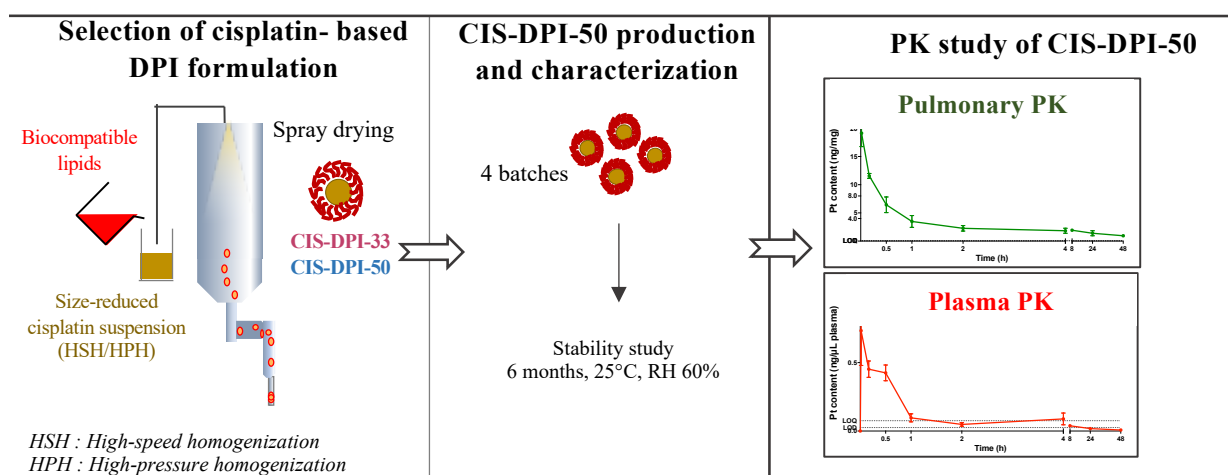
Figure 24:Graphical abstract of the first experimental part.

1. <u>Introduction and aims</u>

The first part of this work consisted of optimizing the cisplatin-based DPI formulation developed by Levet *et al*. Indeed, they have developed a cisplatin-based DPI formulation (referred as CIS-DPI-TS in this work) with controlled-release properties and a high FPF *in vitro* correlated with interesting lung retention *in vivo* [187,203]. This improved the global tolerance *in vivo* as the MTD increased from 0.5 mg/kg for an immediate-release cisplatin DPI to 1 mg/kg for the CIS-DPI-TS, leading to promising efficacy outcomes. Indeed, CIS-DPI-TS administered using the endotracheal (ET) route three times a week for 2 weeks at its MTD (i.e. 1 mg/kg cisplatin) in the M109-HiFR lung carcinoma orthotopic mouse model showed a significantly higher survival rate in comparison to the untreated mice ($p < 0.01$, log rank test). This was not the case with cisplatin in microparticles without controlled-release and lung-retention properties administered at its MTD (i.e. 0.5 mg/kg), showing the limit of an immediate-release formulation due to its DLT [205]. Moreover, this formulation, at 1 mg/kg, showed a level of significance lower than obtained with CIS-IV at the same dose and using the same regimen ($p < 0.01$, log rank test) demonstrating the limit of a loco-regional treatment administered alone. However, it should be mentioned that these treatments were both administered three times per week over 2 weeks, and that this scheme of administration is quite far from clinical-practice reality for IV chemotherapy. Nonetheless, this result showed the importance of modulating the cisplatin release from microparticles to find the optimal balance between local tolerance and efficacy.

Considering Levet *et al*.'s results, CIS-DPI-TS was chosen to be the basis of this research work. Indeed, a preliminary section aimed to produce and characterize CIS-DPI-TS. This was done to ensure the correct handling of the production and characterization techniques and to evaluate the reproducibility of the process. Moreover, several experimental aspects were investigated such as *(i)* the selection of the most suitable single-dose DPI in terms of particle dispersion performance in order to be used as a disposable device, *(ii)* the evaluation of the efficacy of CIS-DPI-TS using a regimen closer to clinical practice and *(iii)* the initiation of *in vitro-in vivo* correlations using GastroPlus™.

New challenges were worth considering for the development of a new cisplatin-based DPI. First, considering the aforementioned efficacy results, this new formulation should give a higher burst effect than CIS-DPI-TS while maintaining a similar controlled release over time.

This is crucial to improve its efficacy while maintaining good pulmonary and renal tolerance. Second, the manufacturing process should be optimized to ease the scale-up step and should use only GRAS and commercially available pharmaceutical grade excipients. This is important to avoid the necessity to change excipients and provide for longer development/toxicological studies during the approval process. Third, the stability of this formulation should be clearly established to avoid any differences in terms of toxicity/efficacy during storage. Fourth, the repeatability of the production process as well as the preservation of the aerodynamic properties should be demonstrated.

Finally, once these characteristics had been demonstrated, it was mandatory to verify whether the aim of developing a formulation with a higher burst effect was achieved *in vivo*. This was also done to characterize the controlled release of cisplatin in the lungs, and its exposure in kidneys and blood. To verify these key properties, a PK study had to be conducted on healthy mice.

2. Materials and methods

2.1. Materials

Cisplatin was purchased from Umicore (Brussels, Belgium), tristearin (TS) from Tokyo Chemical Company (Tokyo, Japan), tocopherol polyethylene glycol 1000 succinate (TPGS) from Sigma-Aldrich (St. Louis, USA). Hydrogenated castor-oil (HCO) Kolliwax and Poloxamer 407 were purchased from BASF (Ludwigshafen, Germany) and DPCC was provided by Lipoid (Steinhausen, Switzerland). Chloroform and methanol were provided by VWR Chemicals (Leuven, Belgium) and dimethylformamide, Suprapur® nitric acid, isopropanol (IPA), ethanol, mannitol, NaCl and L-leucine were obtained from Merck Millipore (Darmstadt, Germany). M109-HiFR cells were purchased from ATCC (Maryland, USA). Folate-free Roswell Park Memorial Institute medium (RPMI), foetal bovine serum (FBS), penicillin-streptomycin solution, gentamycin solution, phosphate buffer saline (PBS) and trypsin-EDTA solution were purchased from Life Technologies (Merelbeke, Belgium). Matrigel® matrix was purchased from Corning (Lasne, Belgium). Ultrapure water was obtained from a Pure-Lab Ultra® purification system (Elgan Lane End, UK). All solvents and chemicals were analytical grade.

2.2. Safety procedures

Cisplatin manipulation included the preparation of high-loaded suspensions of up to 5% w/v and the production and characterisation of DPIs. The handling of such a cytotoxic drug necessitated heavy infrastructure to avoid early and delayed toxicities for humans and environmental contamination. These experiments were conducted in a negative-pressure room equipped with flow cabinets (Protec I and Protec II, ADS Laminaire, Paris, France) with air circulating through high-efficiency particulate absorbing (HEPA) filters before its elimination outside the building. In addition, the manipulators had to use powder-free latex gloves that were immediately in contact with their skin, above which a second pair of powder-free latex gloves were used and changed, at the latest, each hour. A Tyvek® protective gown (DuPont, Mechelen, Belgium) was used only inside the dedicated room and often changed. In addition, an FFP3 respirator mask (3M, Cergy Pontoise, France) was dedicated to this manipulation, as described by Wauthoz *et al*. [189] and following the practice guidelines [208].

2.3. Preliminary studies on CIS-DPI-TS

2.3.1. Production of CIS-DPI-TS

The cisplatin-based DPI formulation using TS 49.5% w/v and TPGS 0.5% w/v (CIS-DPI-TS) was produced as broadly described by Levet *et al*. [187]. Cisplatin was dispersed in IPA (5% w/v) and size-reduced using high speed homogenization with an X620 motor and a T10 dispersing shaft (Ingenieurbüro CAT, M. Zipperer GmbH, Staufen, Germany) at 24 000 rpm for 10 minutes. The suspension was then transferred to an Emulsifex-C5 high-pressure homogenizer (Avestin Inc, Ottawa, Canada) for a further size- reduction step using high-pressure homogenization (HPH) following three cycles: 10 cycles at 5 000 psi, 10 cycles at 10 000 psi and 20 cycles at 20 000 psi. The temperature of the suspension was maintained between 5 and 10°C, to avoid massive solvent evaporation, using a heat exchanger that maintained the circulating medium (propylene-glycol/water 1:1 v/v) at -15°C, using an F32-MA cooling circulator (Julabo GmbH, Seelbach, Germany).

The excipients (TS, TPGS) were solubilized in pre-heated IPA (5% w/v, 65°C) and added to the size-reduced cisplatin suspension to achieve a final concentration of 2% w/v. This suspension was maintained under stirring and then spray dried using a B-290 Mini Spray Dryer (Büchi Labortechnik AG, Flawil, Switzerland) equipped with a B-296 dehumidifier (Büchi Labortechnik AG, Flawil, Switzerland) to maintain RH at 50%. This was conducted using the

following parameters: feed rate, 3.0 g/min; inlet temperature, 70°C (corresponding to an outlet temperature of 38-42°C); 0.7 mm nozzle; compressed air, 800 L/min, and drying air flow, 35m^3/h. The collected mass was divided by the theoretical mass composition to calculate the yield of the recovered powder. The DPI formulation was stored in a desiccator at ambient temperature until further analysis.

2.3.2. *In vitro* characterization of CIS-DPI-TS

2.3.2.1.   Platinum content of *in vitro* samples

The platinum content was quantified by electrothermal atomic absorption spectrometry (ETAAS) using a SpectrAA spectrometer equipped with a Zeeman correction and a GTA-96 graphite tube atomizer (Varian, Mulgrave, Australia). The analyses (samples of 20 μL) were performed in adapted graphite tubes (Spectrotech, Tubize, Belgium) with a platinum hollow cathode lamp (Photron Pty Ltd., Narre Warren, Australia) at a wavelength of 265.9 nm and at 7 mA, with argon (Air Liquide, Liège, Belgium) used as a purge gas at a flow rate of 3.0 L/min. This was conducted following a specific temperature programme **(Table 10)**, as validated and described by Levet *et al.* [187].

Table 10: Furnace temperature programme for platinum content, as described by *Levet et al., 2016* [187].

	Steps	Temperature (°C)	Ramp (s)	Gas flow (L/min)
1		85	5.0	3.0
2	Drying	95	40.0	3.0
3		150	10.0	3.0
4		800	5.0	3.0
5	Charring	800	1.0	3.0
6		800	2.0	0.0
7	Atomization	2700	1.0	0.0
8		2700	4.0	0.0
9	Cleaning	2700	1.0	3.0

To evaluate the cisplatin content in the DPI, 10.0 mg of CIS-DPI-TS was diluted in 10.0 mL of dimethylformamide, ultrasonicated for 1 hour and diluted 2 500-fold with 0.1% v/v Suprapur$^®$ HNO$_3$ (n=3). The platinum quantification was performed on the samples collected during the dissolution test or following the collection of the powder during aerodynamic performance testing. Afterwards, the platinum concentration was converted to cisplatin. This technique was used routinely as platinum nuclear magnetic resonance spectroscopy has demonstrated no degradation of cisplatin during the production process [187], and as the apparatus was more easily accessible. Data are presented as means ± standard deviation (SD) (n=3).

2.3.2.2. Particle size distribution

Evaluation of the geometric PSD of the size-reduced cisplatin suspension and from DPI particles was operated using a Mastersizer® 3000 laser diffractometer (Malvern Instruments Ltd., Worcestershire, UK) connected to a Hydro MV dispenser equipped with a 40 W ultrasonic probe (Malvern Instruments Ltd., Worcestershire, UK). As this technique measures individualized particles, these must be in suspension in a solvent where they are undissolved. Consequently, cisplatin size-reduced microparticles were suspended in cisplatin-saturated IPA and CIS-DPI-TS was suspended in cisplatin-saturated solution (0.1% w/v Poloxamer 407 and NaCl 0.9% w/v), as optimized by Levet *et al.* [187]. The agitation was set at 2 900 or 1 800 rpm according to whether this was measured in IPA or saline, respectively, with a refractive index set at 1.6 and an absorption coefficient at 0.1 using 100% of ultrasonic intensity for 10 s or 1 min for IPA (refractive index 1.377) or saline (refractive index 1.33), respectively. The percentage of particles under 5 μm (% < 5 μm), the mass median diameter dv(50), the volume mean diameter D[4,3], the dv(10) and dv(90), corresponding to 10% and 90% of particles, respectively, with a diameter under the given size, characterized the geometric PSD. Data are presented as means ± SD (n=3).

2.3.2.3. Residual solvent content

The evaluation of the residual solvent was assessed on CIS-DPI-TS using thermogravimetric analysis operated by a Q500 thermogravimetric analyser (TA Instruments, New Castle, USA) and Universal Analysis 2000 software (TA Instruments, New Castle, USA). The analysis was conducted on weighed samples of about 10 mg (n=3), in a range 25-300°C, with a ramp of 10°C/min, and on weight loss between 25°C and 125°C. Data are presented as means ± SD (n=3).

2.3.2.4. Thermal properties

The thermal properties of CIS-DPI-TS were determined using differential scanning calorimetry (DSC), following the use of a Q3000 differential scanning calorimeter (TA Instruments, New Castle, USA) equipped with an RCS90 cooling system (TA Instruments, New Castle, USA). Analysis was carried out on samples of 5.0 mg of CIS-DPI-TS in Tzero aluminium pans, closed using Tzero hermetic lids (TA Instruments, New Castle, USA). The process followed a heating cycle from -10°C to 180°C, then a cooling cycle from 180°C to -10°C and finally a second heating cycle from -10°C to 180°C. This was conducted with nitrogen as blanket gas and an empty pan as a reference, as described previously [187].

2.3.2.5. Aerodynamic behaviour

The aerodynamic performance of CIS-DPI-TS was evaluated according to European Pharmacopeia 10, section 2.9.18 for DPIs. The APSD from a low-resistance RS.01 device (RPC Plastiape, Osnago, Italy) containing a size 3 HPMC capsule (Vcaps, Capsugel-Lonza, Colmar, France) **(Figure 19)** hand-filled with 20.0 ± 0.5 mg powder was determined using a multistage liquid impactor (MsLI, Copley Scientific, Nottingham, UK). The evaluation was also conducted from three other devices: a commercial high-resistance device (n=3) and two different prototypes at high (prototype 1) (n=1) and medium (prototype 2) resistance (n=1) in which the same powder mass was deposited inside each device directly as these devices did not require the use of capsules. This was done to select the device best adapted to CIS-DPI-TS.

A pressure drop of 4 kPa in the device was reached with an aspiration flow rate of 100 L/min for the RS.01, 39 L/min for the commercial high-resistance device, 36 L/min for the prototype 1 high-resistance device and 56 L/min for the prototype 2 medium-resistance device. Considering an inhaled air volume of 4 L, these flow rates were applied for 2.4 s, 6.2 s, 6.7 s and 4.3 s, respectively. The collection of cisplatin particles was performed by means of dimethylformamide and the platinum content of the different collection samples was determined by the validated ETAAS method, as described previously [187].

The collected cisplatin masses were then plotted in Copley Inhaler Testing Data Analysis Software 1 to obtain the FPD and FPF_n as well as the APSD parameters including the MMAD and the GSD. Data are presented as means of $\pm$ SD (n=3).

2.3.2.6. Dissolution release profile

To evaluate the cisplatin release from CIS-DPI-TS particles that were optimally deposited in the lungs (< 5 μm), it was mandatory to first select the particles with a $d_{ae} < 5$ μm, then evaluate their release in simulated lung surfactant. This was performed following a technique called "paddle-over disk" from the US Pharmacopeia (USP), as described by Levet *et al.* **(Figure 25)** [187].

To do so, the respirable fraction of CIS-DPI-TS was selected using an FSI (Copley Scientific, Nottingham, UK). About 3 mg of cisplatin were loaded into a size 3 HPMC capsule and collected at a flow rate of 100 L/min for 2.4 s, using the RS.01. A hydrophilic polycarbonate membrane with 0.4 μm pore size (Isopore®, Merck Millipore, Darmstadt, Germany) covered the collected powder **(Figure 25)**. The cisplatin dissolution profile was then evaluated in a paddle dissolution apparatus (Erweka DT6, ERWEKA GmbH, Heusenstamm, Hesse, Germany) filled with 400 mL of modified simulated lung fluid (mSLF, [209,210]), modified to

be as closest as possible to lung surfactant. To prepare the saline part of mSLF, the chemicals were added following the list described by Marques *et al.* [210].
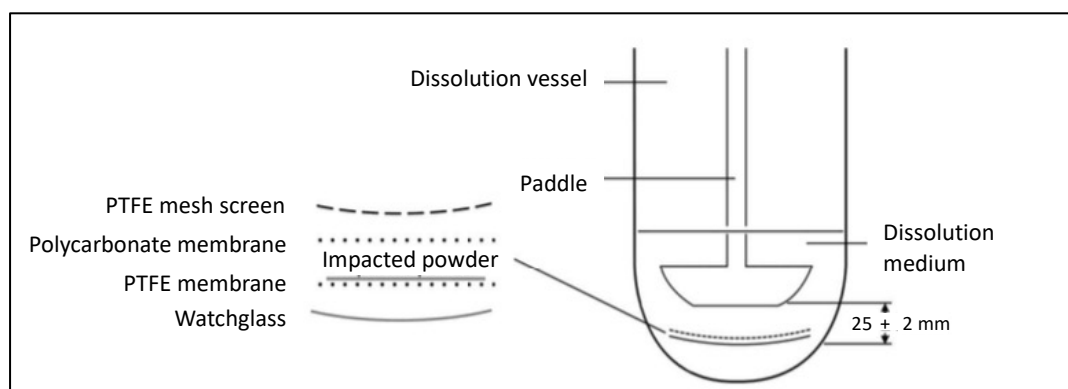

Figure 25: Schematic representation of the dissolution assembly used for the dissolution test, *Levet et al., 2016* [187]. PTFE stands for polyfluorotetraethylene.

In parallel, DPPC suspension was prepared as follows: 200 mg of DPPC was weighed into a round-bottom flask and dissolved in 40 mL of a mixture of chloroform and methanol (1:1), after which the solvent was evaporated using a rotary evaporator [210]. The dry film was rehydrated with 200 mL Milli-Q water at 55°C and agitated for 2h, then ultrasonicated for 1h. The suspension was kept at 4°C (for maximum 48h) and added to the saline part immediately before use [210].

Dissolution testing was performed in accordance with sink conditions at 37 ± 1°C, pH 7.35 ± 0.05, with a paddle rotating speed of 50 ± 2 rpm and the paddles placed at 25 ± 2 mm between the blade and the centre of the dose collector assembly. Volumes of 2.0 mL were sampled at pre-established times between 2 min and 24h, filtered on 0.22 μm pore-size cellulose acetate syringe filters (VWR, Leuven, Belgium) and analysed for their platinum content by the validated ETAAS method [187]. These samples were immediately replaced with 2.0 mL of mSLF. At the end of the dissolution test, the dose collector assembly was opened into the dissolution vessel and incubated for an additional hour to determine the 100% cisplatin dissolution value. Data are presented as the mean percentages of dissolved cisplatin *vs.* time (means ± SD, n=3).

To compare our dissolution profile to the one generated by Levet *et al*., the difference (f_1) and the similarity (f_2) factors were used as recommended by the FDA Guidelines for Industry. Dissolution profiles were considered similar in the case of $f_1 < 15$ (close to 0) and $f_2 > 50$ (close to 100).

2.3.3. *In vivo* **efficacy study of CIS-DPI-TS**

2.3.3.1.   Mouse strains and housing conditions

Female 6-week-old BALB/c mice (for the M109-HiFR-lung carcinoma model) (16-20g) were purchased from Janvier Labs (Le Genest-Saint-Isle, France) and Charles River (Écully, France) and kept under conventional housing conditions (12h/12h night and day cycles, $22 \pm 2°C$, $55 \pm 10\%$ RH) and were given dry food and water *ad libitum*. Once entered in the studies, mice were weighed three times a week and were euthanized if their weight loss exceeded 20% when compared to the first experiment day, or 15% when compared to the last weighing. All experiments were performed in accordance with EU Directive 2010/63/EU for animal experiments and were approved by the CEBEA (Comité d'Ethique et du Bien-Être Animal) of the ULB faculty of medicine under approval number 585N.

2.3.3.2.   Intrapulmonary engraftment

Cell culture and preparation of cell suspension for engraftment

The M109-HiFR mouse-lung carcinoma cells were cultured, as described previously [211]. Briefly, cells were cultured in folate-free RPMI supplemented with 10% (v/v) FBS, 1% (v/v) penicillin-streptomycin and 0.02% (v/v) gentamycin in an incubator with 5% CO_2, at 37°C. The medium was renewed each 2-3 days, as recommended by the ATCC guidelines. The cell suspension was prepared in order to target 1.4 million M109-HiFR cells in 20 μL of a 50:50 (v/v) mixture of folate-free RPMI/Matrigel® and renewed each hour during the intrapulmonary engraftment [211].

Intrapulmonary engraftment

Mice were anesthetized using ketamine (150 mg/kg)/xylazine (2mg/kg) delivered using the intraperitoneal (IP) route, the skin in the upper region was delicately opened and the muscles were torn to obtain a clear view of the intercostal area. After which, the cell suspension was inoculated between the third and fourth costal bone in the lung parenchyma. The muscle and skin were sutured using Ethicon Inc 3-0 silk (Johnson & Johnson, Somerville, USA).

2.3.3.3.   Preparation and administration of CIS-DPI-TS and CIS-IV_1.5
                to mice

CIS-DPI-TS was produced and characterized, as detailed in the previous sections *(sections 2.3.1 and 2.3.2)*. To deliver a dose of 0.5 mg/kg of CIS-DPI-TS to grafted mice, this formulation was first mixed with a dry diluent (spray-dried mannitol-leucine (90:10 w/w)) then administered

using a DP-4M Dry Powder Insufflator™ for a mouse (Penn-Century Inc., USA). To be closer to clinical practice, one week was designated as one cycle of treatment and the treatments were administered over two cycles. Cisplatin was diluted in saline to reach a final concentration of 0.15 mg/mL and was administered via IV (CIS-IV) (200 μl by tail vein) at 1.5 mg/kg (CIS-IV_1.5) the first day of each cycle for two cycles, while CIS-DPI-TS was delivered to grafted mice using the ET route three times per cycle (i.e. Mondays, Wednesdays and Fridays). The treatment administration was initiated 6 days following the intrapulmonary graft. Both CIS-DPI-TS (n=15) and CIS-IV_1.5 (n=6) were compared to the untreated group (n=6). The treatment preparation and the techniques of administration will be further detailed in *sections 2.4.4.2 and 2.4.4.3*.

2.3.4. *In silico* prediction of pharmacokinetic parameters using GastroPlus™ software

2.3.4.1. *In vitro* and *in vivo* data

The *in vivo* data considered for the *in silico* prediction were generated by the PK study done by Levet *et al.* during which an immediate-release cisplatin-based DPI (IR_CIS-DPI) and a cisplatin solution were administered to mice at 1.25 mg/kg using the ET or IV routes. IR_CIS-DPI was prepared as described for CIS-DPI-TS, but without TS (Cisplatin/TPGS: 95:5 (% w/w)). The composition, drug content and dissolution profiles are reported in **Table 11**.

Table 11: Theoretical composition, measured platinum content determined by ETAAS and the *in vitro* released percentages from CIS-DPI-TS. The CIS-DPI-TS was fractionated on an FSI filter (fraction below 5 μm) and packaged onto a watch glass covered with a polyfluorotetraethylene (PTFE) and polycarbonate membrane and a PTFE mesh screen in simulated lung fluid (400 ml, 37.0 ± 0.2°C, pH 7.35 ± 0.05) under 50 rpm of stirring (mean ± SD, n=3), from *Levet et al., 2016*.

Formulation	Theoretical composition (% w/w)	Platinum content (% w/w ± SD, n=9)	Percentage release vs time (% w/w)		
			5 min	1h	2h
IR-CIS-DPI	Cisplatin/TPGS : 95/5	95.6 ± 2.6 %	93.6 ± 8.6 %	97.1 ± 0.6 %	100.0 ± 0.0 %

Platinum quantification and *in vitro* dissolution profiling were performed using the techniques described in the previous *sections 2.3.2.1* and *2.3.2.6*. Cisplatin administration was performed via the IV (CIS-IV_1.25) or ET routes using a cisplatin solution (ET-SOL) or an IR_CIS-DPI (ET- IR_CIS-DPI) to CD1 mice. The techniques of administration will be further detailed in *section 2.4.4.3*.

2.3.4.2.   Converting *in vivo* data into PK parameters using PKPlus^{TM}

The *in vivo* data that illustrate the evolution of the plasma concentration *vs.* time **(Figure 26)** after CIS-IV_1.25, ET-SOL and ET- IR_CIS-DPI administrations of 1.25 mg/kg of cisplatin were loaded into the PKPlus^{TM} module of GastroPlus^{TM} software (Simulation Plus, Lancaster, USA). The PKPlus^{TM} was able to convert the *in vivo* data into PK parameters using non-compartmental and one-, two- or three-compartment models [212]. It then selected the compartmental model that best fitted the *in vivo* data. These parameters were then considered as the observed values derived from the experimental *in vivo* data and were compared to the values simulated by GastroPlus^{TM} software (Simulation Plus, Lancaster, USA). Furthermore, the selected IV PK parameters were used for the ET administration of SOL and DPI to describe the cisplatin distribution and clearance when it arrives in the bloodstream from the lungs.
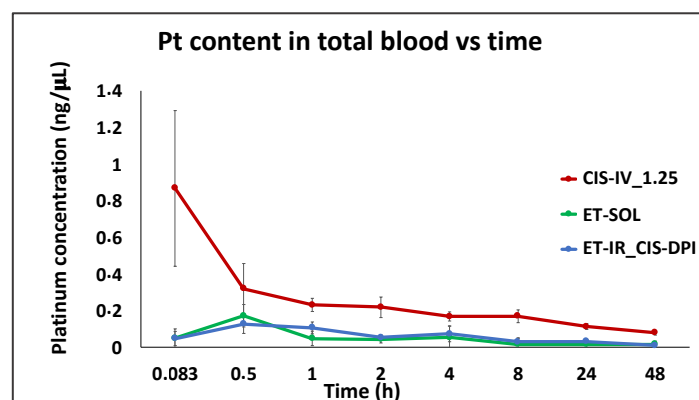

Figure 26 : Plasma concentrations *vs.* time profiles of cisplatin after an IV (CIS-IV_1.25), and ET administrations of a cisplatin solution (ET-SOL) and IR_CIS-DPI of 1.25 mg/kg of cisplatin in mice, from *Levet et al., 2017* [203].

2.3.4.3.   *In vivo* prediction using GastroPlus^{TM}

Compound characteristics

The molecular formula ($Cl_2H_6N_2Pt$), the MW (300.05 g/mol) and the logD (-2.19 at pH=7) of cisplatin were entered manually into the selected compound tab. The dosage form and the initial dose were selected depending on the ongoing simulation (IV or pulmonary (PL); solution, powder). The initial dose was adapted to the mean mouse bw. The solubility of cisplatin in water (2.53 mg/mL) was found in the Merck Index [213]. The default values provided by Gastroplus^{TM} were used for the mean precipitation time (900 sec), and for the drug-particle density value (1.2 g/mL). The diffusion coefficient (0.768×10^5 cm^2/s) was estimated by GastroPlus^{TM}, relying on the cisplatin molecular formula. The default effective permeability provided by GastroPlus^{TM} was used.

Loaded files

To compare the calculated results to the observed ones, the experimental *in vivo* plasma-concentration-time profiles were loaded for the CIS-IV_1.25, ET-CIS and ET- IR_CIS-DPI formulations. These data were only used as a comparison as the software did not take them into account to run the simulation. The experimental values were then automatically plotted graphically. Furthermore, the *in vitro* dissolution profile *vs.* time was also loaded and used by GastroPlus^{TM} to perform the *in vivo* PK IR_CIS-DPI simulation.

Additional dosage routes module: nasal-pulmonary module

The nasal-pulmonary module developed by SimulationPlus^{TM} was used for the ET-SOL and ET-IR_CIS-DPI. The animal model, called "physiology", was switched to mice while the default lymph volume (1.985×10^{-3} mL) and the total lung volume (0.49987 mL) values were kept. Regarding the parameters related to the drug, "the compound" parameters, the lymph transit was set to 0 as the default value given by GastroPlus^{TM}.

The "pulmonary deposition model" describes the percentage deposited in each compartment. It was defined for each formulation based on the drug recovery in the lungs published by Levet *et al.* [187].The actual platinum content was quantified in the lungs 2 min after administration and compared to the theoretical emitted dose from the device (ET-SOL: $21 \pm 9\%$, ET-IR_CIS-DPI: $35 \pm 22\%$) [187]. The drug recovery values were entered directly into the bronchiolar and alveolar-interstitial compartments (50% each).

Values for all the characteristics related to the pulmonary module were set up by default. These characteristics included the pulmonary permeability (PP), metabolic clearance, systemic absorption rate (SAR), binding to mucus or cells, and physiologic characteristics of each compartment. To develop a model that best fitted the cisplatin formulations, two pulmonary parameters – the PP and the SAR – were optimized for the ET-SOL administration before being transposed to the ET-IR_CIS-DPI form. Each of these two pulmonary parameters was decreased or increased by a factor of 10 separately (PP: from 10^{-6} to 10^{6} cm/s, SAR: from $4.82.10^{-5}$ s^{-1} to $4.82.10^{5}$ s^{-1}). Then, the PP and the SAR were both changed using the same factor. As soon as the PK parameters were reached, the pulmonary parameters were considered as optimized, and the simulation results were named "optimized values".

2.4. Preparation and *in vitro* evaluation of new cisplatin DPIs

2.4.1. Preparation of CIS-DPI-33 and CIS-DPI-50

Cisplatin-based DPI were prepared following an adaptation of the protocol described by Levet *et al.* [187], as detailed in the previous *section 2.3.1*. Modifications in terms of excipients, solvent and processes were performed, and are described hereunder. Briefly, 5% w/v cisplatin was suspended in ethanol. The cisplatin was reduced in size by means of, first, high-speed homogenization (following the same parameters as in *section 2.3.1)* then HPH for 40 cycles at 1 000 bars in a closed configuration (EmulsiFlex-C3, Avestin Inc., Ottawa, Canada), with a heat exchanger placed ahead of the homogenizing valve maintained at $15 \pm 1°C$. Samples of the reduced cisplatin were then analysed by means of the laser diffraction method (Malvern Mastersizer 3000 with a Hydro MV dispenser, Malvern Panalytical, Worcestershire, UK) described previously *(section 2.3.2.2)*. HCO and TPGS were added to the pre-heated $(55 \pm 5°C)$ cisplatin suspension to obtain a final concentration of *(i)* 50% w/w cisplatin and 50% w/w HCO/TPGS (99:1 w/w) mixture for CIS-DPI-50, and *(ii)* 33% w/w cisplatin and 67% w/w HCO/TPGS (99:1 w/w) mixture for CIS-DPI-33. The cisplatin suspension mixtures were spray dried (Mini-Spray Dryer B-290, Büchi Labortechnik AG, Flawil, Switzerland) under the same operating parameters as for CIS-DPI-TS *(section 2.3.1)*. The powders were collected from a high-performance cyclone separator with a yield of ~ 60% and stored in a desiccator at room temperature. A single batch of each formulation was prepared and characterized for its cisplatin content *(section 2.3.2.1)*, *in vitro* FPD, particle shape, and morphology and dissolution-release profile (see below).

2.4.2. Characterization of CIS-DPI-33 and CIS-DPI-50

2.4.2.1. Crystalline state

The crystalline states of raw HCO and spray-dried HCO and TPGS were assessed by X-ray powder diffraction using a D5000 diffractometer (Siemens, Munich, Germany) as described previously [187]. This apparatus was equipped with a mounting for Bragg-Brentano diffractometer associated to a monochromator and software (Bruker Belgium SA, Brussels, Belgium).

2.4.2.2. Particle shape morphology

The particle shape and morphology were determined using scanning electron microscopy . The particles were mounted onto 12-mm double-sided sticky carbon pads, coated with platinum

using standard procedures, analysed using a Tecnai FEG ESEM Quanta 200 scanning electron microscope (FEI, Hilsboro, USA) and imaged using iTEM software (FEI, Hilsboro, USA).

2.4.2.3. Determination of the fine particle dose and fraction using a fast-screening impactor

The FPD, and its expression as an FPF_d and an FPF_n, of CIS-DPI-33 and CIS-DPI-50 were determined using an FSI with the low-resistance RS.01 device, selected in the preliminary device study. The process used a size 3 HPMC capsule hand-filled with 20.0 ± 0.5 mg powder as previously described [187]. Briefly, a pressure drop of 4 kPa in the device was reached with an aspiration flow rate of 100 L/min applied for 2.4 s (inhaled air volume of 4 L) and measured using a DFM3 flow meter (Copley Scientific, Nottingham, UK). This flow rate was obtained with an HCP5 air pump (Copley Scientific, Nottingham, UK) connected to a TPK critical flow controller (Copley Scientific, Nottingham, UK). The collection and solubilisation of cisplatin particles was performed by means of dimethylformamide, and the platinum content of the different collection samples was determined by the validated ETAAS method *(section 2.3.2.1)*.

2.4.2.4. Dissolution release profile

Dissolution properties of CIS-DPI-50 and CIS-DPI-33 were established by means of the dissolution system for dose collection developed by Copley Scientific for DPI release-profile studies, with a method adapted from the "paddle over disc" method, as described previously *(section 2.3.2.6)*.

2.4.3. Production and characterization of the selected cisplatin-based DPI formulation

A total of three independent batches of CIS-DPI-50 (batch size of ~3g) were produced following the procedures described in *section 2.4.1*. Yields comprised between 55 and 65%. The three batches were characterized by means of the methods described previously in terms of cisplatin content (ETAAS; *section 2.3.2.1*), PSD (laser diffraction; *section 2.3.2.2*), residual solvent (thermogravimetric analysis; *section 2.3.2.3*) and thermal properties (DSC; *section 2.3.2.4*).

The aerodynamic performance of CIS-DPI-50 was evaluated according to European Pharmacopeia 10, section 2.9.18 for DPIs. The DDU and APSD from an NGI (Copley Scientific, Nottingham, UK – Apparatus E) were determined using the low-resistance RS.01

device previously selected (containing a size 3 HPMC Vcaps capsule hand filled with 20.0 ± 0.5 mg powder). This was performed under the same conditions as in *section 2.3.2.5.*

The collected cisplatin masses were then plotted using Copley Inhaler Testing Data Analysis Software 1 (Copley Scientific, Nottingham, UK) to obtain the FPD and FPF (i.e. FPF_d and FPF_n), calculated as a percentage of the nominal dose, and the APSD parameters, including the MMAD and the GSD. The mean DDU and the APSD evaluation were both determined using 1 capsule/test and repeated on 10 and 3 replicates per batch, respectively. Data are presented as the means of three independent batches $\pm$ SD.

To evaluate the influence of lower respiratory airflows (i.e. for impaired respiratory function of lung cancer patients), the aerodynamic performance of CIS-DPI-50 was characterized using an FSI, the low resistance RS.01 device previously selected (containing a size 3 HPMC Vcaps capsule hand-filled with 20.0 ± 0.5 mg powder), at three different airflows (100 L/min for 2.4 s, 60 L/min for 4 s and 40 L/min for 6 s). This was done to evaluate the dependency of the aerodynamic performance on the airflow. The deposition in the capsule, device, throat and pre-separator were analysed as well the aerodynamic parameters (FPF_n, FPF_d and FPD) using Copley Inhaler Testing Data Analysis Software 1 (Copley Scientific, Nottingham, UK).

Finally, the stability of CIS-DPI-50 over 6 months (after 1 month, 3 and 6 months) for one batch was evaluated under normal conditions (25°C, 60% RH). To do so, CIS-DPI-50 was hand-filled into 3 HPMC Vcaps capsules and put with a desiccant into a container. The residual solvent content, thermal properties *(section 2.3.2.3)*, geometric PSD and APSD parameters (NGI, 100 L/min), were evaluated following the methods described above in this section and in *section 2.3.2.5*. This was compared to the initial parameters (T0) obtained in the week following CIS-DPI-50 production at the latest. This study was conducted in collaboration with Inhatarget Therapeutics.

2.4.4. *In vivo* PK experiment using the selected cisplatin-based DPI formulation

2.4.4.1. Mouse strains and housing conditions

Female 4-8-week-old CD1 mice (for PK studies) (16-20g) were purchased from Janvier Labs (Le Genest-Saint-Isle, France) and Charles River (Écully, France). All experiments were approved by the CEBEA of the ULB faculty of medicine under approval number 719N. All housing conditions were identical to those described in *section 2.3.3.1.*

2.4.4.2.　　　Preparation of CIS-DPI-50 for *in vivo* delivery

CIS-DPI-50 was blended with a previously developed diluent powder for *in vivo* experimentation to deliver a cisplatin inhaled dose with good performance through the ET device adapted to mice [203].

Indeed, Levet *et al*. have already validated an adapted diluent for CIS-DPI-TS in terms of composition and process of production. In addition, they have also optimized the technique of blending with CIS-DPI-TS and validated its homogeneity in terms of dose and content [203]. Consequently, the production of the vehicle, the blending procedure and the uniformity of drug content used routinely will be presented hereunder.

Production of the diluent

A solution of mannitol (1%, w/v) and L-leucine (0.1% w/v) was prepared in Milli-Q water and stirred until full dissolution then spray dried using a B-290 Mini Spray Dryer (Büchi Labortechnik AG, Flawil, Switzerland) equipped with a B-296 dehumidifier (Büchi Labortechnik AG, Flawil, Switzerland) to maintain RH at 50%. This was conducted using the following parameters: feed rate, 3.0 g/min; inlet temperature, 130°C (corresponding to an outlet temperature ~56°C); 0.7 mm nozzle; compressed air, 800 L/min; and drying air flow, 35m^3/h. The collected powder was sieved through a 355 μm stainless steel mesh before blending.

Blending procedure

CIS-DPI-50 was diluted to deliver ~1.0 mg of powder to mice to target 2% of cisplatin to achieve a dose of 1 mg/kg. This was done by blending CIS-DPI-50 and the diluent in a total mass of 250 mg using a 2 mL glass vial following the so-called sandwich method. Practically, to target 2% of cisplatin in the formulation, an amount of 10 mg of CIS-DPI-50 was added to 240 mg of diluent. The powders were blended using a Turbula 2C 3D motion mixer (Bachofen AG, Uster, Switzerland) at 46.2 rpm for 4h. At the end of this process, the blend was sieved twice using a 355 μm stainless steel mesh to deagglomerate the particles.

Uniformity of drug content

Samples of 5.00 mg of the obtained blend were characterized in terms of cisplatin content *(section 2.3.2.1)* and uniformity (n=10, expressed as a percentage of difference from the mean), as recommended by European Pharmacopeia v.10 (contents ranging between 85 and 115% from the mean drug content with maximum one drug content within the 75-125% limits of the mean drug content).

2.4.4.3.   Administration of *in vivo*-evaluated formulations

The delivery of CIS-DPI-50 blend was performed throughout the ET route. Mice were anesthetized using ketamine (150 mg/kg)/xylazine (2mg/kg) delivered using the IP route. Once anesthetized, mice were put in an angled board to deliver the CIS-DPI-50 directly into the mice trachea using an ET device for dry powders (Dry Powder Insufflator™ model DP4-M®, Penn-Century) [214].

The delivery of cisplatin using the IV route (CIS-IV_1.5) was performed at 1.5 mg/kg through the caudal vein, which had been previously pre-heated to vasodilate it. Cisplatin solution was prepared in NaCl 0.9% at 0.150 mg/mL immediately before use, kept protected from light and renewed each day. Mice were weighed immediately before the administration, and the exact volume of CIS-IV solution to target 1.5 mg/kg was adapted for each individual.

2.4.4.4.   Pharmacokinetic profiles of CIS-DPI-50 and CIS-IV_1.5 in healthy mice

CIS-DPI-50 blend was administered at 1 mg/kg cisplatin through ET administration. Retro-orbital blood for plasma (heparinized tubes, centrifuged at 2 000 g for 10 min at 20°C) and organs (lungs, liver, kidneys and spleen) was collected at nine timepoints comprised between 1 min and 48h following the administration of the CIS-DPI-50 blend (n=5-6 mice per timepoint). Organs were washed in PBS and stored at -80°C until platinum content analysis.

The PK profiles of cisplatin in the organs and plasma were established and PK curves of cisplatin and its adducts were graphed as platinum concentration *vs.* time curves. PK parameters were calculated following a standard non-compartmental analysis and included C_{max}, T_{max}, and AUC. The initial and terminal elimination rate constants k_{el}^i and k_{el}^t were calculated from the log regression of platinum concentration *vs.* time curves between the three first and the three last dosing timepoints, respectively. The initial and terminal half-life $t_{1/2}^i$ and $t_{1/2}^t$ were calculated as $\ln(2)/ k_{el}^i$ and $\ln(2)/ k_{el}^t$, respectively. The $AUC_{0-\infty}$ was estimated by means of the trapezoidal method from 1 min to 48h for all organs and plasma. The targeting advantage (T_a) of CIS-DPI-50 was calculated following **Equation 3** ([215]) to be compared with CIS-IV_1.25 and with the T_a obtained with CIS-DPI-TS and IR-CIS-DPI, by Levet *et al.* [203].

$$T_a = \frac{AUC_{lungs}^{CIS-DPI-50}}{AUC_{lungs}^{CIS-IV\_1.25}}$$

Equation 3: Calculation of the targeting advantage (T_a).

To be able to compare the kinetics data obtained with previously published data, PK parameters (C_{max}, $t_{1/2}^i$ and k_{el}^i) were generated with CIS-IV_1.5 following the same procedure. Sampling procedures (see above) were performed at 1-, 10- and 30-min post-administration and C_{max}; $t_{1/2}^i$ and k_{el}^i were calculated for all organs and plasma (n=5 mice per timepoint).

2.4.4.5. Platinum content for *in vivo* samples

The organs were digested in Suprapur® HNO_3 for three hours before platinum assay, as described previously [203]. The platinum assay in plasma was performed by means of an adaptation of a method described previously [203,216]. The limit of detection (LOD) and of quantification (LOQ) of the methods are indicated in the corresponding graphs and were 0.075 and 0.225 ng/mg in lungs and kidneys and 0.025 and 0.075 ng/μL in plasma. These analyses were performed using a SpectrAA 220Z atomic absorption spectrometer equipped with a GTA-96 graphite tube atomizer (Varian, Mulgrave, Australia).

2.5. Statistical analyses

All statistical tests were conducted using GraphPad PRISM® (7.0a) software. The Kaplan-Meier curve, log-rank test and two-way ANOVA with Tukey-multiple comparison test with an analysis of the *p* value by means of the Holm-Šídák method were used for the survival analysis. One-way ANOVA and Bonferroni's post-testing was used to measure the differences observed between flow rates (i.e. 100 L/min, 60 L/min, 40 L/min) in terms of aerodynamic performance. Results were considered as statistically significant (*) for $p < 0.05$, very significant (**) for $p < 0.01$, extremely significant for $p < 0.001$ (***) and extremely significant for $p < 0.0001$(****). Results are presented as the mean value ± SD, unless otherwise indicated.

3. Results and discussion

3.1. Preliminary studies on CIS-DPI-TS

3.1.1. CIS-DPI-TS production and characterization

CIS-DPI-TS demonstrated similar characteristics to those obtained by Levet *et al*. [187]. Indeed, the cisplatin size after HPH was identical ($0.888 \pm 0.008\ \mu$m *vs*. $0.89 \pm 0.01\ \mu$m), with less solvent evaporation (i.e. initial suspension concentration of 5% *w/v*) than reported by Levet *et al*. as the cisplatin content after HPH was $4.61 \pm 0.06\%$ *vs*. 5.3% for Levet *et al*. **(Table 12, [187])**. Moreover, the cisplatin content, once the cisplatin suspension spray dried, was similar, and was close to the theoretical composition ($48 \pm 2\%$ *vs*. $49 \pm 2\%$ for Levet *et al*.). Similar

results were also observed for the residual solvent content ($0.05 \pm 0.002\%$ *vs.* $0.11 \pm 0.02\%$ for Levet *et al.* **Table 12**). The residual solvent content was low in both cases, demonstrating that the spray-drying technique was adapted *(i)* for the solvent evaporation (suggesting low local toxicities related to the use of IPA) and *(ii)* for the elimination of water moisture from the powder (good prognosis for long-term stability).

Table 12: Characterization of CIS-DPI-TS in terms of cisplatin particle size and content after HPH, geometric PSD, cisplatin content after spray drying, residual solvent content and aerodynamic behaviour using a RS.01 device (mean $\pm$ SD, n=3). These data were compared to *Levet et al., 2016* results [187].

Characterization	Generated result	Published result by Levet *et al.*, 2016
Cisplatin size after HPH (Dv 50, µm)	0.888 ± 0.008	0.89 ± 0.01
Cisplatin content after HPH (%, w/w)	4.61 ± 0.06	5.3
Geometric particle size distribution after spray-drying - Dv (10) (µm) - Dv (50) (µm) - Dv (90) (µm) - D [4,3] (µm) - % <5 µm	2.12 ± 0.02 3.55 ± 0.03 5.6 ± 0.1 3.70 ± 0.04 75 ± 2	- 4.2 ± 0.2 - 4.4 ± 0.1 63 ± 3
Cisplatin content after spray-drying (%, w/w)	48 ± 2	49 ± 2
Residual solvent content (% w/w)	0.05 ± 0.02	0.11 ± 0.02
Aerodynamic behaviour - FPF_n (% w/w) - FPD (mg) - MMAD (µm) - GSD (µm)	40 ± 2 3.9 ± 0.2 2.9 ± 0.1 2.1 ± 0.4	37 ± 2 3.7 ± 0.2 2.4 ± 0.2 -

In addition, the DSC curves obtained from the spray-dried powder were similar to those obtained by Levet *et al.*, with the crystalline state of cisplatin being maintained throughout the process and the presence of the stable polymorph β for TS. These results are both promising for the long-term stability of CIS-DPI-TS [187]. However, although close, the geometric PSD was smaller than already published. Indeed, the Dv (50) was 3.55 ± 0.03 μm *vs.* 4.2 ± 0.2 μm for Levet *et al.*, and the fraction of particles under < 5 μm was higher in our case ($75 \pm 2\%$ *vs.* $63 \pm 3\%$, **Table 12**). However, this did not have a major impact on the aerodynamic behaviour as the aerodynamic parameters were close, with similar FPF_n ($40 \pm 2\%$ *vs.* $37 \pm 2\%$), FPD (3.9 ± 0.2 mg *vs.* 3.7 ± 0.2 mg) and MMAD (2.9 ± 0.1 μm *vs.* 3.7 ± 0.02 μm), as represented in **Table 12**.

Cisplatin release from CIS-DPI-TS particles was also assessed and was very similar to that described by Levet *et al*., as illustrated in **Figure 27**. Indeed, the difference factor f_1 was -6.77 (< 15) and the similarity factor f_2 was 87.04 (> 50), which demonstrated statistical similarity between these two profiles. Cisplatin was released from CIS-DPI-TS particles gradually, which demonstrated its controlled-release properties ($31\pm10\%$, $44\pm10\%$ and $55\pm13\%$ within 1h, 6h and 24h, respectively).

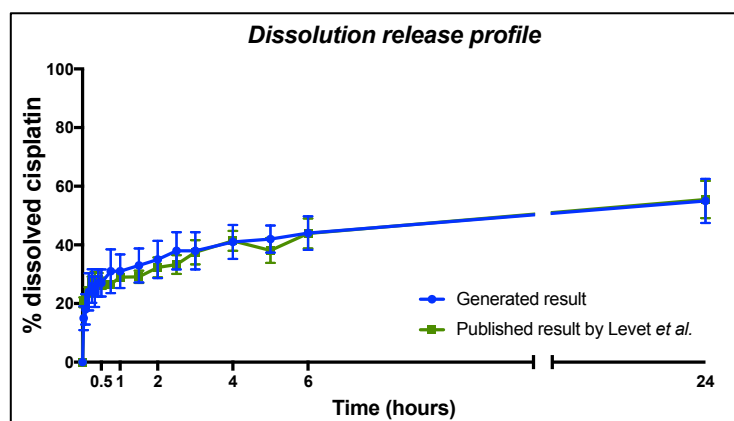Figure 27: Dissolution-release profile of CIS-DPI-TS (mean ± SD, n=3), determined following its impaction on an FSI filter using the RS.01 device (100L/min, 2.4 s). These data were compared to *Levet et al., 2016* results [187].

3.1.2. Selection of the most suitable single-dose device

The aim of this part was also to select a single-dose device characterized by the best aerodynamic performance. These devices were also chosen because they are inexpensive, simple to use, convenient, portable and adapted for single use for DPI formulations of up to 40-50 mg. All these points are needed for the development of inhaled anti-cancer drugs, where an efficient and disposable DPI inhaler is required to limit environmental exposure [173].

It should be mentioned that the quantification of deposition in the capsule was included in the device fraction in **Figure 28**. This is because none of the devices, except RS.01, required the use of a capsule. Interestingly, the cisplatin mass retrieved in the capsule for RS.01 was low, at $1.1 \pm 0.3\%$. The deposition patterns and the aerodynamic parameters showed a more advantageous profile for RS.01 in comparison to the three other devices (**Figure 28**). Indeed, the deposition in the device may explain these differences, as $5 \pm 2\%$ was retrieved for RS.01, while this was 5- to 6-fold higher for the other devices ($32.5 \pm 0.7\%$ for the commercial high-resistance device, 25% for the prototype 1 high-resistance device and 33% for the prototype 2 medium-resistance device).
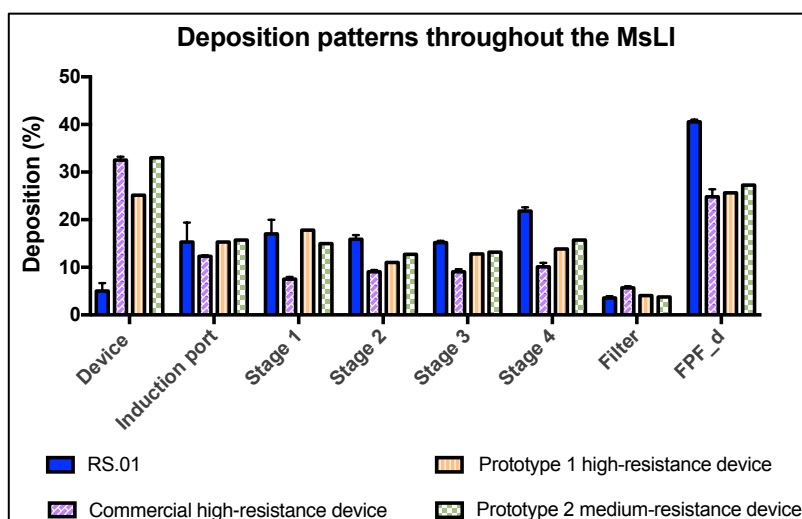
Figure 28: Deposition patterns throughout the MsLI and FPF_d as the fraction of the nominal dose of the CIS-DPI-TS. This was conducted on 20 mg powder mass using an HPMC capsule n°3 for RS.01 (mean ± SD, n=3), or directly in the device for the commercial high-resistance device, the prototype 1 high-resistance device and the prototype 2 medium-resistance device (mean, n=1).

Moreover, except for stage 4 (RS.01: 21.8 ± 0.7%, commercial high-resistance device: 10.1 ± 0.8, the prototype 1 high-resistance device: 14%, the prototype 2 medium-resistance device: 16%) for which relatively higher disparities in terms of deposition between the devices were observed, all other stages (stages 1, 2, 3 and filter) were characterized by similar deposition fractions.

These differences directly impacted the aerodynamic parameters. Consequently, the FPF_d observed for RS.01 (40.6 ± 0.5%) was higher than for the other devices (commercial high-resistance device: 25 ± 2%, prototype 1 high-resistance device: 25.6% and prototype 2 medium-resistance device: 27.3%, **Table 13**). This was related to a similar trend for the FPD (RS.01: 3.77 ± 0.04 mg, commercial high-resistance device: 1.8 ± 0.1 mg, prototype 1 high-resistance device: 1.73 mg, prototype 2 medium-resistance device: 2.17 mg, **Table 13**). These trends all seemed to be related to flow rate intensity. The higher the flow rate was, the higher the FPF_d and FPD and the lower the MMAD and GSD. This observation was directly related to the device resistance. Indeed, as mentioned previously, a device resistance should be high enough to store the energy coming from the patient inspiratory flow and low enough that it can be used by patients with altered pulmonary function. It has been reported that the narrower the internal diameter of the device was, the higher the turbulence, which led to more efficient powder fluidization and to a higher FPF [217]. Indeed, this observation could explain the differences observed between the prototype 1 high-resistance device and the prototype 2

medium-resistance device as these devices had the same geometry but different internal diameters.

Table 13: Aerodynamic performances of CIS-DPI-TS using the different selected devices, RS.01, commercial high-resistance device (mean ± SD, n=3), prototype 1 high-resistance device and prototype 2 medium-resistance device (mean, n=1), at the appropriate flow according to their resistance.

Devices	RS.01	Commercial high-resistance device	Prototype 1 high-resistance device	Prototype 2 medium-resistance device
Deposition flow rate (L/min)	100	39	36	56
FPF_n (% w/w)	39.7 ± 0.5	19 ± 1	18.1	22.4
FPD (mg)	3.77 ± 0.04	1.8 ± 0.1	1.73	2.17
MMAD (μm)	2.77 ± 0.08	4.3 ± 0.2	4.77	3.86
GSD (μm)	1.67 ± 0.02	3.0 ± 0.1	1.85	1.81

Therefore, it seems clear that RS.01 was characterized by the lowest resistance for the same pressure (4 kPa) applied on all devices, RS.01 had the highest air flow rate, followed by prototype 2 (medium-resistance device), prototype 1 (high-resistance device) and finally by the commercial high-resistance device. Considering that lung cancer patients (especially those in advanced stages) often have impaired lung function with limited inspiratory capacity, it is highly probable that they will not be able to achieve high air flows (as with the RS.01 device) using high-resistance devices. Therefore, this would highly impact the deposition in the deeper lung.

3.1.3. Evaluation of the efficacy of CIS-DPI-TS on the M109-HiFR lung carcinoma model

Considering the efficacy results obtained with CIS-DPI-TS on the M109-HiFR lung carcinoma model and the scheme of administration selected by Levet *et al*. [205], as well as our aim to propose CIS-DPI-50 as a combination with IV chemotherapy, it was interesting to investigate the efficacy of CIS-DPI-TS using a regimen closer to clinical practice.

The scheme of administration evaluated so far had been 3 administrations of CIS-IV or CIS-DPI-TS over 2 weeks [205]. However, as our aim is to deliver a cisplatin-based DPI during the off-cycles encountered with CIS-IV, it was interesting to designate each treatment week as a cycle. Therefore, at the beginning of each cycle, a single CIS-IV administration was performed, while 3 administrations of CIS-DPI-TS per cycle (corresponding to treatment administrations during off-cycles) were delivered to M109-HiFR grafted mice.
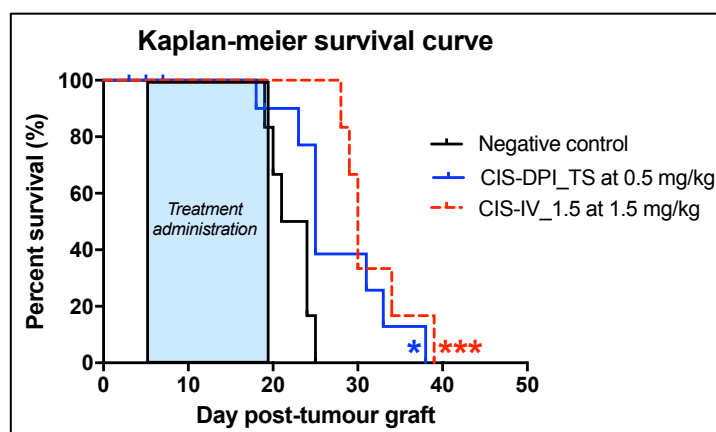
Figure 29: Kaplan-Meier survival curves of M109-HiFR lung carcinoma-grafted mice. Mice were left untreated (negative control, n=6), were treated with CIS-IV_1.5 (n=6) or with CIS-DPI_TS (n=15). The statistical analyses were performed *vs.* the control groups using a log-rank test (*** for $p < 0.001$ and * for $p < 0.05$). No significant difference was found between the CIS-DPI-TS and CIS-IV_1.5 ($p > 0.05$, two-way ANOVA with Tukey-multiple comparison test).

The treatment efficacy was investigated by evaluating the median survivals. Both CIS-DPI-TS at 0.5 mg/kg used once a cycle for two consecutive cycles and CIS-IV_1.5 administered three times a cycle for two consecutive cycles on D6 post-tumour graft showed an anti-tumour response in comparison with untreated mice **(Figure 29)**. Indeed, both treatments significantly prolonged survival in comparison to the negative control group ($p < 0.05$ and $p < 0.001$, respectively). However, for the same cumulative dose, no significant difference in terms of survival was reported between the mouse groups treated with CIS-DPI-TS or CIS-IV_1.5 ($p > 0.05$) **(Figure 29)**. These results confirmed the trends obtained with CIS-DPI-TS and CIS-IV_1 and reported by Levet *et al*. [205].

Considering the similarity in terms of survival between the mice treated with a controlled-release CIS-DPI-TS formulation from which cisplatin was released (i.e. the active fraction) continuously and with CIS-IV_1.5 from which the fraction retrieved in the lungs is 100% active fraction, the modulation of cisplatin release from a cisplatin-based DPI would be promising. Indeed, an increased burst effect (i.e. a higher cisplatin active fraction) would permit the tumour to be attacked directly and a high tumour exposure to be maintained as cisplatin is released continuously. Therefore, one aim to optimize the formulation was to increase its burst effect to have an impact on the PK relevant parameters *in vivo* while maintaining the controlled-release and lung-retention properties to keep a sufficient lung-T_a in comparison to IV administration. As the pulmonary PK as well as the achievement of effective cisplatin concentrations in the lungs have an impact on the tumour exposure and therefore on the efficacy of the treatments, it was interesting to evaluate the effect of modifying the release *in vitro* on the PK parameters.

This was done using a predictive model (i.e. GastroPlus™ software) and by modifying the composition of the formulations.

3.1.4. *In silico* prediction of pharmacokinetic parameters using GastroPlus™ software

Developing an *in vitro-in vivo* correlation using an *in silico* tool is one of the most promising strategies for developing high-quality products as quickly as possible, while trying to limit the number of *in vivo* experiments [218]. The GastroPlus™ software helps to adapt the drug formulation by predicting its likely *in vivo* behaviour in the human body using *in vitro* data only. GastroPlus™ has an Additional Dosage Routes Module (ADRM™) that has a nasal-pulmonary module that can simulate solution and powder distribution after pulmonary administration. Therefore, the aim of this part was to predict cisplatin PK parameters considering only *in vitro* data, using ADRM™. This simulation could help to develop more quickly a more advanced cisplatin formulation presenting a suitable PK profile more efficiently. To do so, the first part consisted of developing an *in silico* model that best fitted the IR-CIS-DPI. Once this model was optimized for an immediate-release form (i.e. IR-CIS-DPI), we attempted to adapt it to controlled-release forms such as CIS-DPI-TS.

The first step was to assess an IV model to check whether the simulation results matched the experimental data. As shown in **Figure 30.A**, the default values for CIS-IV_1.25 matched the *in vivo* experimental plotted values. Furthermore, the AUC were similar for both default and observed values (5.42 μg.h/mL *vs.* 6.31 μg.h/mL), meaning that the curves were alike. However, the T_{max} was slightly different (0.08h *vs.* 0.00h) for the calculated values **(Figure 30.D)**. This 5-minute shift was explained by the fact that this timing corresponded to the time required to take the samples from the mice during the in *vivo* experiment. This can also explain why the C_{max} was slightly higher for the default values than for the observed ones (1.20 μg/mL *vs.* 0.87 μg/mL). Considering the SD described by Levet *et al.* [203], the simulated C_{max} was in the observed range (0.87 ± 0.042 μg/mL). The similarity between the curves illustrated by the similar PK parameters between the observed and default acquisition showed that our model was supported by the software and that the pulmonary simulation could be conducted.

To simplify the process, the pulmonary simulation was first assessed with a cisplatin solution and only afterwards with the IR-CIS-DPI, which was administered using the ET route as explained previously. In the case of cisplatin solution, the software did not start by considering the drug dissolution from the powder, but started with its systemic distribution, once deposited

in the lungs. The default values illustrated in **Figure 30.B, C, D** showed that the observed C_{max} was not reached by the default simulation for ET administration of a cisplatin solution or for IR-CIS-DPI (ET-SOL: 0.03 μg/mL *vs.* 0.17 μg/mL and ET- IR_CIS-DPI: 0.05 μg/mL *vs.* 0.13 μg/mL). Moreover, a longer T_{max} was noticed for both formulations (ET-SOL: 0.50h *vs.* 1.70h and ET- IR_CIS-DPI: 0.50h *vs.* 1.60h). Nevertheless, it seemed clear that from 8h, the curves met the 24h and 48h experimental data for both pulmonary formulations. This showed that GastroPlus™ was able to manage the clearance from the blood compartment, but the permeability from the lungs to plasma was underestimated when the default pulmonary parameters were selected. This underestimation led to a longer time to reach the blood compartment, which explained why the observed C_{max} and the T_{max} were both different from the default values.
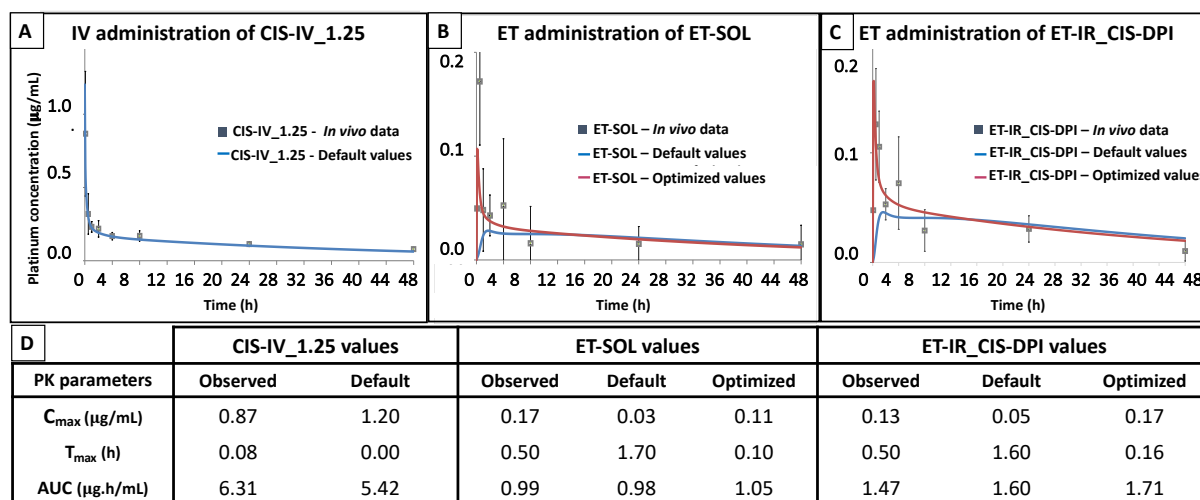

D	CIS-IV_1.25 values		ET-SOL values			ET-IR_CIS-DPI values		
PK parameters	Observed	Default	Observed	Default	Optimized	Observed	Default	Optimized
C_{max} (μg/mL)	0.87	1.20	0.17	0.03	0.11	0.13	0.05	0.17
T_{max} (h)	0.08	0.00	0.50	1.70	0.10	0.50	1.60	0.16
AUC (μg.h/mL)	6.31	5.42	0.99	0.98	1.05	1.47	1.60	1.71

Figure 30: Plasma concentrations *vs.* time profiles simulated by GastroPlus™ using default (blue) and optimized (red) parameters after IV (A) and ET administrations of a cisplatin solution (B) and ET-IR_CIS-DPI (C) compared to the in vivo data (grey dots). The table (D) summarizes the PK parameters values.

The optimization of the pulmonary parameters was previously reported by Salar-Behzadi *et al.* with their study on inhaled budesonide using GastroPlus™ [219]. They reported that better results were obtained when the pulmonary parameters were adapted to a specific drug. During this study, it was noticed that if only one parameter (PP or SAR) was changed, the result remained the same. This meant that the C_{max}, T_{max}, and AUC were not affected (data not shown). This can be explained by the fact that even if a drug can easily cross the pulmonary membrane (characterized by a high PP), it can reach the bloodstream only if the SAR is high enough. Consequently, both pulmonary parameters were changed. Therefore to reach the PK parameters, the PP value was 10-fold higher (optimized value: 10^{-5} cm/s *vs.* default value: 10^{-6}

cm/s) and the SAR value 100-fold higher (optimized value: 10^{-3} s^{-1} *vs.* default value: 10^{-5} s^{-1}) **(Table 14)**. This result was not surprising because cisplatin is a small drug (MW: 300.05 g/mol) compared to others. Its neutral-charge form makes the diffusion across the lipid membranes easier [220]. The drug molecule is reported to use a passive diffusion pathway as well as an active transport mediated by numbers of transporters, mainly OCT1 and OCT2 and CTR1, ATP7A and ATP7B, and multidrug and toxin-extrusion protein 1 (MATE1), as discussed in the introductory part of this work **(Figure 8)** [84]. As a complement, the PP could be verified using *in vitro* tests on Calu-3 cells.

Table 14: PP and SAR values used for the default and optimized simulation.

Pulmonary compartment	Default values		Optimized values	
	PP	SAR	PP	SAR
Extra-thoracic	$1.38.10^{-6}$	$4.82.10^{-5}$	$1.38.10^{-5}$	$4.82.10^{-3}$
Thoracic	$7.38.10^{-6}$	$4.82.10^{-5}$	$7.38.10^{-5}$	$4.82.10^{-3}$
Bronchiolar	$5.57.10^{-6}$	$4.82.10^{-5}$	$5.57.10^{-5}$	$4.82.10^{-3}$
Alveolar-interstitial	$3.05.10^{-4}$	$4.82.10^{-5}$	$3.05.10^{-2}$	$4.82.10^{-3}$

As soon as the PP and SAR were higher, the C_{max} was higher and the T_{max} was lower. These results showed that a larger amount of cisplatin reached the bloodstream faster from the lungs. The optimized curves illustrated in **Figure 30.B, C** after ET administration of a SOL and DPI showed a much better fit to the experimental data than the default curves. This was also confirmed with the PK parameters: the optimized C_{max} was more than 3-fold higher with the optimized pulmonary parameters than with the default ones. This led to a better evaluation of the T_{max}, which was lower than in the default simulation.

Consequently, the optimized PK parameters after ET-SOL administration were closer to the observed values than the default ones. Nevertheless, the C_{max} and the T_{max} were slightly lower than the observed value (e.g. 0.11 μg/mL *vs.* 0.17 μg/mL). On the other hand, the C_{max} was slightly higher for the ET-IR_CIS-DPI but remains in the observed SD range (0.13 $\pm$ 0.05 μg/mL). The T_{max} was also slightly higher during this optimized simulation but was in the same range as the T_{max} after the ET-SOL administration. Nevertheless, it is important to note that the $t_{1/2}$[i] in the lungs is low (ET-SOL: 5.0 min and ET-IR_CIS-DPI: 2.6 min). This result demonstrated that both IR-CIS-DPI and cisplatin solution were absorbed very quickly, as

reported by Levet *et al.* [203], and that the simulated values were consistent with the *in vivo* data.

GastroPlus^{TM} showed that the C_{max} after ET administration of cisplatin solution and IR-CIS-DPI were close, as reported by Levet *et al.* [203]. The software also showed that the powder gives a slightly higher T_{max} than the solution (ET-SOL: 0.10h and ET- IR_CIS-DPI: 0.16h) because it took a minimal time to be dissolved before being recovered in the bloodstream. This may be something that the GastroPlus^{TM} indicated and that can barely be observed *in vivo* because of the experimental difficulties at the first dosing times, as explained before. It also showed that the AUC was higher with the ET-IR_CIS-DPI than with the ET-SOL (1.71 μg.h/mL *vs.* 1.05 μg.h/mL), which was also similar to the experimental data. Moreover, comparing the optimized pulmonary results (ET-SOL and ET-IR_CIS-DPI) to the IV results, there was no doubt that the plasma C_{max} was much higher after the administration of CIS-IV_1.25 than after the administration of ET-SOL or IR-CIS-DPI (1.20 μg/mL *vs.* 0.11 and 0.17 μg/mL). This result was because all the dose went directly into the bloodstream when using the IV route. It also meant that the T_{max} was much lower (0.00h *vs.* 0.10 or 0.16h) and that the AUC was 5- to 3-fold higher (5.42 μg.h/mL *vs.* 1.05 or 1.71 μg.h/mL), as reported by the experimental data.

Once the additional dosage routes module (ADRM^{TM}) was adapted to the solution and the immediate-release formulation powder, our aim was to use a model that can support a controlled-release form from the powder. However, GastroPlus^{TM} does not include controlled-release formulations for pulmonary delivery. This means that this software was not able to establish *in vitro-in vivo* correlations for modified-release DPI formulations. To do so for controlled-release formulations, it was mandatory to develop at least three formulations with different releases and to evaluate their *in vitro* release and *in vivo* biodistribution. These data should have been entered in the GastroPlus^{TM} software to generate a model so that afterwards when the *in vitro* data of a fourth formulation was encoded, its *in vivo* data could be predicted and compared to the generated *in vivo* data obtained in mice. If the predicted PK parameters had matched the obtained results, an IT tool would have been developed by SimulationPlus team to predict *in vivo* data from controlled-release DPI formulations. Moreover, as *(i)* differentiation between the total cisplatin delivered in the lungs and the actual released cisplatin fraction that is retrieved in the bloodstream is impossible, and *(ii)* it is difficult to mimic the lung anatomical specificities *in vitro*, predicting the *in vivo* data of a controlled-release

formulation would increase the difficulty of establishing these models. Unfortunately, these assessments would have taken a lot of time to be assessed and were not further investigated, considering the ultimate objectives of this work. Indeed, as we are aiming to evaluate the feasibility of combining two routes of administration to intensify the therapeutic response against lung cancer, the formulation developed by Levet *et al.* was optimized by selecting other excipients based on their physicochemical properties as well as their ratios. Once the desired *in vitro* release profile was obtained, the formulation was characterized in a PK study in mice.

3.2. Optimization of the cisplatin-based DPI formulation with controlled cisplatin-release and lung-retention properties

3.2.1. Selection of the cisplatin-based DPI formulation

The aim of this part was to develop a cisplatin-based DPI containing lipid and PEGylated excipients to control the release of cisplatin and presenting lung-retention properties using a scalable manufacturing process, biocompatible pharmaceutical-grade excipients and low-toxicity solvents, corresponding to FDA recommendations [221].

As mentioned, cisplatin DPI formulations (CIS-DPI-TS, IR-CIS-DPI) and their manufacturing processes for a high cisplatin content and high FPF_n were initially developed and published by Levet *et al.* [187]. CIS-DPI-TS was composed of *(i)* TS as a highly hydrophobic lipid excipient with good aerodynamic properties and effective controlled-release properties and *(ii)* TPGS as a PEGylated excipient to avoid excessively fast elimination of the delivered particles by the lungs' non-absorptive clearance mechanism. TPGS is an amphiphilic molecule that is concentrated at the surface of the droplets during the drying process and is therefore retrieved at the surface of the particles. The use of TPGS at 0.5% w/w has led to an improved PK profile (i.e. longer retention in the lungs, with limited systemic exposure to cisplatin), when compared to the same formulation without TPGS [203]. Indeed, the PEG chains of TPGS are hydrophilic, and are therefore exposed toward the aqueous media, creating a hydrophilic barrier after their solvation, which limits the recognition of CIS-DPI-TS by AM and therefore avoids their clearance from the lungs. Indeed, PEGylation is a well-known technique to improve the therapeutic ratio of a drug by prolonging its local residence time [222].

Moreover, CIS-DPI-TS administered at 0.5 mg/kg three times a week for 2 consecutive weeks on the M109-HiFR lung carcinoma orthotopic model in mice showed a level of significance lower than that obtained with CIS-IV at 1.5 mg/kg (CIS-IV_1.5) once a week for two weeks **(Figure 29)**. As mentioned previously *(section 3.1.3)*, this result demonstrated the importance

of modulating the cisplatin release from microparticles to boost anti-tumour efficacy while maintaining controlled-release and lung-retention properties to expose the tumour continuously to cisplatin while maintaining an acceptable tolerance. Therefore, this formulation and the manufacturing process were adapted to find this balance.

First, we preferred HCO over TS to slightly increase the hydrophilicity of the particles and therefore the cisplatin release rate over time after deposition in the lungs compared to that observed with CIS-DPI-TS. HCO is a triglyceride mixture, mainly composed of trihydroxystearin, and characterized by a higher melting temperature (85-88°C) than TS (74.9°C, [187]). This higher melting temperature allows the production of inhaled formulations as dry powder while reducing the risk of obtaining an oily and/or sticky phase that would negatively impact the aerodynamic properties of the DPI. Moreover, it is approved by authorities as an excipient for other routes of administration such as the oral and topical routes [221]. Furthermore, HCO has a higher solubility in alcohols (including ethanol) than TS, which has allowed work with a higher concentration of HCO during spray drying (4% w/w total solid *vs.* 2% w/w previously [187]), thus reducing the manufacturing time.

Following a similar preparation process, the minimum TS content to coat the cisplatin microparticles sufficiently to control the cisplatin release was previously reported as 50% w/w [187]. It was also reported that a higher cisplatin-to-lipids ratio (i.e., 75:25 w/w) led to a higher burst effect with a much lower ability to control cisplatin release over time. A sufficient proportion of HCO/TPGS in the cisplatin-based DPI formulations to coat the cisplatin microparticles was considered critical to control the cisplatin release. Considering that HCO is less hydrophobic than TS, lipid (i.e. HCO/TPGS) proportions of 50% w/w related to cisplatin and above in the final powder (i.e. 50% and 67% w/w in CIS-DPI-50 and CIS-DPI-33, respectively) were selected. The selected TPGS content was 0.5% w/w. This content allowed prolonged retention of TS-based DPI formulations in the lungs after inhalation to be achieved [203] and also modulated the encapsulation of cisplatin microcrystals into the lipid matrix during spray drying [187]. Moreover, Levet *et al.* reported that a higher TPGS content (i.e. 5%) in TS-based formulations led to no control of the cisplatin release *in vitro.* This could be explained by the decreased hydrophobicity of the lipid coating in the presence of TPGS and the possible formation of hydrophilic pores in the lipid coating.
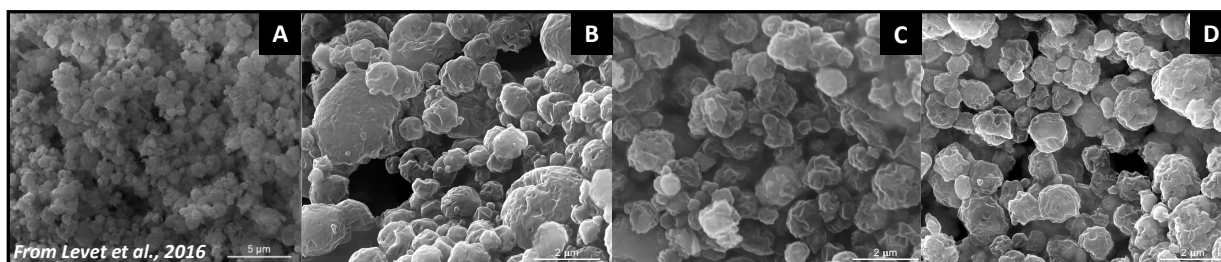
Figure 31: Scanning electron microscopy micrographs of uncoated cisplatin particles (A), spray-dried HCO/TPGS (99:1) powder (B), CIS-DPI-33 (C) and CIS-DPI-50 (D) (magnification 30 000 x).

The coating of cisplatin particles was confirmed in scanning electron microscopy. The CIS-DPI-50 and CIS-DPI-33 particles were roughly spherical and homogeneous and looked very similar to the spray-dried HCO/TPGS (99:1) powder **(Figure 31.B)**, indicating that the cisplatin had been effectively coated by the lipid matrix (**Figure 31).** Conversely, the scanning electron microscopy images of uncoated-cisplatin particles obtained by Levet *et al.* **(Figure 31.A,** [187]**)** showed more agglomerated and sticky particles in comparison to those obtained with CIS-DPI-33 and CIS-DPI-50.
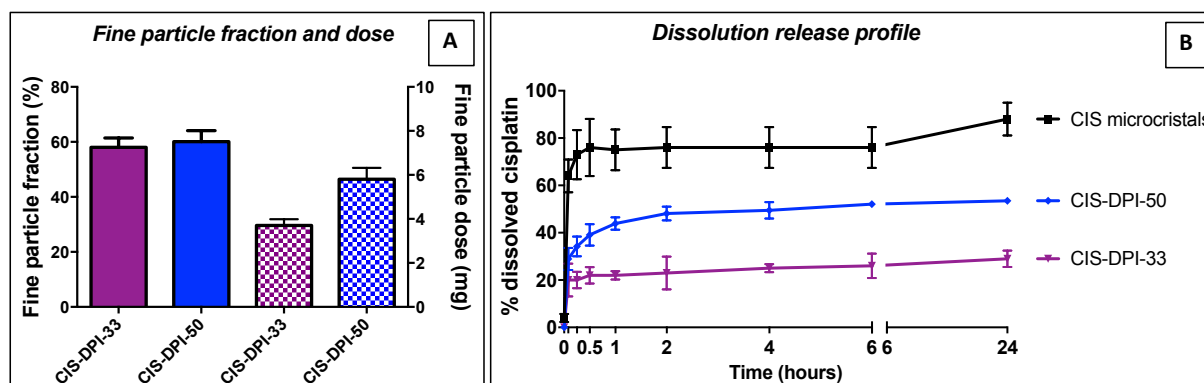

Figure 32: FPF_n and FPD of CIS-DPI-33 and CIS-DPI-50. Impaction studies were performed using the FSI (100 L/min, 2.4 s) on 20 mg of powder hand-filled in an HPMC n°3 capsule in RS.01 inhaler (A). Dissolution profiles of an inhalable fraction of CIS-DPI-33 and CIS-DPI-50 (mean ± SD, n=3) selected from stage 3 (aerodynamic diameter comprised between 2.18 and 3.42 μm) of an NGI using an RS.01 inhaler (100 L/min, 2.4 s) (B).

The differentiation between CIS-DPI-33 and CIS-DPI-50 was performed by characterizing the FPD and FPF using an FSI and on the basis of the *in vitro* cisplatin release over time in mSLF. As illustrated in **Figure 32.A**, both of these formulations demonstrated similar and adequate FPF_d (60 ± 4% for CIS-DPI-50 and 58 ± 6% for CIS-DPI-33) but as predicted, lower FPD for CIS-DPI-33 (3.7 ± 0.5 mg, compared to 5.8 ± 0.9 mg for CIS-DPI-50) due to their different cisplatin contents (28 ± 5% and 49.5 ± 0.6%, respectively).

The dissolution profiles of CIS-DPI-50 and CIS-DPI-33 showed different releases over time **(Figure 32.B)**. After one hour, 44 ± 2% cisplatin was released from CIS-DPI-50 whereas the release observed with CIS-DPI-33 was limited to 22 ± 1% **(Figure 32.B)**. The cisplatin release increased gradually to reach ~50% after 24h from CIS-DPI-50. In contrast, cisplatin release from CIS-DPI-33 was highly limited, reaching ~30% within 24h. These results showed that a higher proportion of HCO, as in CIS-DPI-33, strongly limited the amount of initially dissolved cisplatin and slowed cisplatin release over 24h. This may impair cisplatin total dose release into lung fluids from CIS-DPI-33 and therefore its local activity. It should be noted that DPI formulations with a lower amount of HCO were not selected in order to avoid a much higher cisplatin burst release, which might lead to lower local tolerance. About 80% cisplatin dissolution in 15 min was observed with uncoated cisplatin powder obtained by spray drying the cisplatin particles obtained after the HPH process **(Figure 32.B)**.

Consequently, the results were in favour of CIS-DPI-50 better balancing a burst drug release that is high enough to ensure rapid local activity with a controlled release able to attack the tumour sustainably with limited local toxicity. The release profile observed with CIS-DPI-50 showed a higher burst effect than that obtained from CIS-DPI-TS. Indeed, ~ 44% of cisplatin was released in 1h from CIS-DPI-50 *vs.* ~ 29% from CIS-DPI-TS **(Figure 32.B and Figure 27** [187]**)**. This represented up to 15% of the cisplatin release difference between CIS-DPI-50 and CIS-DPI-TS in 1h. It was only until 6h later that ~ 44% of cisplatin was released from CIS-DPI-TS. The profiles were quite similar after 24h, as 50% of cisplatin was released from CIS-DPI-50 *vs.* 55% for CIS-DPI-TS, demonstrating the sustained-release property of both formulations. In addition, CIS-DPI-50 was preferred over CIS-DPI-33 as it would deliver a higher FPD than CIS-DPI-33 from the same mass of powder delivered. Consequently, CIS-DPI-50 was selected to continue the *in vivo* investigation, as our aim of developing a higher-burst-effect formulation was reached.

It should be noted that there are no pharmacopeia methods or guidelines describing *in vitro* dissolution tests of inhaled products. The main issue with these tests is the difficulty of reproducing *in vitro* the physiological conditions that the aerosol faces once it deposits and disperses in lung fluids. Many methods have been reported with many drawbacks, including difficult handling of the powder, leading to poor reproducibility and targeting [223,224]. In the case of cisplatin-based DPI, this has been accentuated by particle agglomeration related to the highly lipophilic character of HCO, as noticed when the dissolution cup assembly was opened

at the end of the dissolution test to determine the total amount of cisplatin introduced (i.e. 100% release) into the medium.

Therefore, the *in vitro* dissolution profiles for inhaled products must be interpreted with caution as they are used to compare different release patterns from formulations containing the same active ingredient. Dissolution tests for inhaled products are inadequate methods to investigate the release once deposited in the lungs. This is due to poor *in vitro-in vivo* correlation, and the difficulty in building these correlations using simulation software (e.g. GastroPlus^{TM}) [224]. Further development regarding the methodologies used and the composition of medium are thus highly awaited to try to solve these drawbacks.

3.2.2. Characterization of the selected cisplatin-based DPI formulation

The cisplatin mean content of CIS-DPI-50 was 49.2 ± 0.3% w/w and was highly reproducible from batch to batch, with low SD and relative standard deviation (RSD%) observed: 49.5 ± 0.6% (1%); 51 ± 2% (3%); 47.2 ± 0.6% **(Table 15)**.

One of the most crucial parameters for DPI development is the particle size as it is directly correlated to the aerodynamic diameter, which dictates the deposition section in the respiratory tract [169]. The geometric PSD was compatible with a deep lung deposition as the proportion of the particle size under 5 μm was 97 ± 4%, the Dv (50) was 1.9 ± 0.2 μm and the Dv 90 was 4 ± 1 μm **(Table 15)**.

The delivered cisplatin dose for the three independent batches was 8.1 ± 0.4 mg cisplatin and corresponded to 82 ± 2% of the nominal dose, which indicated good aerosolization of the powder with limited powder retention in the device and the capsule. The delivered dose was considered as highly repeatable from batch to batch, as indicated by the low RSD% observed (5%, **Table 15**). Moreover, the DDU was very good (96-104%), with RSD% < 3% for each batch on 10 replicates, and corresponded to the European Pharmacopeia recommendations, i.e. all 10 doses comprised between 65 and 135% and 9 out of 10 doses comprised between 75 and 125% of the mean delivered dose for each batch.

Table 15: *In vitro* evaluation of CIS-DPI-50 in terms of platinum concentration (ETAAS), residual solvent (thermogravimetric analysis), geometric PSD (laser diffraction), delivered dose and uniformity (100 L/min, 2.4 s), and aerodynamic performance (NGI at 100 L/min, 2.4 s) through the RS.01 inhaler (10 mg cisplatin per capsule). The data are presented as the mean values of three independent batches analysed in 3 or 10 (for DDU) replicates ± SD.

Formulation	CIS-DPI-50	
Theoretical composition of CIS-DPI-50 (% w/w)	Component	Proportion
	Cisplatin	50.0
	COH	49.5
	TPGS	0.5
Cisplatin content (% w/w, mean ± SD, n=3)	49.2 ± 0.6	
Residual solvent content (% w/w, mean ± SD, n=3)	0.15 ± 0.09	
Geometric particle size distribution (mean ± SD, n=3)	% < 5 μm	97 ± 4
	Dv (10) (μm)	1.2 ± 0.1
	Dv (50) (μm)	1.9 ± 0.2
	Dv (90) (μm)	4 ± 1
	Dv[4;3] (μm)	2.2 ± 0.5
Delivered dose (mg) (mean ± SD, n=3 batches analysed in ten replicates)	8.1 ± 0.4	
Delivered dose uniformity (min and max % of the mean delivered dose, 10 assays per batches)	96-104%	
Aerodynamic performance **NGI, 100 L/min** (mean ± SEM, n=3)	FPF_d (%)	74.4 ± 0.3
	FPF_n (%)	53 ± 2
	FPD (mg)	5.3 ± 0.2
	MMAD (μm)	2.2 ± 0.2
	GSD (μm)	1.85 ± 0.03

It is commonly considered that particles must have an aerodynamic diameter ranging between 1 and 5 μm to deposit optimally in the lower respiratory tract [169]. This diameter is far more crucial in the development of anticancer drugs as it increases their potential to be deposited broadly in the sections from the bronchioles to the alveolar sacs (i.e. generations 4 to 23). Such deposition avoids two main potential limitations in the treatment. First, particle deposition in the upper airways (i.e. generations 0 to 3, aerodynamic diameter > 5 μm), such as the mouth, throat, trachea, or bronchi of the lower respiratory tract, which can lead to local toxicities without therapeutic action. Second, exhalation of the cytotoxic aerosol (if it presents an aerodynamic diameter between 0.1 and 1 μm), which can induce environmental contamination [173,186].
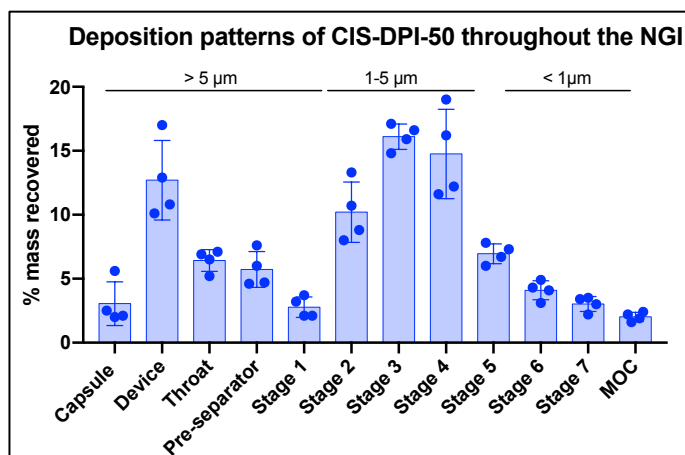
Figure 33: Deposition profiles of the CIS-DPI-50 formulation in an NGI using a RS.01 inhaler (10 mg cisplatin per capsule, 100 L/min, 2.4 s, 1 capsule per test). The cut-off diameters at 100 L/min were 6.12, 3.42, 2.18, 1.31, 0.72, 0.40, 0.24 and 0.07 μm for stages 1, 2, 3, 4, 5, 6, 7 and the micro-orifice collector (MOC), respectively. The data are presented as the mean ± SD of the three batches (dots) analysed in triplicate.

The APSD was in line with these recommendations and described a polydisperse aerosol as CIS-DPI-50 was retrieved at nearly all stages (i.e. from 0.07 to 10 μm, from the MOC to the pre-separator stage). This broad deposition was confirmed by the GSD obtained, i.e. 1.85 ± 0.03 μm, as it was higher than 1.22 μm (the commonly accepted threshold for considering the aerosol as monodisperse [225]). However, a much higher proportion (i.e. 37 ± 6%) of the particles was comprised in stages 2 and 4, i.e. within a range of 1 and 5 μm **(Figure 33)**. In contrast, the cumulative cisplatin doses collected from the induction port (i.e. the throat), the pre-separator and stage 1 were relatively low, i.e. about 16%.

Two main types of adverse reaction might be related to the fraction deposited in the oropharynx. First, this fraction, as part of the fraction deposited in the upper airways, might induce local adverse reactions such as coughing. These local reactions are expected to be immediate, i.e., within 15 min following the administration. Although any occurrence will be investigated in clinical trials, mainly in the first in-humans study, potential local adverse reactions are expected to be limited because *(i)* the fraction deposited in the upper airways is expected to be limited, less than 20% of the nominal dose, according to the APSD evaluation, and *(ii)* this limited fraction is expected to be cleared rapidly due to clearance mechanisms, e.g., coughing, sneezing or swallowing, as described in the literature for inhaled drug particles [226]. Moreover, patients will be advised to rinse their mouth, which will help to reduce this fraction. Secondly, any of the remaining oropharyngeal dose that is subsequently swallowed could potentially be absorbed via the digestive tract, leading to systemic adverse reactions. However, these systemic adverse reactions are expected to be low as *(i)* the cisplatin dose administered to patients will be very

low compared to the usual IV doses and *(ii)* oral bioavailability of cisplatin is limited, i.e., below 0.4 [227].

The MMAD was 2.2 ± 0.2 μm and therefore in the desired range for an anticipated good deposition in the lower airways (< 5 μm) [228]. This good aerodynamic performance led to high FPD (5.3 ± 0.2 mg) and FPF values (FPF_d and FPF_n of $53 \pm 2\%$ and $74.4 \pm 0.3\%$, respectively) **(Table 15)**. In the case of nebulizers (i.e. the only device studied so far in clinical inhaled chemotherapy), it was estimated that 10-15% of the inhaled dose was deposited in the deep lungs in a phase I study with the same drug candidate [178]. The authors reported that despite three sessions of administration of about 20 minutes each per day for up to 3 days per week for 2 weeks, the highest delivered dose per cycle was 60 mg/m^2 and the DLT was not reached [178]. This demonstrated the difficulty of delivering the adequate cisplatin dose using nebulizers [178].

Regarding the aerodynamic performance of CIS-DPI-50, it was concluded that the RS.01 device was suitable for this formulation. Indeed, it confirmed the previous results obtained with CIS-DPI-TS, as it assured a good aerosolization and dispersion and should allow good deposition in the lungs. The selected RS.01 inhaler was a low-resistance version that allowed the highest deposition at the selected flow rate to be achieved and therefore demonstrated the best aerodynamic performance. It is most important to evaluate the dependency of this device on airflow. Indeed, this is all highly important as lung cancer patients might have impaired lung function due to the presence of the tumours, a tobacco-smoking history or COPD [186].

The aerodynamic performance of CIS-DPI-50 using different flow rates (100 L/min, 60 L/min and 40 L/min) was evaluated to investigate its influence on the deposition patterns **(Figure 34)**. As expected, the higher the flow rate was (i.e. patient inspiratory flow), the lower the deposition in the capsule, device, throat and pre-separator and the higher the FPF **(Figure 34)**.

This was correlated with a better aerosolization and deagglomeration of the powder in the case of the highest flow rates. Indeed, the aerodynamic performance significantly decreased with a flow rate of 60 L/min (instead of 100 L/min) **(Figure 34)**. This was observed from a significant decrease of 0.8 mg in the FPD ($p < 0.05$) and 4.5% in the FPF_d ($p < 0.05$), and was related to a significant increase in the proportion of the mass recovered in the device ($p < 0.0001$) and in the throat ($p < 0.0001$), with no difference in the capsule ($p > 0.05$) or in the pre-separator ($p > 0.05$) **(Figure 34)**.
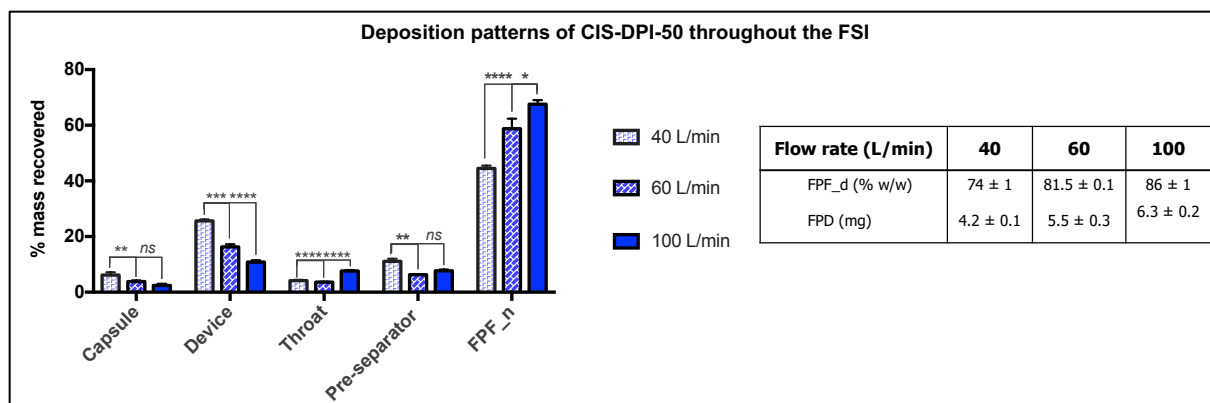
Figure 34: Deposition profiles of the CIS-DPI-50 formulation in an FSI using a low resistance RS.01 inhaler filled with 10 mg cisplatin per capsule at 40 L/min (6 s), 60 L/min (4 s) and 100 L/min (2.4 s). The data are presented as the mean ± SD of one batch analysed in triplicate. The statistical analyses were performed *vs.* 100L/min using one-way ANOVA and Bonferroni's post-test (**** for $p < 0.0001$, *** for $p < 0.001$,** for $p < 0.01$ and * for $p < 0.05$).

As expected, the aerodynamic performance was more strongly impacted when the flow rate was lowered from 100 L/min to 40 L/min as a significant decrease of 2.1 mg in the FPD ($p < 0.0001$), and of 12% in the FPF_d ($p < 0.0001$) was reported. This was related to a significant increase in the proportion of the mass recovered in the capsule ($p < 0.01$), in the device ($p < 0.0001$), in the throat ($p < 0.0001$) and in the pre-separator ($p < 0.01$) **(Figure 34)**.

According to these results, although a 40%-fold lower inspiratory flow rate (i.e. 60 L/min) was not able to impair the powder from leaving the capsule, a 60%-fold lower inspiratory flow rate (i.e. 40 L/min) was. This was demonstrated by a significant difference ($p < 0.05$) between these two flow rates (i.e. 60 L/min and 40 L/min) in the masses recovered in the capsule. However, the ability to leave the device was impacted, which was demonstrated by a significantly lower delivered dose (60 L/min *vs.* 100 L/min: $p < 0.01$, and 40 L/min *vs.* 100 L/min: $p < 0.0001$), leading to impaired aerosolization at both lower flow rates. In addition, the powder de-agglomeration/dispersion at both lowered flow rates was also affected as a significantly higher mass was recovered in the throat and pre-separator, leading to lower FPD and FPF_n, as represented in **Figure 34**. Moreover, the differences between 60 L/min and 40 L/min in terms of delivered dose ($p < 0.05$), FPD ($p < 0.001$) and FPF_d ($p < 0.0001$) were also significant, confirming the device dependency on the flow rate.

However, it should be mentioned that the overall aerodynamic performance was very good regardless of the flow rate. Indeed, the FPF_d ranged between 74 ± 1%, for a deposition flow rate of 40 L/min, to 81.5 ± 0.1% for 60 L/min and 86 ± 1% for 100 L/min and corresponded to an FPD of 4.2 ± 0.1 mg, 5.5 ± 0.3 mg and 6.3 ± 0.2 mg, respectively **(Figure 34)**. It should be

mentioned that even severe COPD patients, with a significantly affected lung function, mostly have a peak inhalation flow (i.e. maximum flow reached during inspiration) ranging between 60 and 89 L/min using such low-resistance devices [229,230]. This tended to show that it is probable that lung cancer patients, with past or concomitant COPD, would have a peak inhalation flow in the same range as severe COPD patients, with a lower probability of reaching inspiratory flows down to 40 L/min. However even if this was the case, both the delivered dose and the FPD/FPF_d would show good aerodynamic performance.

One interesting criteria is that the RS.01 device is activated and controlled by the patient inspiratory flow, and the drug retrieved in the air seems to be negligible (i.e., 0.2% exhaled after the inhalation of a tobramycin based DPI by healthy volunteers [190]). This would counteract the limitation observed with nebulizers during the previous clinical studies.

3.2.3. Evaluation of the stability of CIS-DPI-50

The preliminary investigation of the stability of CIS-DPI-50 was promising. Indeed, the loss on drying was limited (< 0.2% w/w, **Table 15**) and corresponded to the total residual content of ethanol and water. This was aligned with the European Pharmacopeia recommendations, as the use of ethanol as a class III solvent can be used with no justification but should not exceed a threshold of 0.5% w/w. Moreover, this result was also a good prognostic for the long-term stability of the product during storage as stability could be impaired by a high residual solvent content.

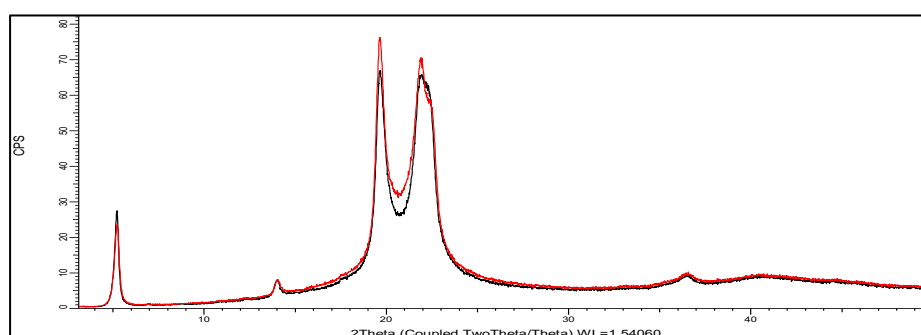Figure 35: X-ray diffractogram obtained from the spray-dried HCO and TPGS powder (red curve) and raw HCO obtained from the manufacturer (black curve).

Another indicator of potential good long-term stability was that the more stable polymorph of HCO (*β*-form) was preserved during spray drying as it was similar to that of the initial raw material, thus providing reassurance of its physicochemical stability during storage, as

illustrated in the X-ray diffractogram in **Figure 35**. Indeed, these results were confirmed by the thermal analysis as the HCO DSC pattern was similar to that observed for CIS-DPI-50 **(Figure 36)**.

The slight difference in terms of peak intensity and surface could be attributed to the amount of HCO in CIS-DPI-50 (49.5% *vs.* 100%). These DSC curves showed that the two endothermic peaks observed during the first heating cycle (blue curve from HCO at 78.7°C and red curve from CIS-DPI-50 at 85.8°C) indicated the melting of the *β*-form of the main component of HCO (i.e. trihydroxytristearin). During the cooling cycle, the *β*-form recrystallized to the *α*-form (green curve from HCO at 66.2°C and yellow curve from CIS-DPI-50 at 52.3°). Finally, the three peaks (i.e. burgundy curve from HCO and black curve from CIS-DPI-50) observed during the last cycle showed the melting of the *α*-form (58°C) and the *β*-form **(Figure 36)**. These results were similar to those reported by Levet *et al*. for CIS-DPI-TS [187]. However, even if these results were encouraging for the long-term stability of CIS-DPI-50, it was essential to investigate the stability according to ICH guidelines [231].
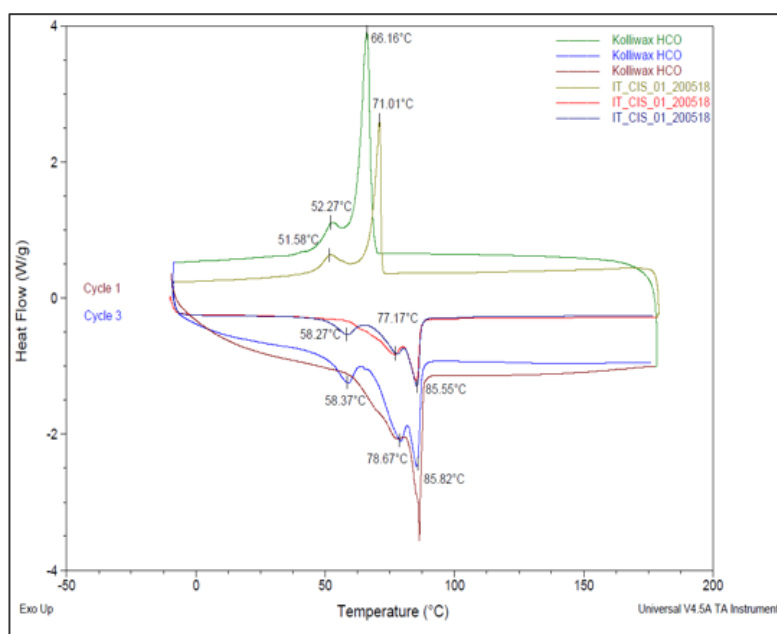
Figure 36: Thermal behaviour of HCO and CIS-DPI-50 from DSC analysis. The blue and red curves correspond to the first heating cycle for HCO and CIS-DPI-50, respectively. The green and yellow curves correspond to the cooling cycle for HCO and CIS-DPI-50, respectively. Finally, the burgundy and black curves correspond to the second heating cycle for HCO and CIS-DPI-50, respectively.

Therefore, the stability of CIS-DPI-50 was evaluated under normal storage conditions (25°C, 60% RH) over 6 months and demonstrated no modification of the physicochemical and aerodynamic characteristics between T0 and 6 months **(Figure 37)**. Indeed, similar residual

solvent content (T0: $0.05 \pm 0.05\%$ *vs.* $0.02 \pm 0.03\%$, after 6 months) was observed, demonstrating the low hygroscopicity of the powder. In addition, thermal properties demonstrated that the *β*-form of HCO as well as the crystalline state of cisplatin were maintained during the 6 months of storage **(Figure 38)**. Moreover, the geometric PSD (Dv (50) of 1.99 ± 0.06 *µ*m at T0 *vs.* 1.89 ± 0.09 *µ*m, after 6 months) and APSD (FPF_d of $81.0 \pm 0.6\%$ at T0 *vs.* $81 \pm 2\%$ after 6 months) were similar, as were the NGI deposition patterns reported over 6 months, as illustrated in **Figure 37.B**.

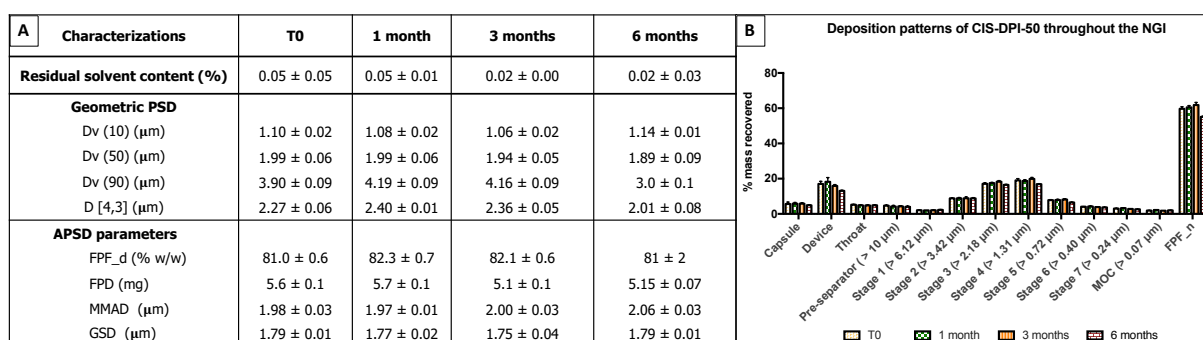| A Characterizations	T0	1 month	3 months	6 months
Residual solvent content (%)	0.05 ± 0.05	0.05 ± 0.01	0.02 ± 0.00	0.02 ± 0.03
Geometric PSD				
Dv (10) (µm)	1.10 ± 0.02	1.08 ± 0.02	1.06 ± 0.02	1.14 ± 0.01
Dv (50) (µm)	1.99 ± 0.06	1.99 ± 0.06	1.94 ± 0.05	1.89 ± 0.09
Dv (90) (µm)	3.90 ± 0.09	4.19 ± 0.09	4.16 ± 0.09	3.0 ± 0.1
D [4,3] (µm)	2.27 ± 0.06	2.40 ± 0.01	2.36 ± 0.05	2.01 ± 0.08
APSD parameters				
FPF_d (% w/w)	81.0 ± 0.6	82.3 ± 0.7	82.1 ± 0.6	81 ± 2
FPD (mg)	5.6 ± 0.1	5.7 ± 0.1	5.1 ± 0.1	5.15 ± 0.07
MMAD (µm)	1.98 ± 0.03	1.97 ± 0.01	2.00 ± 0.03	2.06 ± 0.03
GSD (µm)	1.79 ± 0.01	1.77 ± 0.02	1.75 ± 0.04	1.79 ± 0.01

Figure 37: Characterization of CIS-DPI-50 in terms of residual solvent content, geometric PSD and APSD parameters (A) immediately after its production (T0), and after 1, 3 and 6 months of storage at 25°C, 60% RH). The NGI deposition profiles of the CIS-DPI-50 formulation using a RS.01 inhaler (10 mg cisplatin per capsule, 100 L/min, 2.4 s) were evaluated at the same timings. The data are presented as the mean ± SD.
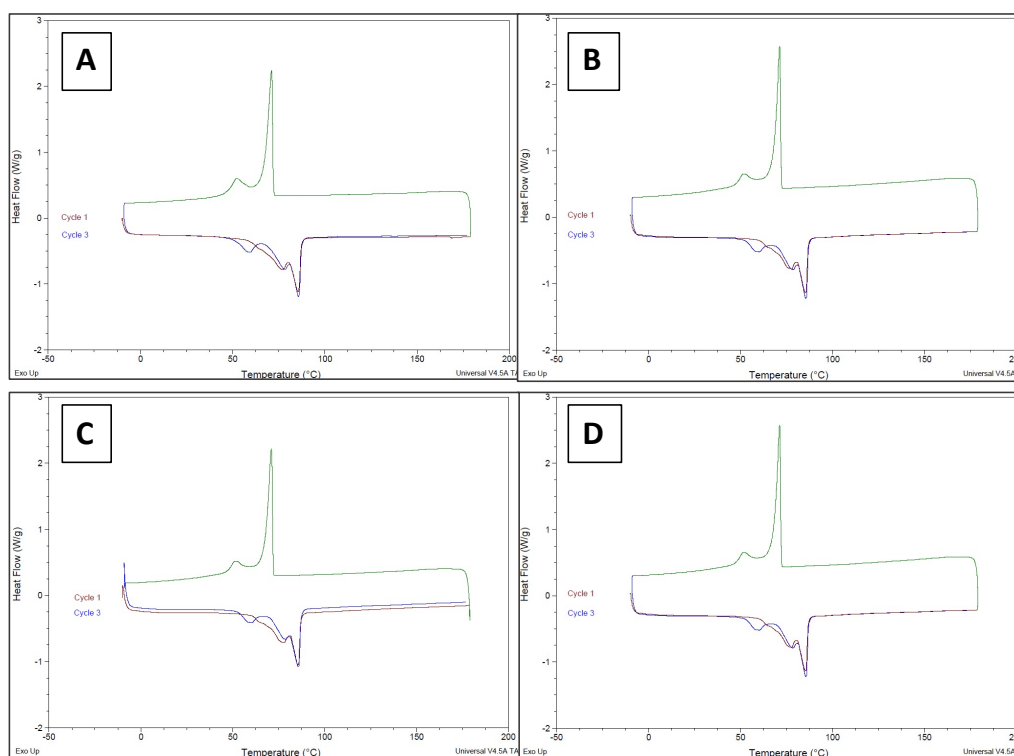

Figure 38: Thermal behaviour of CIS-DPI-50 at T0 (A), 1 month (B), 3 (C) and 6 months (D) of storage at 25°C and 60% RH. The burgundy curve corresponds to the first heating cycle, the green curve corresponds to the cooling cycle and the blue curve to the second heating cycle.

3.2.4. Biodistribution and pharmacokinetic profiles after cisplatin administration to healthy mice

As detailed in the general introduction, lungs present anatomical specificities (i.e. a huge deposition surface and rapid drug absorption) that are difficult to mimic *in vitro*. Moreover, the non-absorptive clearance mechanisms such as the mucociliary escalator and AM uptake defining the potential lung-retention properties of the formulation are not taken into account during *in vitro* dissolution experiments. It was therefore essential to investigate the fate of CIS-DPI-50 *in vivo*.

The *in vivo* PK profiles of cisplatin (followed by the quantification of platinum) from the selected formulation were established in healthy mice. This study was crucial to verify whether the increased burst effect observed *in vitro* was kept *in vivo* while still maintaining controlled drug release. This was subsequently useful to evaluate the exposure of lung and plasma as well as kidney to determine the combination regimen of repeated CIS-DPI-50 administrations with CIS-IV-based treatment that offered the best compromise between enough lung (and therefore tumour) exposure to cisplatin and minimising the related potential local and systemic toxicities.
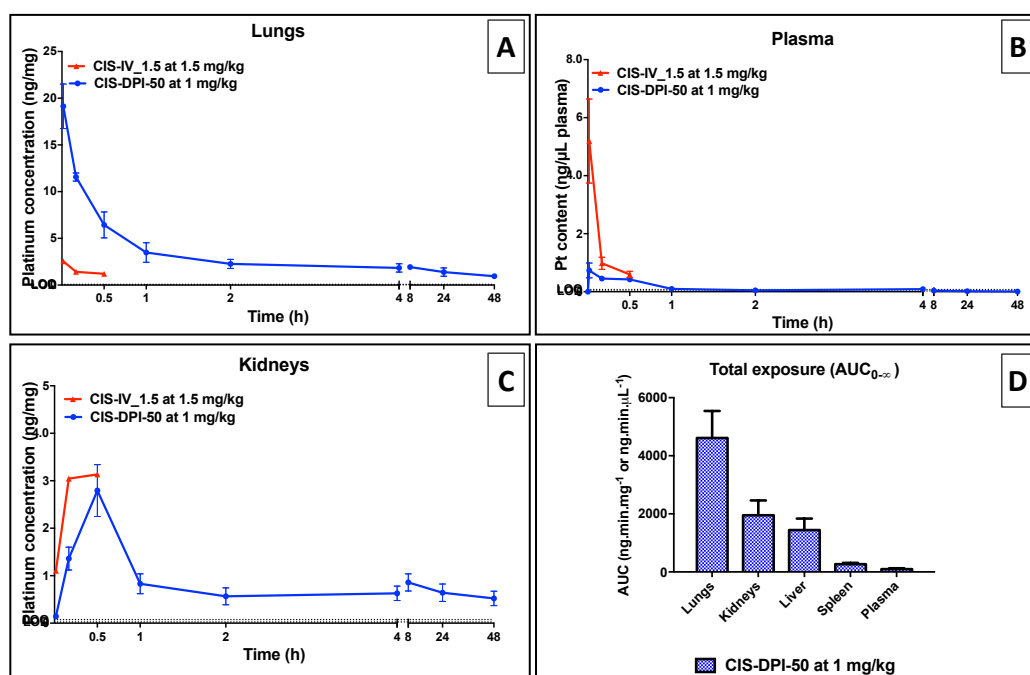

Figure 39: PK study of CIS-DPI-50 and CIS-IV_1.5 (1 and 1.5 mg/kg, respectively) in healthy mice. Platinum concentration was evaluated in the lungs (A), plasma (B) and kidneys (C). Total AUC for different organs of CIS-DPI-50 (D). All results are expressed as means ± standard error of the mean (SEM) (n=5-6 per timepoint).

The PK curve of platinum lung concentrations obtained over time after the administration of CIS-DPI-50 at 1.0 mg/kg cisplatin and CIS-IV_1.5 at 1.5 mg/kg cisplatin, are represented in

Figure 39. As the bioanalytic method was not selective to cisplatin but to platinum (as commonly referred to in clinical trials for platinum salts including cisplatin [177,178]), lung platinum concentrations measured over time with CIS-DPI-50 and CIS-IV_1.5 consisted of unbound (i.e. dissolved) active cisplatin, inactive platinum adducts and bound cisplatin as particles not yet dissolved in lung fluids. The PK profile of CIS-IV_1.5 is known and has been investigated in depth and reported in healthy mice by Levet *et al.* [203]. However, the protocol slightly differed from this study (e.g. timepoints, cisplatin dose, blood sampling). The exposure to platinum following CIS-IV_1.5 at 1.5 mg/kg cisplatin (the MTD determined by Levet *et al.* [205]) following the protocol of the present study was therefore investigated. Only the three first timepoints were evaluated, i.e., 1 min, 10 min, and 30 min, which allowed us to determine the C_{max}, k_{el}^i, and $t_{1/2}^i$.

As anticipated, platinum C_{max} in the lungs was obtained immediately following the administration of CIS-DPI-50 and CIS-IV_1.5, at the first timepoint (i.e. 1 min), which corresponded to the time required to euthanize the mice and collect the lungs. The C_{max} in the lungs for CIS-DPI-50 was 19 ± 2 ng/mg, corresponding to $26 \pm 3\%$ cisplatin recovered from the actual delivered dose **(Table 16)**.

Table 16: PK parameters of PK study of CIS-DPI-50 and CIS-IV_1.5 (1 and 1.5 mg/kg, respectively) in healthy mice. These parameters were determined on the PK curves obtained in **Figure 39**. All results are expressed as means $\pm$ SEM (n=5-6 per timepoint). T_a is expressed as the ratio of the platinum AUC in the lungs from CIS-DPI-50 to the AUC from CIS-IV_1.25 (i.e. 558 ng.min.mg^{-1}, as determined by Levet *et al.*[203]).

Pharmacokinetics	CIS-DPI-50			CIS-IV_1.5		
	Lungs	Plasma	Kidneys	Lungs	Plasma	Kidneys
C_{max} (ng/mg – ng/μL)	19 ± 2	0.7 ± 0.6	2.8 ± 0.6	2.6 ± 0.8	5 ± 1	3.1 ± 0.2
T_{max} (min)	1	1	30	1	1	30
AUC$_{0-\infty}$ (ng.min.mg^{-1} - ng.min. μL^{-1})	4611 ± 932	95 ± 30	1952 ± 510	-	-	-
K_{el}^i (min^{-1})	0.036			0.023	0.066	0.03
$t_{1/2}^i$ (min)	19			30	10	23
K_{el}^t (h^{-1})	0.00029					
$t_{1/2}^t$ (h)	39					

The C_{max} of CIS-IV_1.5 in the lungs (i.e. 5 ± 1 ng/mg, **Figure 39**) was nearly four-fold lower than for CIS-DPI-50, despite the higher cisplatin dose delivered (i.e. 1 *vs.* 1.5 mg/kg, respectively). The platinum concentration in the lungs first decreased from 19 ± 2 ng/mg to 6 ± 2 ng/mg 30 min after the administration of CIS-DPI-50, with a k_{el}^i and $t_{1/2}^i$ of 0.036 min^{-1} and 19 min, whereas following CIS-IV_1.5 administration, k_{el}^i and $t_{1/2}^i$ were 0.023 min^{-1} and 30

min. Levet *et al.* reported a more rapid elimination from the lungs, with a k_{el}^i and $t_{1/2}^i$ of 0.26 min^{-1} and 2.6 min following the administration of cisplatin microparticles without lipid excipients [203]. The initial clearance profile could be related to the clearance of the released cisplatin from the lungs, mainly by absorption to the systemic compartment. This is because cisplatin is a small molecule, which could facilitate its diffusion though the lung epithelium once released from microparticles in lung fluids as observed previously with ET delivery of ET-SOL and ET-IR_CIS-DPI [203]. Therefore, the retention time of cisplatin in the lungs consecutive to a single CIS-DPI-50 administration was estimated to be around 2.2h (seven times the $t_{1/2}^i$). This retention time was more than 7-fold higher than for cisplatin microparticles without lipid excipients (18.2 min) [203]. These parameters clearly indicated a delay in the lung clearance of cisplatin due to the presence of the lipid matrix and the PEGylated excipient (TPGS). The clearance PK (K_{el}^i: 0.036 min^{-1} and $t_{1/2}^i$: 19 min) showed a 3-fold higher clearance of CIS-DPI-50 than for CIS-DPI-TS (K_{el}^i: 0.012 min^{-1} and $t_{1/2}^i$: 59.9 min [203]).

Between 2 and 8h, the platinum concentrations in the lungs remained constant around 2 ng/mg, i.e. 2-fold higher than the lung C_{max} of CIS-IV_1.5. These concentrations then continued to decrease to 0.94 ± 0.4 ng/mg after 48h (k_{el}^t and $t_{1/2}^t$ of 0.00029 h^{-1} and 39h, **Table 16**). This terminal clearance profile could be attributed more to the clearance of platinum adducts from the tissue [203], which can remain for months following administrations [232]. The $AUC_{0-\infty}$ in the lungs was $4\ 611 \pm 932$ ng.min.mg^{-1}, which also demonstrated the prolonged retention of CIS-DPI-50 within the lungs ($AUC_{0-\infty}$ of $1\ 462$ ng.min.mg^{-1} for IR-CIS-DPI [203]). As anticipated, the use of HCO instead of TS decreased the lung AUC ($AUC_{0-\infty}$ of $6\ 072$ ng.min.mg^{-1} for CIS-DPI-TS [203]), tending to indicate a more rapid release profile (and thus a shorter lung retention) of cisplatin with an HCO-based DPI. Consequently, a lower T_a was observed for CIS-DPI-50 in comparison to CIS-DPI-TS (8.3 *vs.* 10.9 [203]). However, CIS-DPI-50 T_a was still higher in comparison to the IR-CIS-DPI (i.e. T_a of 2.6 [203]) or to CIS-IV_1.25 (i.e. T_a of 1 [203]), confirming the controlled-release and lung-targeting properties of CIS-DPI-50. Consequently, these results (K_{el}, $t_{1/2}$, AUC and T_a) confirmed the burst effect observed *in vitro*. Therefore our objective of developing a formulation with a higher burst effect was achieved.

As expected, the C_{max} in plasma following CIS-DPI-50 administration was more than 6-fold lower than for CIS-IV_1.5 (0.7 ± 0.6 *vs.* 5 ± 1 ng/μL, respectively, **Table 16**). Overall, these data confirmed the advantage of CIS-DPI-50 in terms of targeting the lungs compared to CIS-

IV, with a 7-fold increase and decrease in the C_{max} in lungs and in plasma, respectively. As expected, total exposure of untargeted organs to platinum after CIS-DPI-50 delivery was limited compared to the lungs, with lower $AUC_{0-\infty}$ values **(Figure 39.D)**. These values demonstrated the PK advantage of CIS-DPI-50, compared to CIS-IV [203], for a lung-targeting therapeutic approach.

Interestingly, the results observed on renal exposure (renal C_{max}: 2.8 ± 0.6 ng/mg, renal $AUC_{0-\infty}$: $1\,952 \pm 510$ ng.min.mg^{-1}, **Figure 39.D)** were higher than those previously reported with CIS-DPI-TS (renal C_{max}: 1.1 ± 0.6 ng/mg, renal $AUC_{0-\infty}$: $1\,568 \pm 788$ ng.min.mg^{-1}[203]). Both the renal C_{max} and $AUC_{0-\infty}$ values were higher than with ET-SOL (renal C_{max}: 1.1 ± 0.5 ng/mg, renal $AUC_{0-\infty}$: 709 ± 205 ng.min.mg^{-1}) and ET-IR_CIS-DPI (renal C_{max}: 0.6 ± 0.2 ng/mg, renal $AUC_{0-\infty}$: 1070 ± 266 ng.min.mg^{-1}[203]). Renal excretion though a non-linear and saturable process is the main elimination process for cisplatin and its metabolites [126]. This seems to be the most plausible explanation of this renal exposure for inhaled cisplatin-based DPI, with prolonged lung retention leading to prolonged renal exposure to cisplatin and derivatives (all quantified as platinum here). Although the nephrotoxicity of cisplatin and its metabolites is directly related to their concentrations, the presence of platinum in the kidneys after administration does not necessarily imply renal toxicity. This is because not all metabolites or platinum adducts induce renal impairment [126]. However, renal tolerance should be investigated in depth, and will be discussed in the *Experimental parts III and IV*.

The results observed during the PK study in mice, in terms of lung targeting and reduced systemic exposure, were confirmed in a healthy sheep model that was administered CIS-DPI-50 and CIS-IV_1 at 1 mg/kg [233]. Indeed, a very low systemic exposure to cisplatin with CIS-DPI-50 compared to CIS-IV_1 was observed, with 10-fold reduced C_{max} and $AUC_{0-\infty}$ in the plasma at the same dose [233]. The major differences observed between the mice and sheep models were: *(i)* a longer T_{max} for sheep in comparison to mice, *(ii)* a higher $AUC_{0-\infty}$ in the sheep plasma and a *(iii)* quicker elimination (higher K_{el}^{i} and lower $t_{1/2}^{i}$) from mice than from sheep plasma. This longer T_{max} (i.e. 10-min and 30-min-shift for ET and IV routes, respectively) can be explained by the differences in terms of techniques of administration between species (i.e. ET administration following a 10 min ventilation and IV infusion over 30 min for sheep *vs.* immediate ET or IV delivery over a few seconds for mice). Moreover, the differences observed between the two models in terms of $AUC_{0-\infty}$ and T_{max} can also be attributed to physiological differences between species. Indeed, a lower specific metabolic rate is observed

for larger animals and an increased blood flow to the liver and kidneys is achieved in smaller animals leading to a faster elimination, especially for drugs such cisplatin that are highly cleared by the kidneys [234].

4. **Conclusion**

This study succeeded in optimizing a promising cisplatin-based DPI formulation with controlled cisplatin-release and lung-retention properties. The manufacturing of this formulation was performed using GRAS excipients by means of a scalable and reproducible process. This formulation was characterized by an interesting aerodynamic performance with the use of a low-resistance device that offered good aerosolization and potential low contamination of the environment by the cytotoxic aerosol. Moreover, these aerodynamic performances were maintained even at lower flow rates (i.e. in the case of impaired respiratory function of lung cancer patients). Finally, the stability of this formulation over 6 months in normal conditions was also confirmed and showed limited modifications over time. As expected, a higher burst effect was confirmed *in vivo* during a PK study in healthy mice, in comparison with the previous CIS-DPI-TS. These PK results will therefore be considered for the construction of a monotherapy regimen based on repeated administrations of CIS-DPI-50.

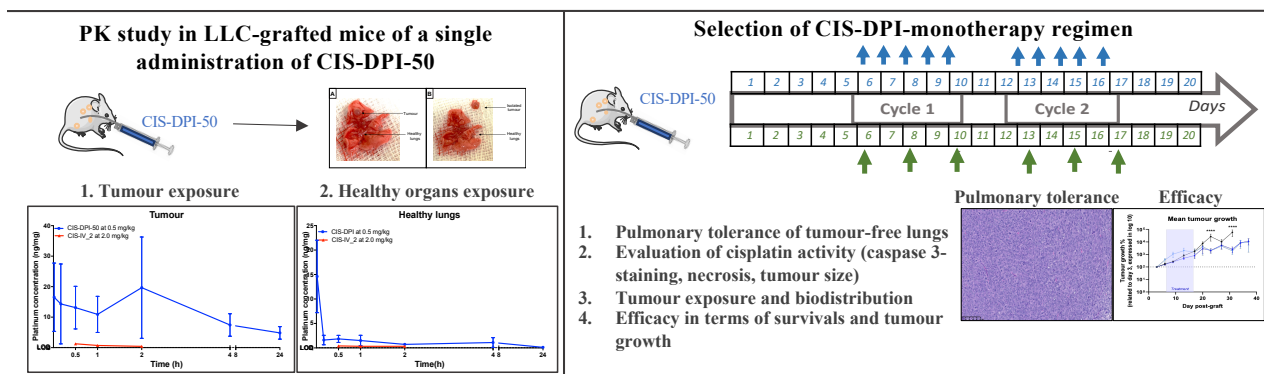# Part II: Selection of the most appropriate CIS-DPI-50 monotherapy regimen

Figure 40: Graphical abstract of the second experimental part.

1. <u>Introduction and aims</u>

In the first experimental part, a cisplatin-based DPI (CIS-DPI-50) was developed using GRAS and pharmaceutical-grade excipients following a scalable process. Three batches of this formulation were produced and characterized and demonstrated controlled-release properties and good aerodynamic performance. These properties were maintained as stable over 6 months at normal storage conditions (25°C, 60% RH). In addition, this formulation showed a higher burst effect than CIS-DPI-TS while maintaining controlled-release and lung-retention properties. This led to a higher lung targeting (i.e. higher T_a) and retention in mice in comparison to CIS-IV.

Considering the intent to combine CIS-DPI-50 to conventional IV chemotherapy, it was crucial to first select the most promising CIS-DPI-50 monotherapy regimen constructed from repeated administrations of CIS-DPI-50. This selection should take into account different factors such as *(i)* the biodistribution in the tumour and in healthy tissues, *(ii)* the anti-tumour efficacy and *(iii)* the tolerance. Therefore in this *Experimental part II*, the aim was to assess the biodistribution (platinum quantification) in grafted mice after the administration of *(i)* CIS-DPI-50 once or *(ii)* repeatedly following several regimens (different doses and frequency). This was coupled with the evaluation of cisplatin activity (i.e. necrosis using histology and apoptosis using caspase-3 staining) and the investigation of the lung tissue tolerance (i.e. histology).

Last but not least, the most promising monotherapy regimens were selected to be evaluated during an efficacy study in terms of survival, tumour size and proportion of responders.

2. <u>Materials and methods</u>

2.1. Materials

Dulbecco's Modified Eagle's Medium (DMEM) and formaldehyde (FMA)-buffered pH 6.9 for histology were purchased from Sigma-Aldrich (St. Louis, USA) and Lewis lung carcinoma cells (LLC1) were provided by ATCC (Maryland, USA). All the reagents used for the immunostainings were obtained either from Vector Labs (Peterborough, UK) (caspase-3 and CD31) or from Ventana Discovery XT™ (Arizona, USA) (CD3). All other materials used in this part are detailed in *Experimental part I-section 2.1.*

2.2. *In vivo* studies

Female 6-week-old BALB/c mice (for the M109-HiFR-*Luc*2 lung carcinoma model) (16-20g), or 8-week-old C57BL/6J (for the LLC1 model) were purchased from Janvier Labs (Le Genest-Saint-Isle, France) and Charles River (Écully, France). All experiments were approved by the CEBEA of the ULB faculty of medicine under approval numbers 585N, 719N, and CMMI-2017-01. The housing conditions were identical to those described in *Experimental part I-section 2.3.3.1.*

2.3. Development of Lewis lung carcinoma expressing luciferase model

The development of the Lewis lung carcinoma expressing luciferase (LLC1-*Luc*) model was performed in collaboration with Inhatarget Therapeutics. The LLC1 cell line was provided by ATCC and its transfection was performed using pLenti EF1-*luc* MOI 100 by GiGa Uliège. The cells were cultured in DMEM, supplemented with 10% (v/v) FBS, 1% (v/v) penicillin-streptomycin, and 0.02% (v/v) gentamycin in an incubator with 5% CO_2, at 37°C. The medium was renewed each 2-3 days, which corresponded to 70-80% of confluence, as recommended by the ATCC. In the literature, the implantation of these cells in C57BL/6J mice has already been performed using the intrapulmonary engraftment [235,236]. The cell suspension (5.10^4 cell/mL) was implanted following the intrapulmonary graft as described in *Experimental part I-section 2.3.3.2. In vivo* tumour growth (primary tumour and metastases) was followed by bioluminescence imaging (BLI) of the whole mice performed two times a week (on D3, D6, D9, D13). BLI imaging was performed by means of a Photon Imager Optima (Biospace Lab, France) that dynamically counted the emitted photons for at least 25 min, with the mice under anaesthesia (3.5% and 2% isoflurane for initiation and maintenance, respectively) and after subcutaneous administration of 150 mg/kg of D-luciferin (Promega, Leiden, Netherlands) [237]. Image analysis was performed with M3Vision software (Biospace Lab), and signal intensities were quantified individually for a time lapse of 5 min corresponding to the maximum signal intensity plateau. In addition, to visualize the tumour mass, mice were scarified on D6, D8, D10, D13 and D20 and images were taken.

2.4. PK study on LLC1-*Luc* grafted mice

LLC1-*Luc* grafted mice were administered CIS-DPI-50 at 0.5 mg/kg and CIS-IV_2 at 2 mg/kg (their MTDs, as will be discussed in *Experimental part III-section 3.1*) 6 days following the intrapulmonary engraftment.

The CIS-DPI-50 blend was prepared and administered to mice following the same techniques as those described in *Experimental part I-section 2.4.4.3*, except for the anaesthesia. Indeed, to lighten the impact of repeated anaesthesia, mice were anesthetized after being placed in a chamber with 3.5% of isoflurane for 5 minutes.

Retro-orbital blood for plasma (heparinized tubes, centrifuged at 2 000 g for 10 min at 20°C) and organs (lungs, tumours) were collected at 1 min, 10 min, 30 min, 1h, 2h, 4h, 8h and 24h following the administration of CIS-DPI-50 blend (n=6-7 mice per timepoint), and at 30 min, 1h and 2h following the administration of CIS-IV_2 (n=5 per time point). Organs were washed in PBS and stored at -80°C until platinum content analysis. The tumour was washed in 100 μL of PBS (i.e. tumour fluid) and quantified to evaluate the platinum that was on the periphery of the tumour.

The PK profiles of cisplatin in the organs and plasma were established and PK curves of cisplatin and its adducts were graphed as platinum concentration *vs.* time curves. PK parameters were calculated following the procedure described in *Experimental part I-section 2.4.4.4.*

2.5. Biodistribution of CIS-DPI-50 and immunohistochemistry labelling following the administration of different regimens

To select the regimen that accumulated the most cisplatin in the tumour, four regimens were evaluated, as illustrated in **Figure 41**. LLC1-*Luc* grafted mice were administered CIS-DPI-50 blends, following the same techniques as described in *section 2.4.* These administrations were performed five times per week (designated as a cycle) for two cycles. This was done at 0.3 mg/kg (0.3 x 5), 0.5 mg/kg (0.5 x 5) and 1 mg/kg (1 x 5). CIS-DPI-50 blends were prepared and administered to mice following the techniques described in *Experimental part I-section 2.4.4.2* and *section 2.4.* In addition, to evaluate the effect of the frequency of administration for the same cumulative dose, CIS-DPI-50 blend was also administered three times per cycle (0.5 x 3) over two cycles and was compared to the group treated with the lower dose, more frequently (0.3 x 5). Blood and organs sampling was performed after the first treatment cycle (groups identified as 1_*group name*) and also after the second cycle (2_*group name*) as illustrated in **Figure 41**, to evaluate potential accumulation of platinum adducts in the tumour. As previously performed for the PK study in LLC1-*Luc* grafted mice, blood, tumour-free lungs and kidneys were collected at the T$_{max}$ for the tumours determined previously (i.e. 2h). Blood and organs followed the same protocol as in *Experimental part I-sections 2.4.4.4 and 2.4.4.5,* to evaluate their platinum concentrations.

In addition, mice treated with the CIS-IV_2 and CIS-DPI-50 regimens and untreated mice were euthanized 3 days after the end of each cycle **(Figure 41)** for histopathological analyses. This was done on mice in D6, D13 and D20, which were referred to as previously explained for the treated groups or as CTRL-D6, CTRL-D13 and CTRL-D20 for the untreated ones. Their lungs were harvested and immersed in FMA for 24h, then cleaned in water for 15 minutes before being put in IPA for 24h. Then, they were embedded in paraffin for histopathological analyses using HE staining and immunostaining. Analyses of HE staining were performed to evaluate lung tissue damage in a randomized, blind study by an independent pathologist following the process described by Jones *et al.* [238]. Moreover, the response to the treatment was investigated following the recommendations described by Travis *et al.* [239]. The severity of each observation was scored from 0 to 5, and the mean score was determined by calculating the average among each group. In addition, the frequency was evaluated and was expressed as the number of animals in which the observation was encountered.
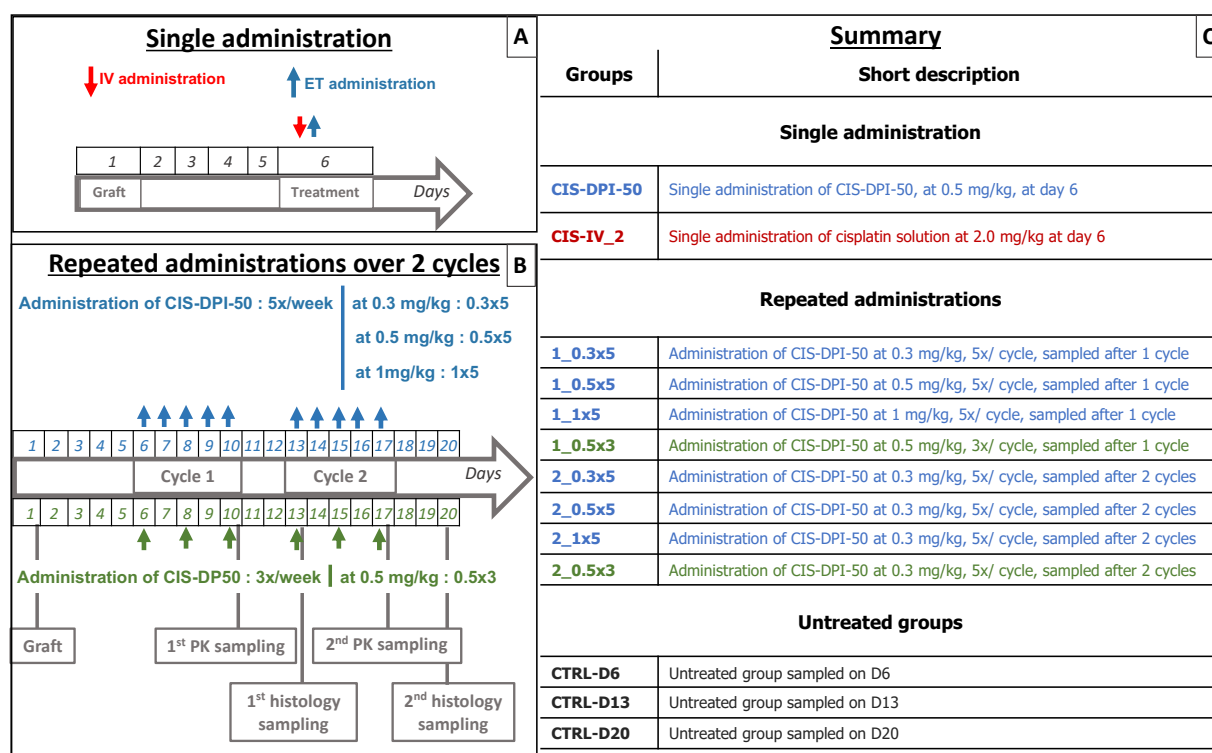

Figure 41: Scheme of administration of cisplatin formulations and sampling.

In addition, activated caspase 3 staining and CD3 and CD31 immunostainings were performed to evaluate the intensity of apoptosis related to cisplatin activity (activated caspase 3, [240]), and the involvement of T LYM (CD3, [241]), as well as the intensity of tumour angiogenesis (CD31 is expressed by endothelial cells, circulating platelets (PLT), MON, NT-GRA and some

T LYM [242]). These stainings were outsourced to DiaPath (CMMI, Biopôle ULB-Umons). This was performed for all mice lungs, using two impaired sections per lung and spaced by 150 μm. Lung sections were deparaffinized, rehydrated and washed in PBS and stained using an automated Ventana Discovery XT^{TM} IHC platform (Arizona, USA) for caspase 3, CD31 and CD3 or Dako PT Link/Autostainer Link 48 for CD8 (Agilent, Santa Clara, USA). The heat antigen retrieval for all the immunostainings was performed by putting the sections in EDTA (pH 8.4) for 8 min at 95°C, then 28 min at 100°C.

The sections were washed with PBS at each step and incubated with primary antibody then secondary antibody, then washed again and incubated with avidin-biotin complex (ABC) solution (Vector Labs, Peterborough, UK), rinsed once again and incubated with the 3,3'-diaminobenzidine (DAB) substrate (Vector Labs, Peterborough, UK) for 5 min.

The incubation time and dilution of the primary and secondary antibodies differed from one staining to another. For the staining of activated caspase 3 in the cell cytoplasm, the primary antibody was a rabbit immunoglobulin (Vector Labs, Peterborough, UK), diluted 1/200 and incubated at 37°C for 1h. After the washing steps, sections were incubated with the secondary antibody, biotinylated anti-rabbit (Vector Labs, Peterborough, UK) previously diluted 1/200, and incubated at 37°C for 24 min. For the staining of CD31 in the cell membrane, the primary antibody was a rabbit immunoglobulin (Vector Labs, Peterborough, UK), diluted 1/100 and incubated at room temperature for 1h. The secondary antibody, a biotinylated anti-rabbit (Vector Labs, Peterborough, UK) previously diluted 1/200, was incubated at 37°C for 28 min. For the staining of CD3 in the cell membrane and cytoplasm, the primary antibody staining, a rabbit immunoglobulin (Ventana Discovery XT^{TM}, Arizona, USA) was used as provided by the manufacturer and incubated at 37°C for 12 min. The secondary antibody, an OmniMap anti-rabbit horseradish peroxidase (HRP) (Ventana Discovery XT^{TM}, Arizona, USA), was used as provided by the manufacturer and incubated at 37°C for 12 min.

The quantification of the region of interest from caspase 3 and CD31 stainings within the tumour was performed using Visiopharm software 2020.09 (Copenhagen, Denmark). Results from caspase 3 were expressed as the positive fraction area calculated from the positively stained area and normalized by the combined area of positively and negatively stained pixels. To compare the vascularisation between tumour-free lungs and tumoral tissue, results from CD31 were instead expressed as the positive fraction area, calculated from the positively stained area and normalized by the total analysed tissue area.

2.6. Efficacy study on M109-HiFR-*Luc*2 lung carcinoma model

To evaluate the efficacy of CIS-DPI-50 in terms of tumour size during the treatment administration, it was mandatory to transfect the M109-HiFR mouse lung carcinoma cells with a luciferase reporter gene *luc2* (pGL4.10[luc2] vector, Promega, Leiden, Netherlands), as performed for LLC1-*Luc*, in collaboration with Inhatarget Therapeutics. The development of this model consisted of an intrapulmonary graft of $1.4.10^4$ cells, as described in *Experimental part I-section 2.3.3.2.*

On the third day post cell engraftment (i.e. D3), mice were randomly allocated to one of the four groups of investigation. CIS-DPI-50 blends were prepared and administered to mice following the techniques described in *Experimental part I-section 2.4.4.2* and *section 2.4*. Treatments were administered from D6 for two cycles and were established as follows: *(i)* negative control untreated group (n=8); *(ii)* CIS-DPI-50 blend at 0.3 mg/kg five times per cycle for two consecutive cycles (n=15); *(iii)* CIS-DPI-50 blend at 0.5 mg/kg three times per cycle for two consecutive cycles (n=15).

BLI of the whole mice was performed following the technique described in *section 2.3*, two days per cycle at D3, D6, D10, D13, D17, D20, D23, D27, D30, D33 and D37. Finally, Kaplan-Meier survival curves were established by excluding deaths related to the ET administration procedure, as previously reported [192,205,243]. A responder was defined as a mouse with tumour growth < 150% in comparison to the 100% value measured at D3.

2.7. Statistical analyses

All statistical tests were conducted using GraphPad PRISM® (7.0a) software. The Kaplan-Meier curve and log-rank test with an analysis of the *p* value by means of the Holm-Šídák method were used for the survival analysis. Two-way ANOVA with Tukey-multiple post-testing was used to analyse mean tumour growth over time. One-way ANOVA and Bonferroni's post-testing was used to analyse the difference in terms of positive fraction area for caspase 3 staining and platinum concentration between groups. Results were considered as statistically significant (*) for $p < 0.05$, very significant (**) for $p < 0.01$, extremely significant for $p < 0.001$ (***), and extremely significant for $p < 0.0001$(****). Results are presented as the mean value ± standard error of the mean (SEM), unless otherwise indicated.

3. <u>Results and discussion</u>

3.1. PK study of CIS-DPI-50 on Lewis lung carcinoma grafted mice

3.1.1. Development of Lewis lung carcinoma model

The LLC1-*Luc* model was developed to evaluate the efficacy and the tumour accumulation of CIS-DPI-50 on the most common reproducible syngeneic and orthotopic murine model of the literature. The advantage of this model is that the tumour microenvironment can be accurately depicted in the preclinical model [244]. Indeed, this was much needed in the study as in parallel to the biodistribution of CIS-DPI-50, the involvement of the immune cells in the tumour was also investigated. Moreover, this model was highly tumorigenic a few days following the engraftment, which would allow us to obtain an appropriate tumour mass for isolation and quantification.

Different cell suspension concentrations were tested by Inhatarget Therapeutics. The cell suspension characterized by the longest median survival (i.e. 21 days) was selected. A long median survival was crucial in our case as our aim was to evaluate the PK biodistribution following the administration of CIS-DPI-50 repeatedly up to two cycles (i.e. 14 days). The intrapulmonary graft at the selected concentration (i.e. 5.10^4 cells/mL) mice showed BLI signals located in the mice thoracic cage, starting in D3, which proved the success of the graft. The signals increased exponentially from D3 until D13. Therefore this model was selected as it described a pulmonary localized tumour with a success of graft of 90%, as represented in **Figure 42.A**. In addition, lungs were harvested to visually evaluate the tumour mass to see whether it can be easily separated from tumour-free lungs, as illustrated in **Figure 42.B, C and D.**
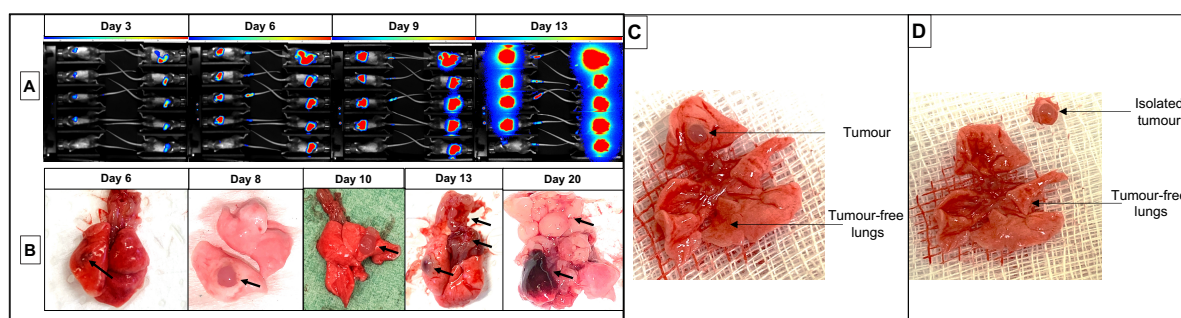

Figure 42: Characterization of the LLC1-*Luc* model in mice in terms of BLI of intrapulmonary grafted mice with 5.10^4 cells/mL at D3, D6, D9 and D13 (A). Mice lungs were harvested to visualize the evolution of lung tumours at D6, D8, D10, D13 and D20 (B). Representative images of the tumour implanted in the lungs (C) and its isolation from tumour-free lungs (D). The black arrows indicate the location of the tumour.

The results from this study confirmed the ability of the LLC1-*Luc* lung cancer model to induce the development of pulmonary tumours inside the thoracic cage, with limited metastases detected elsewhere (only low signals in the tails) from D3 to D13, as illustrated in **Figure 42.A**. The images taken from harvested days showed that the primary inoculation site on the left lung continued to grow from D6 up to D10. It is only from D13, that the tumour grew outside the left lung, and more precisely between the lungs. This tumour continued to expand until D20, and maintained its position between the lungs. On that day, the left lung was nearly completely necrotic while the tumour-free lungs were still constituted of normal tissue only, as illustrated in **Figure 42.B**.

3.1.2. PK results and tumour accumulation following a single administration of CIS-DPI-50

Considering the fast development of the tumour (i.e. median survival up to D21), and the length of CIS-DPI-50 regimens (i.e. two-week treatments), it was interesting to initiate the treatment at the earliest to *(i)* better control the tumour growth, and *(ii)* assure the ability to deliver two treatment cycles before mice death due to their tumour mass. As illustrated in **Figure 42.C and D**, the separation of the tumour mass from lung tissue was feasible on D6. Indeed, on that day, the tumour was large enough to be easily isolated from lung tissue. Therefore, the PK study on grafted mice was initiated on D6. CIS-DPI-50 and CIS-IV_2 were administered at their respective MTD, i.e. 0.5 mg/kg and 2 mg/kg. The determination of the MTD will be further detailed in *Experimental part III-section 3.1.*
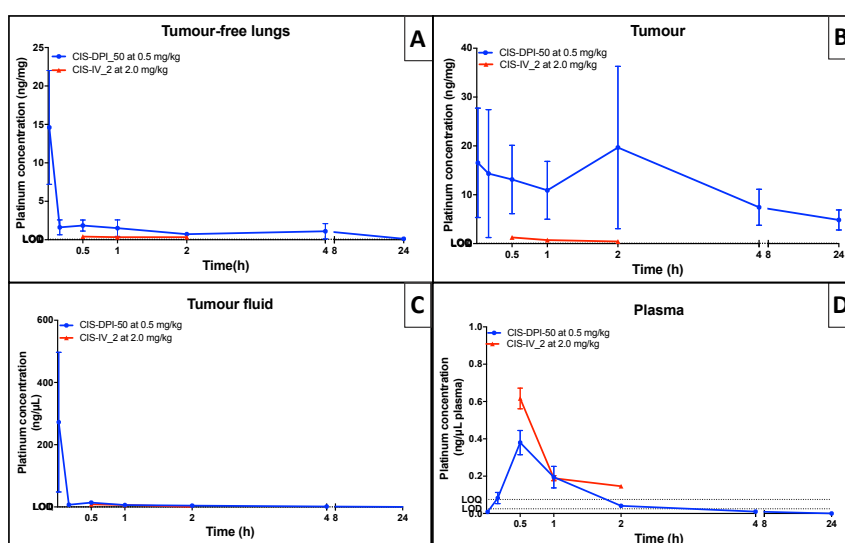

Figure 43: PK study following a single administration on D6 of CIS-DPI-50 or CIS-IV_2 (0.5 and 2 mg/kg, respectively) in LLC1-*Luc* grafted mice. Platinum concentrations were evaluated in tumour-free lungs (A), tumour (B), tumour fluid (C) and plasma (D). All results are expressed as means ± SEM (n=5-7 per timepoint).

As expected, CIS-DPI-50 C_{max} in tumour-free lungs (i.e. both left and right lungs) was reached immediately (i.e. 1 min corresponding to the time required to euthanize the mice and collect organs) following its administration using the ET route, and was up to 15 ± 7 ng/mg **(Table 17)**. This corresponded to $29 \pm 13\%$ of the delivered dose, and was similar to the percentage previously obtained in healthy mice ($26 \pm 3\%$). The high SEM values can be related to the variability of administration, which can directly lead to higher variations of the C_{max} in the tumour-free lungs and plasma.

Table 17: PK parameters of PK study of CIS-DPI-50 at 0.5 mg/kg in LLC1-*Luc* grafted mice. These parameters were determined on the PK curves obtained in **Figure 43**. All results are expressed as means $\pm$ SEM (n=5-7 per timepoint).

Pharmacokinetics	CIS-DPI-50 at 0.5 mg/kg		
	Tumour-free lungs	Tumour	Plasma
C_{max} (ng/mg – ng/µL)	15 ± 7	20 ± 16	0.38 ± 0.07
T_{max} (min)	1	120	30
$AUC_{0-\infty}$ (ng.min.mg^{-1} - ng.min. µL^{-1})	1071 ± 825	10683 ± 5836	30 ± 9
K_{el}^{i} (min^{-1})	0.058	0.0074	
$t_{1/2}^{i}$ (min)	12	94	
K_{el}^{t} (min^{-1})	0.0015	0.00078	
$t_{1/2}^{t}$ (h)	8	15	

Following the administration of CIS-DPI-50, the platinum concentration quickly decreased from 15 ± 7 ng/mg to 2 ± 1 ng/mg in 30 minutes and was still decreasing 4h later when it reached 1 ± 1 ng/mg **(Figure 43.A)**. The elimination from the tumour-free lungs followed two major phases, as observed in healthy mice **(Figure 39)**. Indeed, it was characterized first by clearance of cisplatin, with a K_{el}^{i} of 0.058 min^{-1} and $t_{1/2}^{i}$ of 12 min (versus 19 min in healthy mice), then of its adducts with a K_{el}^{t} of 0.0015 min^{-1} and $t_{1/2}^{t}$ of 8h (versus 39h in healthy mice). Even considering this profile, and the 4-fold higher dose for CIS-IV_2 in comparison to CIS-DPI-50, the cisplatin concentration in tumour-free lungs was more than 4-fold higher for CIS-DPI-50 than for CIS-IV_2, 30 min after their administrations (1.9 ± 0.7 ng/mg for CIS-DPI-50 *vs.* 0.42 ± 0.03 ng/mg, **Figure 43.A**).

This biodistribution profile was close to that obtained during the PK study conducted on healthy mice as the T_{max} (1 min), K_{el}^{i} (0.036 min^{-1}) and $t_{1/2}^{i}$ (19 min) were similar **(Table 16)**. However, considering the 2-fold difference in terms of dose between the PK studies (i.e. CIS-DPI-50 at 0.5 mg/kg *vs.* 1.0 mg/kg), the C_{max} obtained in grafted mice was not proportionally lower than that obtained in healthy mice (19 ± 2 ng/mg, **Table 16**). This can be attributed to the differences in terms of lung masses between mice (i.e. 115 ± 2 mg for grafted-mice *vs.* 181 ± 2 mg for

healthy mice). In addition, the K_{el}^t (0.00029 min^{-1}) and $t_{1/2}^t$ (39h) described a longer elimination in healthy mice. However, these comparisons should be considered with a great deal of precaution as the mice strains were different (CD1 and C57BL/6J mice), which could alter the drug biodistribution [245]. Indeed, differences in enzyme kinetics, metabolite formation, enzyme abundance and inducibility have been reported between strains [246,247].

The biodistribution profile in tumour-free lungs was correlated to a progressive diffusion of platinum in the tumour. Indeed, the PK profiles in the tumour demonstrated the presence of a relatively high constant platinum concentration during the first hour (11 ± 6 ng/mg) following the administration of CIS-DPI-50 until reaching a peak concentration 2 hours later (20 ± 16 ng/mg). The platinum concentration then slowly decreased until reaching 7 ± 4 ng/mg 4 hours later and 5 ± 2 ng/mg 24 hours later **(Figure 43.A)**. The platinum concentration in the tumour following CIS-IV_2 administration was the highest at 30 minutes. At that timing, the platinum concentration following the administration of CIS-DPI-50 at a dose 4-fold lower was more than 10-fold higher in the tumour (13 ± 7 ng/mg *vs.* 1.2 ± 0.1 ng/mg) **(Figure 43.A)**. However, it is worth reporting that the first timing points were not considered in this study since in the first time points, the platinum concentration in plasma is high, as reported in healthy mice. Therefore, once isolated, the total platinum quantification inside the tumour could be attributed to the fraction of platinum retrieved in the tumour vessels and not to the fraction of platinum fixed within the tumour. Consequently, to avoid this bias, it was important to select time points at which the platinum concentration in plasma was at its lowest, while considering that the platinum concentration in the tumour would be the earliest in the first time points. To do so, the plasma platinum concentrations reported by Levet *et al.* 30 minutes following the administration of CIS-IV_1.25 and by our PK study, following the administration of CIS-IV_1.5, both in healthy mice, were 0.32 ± 0.06 ng/μL and 0.6 ± 0.1 ng/μL, respectively [203], and were even lower 1h later. Therefore, the PK study following the administration of CIS-IV_2 was conducted at 30 min, 1h and 2h to consider the fraction of platinum retrieved in the tumour once cisplatin was cleared from plasma. **Figure 43.D** showed that the platinum concentration in the plasma was at its highest 30 minutes (0.6 ± 0.1 ng/μL) following the administration of CIS-IV_2 and decreased until reaching 0.15 ± 0.01 ng/μL 2h later. This would have been certainly higher if the sampling was performed earlier.

The evaluation of the platinum concentration in tumour fluid was assessed to verify whether the platinum quantified for the tumour was fixed within it or was deposited on its periphery,

without penetrating inside the tumour. As observed, the platinum concentration in the tumour fluid was at its highest 1 min following the administration of CIS-DPI-50 (272 ± 224 ng/μL), was more than 19-fold lower 30 min later (14 ± 6 ng/μL), and continued decreasing until reaching 2 ± 1 ng/μL 4 hours later **(Figure 43.C)**. This result correlated with the concentration in the tumour and tended to demonstrate a diffusion from the tumour periphery to the tumour core. This was also observed for CIS-IV_2, but to a lower extent, as the platinum concentration in tumour fluid was 8 ± 2 ng/μL at 30 min and was 0 ± 1 ng/μL 2h later. The difference in terms of tumour fluid concentration between CIS-DPI-50 and CIS-IV_2 can be attributed to a difference in terms of diffusion. Indeed, this was hypothesized considering that *(i)* the tumour fluid corresponded to the liquid in which the tumour was rinsed and *(ii)* the concentration drop in the tumour fluid was correlated with an increase within the tumour.

These results were very encouraging, as the concentration in the tumour was immediately high following the administration of CIS-DPI-50 and increased slowly until reaching its peak 2h later, while platinum elimination was slow. Indeed, platinum was eliminated following two phases: a first elimination of cisplatin from lungs and tumours with a $t_{1/2}{}^i$ of 12 min and 94 min, respectively; and a second elimination, probably of cisplatin adducts, with a $t_{1/2}{}^i$ of 8h and 15h, respectively. Consequently, this was correlated with an $AUC_{0-\infty}$ of $10\ 683 \pm 5\ 836$ ng.min.mg^{-1} in the tumour, which was nearly 10-fold higher in comparison with the $AUC_{0-\infty}$ in the tumour-free lungs ($1\ 071 \pm 825$ ng.min.mg^{-1}) **(Table 16)**. This result is very promising as it showed that following the administration of CIS-DPI-50, the tumour is more exposed and for a longer time to cisplatin than tumour-free lungs. Indeed, this would lead to a higher efficacy, with limited pulmonary injury from cisplatin in tumour-free lungs.

This higher exposure in the tumour can be explained by factors intrinsic to both the tumour and to the molecule that can lead to a defect in the transit of cisplatin within it [248]. Indeed, apart from the drug size and its elimination half-time ($t_{1/2}$), the distribution of a drug in the tumour depends on the degree of vascularization and angiogenesis of the cancerous tissue [248]. "Solid stress" related to uncontrolled cancer cell mitoses often leads to an incomplete angiogenesis. Angiogenesis is therefore often anarchic, with a low vascular density leading to irregular blood flow. In this case, the blood and lymphatic vessels often undergo compression by the tumour. Consequently, an increase in the interstitial fluid pressure of $\sim$ 10-20 mm Hg is observed within the tumour in comparison to healthy tissue, leading to impediments to delivery and convection of small molecules and therefore to low clearance [70,249]. Moreover, as the cells and the

extracellular matrix (high levels of collagen and polysaccharide networks) are abnormally denser than with normal cells, both diffusion and convection are difficult to achieve, which increases this drug entrapment [70,249].

Three main mechanisms related to the gradient concentration are involved in the penetration of a drug in a tissue, as explained by Minchinton *et al.* [70]. The first parameter is drug supply and mostly depends on the dose and the PK. Indeed, the drug penetration inside the tumour is determined by the rate of diffusion through the tissue, which is dictated by the physiochemical properties of drugs (e.g. MW, charge and aqueous solubility). As cisplatin is a small, non-charged molecule, it can diffuse through the plasma membrane using mostly passive diffusion, but this is achieved slowly as it is a hydrophile [91]. The second parameter is the flux. Once inside the cell, the low chloride concentration leads to the transformation of cisplatin into positively charged species (mono and di-aqua-cisplatin) that are able to undergo diffusion in the tissue through extracellular pathways [70]. In addition, as the extracellular matrix is known to have a rapid turnover, its modification is able to alter the penetration of the drug through the tumour, as cisplatin reactive species can bind to this matrix. Finally, the last parameter is consumption. Depending on the binding, metabolism and sequestration of the drug, the penetration can also differ [70]. Indeed, a low drug penetration is observed in the case of a high cellular metabolism or a high binding or sequestration (which both increase the concentration of a drug within the tissue). In the case of cisplatin, it is probable that the positively charged species, which are highly reactive, bind to the tissue, which would increase the tissue concentration and limit its penetration inside the deep layers. This can therefore explain the high tumour concentration in the tumour and its slow release.

The platinum profiles in the tumour following the administration of CIS-DPI-50 showed a high variability among mice, while this was not observed in tumour-free lungs or in plasma for example. This could be attributed to the variation between tumours in terms of localisation (junctions between the bronchioles and alveoli), size (mass, volume) and also to the tumour microenvironment, as already reported for other cytotoxic drugs such as doxorubicin or etoposide, for example [70].

Following the administration of CIS-DPI-50, the plasma C_{max} was 0.38 ± 0.07 ng/μL, the lowest in comparison to the tumour and tumour-free lungs. This was related to an $AUC_{0-\infty}$ of 30 ± 9 ng.min. μL^{-1}. These results were comparable to the PK parameters obtained in healthy mice with a 2-fold higher dose (i.e. 1.0 mg/kg *vs.* 0.5 mg/kg). The plasma concentration 30 min after

the treatment administration was 2-fold higher (0.7 ± 0.6 ng/μL) and the AUC$_{0-\infty}$ more than 3-fold higher (95 ± 30 ng.min.μL^{-1}) in healthy mice **(Figure 39)**. The difference in terms of AUC$_{0-\infty}$ can be attributed to the difference between mouse strains, as previously argued, and/or to the difference in the selected time points (up to 48h for the PK study in healthy mice *vs.* up to 24h for the PK study in grafted mice). However, the main difference between the two PK studies was the T$_{max}$ shift. Indeed, while this was observed immediately after the administration of CIS-DPI-50 in healthy mice, this was only described after a delay of 30 min for grafted mice **(Table 16 and Table 17)**. This demonstrated that the presence of the tumour would have disturbed the normal biodistribution in terms of absorption/elimination mechanisms, leading to impaired clearance mechanisms. It is possible that cisplatin diffused from tumour-free tissue to the tumour before being eliminated in plasma, which led to a delay in reaching the plasma C$_{max}$. In addition, as the tumour micro-environment is able to retain cisplatin, the elimination from the tumour could have been delayed, leading to a longer T$_{max}$.

As expected, and as previously reported, the platinum concentration in plasma was higher for CIS-IV_2 than CIS-DPI-50, with a value of 0.6 ± 0.1 ng/μL, similar to that observed in healthy mice at 1.5 mg/kg and at the same timing (CIS-IV_1.5: 0.6 ± 0.1 ng/μL).

Overall, the biodistribution of CIS-DPI-50 administered using the ET route to LLC1-*Luc*-grafted mice demonstrated promising results in terms of tumour exposure, with a favourable AUC$_{0-\infty}$ and clearance. On the other hand, a low plasma and tumour-free lung exposure was reported. Both results are good prognoses for CIS-DPI-50 efficacy as well as its pulmonary and systemic tolerance. Indeed, Kim *et al.* have reported a significant correlation between tissue platinum concentration and efficacy in terms of reduction of the tumour size, and increased survival and time to recurrence of the disease [204].

3.2. Selection of the most appropriate CIS-DPI-50 monotherapy regimen

Despite the promising tumour exposure to cisplatin following a single administration of CIS-DPI-50, the strategy of maintaining high platinum concentrations in the tumours during the off-cycles observed with IV chemotherapy can be successful only if CIS-DPI-50 is administered frequently. Therefore, the aim of this part was to select the regimen that most accumulated platinum in the tumours with limited concentration in healthy organs (tumour-free lungs, and kidneys) and in plasma. To do so, the platinum concentration in healthy tissues, plasma, and in the tumour were compared following repeated administrations of CIS-DPI-50 through different

regimens, as illustrated in **Figure 41**. Moreover, these regimens were administered over two cycles to evaluate whether the platinum accumulated during the treatment cycles.

To do so, mice were administered, from D6 following the intrapulmonary graft, CIS-DPI-50 at three different doses (0.3, 0.5 and 1 mg/kg) over five times per cycle, for two cycles. To evaluate the effect of the frequency of administration, a fourth group was administered CIS-DPI-50 at 0.5 mg/kg, three times per cycle (0.5 x 3), and was compared to the group treated with 0.3 mg/kg, five times per cycle (0.3 x 5). Indeed, both groups had the same cumulative doses but fractionated into different days. Mice were euthanized at the end of each cycle (D10 and D17) at the T_{max} selected in the previous study (i.e. 2h).

3.2.1. Body weight profiles

Following the administration of CIS-DPI-50 regimens, mice bw profiles were relatively stable and similar between all groups during the first cycle. At the end of the first cycle (D10), it should be mentioned that the 0.5 x 3 group showed the highest bw increase ($3.9 \pm 0.6\%$) among all treated groups, while the 1 x 5 group showed the lowest (1 x 5: $0.8 \pm 0.7\%$) **(Figure 44)**. This was certainly related to the toxicity of the cumulative dose of cisplatin: 1.5 mg/kg for 0.5 x 3 *vs.* 5 mg/kg for 1 x 5. However, these toxicities were limited as no bw loss was reported. The bw of all the treated mice increased between D10 and D13 as no treatment was administered during these two days **(Figure 41),** while the bw remained stable for the untreated group.
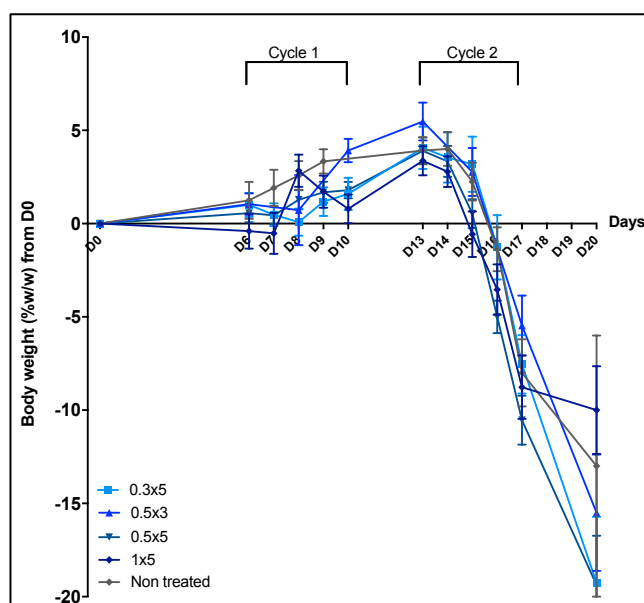

Figure 44: Bw profiles of untreated or treated LLC1-*Luc*-grafted mice, administered with CIS-DPI-50 either five times per week at 0.3 mg/kg (0.3 x 5), 0.5 mg/kg (0.5 x 5) or at 1 mg/kg (1 x 5) or three times per week at 0.5 mg/kg (0.5 x 3). All results are expressed as means ± SEM (N=15-25).

Following the first administration during the second cycle (i.e. D13), all mouse groups started losing weight sharply until reaching, at the lowest, -6 ± 2% for 0.5 x 3, and at the highest, -11 ± 1% for 0.5 x 5 and -9 ± 2% for 1 x 5 on D17 **(Figure 44)**. The bw of all mouse groups continued decreasing until D20. As these trends were followed by both treated and non-treated mice, these profiles demonstrated the aggressiveness of the LLC1-*Luc* model (bw losses of untreated mice) **(Figure 44)**.

3.2.2. Histology and immunohistochemistry investigation on Lewis lung carcinoma grafted mice

Prior to the evaluation of platinum accumulation, it was interesting to investigate the lung tissue (i.e. tumours and tumour-free tissue) of the LLC1-*Luc* grafted mice. This was crucial for *(i)* understanding the cisplatin distribution within the tumour, *(ii)* the evaluation of the pulmonary inflammation of tumour-free tissue and *(iii)* the assessment of the tumour response to cisplatin.

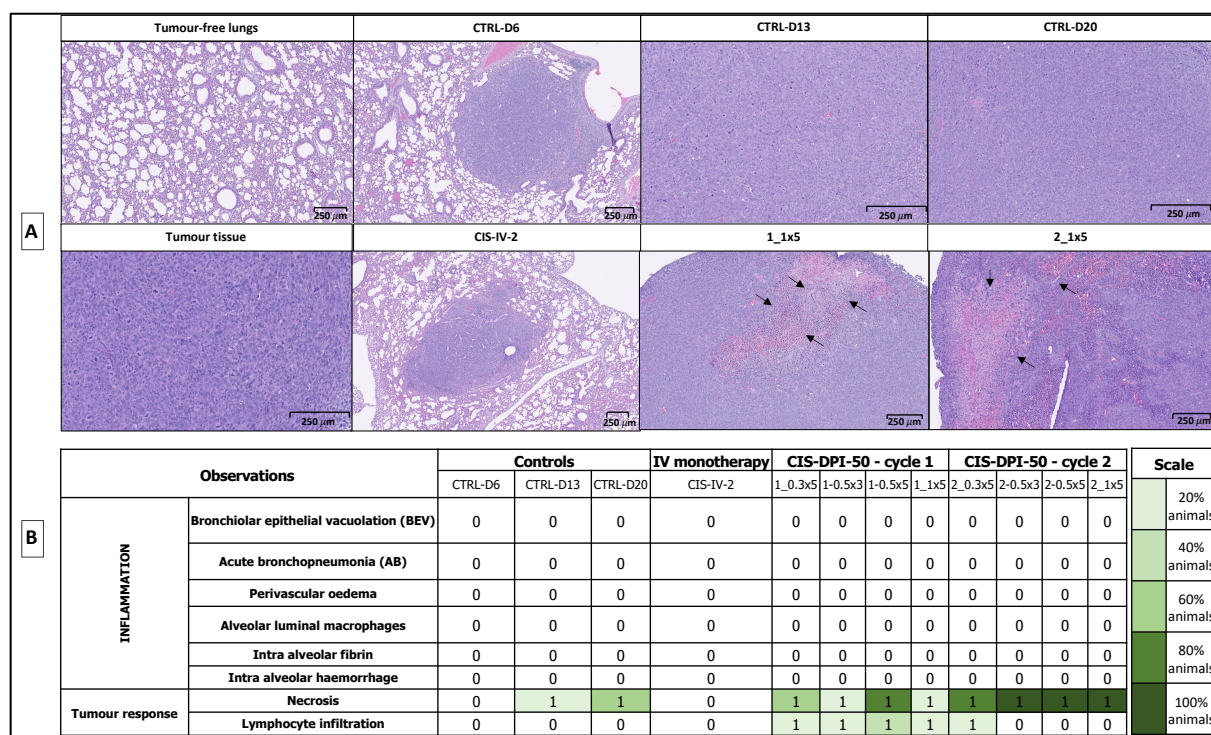|		Controls			IV monotherapy	CIS-DPI-50 - cycle 1				CIS-DPI-50 - cycle 2				Scale
Observations		CTRL-D6	CTRL-D13	CTRL-D20	CIS-IV-2	1_0.3x5	1-0.5x3	1-0.5x5	1_1x5	2_0.3x5	2-0.5x3	2-0.5x5	2_1x5	
INFLAMMATION	Bronchiolar epithelial vacuolation (BEV)	0	0	0	0	0	0	0	0	0	0	0	0	20% animals
	Acute bronchopneumonia (AB)	0	0	0	0	0	0	0	0	0	0	0	0	40% animals
	Perivascular oedema	0	0	0	0	0	0	0	0	0	0	0	0	60% animals
	Alveolar luminal macrophages	0	0	0	0	0	0	0	0	0	0	0	0	80% animals
	Intra alveolar fibrin	0	0	0	0	0	0	0	0	0	0	0	0	100% animals
	Intra alveolar haemorrhage	0	0	0	0	0	0	0	0	0	0	0	0	
Tumour response	Necrosis	0	1	1	0	1	1	1	1	1	1	1	1	
	Lymphocyte infiltration	0	0	0	0	1	1	1	1	1	0	0	0	

Figure 45: Histopathology of lung tissue of untreated (sampled on D6 (CTRL-D6), D13 (CTRL-D13) or D20 (CTRL-D20)) or treated LLC-grafted mice, exposed to CIS-IV_2 alone, or after the administration of repeated administrations of CIS-DPI-50 following different regimens over two cycles. The groups' abbreviations are described in **Figure 41.** Representative images of treated and untreated groups (A) and heat map of adverse observations (in scale of concerned proportion of mice) and severity scores (from 0 to 5) depending on lung tissue inflammation and response scores (from 0-1) depending on tumour response (B). The evaluation of the mouse-lung histopathological sections was performed to analyse the pulmonary inflammation and to investigate the tumour response to the treatment by evaluating necrosis and LYM infiltration. The black arrows indicate the necrotic areas.

The evaluation of the inflammation did not show any inflammation of tumour-free tissue for any group as no adverse side-effect was reported **(Figure 45.B)**. Indeed, no bronchiolar epithelial vacuolation (BEV), acute bronchopneumonia (AB), perivascular oedema, alveolar luminal macrophages, intra-alveolar fibrin or intra-alveolar haemorrhage were reported. This was an interesting result as the lungs of this specific mouse strain seemed to tolerate up to 10 mg/kg of cisplatin as a cumulative dose delivered continuously using CIS-DPI-50 (i.e. 1 mg/kg administered five times per cycle, over two cycles).

The tumour-free lung tissue showed a well-spaced organization, with the bronchioles and the alveoli clearly represented **(Figure 45.A)**. In contrast, the tumour tissue showed a higher density, uncontrolled mitoses and anarchic organization **(Figure 45.A)**. To evaluate the treatment efficacy, we followed the new recommendations on how to determine whether an antitumour response has occurred on neoadjuvant chemotherapy prior to resection [239]. This evaluation was performed by an independent pathologist and was mostly done by analysing the presence of necrosis in the tumour tissue and LYM infiltration, demonstrating the ongoing response to the treatment. The analyses of the untreated groups did not show any major difference in terms of tumour response, irrespective of the day post-graft **(Figure 45.B)**. However, localized necrosis outbreaks were reported for untreated groups on D13 and D20 (CTRL-D13, CTRL-D20). These observations were light and concerned fewer than 20-50% of the mice. Indeed, higher necrosis was retrieved for CTRL-D13 in comparison to CTRL-20. Despite the fact that the latter has an increased tumour mass, it is worth mentioning that this group was only composed of two mice, as they died from their tumour (i.e. median survival of untreated groups: 21 days). For both groups, this can be attributed to the necrosis within the tumour due to its inability to exchange with bloodstream (oxygen, nutriments) efficiently, leading to tumour hypoxia [70]. Indeed, as represented in **Figure 46**, a huge gap is observed in terms of vascularization (i.e. CD31 staining) between the tumour-free lungs and the tumour tissue. Moreover, as the days post-graft passed (CTRL-D6, CTRL-D13 and CTRL-D20), the tumour got bigger and invaded the tumour-free lungs, leading to a decreased CD31 staining **(Figure 46.B, C and D)** and to the necrosis of cells from the core of the tumour. To assess objectively the difference in terms of vascularization between the tumour-free lungs and the tumour, the CD31 immunostaining was quantified by analysing the positive fraction area of the endothelial cells from both tissues and was normalized by the total analysed surface **(Figure 46.A)**. These results confirmed these illustrations as the positive area fractions from the tumour were lower than those obtained with tumour-free lungs. Indeed, the positive area fraction of the tumour-free lungs in comparison to the tumour tissue was 1.4-fold higher for CTRL-D6 ($p >$

0.05), 5-fold higher for CTRL-D13 ($p < 0.01$) and up to 6-fold higher for CTRL-D20 ($p < 0.001$). This observation also showed that the more the tumour size increased, the more the gap in terms of vascularization was significant. This phenomenon is one of the most limiting factors for the efficacy of cytotoxic drug as the access to the tumour cells is congested [70].
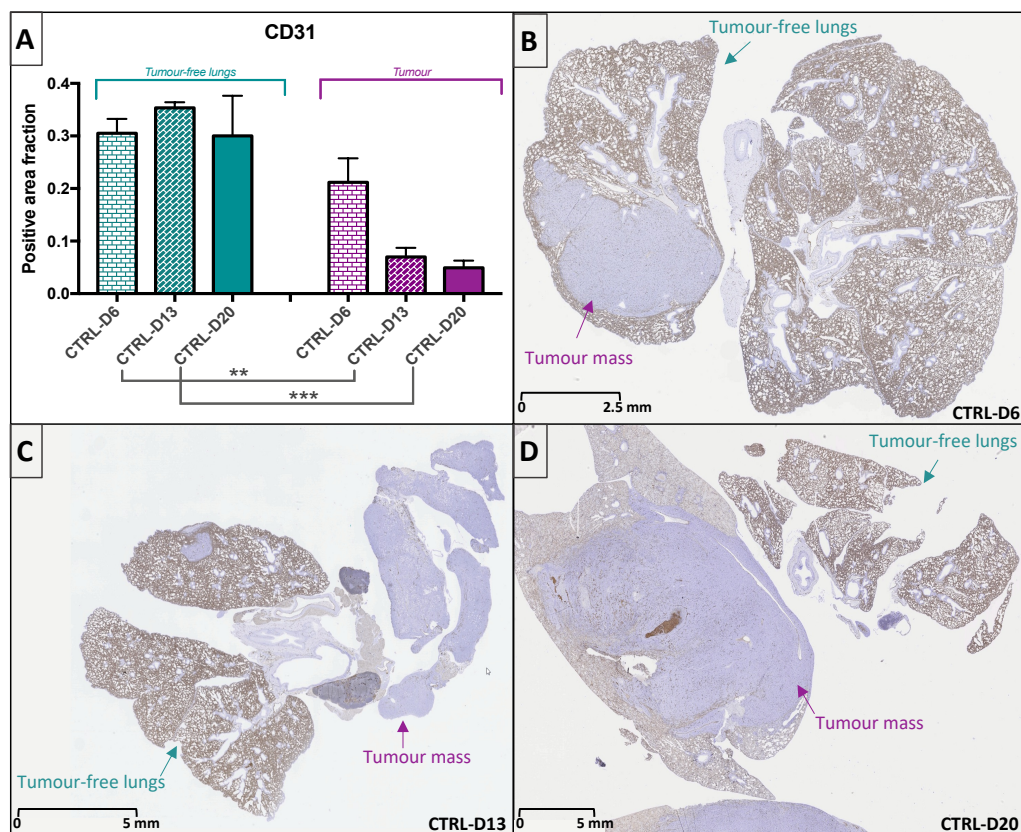

Figure 46: Positive area fraction of activated CD31 staining on level 2, of the untreated groups on D6 (CTRL-D6), D13 (CTRL D13) and D20 (CTRL-D20) post-graft (A). Results are expressed as means ± SEM (n=2-8). The statistical analyses were performed *vs.* their corresponding group using one-way ANOVA and Bonferroni's post-test (*** for $p < 0.001$ and ** for $p < 0.01$). Representative images of CD31 immunostaining of the following untreated groups are given: CTRL-D6 (B), CTRL D13 (C) and CTRL-D20 (D).

No sign of tumour response in terms of necrosis or LYM infiltration was reported following a single administration of CIS-IV_2 **(Figure 45.B)**. However, this was observed for a less cumulative dose (i.e. 1.5 mg/kg) when CIS-DPI-50 was administered following a one-cycle administration of the 0.3 x 5 regimen. Moreover, all the groups treated with CIS-DPI-50 demonstrated an increased response to the treatment irrespective of the dose or the frequency. Indeed, this was observed by an increase in the proportion of animals who developed necrosis (i.e. 20-60% of the mice) as well as increased LYM infiltration. This demonstrated the ongoing interaction with the immune system to either eliminate tumour cells and/or to initiate inflammation [250] **(Figure 45.B)**.

Following the two-cycle administration, the tumour response seemed to be increased as all the treated groups demonstrated increased necrosis (i.e. 80-100% of the mice) as well as increased LYM infiltration when compared to their respective control, as represented in **Figure 45.B**. Arrows were displayed in **Figure 45.A** to visualize these necrosis areas from which cells are lacking, demonstrating the activity of cisplatin after its release from CIS-DPI-50.

To visualize the T LYM infiltration, CD3 was used as a marker for T LYM identification and showed an increased staining intensity for the highest dosed groups in comparison to their control **(Figure 47)**. Indeed, while limited staining intensity was observed for CIS-IV_2, a higher staining was observed following the two-cycle treatment. Therefore this result tended to confirm the observation obtained on HE-stained slides. However, it should be mentioned that the immunostaining of CD3 was not quantified and is represented in **Figure 47** as a qualitative result. To effectively distinguish the effect of the treatment in terms of dose and frequency of administration on T LYM infiltration, the CD3 staining should be quantified.
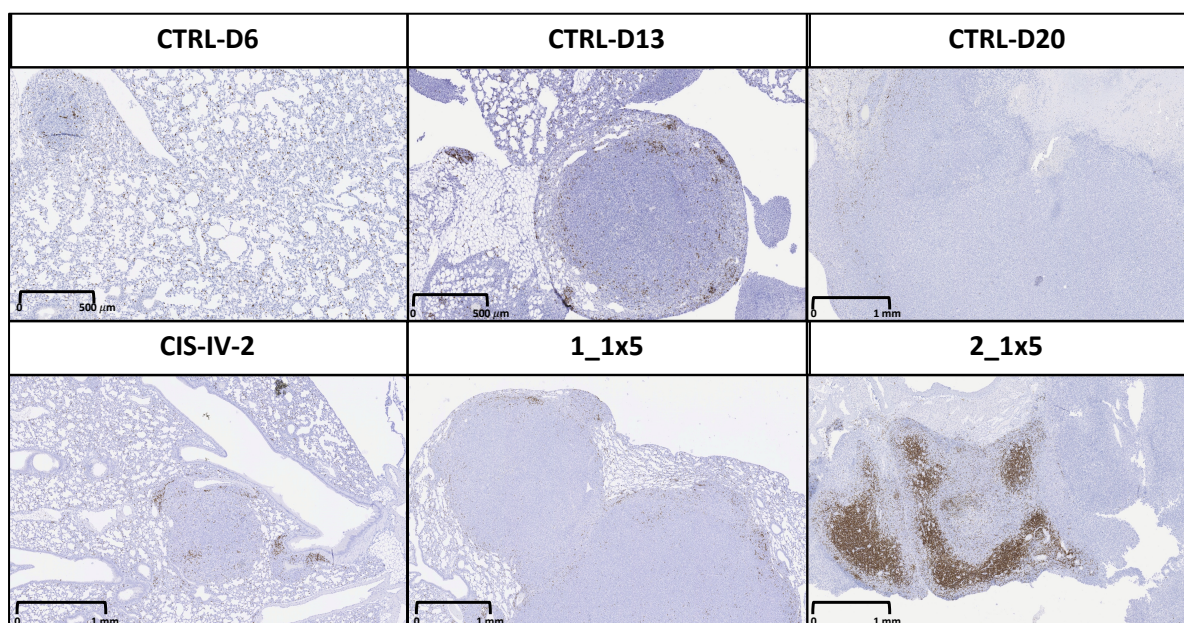

Figure 47: Representative images of CD3 immunostaining of treated groups following a single administration of CIS-IV_2, or repeated administrations of CIS-DPI-50 at the highest dose over two cycles and their corresponding controls. The groups' abbreviations are described in **Figure 41.**

Apart from necrosis, which is one of the two main mechanisms of cisplatin, the activity of caspase 3 as a marker of apoptosis was selected as it is commonly used as a cytoplasmic marker to detect cisplatin antitumour effect [251] **(Figure 48.C)**. Indeed, once cisplatin is in the cells, it converts into highly reactive metabolites that are able to *(i)* interact with several targets such as mitochondria and DNA and *(ii)* generate various ROS leading to the activation of caspases.

A general consequence of these mechanisms is apoptosis [128]. The identification of caspase 3 was performed on two levels spaced by 150 μm to evaluate whether cisplatin activity was maintained deeper in the tumour, thus demonstrating its penetration in the tumour tissue.

A non-significant increase was observed in terms of the caspase 3 positive area fraction between the untreated groups (CTRL-D6, CTRL-D13 and CTRL-D20), at both levels. Indeed, as the days post-graft passed, this fraction was 19-fold higher between CTRL-13 and CTRL-D6 and up to 27-fold higher between CTRL-D20 and CTRL-D6. This tended to demonstrate an increase apoptosis of untreated cancerous cells, which can be observed in hypoxic areas as described previously [252]. Indeed, hypoxia can result from the incomplete vascularization of the tumour, as represented with CD31 immunostaining in **Figure 46**.
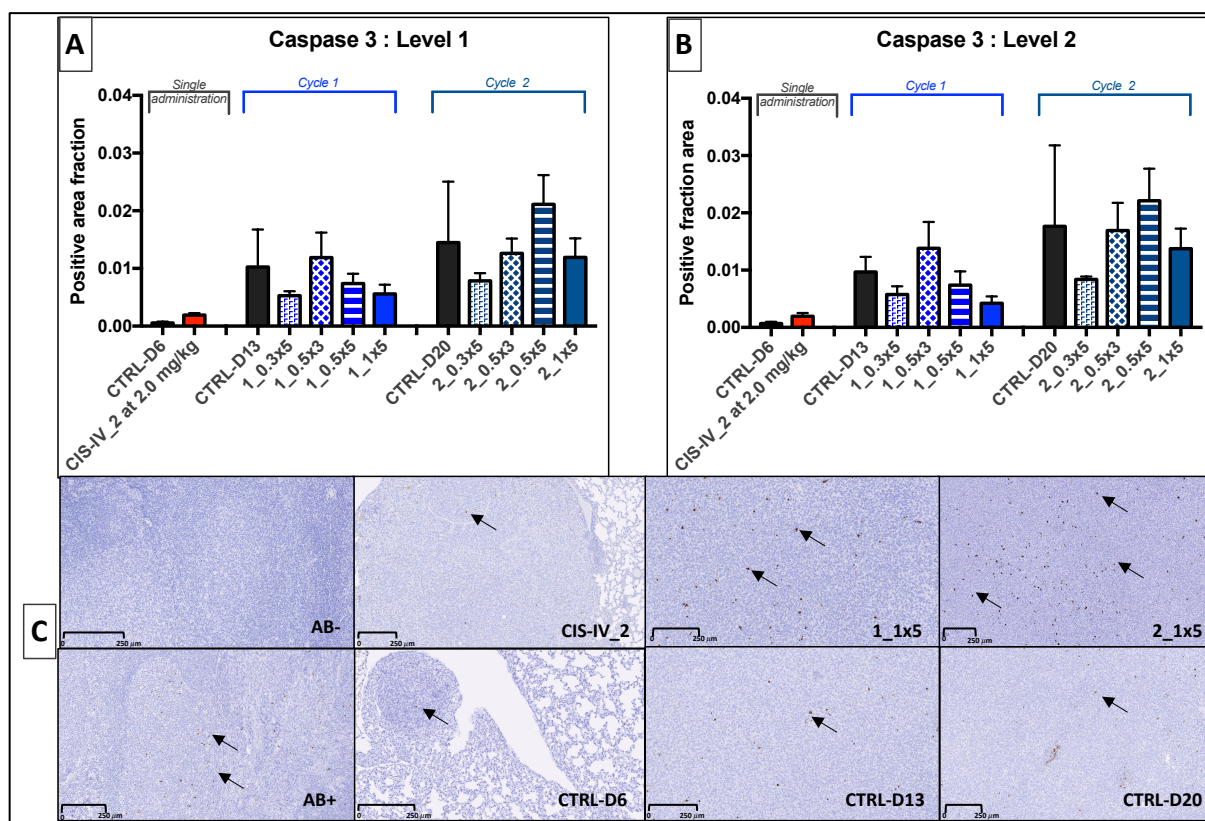

Figure 48: Positive area fraction from the positively activated caspase-3-stained area normalized by the positively and negatively stained pixels in the tumour at two levels (A and B), separated by 150 μm, following the administration of CIS-IV_2 and one- or two-cycle treatment of CIS-DPI-50. The groups' abbreviations are described in **Figure 41**. Results are expressed as means ± SEM (n=2-8). Representative images (C) of activated caspase-3 immunostaining of the untreated groups (CTRL-D6, CTRL-D13 and CTRL-D20) and of the groups treated with the most drastic conditions in terms of cisplatin total dose (CIS-IV_2, 1 x 5) following one- and two-cycle treatment. The slices from AB$^-$ (negative control) were not treated with the primary antibody (AB) whereas this was done for the AB$^+$ (positive control).

Following a single administration of CIS-IV_2, no statistically significant difference ($p > 0.05$) in terms of positive caspase 3 area fraction was observed at any level **(Figure 48.A and B)** in

comparison with their relative untreated groups CTRL-D6, CTRL-D13 and CTRL-D20. In addition, none of the groups treated with CIS-DPI-50 significantly increased the caspase 3 positive area fraction in comparison with their corresponding negative control after both treatment cycles and at both levels **(Figure 48.A and B)**. This was regardless of the dose and frequency of administration. The variabilities observed within these groups can be related to the tumour variability in terms of size, location and microenvironment, as explained previously [70]. Moreover, this also showed the difficulty of cisplatin in killing tumour cells. This difficulty probably resulted from the high density of the tumour tissue, which would prevent the drug from diffusing efficiently [70].

Overall, these results showed the limited efficacy of cisplatin activity, irrespective of the regimen. Moreover, the results obtained in terms of tumour masses between groups were aligned with these observations. Indeed, as illustrated in **Figure 49.B**, no significant difference in terms of tumour masses were reported between treated and untreated groups ($p > 0.05$). This observation demonstrated the limited efficacy of cisplatin on this model, as previously reported in preclinical studies [253,254].

Days	Tumour mass (mean ± SEM)
D6	9.9 ± 0.9
D10	23 ± 3
D17	533 ± 23

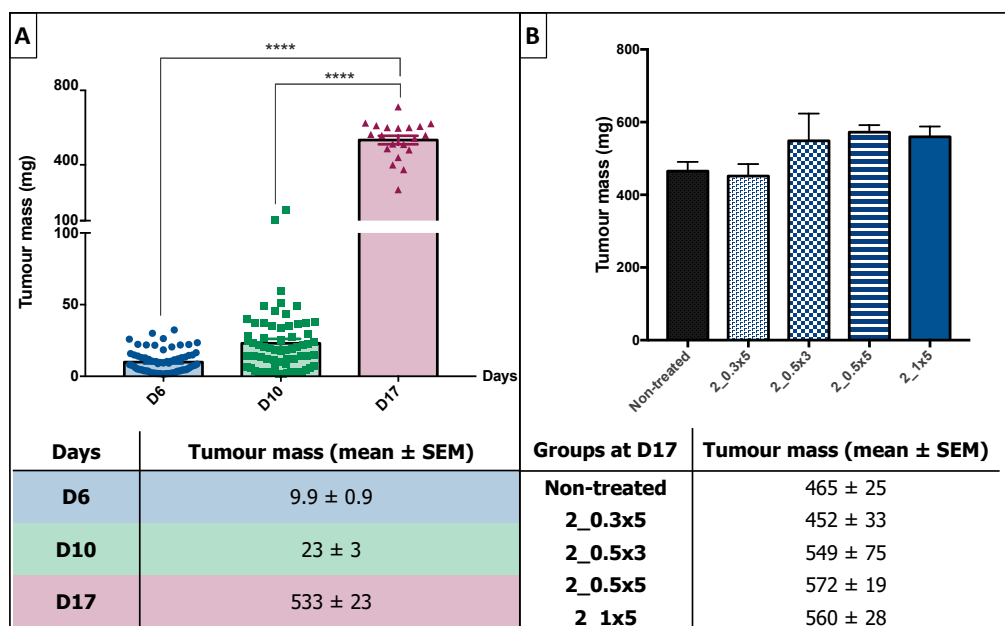| Groups at D17	Tumour mass (mean ± SEM)
Non-treated	465 ± 25
2_0.3x5	452 ± 33
2_0.5x3	549 ± 75
2_0.5x5	572 ± 19
2_1x5	560 ± 28

Figure 49: Tumour masses of all the grafted treated and non-treated mice (A). Tumour masses of the non-treated group and treated groups (0.3x5, 0.5x5, 0.5 x3 and 1x5), following two cycles of treatment, on D17 (B). The groups' abbreviations are described in **Figure 41.** All results are expressed as means ± SEM (N=4-71). The statistical analyses were performed *vs*. their corresponding negative control group using one-way ANOVA and Bonferroni's post-test and were described as **** $p < 0.0001$.

Therefore to select the most promising regimen in terms of drug accumulation in lung tumours, it was interesting to investigate the platinum concentration following the administration of CIS-IV_2 and of the different regimens of CIS-DPI-50.

3.2.3. Platinum accumulation

Following the administration of the first cycle of CIS-DPI-50 regimens, no significantly platinum accumulation was reported in tumour-free lungs, tumour, plasma or kidneys in comparison with a single administration of CIS-DPI-50 **(Figure 50)**.
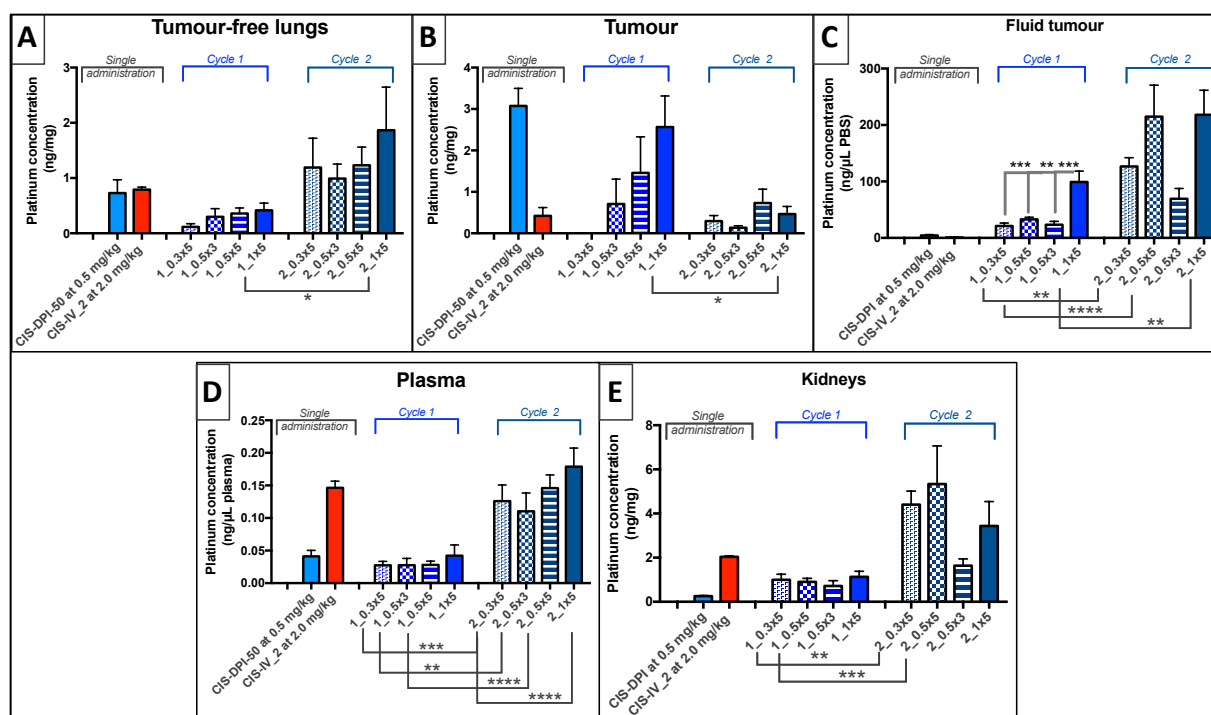
Figure 50: Platinum concentration in tumour-free lungs (A), tumour (B), tumour fluid (C), plasma and kidneys in LLC grafted mice on D6 2h following a single administration of CIS-DPI-50 at 0.5 mg/kg or CIS-IV_2 at 2.0 mg/kg (illustrated from the results obtained from **Figure 43**) or repeated administrations of CIS-DPI-50 following different doses and frequencies over two cycles. The groups' abbreviations are described in **Figure 41**. All results are expressed as means ± SEM (n=7-11 per timepoint). The statistical analyses were performed *vs.* their corresponding group using one-way ANOVA and Bonferroni's post-test (**** for $p < 0.0001$, *** for $p < 0.001$,** for $p < 0.01$ and * for $p < 0.05$). To simplify the figures, only the statistical results between 2_groups and 1_groups, and CIS-DPI-50 and CIS-IV_2, were represented.

No statistically significant change ($p > 0.05$) in terms of platinum concentration was observed in tumour-free lungs among the groups **(Figure 50.A)**. In addition, the platinum concentrations were lower, but not statistically different, from a single administration of CIS-DPI-50 (i.e. 0.7 ± 0.2 ng/mg), as reported in the previous PK study in LLC grafted-mice **(Figure 43.A)**. These results confirmed the trends obtained with the previous PK study in grafted mice, demonstrating that CIS-DPI-50 was completely cleared from the lungs within 24h **(Figure 43.A)**. This trend

was also observed in a PK study made in healthy CD1 mice, even it was made on another strain of mice **(Figure 39)**.

The platinum concentration in the tumour 2h following the single administration of a 4-fold lower dose of CIS-DPI-50 was more than 7-fold higher than CIS-IV_2 ($p < 0.05$, **Figure 50.B**). The platinum concentration in the tumour following repeated administrations of CIS-DPI-50 during one cycle showed no sign of accumulation in comparison with a single administration of CIS-DPI-50 ($p > 0.05$, **Figure 50.B**). Indeed, no higher platinum concentration was reported for these groups in comparison to a single administration of CIS-DPI-50 (1_0.3 x 5: < LOQ, 1_0.5 x 5: 1.5 ± 0.9 ng/mg, 1_1 x 5: 2.6 ± 0.8 ng/mg, *vs.* 3.1 ± 0.2 ng/mg for a single administration of CIS-DPI-50, **Figure 50.B)**. Moreover, no significant difference was reported between them at the end of the first cycle. These results were aligned with those obtained with the quantification of caspase 3 in terms of cisplatin activity **(Figure 48)**. The variabilities observed in these trends can be related to the technique of administration and to the tumour variability, as explained previously. In addition, **Figure 49.A** showed that even though this was not statistically significant, the tumour masses were more than 2-fold higher in D10 in comparison to D6 in all treated mice (23 ± 3 mg *vs.* 9.9 ± 0.9 mg), which would alter the access and penetration of cisplatin inside the tumour. Indeed, a bigger tumour would have denser and more complex extracellular matrixes, which could limit the exposure of all the tumour cells to cisplatin [70].

Interestingly, the platinum concentrations in the tumour were higher than those observed in tumour-free lungs for all groups except 1_0.3 x 5, for which the platinum concentration in tumour-free lungs was very low (0.12 ± 0.06 ng/mg). Indeed, the platinum concentration in the tumour was 2-fold (1_0.5 x 3), 4-fold (1_0.5 x 5) and up to 6-fold higher (1_1 x 5) in the tumour than in tumour-free lungs. Moreover, it seemed that the higher the cumulative dose was, the higher the dose in the tumour, which tended to demonstrate a higher penetration within the tumour than in tumour-free lungs. Therefore, it can support the diffusion theory based on the gradient of concentration, with a higher concentration gradient that led to a higher penetration in the tumour, as previously explained [70]. It seemed that for a lower dose than 0.5 mg/kg, the concentration gradient generated was not high enough to potentialize the penetration of cisplatin inside the tumour.

The results of platinum concentration in tumour fluid (i.e. tumour lavage fluid) were all higher at the end of the first cycle treatment, when compared to a single administration of CIS-DPI-

50. However, this was only statistically significant for the highest cumulative dose (1_1 x 5, *p* < 0.05, **Figure 50.C**). In addition, the tumour fluid concentration following 1_1 x 5 was statistically different from that observed for all the other treated groups, irrespective of the cumulative dose (*p* < 0.001 for 1_0.3 x 5, *p* < 0.01 for 0.5 x 5) or the frequency of administration (*p* < 0.001 for 1_0.5 x 3). This demonstrated that the most repeated administration of the highest dose of CIS-DPI-50 led to an increased platinum concentration in the tumour periphery in comparison to less-dosed or less frequent regimens. Administering the 1_1 x 5 regimen could favour a higher concentration gradient and therefore lead to a higher penetration of cisplatin in the tumour, as demonstrated by the highest concentration reported for this group in the tumour fluid and in the tumour **(Figure 50.B)**. Indeed, drug supply is the first parameter that governs the gradient concentration and triggers the penetration of a drug in a tissue [70], as described in the previous section.

As expected, and as already reported in *Experimental part I,* the platinum concentration in plasma following the administration of CIS-IV_2 was more than 3-fold higher in comparison to CIS-DPI-50 2h following their administration (0.15 ± 0.01 ng/μL *vs.* 0.041 ± 0.009 ng/μL, *p* < 0.0001) **(Figure 50.D)**. No statistically significant difference in terms of platinum concentration in plasma was observed following repeated CIS-DPI-50 administrations during one cycle in comparison to a single administration of CIS-DPI-50, irrespective of the cumulative dose, and the frequency (*p* > 0.05, **Figure 50.D**). In addition, no significant difference among the groups treated for one cycle was reported (*p* > 0.05, **Figure 50.D**). These results confirmed those obtained in plasma in terms of clearance during the PK study of a single administration of CIS-DPI-50 in healthy CD1 mice **(Figure 39)**, even it was made on another mouse strain. Indeed, a 24h-delay between CIS-DPI-50 administrations was enough to avoid platinum accumulation following repeated administrations and therefore would avoid systemic toxicities, as no differences were observed between the groups administered CIS-DPI-50 in a single administration, or the ones treated with 1_0.3 x 5 or 1_0.5 x 3 **(Figure 50.D)**.

Considering that the cisplatin DLT (i.e. nephrotoxicity) is related to the platinum concentration (C_{max} or AUC) within the tissue [255], the evaluation of platinum concentration in the kidneys was tremendously important. As previously observed in plasma, the platinum concentration in the kidneys following the administration of CIS-IV_2 was more than 7-fold higher in comparison to CIS-DPI-50 2h following their administration (2.03 ± 0.04 ng/mg *vs.* 0.26 ± 0.03 ng/mg *p* < 0.05) **(Figure 50.D)**. No statistically significant differences in terms of platinum concentration in the kidneys were observed between the groups administered CIS-DPI-50

repeatedly for one cycle and a single administration of CIS-DPI-50 ($p > 0.05$, **Figure 50.E**). Moreover, this was not reported between the groups treated for one cycle irrespective of the cumulated dose and regimens ($p > 0.05$, **Figure 50.E**). As expected, the lowest concentration among these groups resulted from 1_0.5 x 3 as the platinum concentration in kidneys was 0.7 ± 0.2 ng/mg **(Figure 50.E)**.

Following the second treatment cycle, considerable increases in terms of platinum concentration in the tumour-free lungs, fluid tumour, plasma and kidneys were reported for all the regimens **(Figure 50)**. Moreover, these were correlated with a significant drop in terms of platinum accumulation in the tumours.

Indeed, in the tumour-free lungs, even when non-significant ($p > 0.05$), all platinum concentrations were higher for all groups at the end of the second cycle, in comparison to those treated with one cycle of administration of CIS-DPI-50 **(Figure 50.A)**. The platinum concentration was 10-fold higher for 2_0.3 x 5 than for 1_0.3 x 5, more than 3-fold higher for 2_0.5 x 5 *vs.* 1_0.5 x 5 and for 2_0.5 x 3 *vs.* 1_0.5 x 3, and more than 4-fold higher for 2_1 x5 *vs.* 1_1 x 5 **(Figure 50.A)**. These differences were only statistically significant for 2_1 x 5 in comparison with 1_1 x 5 ($p < 0.05$).

In the tumour, the platinum concentrations for almost all groups (except for 2_0.3 x 5) significantly decreased in comparison to a single administration of CIS-DPI-50 (D6). Indeed, these differences were statistically significant for 2_0.3 x 5 ($p < 0.01$), 2_0.5 x 5 ($p < 0.05$), 2_1 x 5 ($p < 0.01$) and even for the group treated less frequently 2_0.5 x 3 ($p < 0.01$) **(Figure 50.B)**. Moreover, these concentrations were also lower in comparison to the groups treated until the end of the first treatment cycle (D10), as illustrated in **Figure 50.B**. This decrease was not statistically significant for these groups in comparison to their respective groups treated for one cycle, except for 1 x 5 ($p < 0.05$ between 2_1 x 5 and 1_1 x 5).

In the tumour fluid, following the second cycle of administration, all the platinum concentrations were higher than with a single administration of CIS-DPI-50, irrespective of the regimen **(Figure 50.C)**. However, these results were only significant for the groups treated five times per cycle ($p < 0.001$ for 2_0.3 x 5, $p < 0.0001$ for 2_0.5 x 5, and $p < 0.0001$ for 2_1 x 5, **Figure 50.C**). In addition, the groups treated five times per cycle for two cycles showed significantly higher concentrations in comparison to their related groups treated for one cycle ($p < 0.01$ for 2_0.3 x 5, $p < 0.0001$ for 2_0.5 x 5, and $p < 0.01$ for 2_1 x 5, **Figure 50.C**).

In plasma, following the second cycle of administration, the platinum concentrations of the 2-cycle treated groups were statistically all higher than both CIS-DPI-50 administered alone or for one cycle. Indeed, the ratios of platinum-concentration increase for these groups increased proportionally to the cumulative dose **(Figure 50.D).** Moreover, all the groups treated for two cycles showed statistically higher platinum concentrations in plasma in comparison to their respective groups treated over one cycle. The platinum concentration for 2_0.3 x 5 was more than 4-fold higher than for 1_0.3 x 5 ($p < 0.001$), the concentration for 2_0.5 x 3 was 3-fold higher than for 1_0.5 x 3 ($p < 0.01$), the concentration for 2_0.5 x 5 was more than 5-fold higher than for 1_0.5 x 5 ($p < 0.0001$), and for 2_1 x 5 was more than 4-fold higher than for 1_1 x 5 ($p < 0.0001$).

In the kidneys, the platinum concentrations for all groups following the second cycle were higher than for CIS-DPI-50 administered alone or for one cycle. Indeed, the platinum concentration in the kidneys following 2_0.3 x 5 was more than 4-fold higher than for 1_0.3 x 5 ($p < 0.01$), the concentration for 2_0.5 x 5 was more than 5-fold higher than for 1_0.5x5 ($p < 0.001$), and for 2_1x5 was 3-fold higher than for 1_1x5 ($p > 0.05$, **Figure 50.E**). Moreover, the platinum concentrations in kidneys of all groups were all similar as no significant difference was observed among these groups ($p > 0.05$, **Figure 50.E**).

The differences in terms of platinum concentration in the tumour and tumour fluid obtained from the mice treated for two cycles were related to the statistically increased tumour masses **(Figure 49, and Figure 50.B and C)** and density. Indeed, a higher platinum concentration in the tumour fluid was retrieved on D17 in comparison to D10. However, this higher concentration was not able to trigger an increased platinum concentration in the tumour, showing that cisplatin had difficulty in penetrating a denser, less-organized and bigger tumour, while the penetration into a smaller tumour was certainly easier [70]. Indeed, on D17 (i.e. the end of the second cycle), the tumour mass of all treated mice was more than 20-fold higher in comparison to D10 ($p < 0.0001$) and more than 50-fold higher than tumour masses on D6 ($p < 0.0001$, **Figure 49.A)**, as observed as in **Figure 42.B**.

Moreover, considering the sharp bw losses starting from D13 (i.e. the first day of the second cycle) **(Figure 44)** as well as the deterioration in the overall condition (dehydration, curled in bowls), most of the mice were considered to be in a moribund state by D17 [256–258]. This was mainly due to the *(i)* the aggressiveness of the model (i.e. rapid tumour development), illustrated by a low median survival of untreated mice (i.e. 21 days) and *(ii)* the lack of sensitivity of the LLC-carcinoma model to cisplatin, as observed by the results obtained with

the tumour masses and with the caspase-3 activity [253,254]. Moreover, due to the uncontrolled mitoses and the necrosis of the tumour-free lungs by the tumour, it is probable that the lungs started losing their clearance function, leading to an increased accumulation in the tumour periphery and in tumour-free lungs. Indeed, various reviews have reported cilia and macrophage phagocytosis clearance dysfunction in the case of lung tumours [259,260]. Although not observed following the one-cycle treatment, the accumulation in tumour-free lungs was significantly higher than in the tumour following the two-cycle treatment. The platinum concentration in tumour-free lungs was 4-fold higher for 2_0.3 x 5, 2-fold higher for 2_0.5 x 5, and 4-fold higher for 2_1 x 5 than in tumour, irrespective of the cumulative dose. This could be related to the obstruction of the airways, leading to a deviation of the delivered CIS-DPI-50 to the tumour-free lungs. Animals in a moribund state experience a decreased food and water intake, leading to severe bw losses and dehydration [256–258]. This could have led to increased concentrations of cisplatin in plasma and kidneys. In parallel, this moribund state could have led to a filtration defect in the kidneys and to an accumulation of cisplatin in the kidneys and thus in plasma.

Therefore, selecting a regimen as promising on the basis of the results obtained after the two-cycle treatment could be skewed. In addition, considering the proportion of tumour masses in comparison to the tumour-free tissue, the overall condition of the mice was moving away from what could be observed in lung cancer patients **(Figure 42.B)**. Consequently, the selection of the most promising regimen was based on the PK results obtained after a one-cycle treatment.

The differences observed in terms of platinum accumulation in plasma, kidneys and tumour-free lungs between the regimens were non-statistically significant. Therefore, the selection of the most appropriate regimen could be done on the basis of the highest accumulation in the tumour. Even though non-statistically significant, the highest platinum accumulations in the tumours were reported for the most dosed regimens (i.e. 0.5 x 5 and 1 x 5) in comparison with the other regimens. Therefore, if these regimens were intended to be administered alone, they would have been selected to potentialize the efficacy of CIS-DPI-50 as a monotherapy. However, considering that the aim of this work was to combine several administrations of these regimens with conventional IV chemotherapy, it was safer to consider regimens with the less cumulative cisplatin dose, i.e. 0.3 x 5 and 0.5 x 3. Indeed, this was done to avoid cumulative toxicities from the combination of IV chemotherapy and CIS-DPI-50 regimens. The consideration of the tolerance at this step is crucial as IV chemotherapy is, on its own,

responsible for high systemic toxicities and, most importantly, for severe DLTs such as nephrotoxicity with cisplatin. Therefore, the 0.3 x 5 and 0.5 x 3 regimens were both selected to be evaluated in terms of efficacy on another lung carcinoma model that is sensitive to cisplatin. Indeed, this study aimed to compare the efficacy of the administration of a lower dose more frequently (i.e. 0.3 x 5) with a higher dose less frequently (i.e. 0.5 x 3), considering the same cumulative dose (i.e. 1.5 mg/kg per cycle).

3.3. Efficacy study

3.3.1. Development of M109-HiFR-*Luc2* lung carcinoma model

Due to the limited sensitivity of cisplatin on LLC1-*Luc* reported in the previous section, in other *in vivo* studies conducted by Inhatarget Therapeutics and in the literature [253,254], the efficacy of the selected regimens was assessed on another syngeneic and orthotopic model: the M109-HiFR-*Luc2* lung carcinoma model. Therefore, to evaluate the tumour size, which is a crucial marker of the treatment efficacy, it was mandatory to transfect M109-HiFR cells by *Luc2* to follow their progression using BLI analysis. The intrapulmonary graft of 1.4×10^4 cells was the standard protocol optimized previously [211] to obtain lung tumours localized in the thoracic cage. Following the graft, all grafted mice developed lung tumours on D5 (5/5, 100%), validating the method optimized by Rosière *et al*. [211], as represented in **Figure 51**. One week later, these signals were more intense and were still localized in the same area, demonstrating the continuous development of lung cancer cells in the thoracic cage, leading to mouse death 23 days post-graft. Therefore, this model was selected as the preclinical model on which the efficacy study would be conducted.
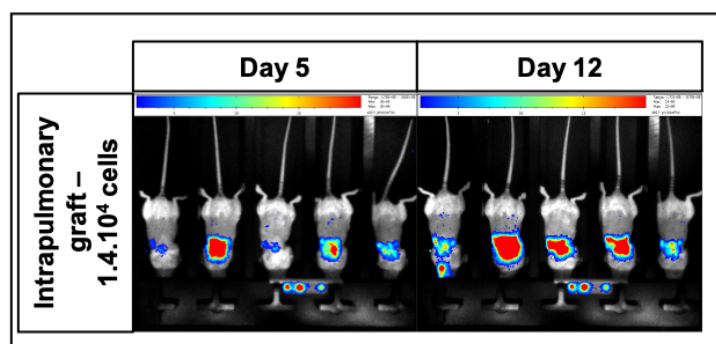

Figure 51: Characterization of M109-HiFR-*Luc2* lung carcinoma model in mice in terms of BLI grafted mice at day 5 and 12 following an intrapulmonary graft of 1.10^4 cells/mL.

3.3.2. Body weight profiles

To evaluate the influence of the frequency of administration on the overall condition, BALB/c mice were intrapulmonary grafted and were randomized before receiving CIS-DPI-50 administered on D6 at the same cumulative dose (i.e. 1.5 mg/kg) following the two selected regimens (i.e. at 0.3 mg/kg five times per cycle – 0.3 x 5, or at 0.5 mg/kg three times per cycle 0.5 x 3) that would both be compared to untreated mice **(Figure 41)**.

The evaluation of bw profiles showed limited bw losses among all groups. The bw of untreated groups increased until D17 (3 ± 1%), and started decreasing from D20, until reaching -3.5 ± 0.5% on D27 **(Figure 52)**. However, bw losses were noticed earlier for the treated mice groups and reached -6 ± 2% for 0.3 x 5 and -3 ± 2% for 0.5 x 3 on D17, and were correlated to the administration of CIS-DPI-50. This was certainly related to the cumbersomeness of the technique of administration (involving anaesthesia, ET intubation and delivery of powder into the lungs using several air puffs), and to the drug toxicity. These losses continued to decrease until reaching -10 ± 5%, for 0.3 x 5 and -11 ± 3% for 0.5 x 3, on D27. Even though the bw losses were similar for the treated groups, the increased frequency of administration led to slightly stronger bw losses in the middle and by the end of the second treatment cycle (i.e. D13, D17), as illustrated in the profiles in **Figure 52**. However, the decreases in bw were lower than 10% and were therefore considered as acceptable as the limit point is 20%.
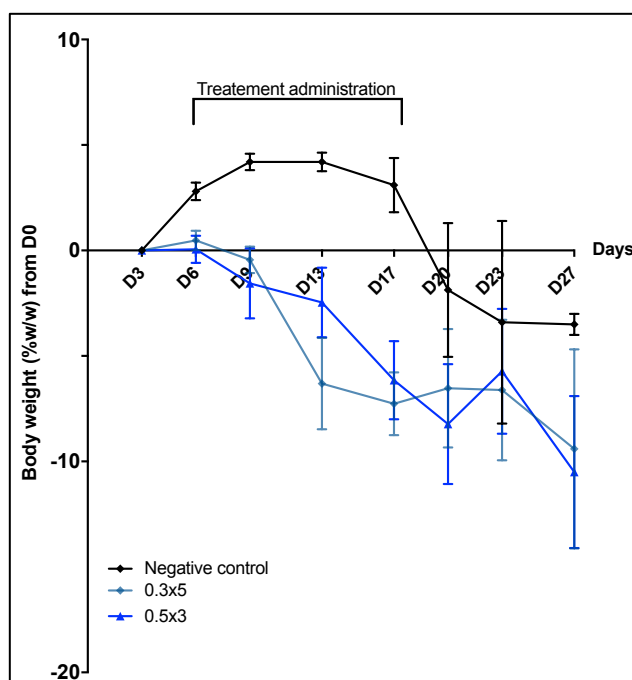

Figure 52: Bw profiles of untreated grafted mice or grafted mice (M109-HiFR-*Luc2*) treated with CIS-DPI-50, administered either five times per week at 0.3 mg/kg (0.3 x 5) or three times per week at 0.5 mg/kg (0.5 x 3). All results are expressed as means ± SEM (N=8-19) from D3 to D27 (i.e. last day untreated mice alive)

3.3.3. Tumour size and responder rate

Tumour growth results indicated an exponential increase in untreated control mice **(Figure 53.A)**, with a steep slope, illustrating the aggressiveness of the M109-HiFR-*Luc2* lung carcinoma model. The administration of CIS-DPI-50 repeatedly following 0.3 x 5 and 0.5 x 3 showed a slower increase in the tumour growth in comparison with untreated groups **(Figure 53.A, B, C)**. This showed that the administration of CIS-DPI-50 seemed to slow down the tumour growth.

Figure 53.D showed that during the first 17 days (i.e. until the end of the treatment), the mouse group treated with 0.3 x 5 had a slightly higher tumour growth rate in comparison with the untreated group and with the group treated with 0.5 x 3. As soon as the treatment was discontinued, the negative control group tumour growth rate continued to increase exponentially until D31, while the tumour growth rate was slowed down for both treated groups (i.e. different slopes between treated and untreated groups). The difference between the treated and untreated groups was statistically significant on D23 and D31, i.e. 6 and 14 days following the treatment administration ($p < 0.001$, **Figure 53.D**).
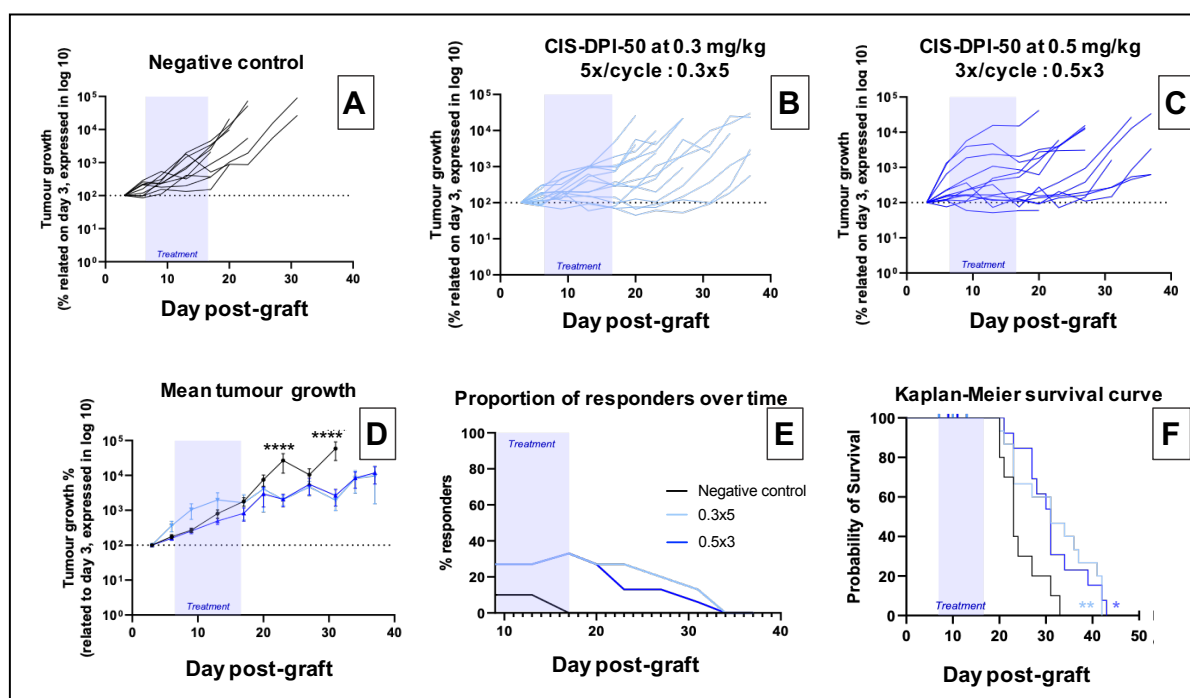

Figure 53: Tumour growth (log 10, % related to day 3) according to BLI and expressed per subject for the negative control group (A) and following the administration of CIS-DPI-50 at 0.3 mg/kg 5x/cycle (B) or at 0.5 mg/kg 3x/week (C) or as mean ± SEM (D) (n=8-19). The proportion of responders over time (E) as well as the Kaplan-Meier curves of these groups (E) are represented. * $p < 0.05$, ** $p < 0.01$ and **** $p < 0.0001$ between the negative control and the two treated groups (two-way ANOVA with Tukey-multiple comparison test).

A responder was defined as a mouse with tumour growth < 150% in comparison to the 100% value measured at D3. Therefore the untreated mice for which a tumour growth was slower than 150% were plotted as "responders" to this graft but should not be considered as such. Consequently, as these mice are untreated, the tumour masses increased over time leading to the disappearance of this signal by the end of the treatment period. As anticipated, mice treated with CIS-DPI-50 at both regimens showed a percentage of responders of up to 33% **(Figure 53.E)**. This confirmed the activity of CIS-DPI-50 on the M109-HiFR-*Luc2* lung carcinoma model, irrespective of the frequency. Following the administration of 0.3 x 5 and 0.5 x 3, the percentage of responders reached 27% on D9 and continued its increase until reaching a peak on D17. This was maintained until D20 when a decrease was then noticed, certainly due to the end of the treatment administration **(Figure 53.E)**.

3.3.4. Survival analysis

The survival analysis confirmed the trends obtained from tumour growth rate and responder proportion analyses. Indeed, the added value of the administration of CIS-DPI-50 following both the 0.3 x 5 and 0.5 x 3 regimens increased significantly the median survivals ($p < 0.01$ and $p < 0.05$, respectively, log rank test), in comparison with untreated mice (median survival time of 31 *vs.* 23 days, **Figure 53.F**). Moreover, these results also confirmed that no significant difference between 0.3 x 5 and 0.5 x 3 was observed ($p > 0.05$), as their median survival days were both observed at 31 days **(Figure 53.F)**.

The difference in terms of efficacy observed between the LLC1-*Luc* and the M109-HiFR-*Luc2* once CIS-DPI-50 administered could be explained by *(i)* the intrinsic difference between the models as well as *(ii)* their sensitivity to cisplatin. Indeed, the cell growth rate *in vitro* was nearly two-fold higher for LLC1-*Luc* in comparison with the M109-HiFR-*Luc2*. Moreover, the doubling time *in vivo* followed the same trend and was 48h for M109-HiFR-*Luc2* and 24h for LLC1-*Luc* (data not shown). Finally, the half maximal inhibitory concentration (IC50) was more than 1 000 fold higher for LLC1-*Luc* in comparison with the M109-HiFR-*Luc2* (data not shown). Therefore, for a similar efficacy, the cisplatin concentration in the tumours should be more than 1 000 fold higher for LLC1-*Luc*, which would hardly be achievable *in vivo* regarding cisplatin MTD.

Overall, the efficacy study showed similar results in terms of tumour growth, proportion of responders and survival between the 0.3 x 5 and the 0.5 x 3 regimens. This tended to

demonstrate that the efficacy was more related to the cumulative dose than the frequency of administration.

A higher risk of cumulative toxicities could be observed when the 0.3 x 5 regimen was combined to CIS-IV than the 0.5 x 3 regimen. Therefore the scheme of administration of CIS-DPI-50 at 0.5 mg/kg was selected to be administered three times per cycle at 0.5 m/kg (0.5 x 3) for two cycles, in combination with the conventional IV chemotherapy, to find the best compromise between antitumor activity and local and systemic tolerance.

4. Conclusion

Overall, a single administration of CIS-DPI-50 at 0.5 mg/kg in LLC1-*Luc* grafted mice showed interesting tumour penetration, with limited exposure in tumour-free lungs and plasma, unlike results observed for CIS-IV_2 even at a 4-fold higher dose. The repeated administrations of CIS-DPI-50 for one cycle following different doses and schemes of administration did not show any higher exposure in tumour-free lungs, tumour, plasma or kidneys. However, the lack of sensitivity of the LLC to cisplatin (i.e. similar caspase 3 activity and tumour masses between treated and untreated groups) led to the uncontrolled development of tumours and therefore to the degradation of the overall condition of the mice. This therefore disturbed the steady-state physiological condition and led to *(i)* the accumulation of platinum in healthy organs, and *(ii)* a drop of the platinum concentration in the tumour, probably due to the difficulty of cisplatin in penetrating denser tumours and to the obstruction of pulmonary airways. Therefore, as these regimens are intended to be combined with an IV chemotherapy (a highly nephrotoxic treatment on its own), the regimens with the lowest cumulative dose (i.e. 0.5 mg/kg, three times per cycle *vs.* 0.3 mg/kg, five times per cycle) were selected to be evaluated on the M109-HiFR-*Luc2* lung carcinoma model. Efficacy analyses in terms of tumour growth rate, proportion of responders and survival curves showed similar results between these two groups. Therefore the less frequent regimen of 0.5 mg/kg administered three times a week for two cycles was selected to be combined to conventional IV chemotherapy in the aim to prevent cumulative toxicities.

Part III: Evaluation of the combination of CIS-DPI-50 and IV cisplatin-based platinum doublet

Parts of these results are published in

the *International Journal of Pharmaceutics*,

the *European Journal of Pharmaceutics and Biopharmaceutics*,

the conference proceedings of "Respiratory Drug Delivery 2020"

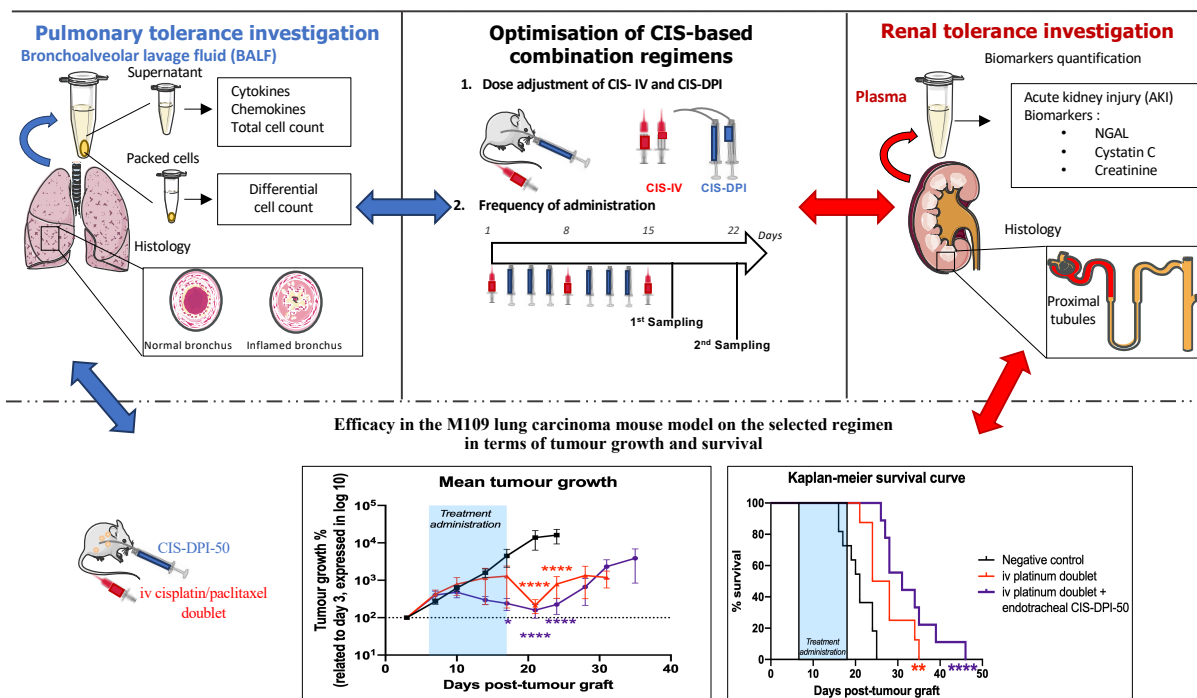and the conference proceedings *"12th World Meeting on Pharmaceutics, Biopharmaceutics and Pharmaceutical Technology"*

Figure 54: Graphical abstract of the third experimental part.

1. <u>Introduction and aims</u>

CIS-DPI-50 was produced, fully-characterized *in vitro* and its stability demonstrated over 6 months under normal conditions. Moreover, its lung T_a was also assessed in healthy mice in *Experimental part I*. Considering that the PK parameters can be altered by the presence of the tumour, CIS-DPI-50 was administered either once or following several regimens to LLC1-*Luc*-grafted mice to evaluate its biodistribution in the tumour and healthy organs, as well as its pulmonary tolerance and efficacy. Therefore, the most appropriate CIS-DPI-50 monotherapy regimen (i.e. 0.5 x 3) was selected in *Experimental part II*.

Delivering the CIS-DPI-50 regimen during the resting period encountered with conventional IV chemotherapy could be a promising strategy to expose the lung tumours and locoregional invasion more often to cisplatin and therefore increase the opportunity to cure patients or to prolong their survival [68]. This hypothesis was correlated with the promising efficacy results obtained in NSCLC patients from a phase II study during which carboplatin was administered using the ET route and combined to IV docetaxel-carboplatin, as previously discussed [79].

Therefore, adding CIS-DPI-50 regimen to CIS-IV can be promising as long as pulmonary and renal toxicities remain acceptable. Indeed, the dissolved part from CIS-DPI-50 could further increase the C_{max} related to the CIS-IV administration in the lungs and kidneys and be responsible for a higher pulmonary and renal toxicity. The aim of this study was to investigate lung and renal tolerance of: *(i)* cisplatin monotherapies administered three times a cycle using the pulmonary route for CIS-DPI-50 (0.5 x 3 regimen) and once a cycle for CIS-IV; and *(ii)* their combinations at different doses. The optimization of the combinations should include both doses (total and fractionated dose) and days of administration to find the best balance between the highest dosage and most frequent regimen (i.e. potentially related to efficacy) and their tolerance. Indeed, considering the elimination of CIS-IV, it was important to evaluate whether the CIS-DPI-50 regimen should be added to CIS-IV the same day, 24h or 48h later, and at which CIS-IV dose to ensure the preservation of both pulmonary and renal tolerance. Finally, the second part of this study aimed to evaluate the added value of the best tolerated, least-spaced and most dosed regimen on M109-HiFR-*Luc2*-grafted mice in comparison with conventional cisplatin-based IV chemotherapy.

2. <u>Material and methods</u>

2.1. Materials

Paclitaxel was purchased from Carbosynth (Berkshire, UK). Periodic acid Schiff (PAS) was provided by Life-Technologies (Merelbeke, Belgium). Primary antibodies used for immunostaining were rabbit anti-NGAL purchased from Invitrogen (Carlsbad, USA). The secondary antibody, the DAB, the blocking kit and the avidin-biotin complex (ABC) kit were all obtained from Vector Labs (Peterborough, UK). All other materials used in this part are detailed in *Experimental part II-section 2.1*.

2.2. CIS-DPI-50 formulation production and characterization (DPI-0.5 and DPI-1)

CIS-DPI-50 was produced, characterized and prepared for *in vivo* delivery as detailed in *Experimental part I-section 2.4.4.2*. For this study, the diluent was added to CIS-DPI-50 to target 1% and 2% cisplatin for DPI-0.5 (CIS-DPI-50 at 0.5 mg/kg) and DPI-1 (CIS-DPI-50 at 1.0 mg/kg), respectively, in a total mass of 250 mg using a 2 mL glass vial following the so-called sandwich method.

2.3. *In vivo* toxicity studies

Female 6-week-old BALB/cAnNRj mice (16-18 g) were purchased from Janvier Labs (Le Genest-Saint-Isle, France) and Charles River (Écully, France). All experiments and manipulations were approved by the CEBEA of the faculty of medicine (ULB) under approval number 585N (toxicity studies) and CMMI-2017-01 (efficacy studies). The housing conditions were identical to those described in *Experimental part I-section 2.3.3.1*.

2.3.1. Renal tolerance

2.3.1.1. Maximum tolerated dose evaluation

The CIS-DPI-50 MTD was defined for this study as "the highest dose for which mean bw loss did not exceed 5% w/w during the follow-up after the first dosing". Considering that CIS-DPI-TS has shown an MTD at 1 mg/kg [205], we tested this new formulation at the same dosage (DPI-1) and at a reduced dose of 50% (i.e. 0.5 mg/kg, DPI-0.5). The treatment administration to mice was performed as described in *Experimental part II-section 2.4*.

The CIS-IV MTD was defined in this study as the "the lowest dose that increased the nephrotoxicity biomarkers and for which mean bw loss did not exceed 5% w/w". Five groups

of six mice were administered CIS-IV one time per week for 3 weeks at 1.5, 1.75, 2.0, 2.25 and 2.5 mg/kg. They were compared to a negative control group (n=6) that received only a saline solution. Briefly, mice were immobilized using a restraint device from which the tail protruded. Immediately after, the tail was vasodilated by applying a wet heated paper to facilitate the injection in the caudal vein. Blood was collected using retro-orbital terminal sampling and centrifuged to collect plasma, as discussed below. Plasma NGAL, cystatin C and creatinine were quantified to evaluate the lowest dose at which the selected biomarkers increased. Cisplatin solutions were prepared at 0.15, 0.175, 0.20, 0.225 and 0.25 mg/mL in 0.9% NaCl at pH 4, kept protected from light and used within 24h. All the mice were weighed three times a week, i.e. on Mondays, Wednesdays and Fridays.

2.3.1.2. Monotherapies

Once the MTD was identified for CIS-IV and CIS-DPI-50, these formulations were tested first as monotherapies using either the ET or IV route. One week was designated a cycle of treatment.

Four mouse groups were administered cisplatin using the ET route three times per cycle for two cycles **(Figure 55)** following the procedure described in *Experimental part II-section 2.4*. The first treated group received the vehicle (DPI placebo without cisplatin, DPI-V (n=14)), the second group CIS-DPI-50 at 0.5 mg/kg (DPI-0.5) (n=10) and the third group CIS-DPI-50 at 1.0 mg/kg (DPI-1) (n=9). Negative control groups received a saline solution (NaCl, 0.9%) (ET-saline) (n=12) and the positive control group received ~1 μg of LPS (ET-LPS) from *E. coli* (n=6). The ET-saline groups followed the same regimen as the treated groups **(Figure 55)**. The ET-LPS groups were administered the treatment 18h before each sampling according to the kinetic of the inflammatory biomarkers, following the procedure described in *Experimental part II-section 2.4*, and using an ET device for the solutions (Microsprayer™ model IA-1C® equipped with an FMJ-250 high-pressure syringe, Penn-Century). These biomarkers have been characterized by a peak between 12 and 24h following exposure to LPS [261]. The control groups (i.e. ET-saline and ET-LPS) were re-evaluated each sampling day. All the ET-LPS groups increased all the inflammatory biomarkers when compared to ET-saline. Biomarkers for the ET-LPS groups ranged between 74.7 and 209.6 pg/mL for TNF-α, 72.7 and 207.58 pg/mL for IL-6, 35.7 and 140.3 pg/mL for IL-1β, 290.5 and 433.28 pg/mL for CXCL1, 37.7 and 64.9 pg/mL for CXCL2 and 251.9 and 350.4 μg/mL for protein content. To simplify the figures, only figures for one ET-LPS group were reported to assess the difference between the tested groups and the LPS level.

ET groups were compared to IV groups, which were administered cisplatin the first day of each cycle for a total of three administrations **(Figure 55)**. CIS-IV was administered at 2.0 mg/kg (CIS-IV_2) (n=20) and 1.5 mg/kg (CIS-IV_1.5) (n=12), following the procedure described in *Experimental part I-section 2.4.4.3*. These groups were compared to saline (IV-saline) (n=12). The last IV administration was performed 24h before the first sampling according to the kinetics of nephrotoxicity biomarkers.
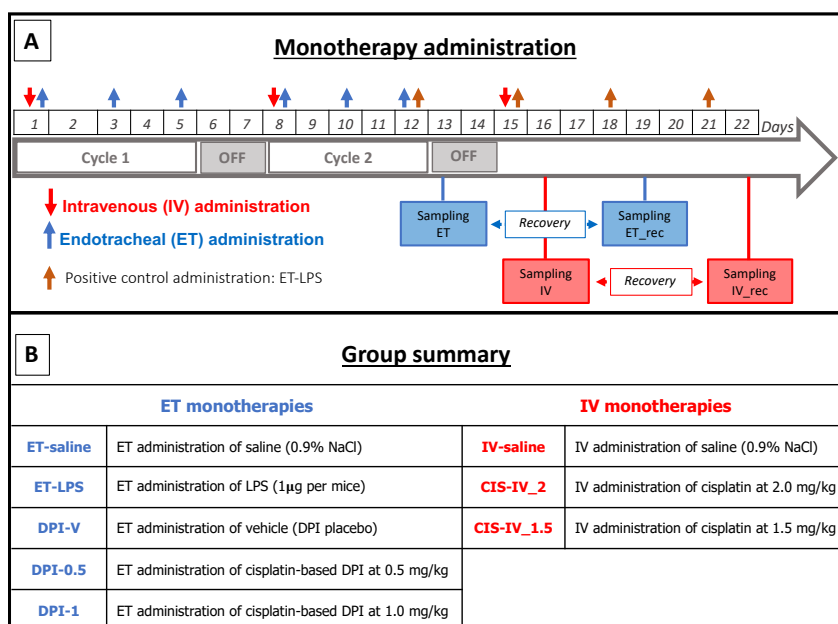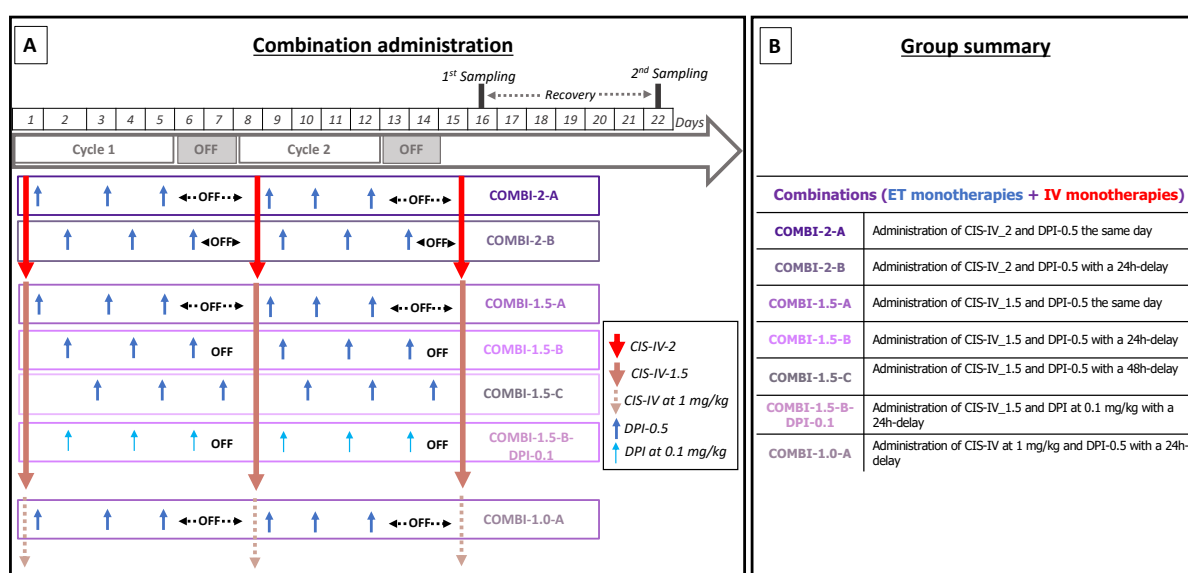

Figure 55: Time course of cisplatin monotherapy administrations (A) and sampling procedures 24h following the last treatment administration and after one week of recovery (_rec) of all the groups (B).

2.3.1.3.   Combination therapies

Different regimens were administered by combining CIS-IV and CIS-DPI-50 at their MTD, or *(i)* decreasing the IV MTD (by 25%, or by 50%) while maintaining the MTD for CIS-DPI-50, or *(ii)* decreasing the IV MTD by 25% and the CIS-DPI-50 dose by 80%. Delaying the administration of CIS-DPI-50 after CIS-IV by 24h, and by 48h was also tested. These adaptations (dose reduction and/or delayed days of administration) were integrated into this study to evaluate the pulmonary and renal tolerance of these adapted regimens in case of cumulative toxicity that may result following the administration of CIS-IV and CIS-DPI-50 at their MTD and on the same day.

To evaluate the tolerance of the combinations, CIS-IV and CIS-DPI-50 blends were administered following seven different regimens **(Figure 56)**. These groups were compared to the negative control group (IV-saline) (n=20).

COMBI-2 combined the IV and ET MTD (i.e. CIS-IV_2 and DPI-0.5). DPI-0.5 was either administered the same day within 1 hour (COMBI-2-A) (n=31) or delayed by 24h (COMBI-2-B) (n=36) after the CIS-IV_2.

COMBI-1.5 combined an IV dose decreased by 25% with the ET MTD (i.e. CIS-IV_1.5 and DPI-0.5) and DPI-0.5 was administered the same day (COMBI-1.5-A) (n=12), delayed by 24h (COMBI-1.5-B) (n=10) or by 48h (COMBI-1.5-C) (n=12) after the CIS-IV_1.5. COMBI-1.5-B_DPI-0.1 combined an IV dose decreased by 25% with an ET dose decreased 5-fold (i.e. CIS-IV_1.5 and DPI at 0.1 mg/kg), administered with a 24h-delay (n=12).

Last but not least, COMBI-1.0-A combined an IV dose decreased by 50% with the ET dose MTD (i.e. CIS-IV at 1.0 mg/kg and DPI-0.5), administered with a 24h-delay.

Figure 56: Time course of cisplatin combinations administrations (A) and sampling procedures 24h following the last treatment administration and after one week of recovery (_rec) of all the groups (B).

For both the monotherapy and the combination groups, the sampling was performed immediately or after a recovery period (_rec groups) of 1 week following the 2-week treatment, i.e. 24h or 1 week after the last administration. For clarity, **Figure 55.B and Figure 56.B** summarized the mouse groups exposed to the monotherapies or to the combinations described above.

2.3.2. Pulmonary tolerance evaluation

To evaluate the local tolerance, BALF and lungs were collected as described previously [211]. Briefly, the neck region was opened and a 20-gauge canula (Surflo® catheter, Terumo, Leuven, Belgium) was introduced into the trachea and fixed with a silk thread. The lungs were directly flushed three times using 0.7 ml PBS at 4°C and BALF was collected in centrifuge tubes (VWR Chemicals, Leuven, Belgium). Lungs were harvested and immersed in FMA for 24h, then cleaned in water for 15 minutes before being put in IPA for 24h. Then, they were embedded in paraffin for histopathological analyses using HE staining. Analyses were performed in a randomized, blind study by an independent pathologist following the process described by Jones *et al*. [238]. This was performed for all mouse lungs, using two impaired sections per lung. The severity of each observation was scored from 0 to 5, and the mean score was determined by calculating the average among each group. In addition, the frequency was evaluated and was expressed as the number of animals in which the observation was encountered.

BALF were kept on ice, vortexed and the total cell count was performed using an automated cell counter (Countess II FL, Life Technologies, Zellik, Belgium). BALF were immediately centrifuged at 160 g at 4°C for 5 minutes. The supernatant was collected, aliquoted and stored at -80°C. The packed cells were resuspended in 200 μL of cold PBS and then cytospinned to set them on slides. Slides were stained using May-Grünwald Giemsa stain to investigate the differential cell count. AM, NT-GRA, LYM and EOS were counted manually on a total of 200 cells to determine the proportion of each cell type.

To evaluate the local tolerance, both inflammation and cytotoxicity were investigated. The pro-inflammatory cytokines (TNF-α, IL-6 and IL-1β) and specific mouse chemokines (CXCL1 and CXCL2) were selected. All these biomarkers were quantified using an ELISA method as described by the manufacturer (Duoset, RnD Systems, Abingon, UK).

To evaluate cytotoxicity, the LDH activity was quantified following the protocol described in the Cayman Chemical LDH Cytotoxicity Assay Kit (Ann Arbor, MI, USA). Results were expressed as LDH/LDH $_{\text{Negative control}}$. The total protein content was also quantified using a Pierce bicinchoninic acid (BCA) Protein Assay Kit (Thermo Fisher Scientific, Zellik, Belgium).

All analyses were performed in duplicate and each group was compared to positive (LPS) and negative (saline) controls, as described previously.

2.3.3. Renal tolerance evaluation

2.3.3.1. Acute kidney injury plasma biomarkers

In a preliminary study aiming to evaluate early AKI, the time course of several plasma and urine biomarkers of AKI was investigated after the administration of a single dose of cisplatin at 15 mg/kg using the IP route [262]. Mice were euthanized 6, 12, 24, 48 and 72h after cisplatin administration using an IP administration of sodium pentobarbital at 12 mg/kg. Urine was removed by a puncture directly in the bladder, aliquoted and stored at -80°C. Blood and kidneys were collected and stored as described above. To evaluate early AKI, urinary and plasma NGAL, KIM-1 and plasma cystatin C were quantified in duplicate using a mouse-specific ELISA following the manufacturer's protocol (Duoset and Quantikine, RnD Systems, Abingdon, UK). Plasma creatinine was evaluated using a high-performance liquid chromatography (HPLC) method and urinary creatinine was quantified using the Jaffé method as described previously [263]. Urinary NGAL and urinary KIM-1 were normalized using urinary creatinine.

Considering these preliminary results and the erratic availability of urine samples in mice (i.e. high variability among groups due to the small urine samples available per group, with no urine for the group that was sampled 72h later), the following experimental procedures focused on plasma biomarkers of AKI (NGAL, cystatin C and creatinine).

2.3.3.2. Sample collection, histology and immunohistochemistry

During sampling, blood was directly collected by retro-orbital puncture in lithium heparin tubes (Sarstedt, Cologne, Germany). Blood was centrifuged for 10 minutes at 2 000 g and 20°C. Then, plasma was aliquoted and stored at -80°C for further analysis. Kidneys were harvested from mice and put in a buffered 4% FMA for 24h. They were then rinsed in water for 15 min, preserved in IPA for 24h and then embedded in paraffin for histopathological analyses using HE and PAS staining. This was performed in a randomized, blinded study as described previously [263]. The severity of each observation was scored from 0 to 5, and the mean score was determined by calculating the average among each group.

NGAL immunostaining was also performed and was adapted from Luo *et al.* [144]. Briefly, once deparaffinized, kidney sections (5 μm) were rehydrated and washed in PBS. The heat antigen retrieval was performed by putting the sections in 10 mM of citrate buffer in a microwave for 15 minutes. The endogenous peroxidase activity was eliminated following incubation for 20 min in 3% H_2O_2. After several washes in PBS-Tween 1% (v/v), the sections were blocked using a blocking solution (Vector Labs, Peterborough, UK) for 20 min in a

humidity chamber. Sections were rinsed in the same buffer and incubated in a humidity chamber overnight with the primary antibody (Thermo Fisher Scientific, Zellik, Belgium) at 10 µg/mL. After the washing steps, sections were incubated with mouse anti-rabbit secondary antibody (Vector Labs, Peterborough, UK) for 30 min, before being washed again and incubated with the avidin-biotin complex (ABC) solution (Vector Labs, Peterborough, UK). Sections were rinsed once again and DAB substrate (Vector Labs, Peterborough, UK) was added for 5 minutes. A haematoxylin counterstain was performed to identify the cell nuclei. Each time that the assay was conducted, a kidney section without primary antibody was assessed as a control to verify the specificity of the experiment.

2.4. Efficacy study

The anti-tumour efficacy of the ET CIS-DPI-50 blend combined with a conventional IV platinum doublet combining cisplatin and paclitaxel was investigated on the M109-HiFR-*Luc2* lung carcinoma orthotopic model in mice [211]. The cell preparation and the technique of engraftment were detailed previously in *Experimental part I-section 2.3.3.2.*

On the third day post cell engraftment (i.e., D3), mice were randomly allocated to one of the four groups of investigation. Treatments were administered from D6 for two cycles of one week and were established as follows: *(i)* IV saline negative control untreated group (n=11); *(ii)* IV solution delivering 1.5 mg/kg cisplatin and 10 mg/kg paclitaxel (IV platinum doublet, n=8), one administration per week (on Mondays) for 2 consecutive weeks; and *(iii)* combination of the IV platinum doublet (on Mondays) with ET CIS-DPI-50 at 0.5 mg/kg cisplatin (n=15), three administrations per cycle regimen (0.5x3, on Tuesdays, Thursdays, and Saturdays) for 2 consecutive weeks **(Figure 57)**.
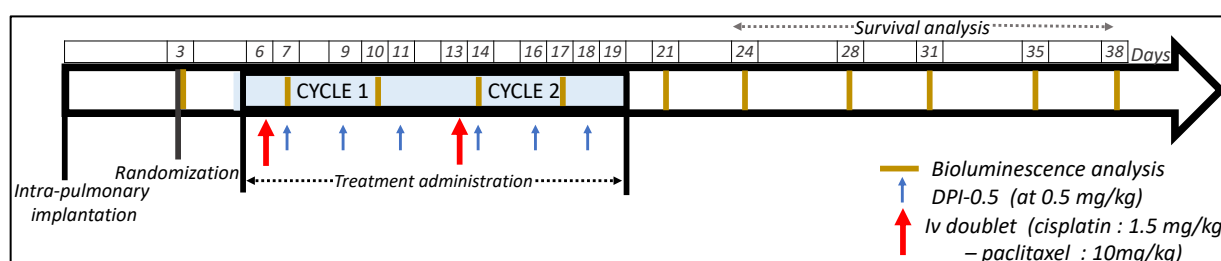

Figure 57: Efficacy study scheme of administration and follow-up.

179

The paclitaxel solution, a Taxol-like solution [211], was prepared at 6 mg/mL using a mixture of Cremophor® El (BASF, Ludwigshafen, Germany) and absolute ethanol (50:50 v/v). The IV platinum doublet was made by mixing the solution of paclitaxel in the cisplatin solution to obtain final concentrations of 1 mg/mL and 0.15 mg/mL, respectively. These solutions were kept protected from light and prepared immediately before use.

BLI of the whole mice was performed two times a week to follow *in vivo* tumour growth (primary tumour and metastases) and was expressed as the tumour growth % relative to D3. BLI was performed by means of a Photon Imager Optima (Biospace Lab, France) that dynamically counted the emitted photons for at least 25 min, with the mice under anaesthesia (3.5% and 2% isoflurane for initiation and maintenance, respectively) and after subcutaneous administration of 150 mg/kg of D-luciferin (Promega, Leiden, Netherlands) [237]. Image analysis was performed with M3Vision software (Biospace Lab). Regions of interest were drawn on the mice thorax, and signal intensities were quantified individually for a time lapse of 5 min corresponding to the maximum signal intensity plateau. Kaplan-Meier survival curves were established by excluding deaths related to the ET administration procedure, as previously reported [192,205,243]. **Figure 57** describes the *in vivo* procedure, from tumour grafting, randomization and scheme of treatment administration to follow-up in terms of BLI and survival analysis.

2.5. Statistical analyses

All statistical tests were conducted using GraphPad PRISM® (7.0a) software. One-way ANOVA and the Bonferroni's post-test were used to compare toxicity biomarkers *vs.* the negative control groups (NGAL, creatinine, cystatin C, IL-6, TNF-α, IL-1β, CXCL1, CXL2, protein content and LDH ratio). For the efficacy study, the Kaplan-Meier curve and log-rank test with an analysis of the p value by means of the Holm-Šídák method were used for the survival analysis. Two-way ANOVA with Bonferroni post-testing was used to analyse mean tumour growth over time. Results were considered as statistically significant (*) for $p < 0.05$, very significant (**) for $p < 0.01$ and extremely significant for $p < 0.001$ (***) and for $p < 0.0001$(****).

3. <u>Results and discussion</u>

3.1. Overall tolerance

Toxicity was evaluated for both mono and combined IV and ET therapies to select the highest dose and frequency of administration that were well-tolerated.

The MTD was first determined for the ET or IV route. The CIS-IV MTD was observed at 2.0 mg/kg and the CIS-DPI-50 MTD at 0.5 mg/kg, as 1.0 mg/kg by the ET route induces a bw decrease of -7±3% **(Figure 58.A)**. Therefore, a combination was made of CIS-IV at 2.0 mg/kg and CIS-DPI-50 at 0.5 mg/kg (COMBI-2) as well as with lower doses of CIS-IV (i.e. 1.5 mg/kg and CIS-DPI-50 at 0.5 mg/kg, for COMBI-1.5, and 1.0 mg/kg and CIS-DPI-50 at 0.5 mg/kg, for COMBI-1.0), and of CIS-IV and CIS-DPI-50 (i.e. CIS-IV at 1.5 mg/kg and CIS-DPI-50 at 0.1 mg/kg, for COMBI-1.5-B-DPI-0.1). These lowered dosages were evaluated because combined administrations usually increase toxicity as cisplatin nephrotoxicity is dose-duration-frequency-dependent [125]. As anticipated, combining cisplatin using both routes increased the bw losses but these did not exceed 10%, irrespective of the doses or regimen. The bw profiles showed similar patterns between all combination groups with a decrease following CIS-DPI-50 administration and an increase between two administrations and during off-cycles as represented in **Figure 58.A**.
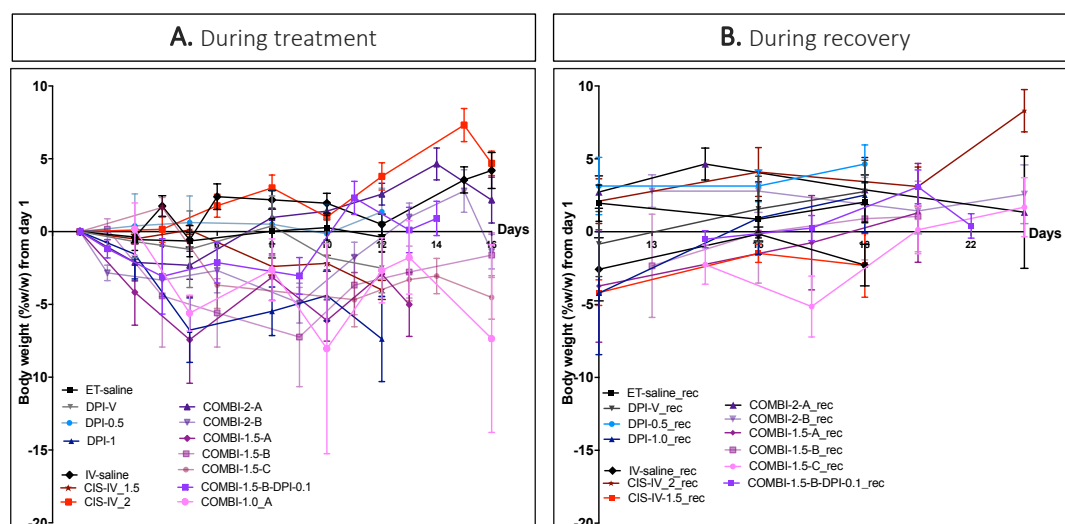

Figure 58: Evaluation of bw loss following the 2-weeks treatment (A) and the one-week recovery (B). The groups' abbreviations are described in **Figure 55 and Figure 56.** All results are expressed as means ± SEM (N=4-17).

Moreover, during the recovery week, the bw increased for all groups except for COMBI-2 (A and B), under which some mice died (5% *vs.* 2.5%, respectively, **Figure 58.B**). This showed that they were not able to recover from the toxicity generated by the cycles of administration

of high doses of cisplatin using both routes under COMBI-2. This toxicity was also related to the cumbersomeness of the technique of administration (use of anaesthesia, ET intubation and the delivery of several puffs per administration) as shown by the weight stabilisation (i.e. no weight increase) for the negative control group during the treatment administration period.

To investigate the possible pulmonary and renal toxicities associated with monotherapies and combinations, biomarkers were quantified and histopathological analyses assessed to identify the tissue damage and the inflammatory mediators involved.

In the case of monotherapies, the pulmonary tolerance following CIS-IV administration and the renal tolerance following CIS-DPI-50 administration should be preserved, as the PK results presented in *Experimental part I* demonstrated a 7-fold increase and decrease in C_{max} in lungs and plasma respectively for CIS-DPI-50 in comparison to CIS-IV_1.25 (C_{max} in the lungs for CIS-DPI-50: 19 ± 2 ng/mg *vs.* 2.6 ± 0.8 ng/mg for CIS-IV_1.25; and C_{max} in the plasma for CIS-DPI-50: 0.7 ± 0.6 ng/μL *vs.* 5 ± 1 ng/ μL for CIS-IV_1.25).

As described previously, samples of all groups were collected 24h after the two cycles and one week later (_rec groups) **(Figure 55 and Figure 56)** to evaluate potential pulmonary and/or renal toxicity found and their reversibility.

3.2. Pulmonary tolerance assessment of CIS-DPI-50, CIS-IV and their combinations

To investigate pulmonary tolerance, it was mandatory to evaluate inflammation as well as cytotoxicity related to the cisplatin mode of action by both quantifying specific biomarkers and identifying lung damage. This was assessed for the monotherapy groups (DPI-V, DPI-0.5, DPI-1, CIS-IV_2 and CIS-IV_1.5), and for the combinations with the most drastic conditions in terms of cumulative dose and with the lowest staggering between CIS-DPI-50 and CIS-IV administrations (i.e. COMBI-2 and COMBI-1.5 A and B). This evaluation was performed 24h following the last treatment administration following the kinetic of biomarkers involved in the early phase of inflammation. Inflammation, in its exudative phase, was evaluated in BALF to quantify the biomarkers in their site of origin [133]. As TNF-α, IL-6 and IL-1β have been widely investigated in animal models and remain the most frequently involved in the evaluation of animal toxicity, they were selected in this study [133,163]. During a tolerance study of CIS-DPI-TS, an increased proportion of NT-GRA was observed [205]. Consequently, to estimate the NT-GRA recruitment, mouse chemokines (CXCL1, CXCL2) were also selected for this

study [264]. Cytotoxicity was evaluated by assessing LDH activity and the total protein content in BALF [265].

3.2.1. Pulmonary inflammation evaluation

As anticipated, all the positive controls (i.e. ET-LPS) led to higher values in terms of pro-inflammatory cytokine contents in BALF than their respective baseline (i.e. negative control groups: ET-saline and IV-saline) **(Figure 59)**. Indeed, these biomarkers are released in the acute phase of inflammation as a response to injury or a toxin such as LPS [163].

No significant TNF-α, IL-6 or IL-1β increase was observed following the administration of DPI-V, DPI-0.5, DPI-1 or COMBI-1.5-A (24h and _rec). TNF-α results showed a higher expression after the administration of IV when compared to ET **(Figure 59.A)**. CIS-IV_1.5 and CIS-IV_2 were significantly higher when compared to their negative controls. Both COMBI-2-A and COMBI-2-B tended to increase the TNF-α levels, but this increase was only significant for COMBI-2-A, the highest drug and most frequent dosage regimen ($p < 0.01$). One week later, these increases were maintained and COMBI-2-B_rec became significant **(Figure 59.A)**, showing the expansion of the inflammation.
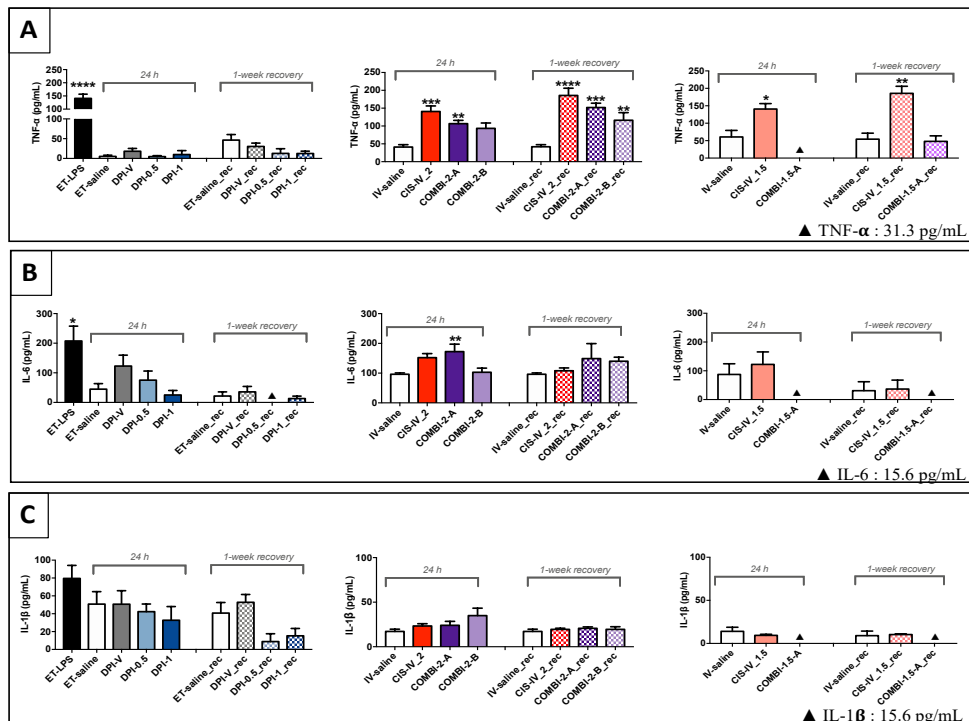
Figure 59: Evaluation of TNF-α (A) IL-6 (B) and IL-1β (C) in BALF 24h following the treatment administration and after one week of recovery (_rec). The groups' abbreviations are described in **Figure 55 and Figure 56.** All results are expressed as means ± SEM (N=4-17). The statistical analyses were performed *vs.* their corresponding negative control group using one-way ANOVA and Bonferroni's post-test (**** for $p < 0.0001$, *** for $p < 0.001$, ** for $p < 0.01$ and * for $p < 0.05$).

However, TNF-α levels did not seem to increase following COMBI-1.5-A administration. This may be related to cytokine fluctuations as high variations are predicted during *in vivo* experiments. It has been demonstrated that stress was able to increase pro-inflammatory cytokine levels and change their kinetics [266]. In our case, cumbersome administration techniques (repeated IV and ET administrations) could generate stress leading to unexpected fluctuations from the baseline. Biomarker levels must be interpreted with caution and should be combined with additional investigations such as cell counts and histology. Therefore, a negative control group (ET-saline) that followed the same procedure of manipulation and administration was sampled the same day as the tested groups to avoid these day-to-day fluctuations. Even though non-significantly different, these day-to-day fluctuations ranged between 5 ± 3 pg/mL and 46 ± 14 pg/mL for ET-saline and ET-saline_rec (one week of recovery later), and between 41 ± 7 pg/mL to 61 ± 19 pg/mL for IV-saline and IV-saline_rec (one week of recovery later) in terms of TNF-α levels **(Figure 59.A)**.

IL-6 was significantly higher only for COMBI-2-A **(Figure 59.B)**. IL-1β showed no significant increase in any group when compared to the negative controls **(Figure 59.C).** CIS-IV seemed to increase TNF-α and IL-6 levels more than CIS-DPI-50 (i.e. DPI-0.5 and DPI-1). This may be explained by the fact that a higher solubilized cisplatin fraction was delivered to the lungs after the IV administration and may be responsible for a higher toxicity when compared to a controlled-release DPI formulation, from which cisplatin is gradually released ($50.6 \pm 0.3\%$ after 6h). As described above, cytokine levels must be interpreted with caution as they might be influenced by mouse stress levels, and should be combined with other investigations. However, in this study, the comparison was made with the control group that have followed the same procedure of manipulation and administration (ET-saline) to take the stress contribution into account in the evaluation of CIS-DPI-50. This was not done for COMBI groups, where the comparison was made with the IV-saline group.
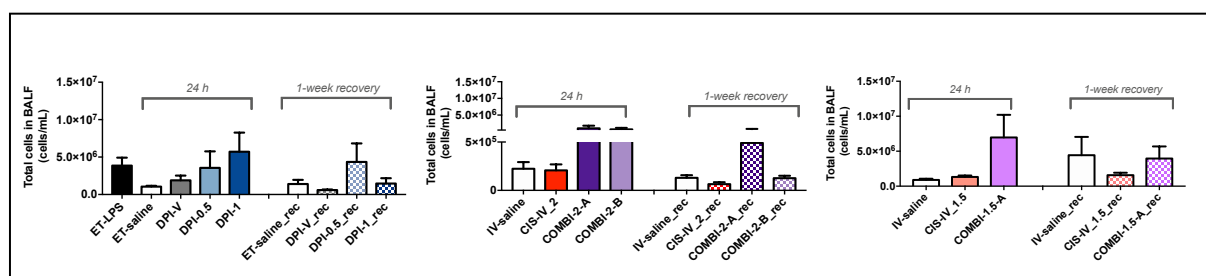

Figure 60: Evaluation of total cells in BALF 24h following the 2-week treatment and the one-week recovery (_rec). The groups' abbreviations are described in **Figure 55 and Figure 56.** All results are expressed as means ± SEM (N=4-17). The statistical analyses were performed *vs.* the control groups using one-way ANOVA and Bonferroni's post-test.

To complete the pro-inflammatory cytokine evaluation, cells in the BALF (AM, NT-GRA, LYM and EOS) were counted **(Figure 60)**. Although non-significant, the total count showed a dose-dependent increase for DPI-0.5 and DPI-1 (4 ± 2 $x10^6$ and 6 ± 3 $x10^6$ cells/mL, respectively *vs.* 1.0 ± 0.1 $x10^6$ cells/mL for the negative control group ET-saline), as with the positive control groups (ET-LPS). An increase was also observed for the combination groups when compared to their respective controls (COMBI-2-A, COMBI-2-B and COMBI-1.5-A, with 1.0 ± 0.8 x 10^6 cells/mL *vs.* 2.0 ± 0.7 x 10^5 cells/mL for IV-saline, 7 ± 5 x 10^5 cells/mL *vs.* 2 ± 0.7 x 10^5 cells/mL for IV-saline, and 7 ± 3 x 10^6 *vs.* 9.0 ± 0.2 x 10^5 cells/mL for IV-saline, respectively). This increase was reversible for all groups except DPI-0.5_rec. As NT-GRA were the only cell type observed during the differential cell count analysis, other than AM and LYM, this increase was certainly related to their recruitment. AM are not adequate to assess phagocytosis in normal conditions [267]. However, their number is increased and their function increased by the dendritic cells in the case of inflammation and/or infection [267,268]. Foamy macrophages were retrieved in the packed cells, showing their ongoing phagocytosis against inhaled foreign particles in the alveolar zone **(Figure 61)**. Moreover, NT-GRA are the first inflammatory cells recruited directly at the acute inflammation site [163], as illustrated in the packed cells for the ET-LPS group **(Figure 61)**. It was therefore interesting to evaluate their proportion among the BALF cells.
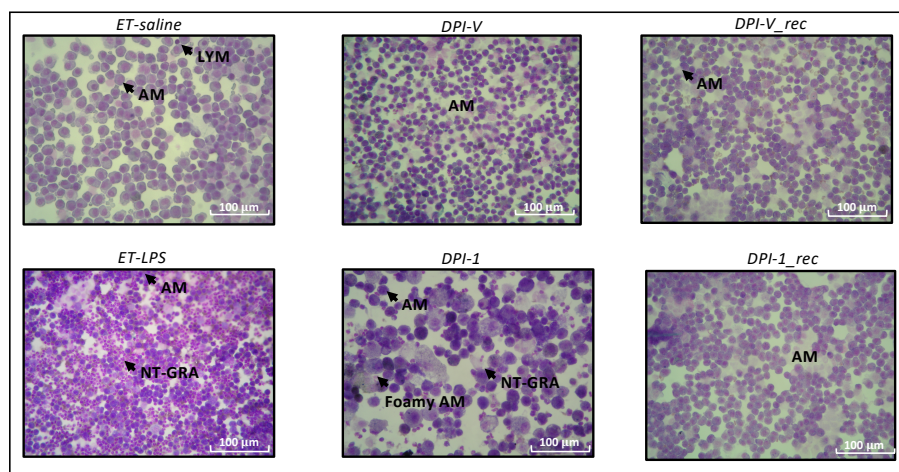

Figure 61: Differential cell count analysis: AM, LYM and NT-GRA are represented for each group. The groups' abbreviations are described in **Figure 55 and Figure 56.**

As expected, all the positive control groups showed a significant NT-GRA increase, as observed in **Figure 61,** and as reported in **Figure 62.A**. No NT-GRA increase was observed when the vehicle (DPI-V) was administered, showing that the excipients were well-tolerated and did not

induce inflammation. This result is confirmed by the representative images of differential cell counts as only AM were retrieved for DPI-V, as observed for the negative control group (ET-saline) **(Figure 62)**. Therefore, all the following increases were attributable to the sustained release of cisplatin from the CIS-DPI-50 particles, and not to the presence of the vehicle.
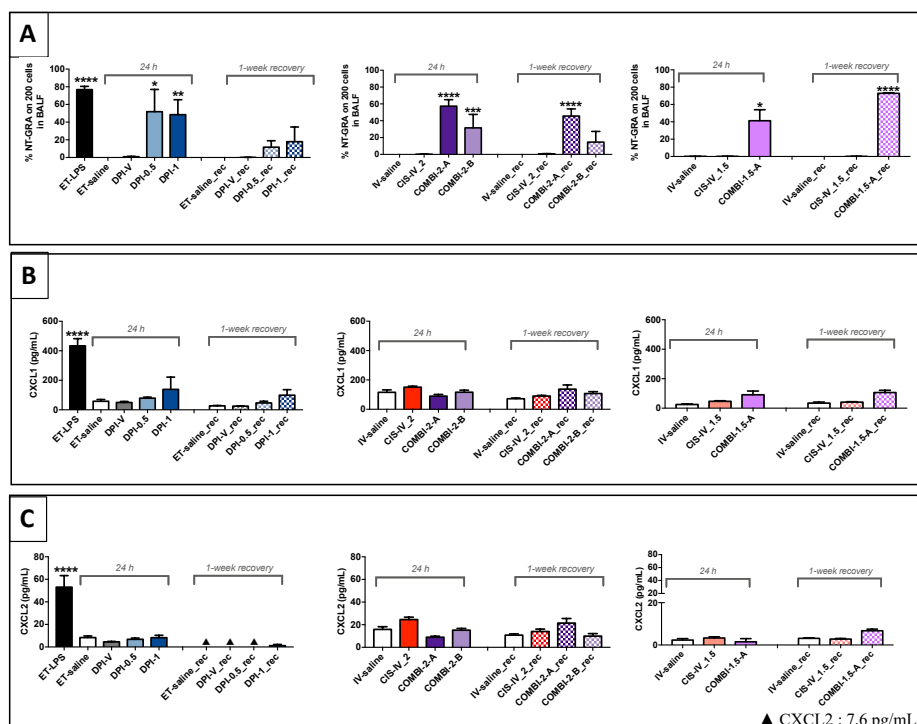

Figure 62: Evaluation NT-GRA as a proportion of 200 BALF cells (A), CXCL1 (B) and CXCL2 (C) in BALF 24h after the treatment administration and after one week of recovery (_rec). The groups' abbreviations are described in **Figure 55 and Figure 56.** All results are expressed as means ± SEM (n=4-17). The statistical analyses were performed *vs.* their corresponding negative control group using one-way ANOVA and Bonferroni's post-test (**** for $p < 0.0001$, *** for $p < 0.001$, ** for $p < 0.01$ and * for $p < 0.05$).

It was also noticed that all the groups that were administered CIS-DPI-50 using the ET route (as monotherapy or combination) increased the NT-GRA proportion significantly in comparison with the IV route as monotherapy. This may be explained by the fact that, as demonstrated by the PK studies, CIS-DPI-50 led to a long lung exposure to cisplatin during which cisplatin was slowly released from CIS-DPI-50 particles, unlike CIS-IV (AUC$_{0-\infty}$ in the lungs for CIS-IV_1.25: 558 ng.min.mg^{-1} ([203]) *vs.* 4611 ± 932 ng.min.mg^{-1} for CIS-DPI-50). The most significant exposures were for COMBI-2-A and COMBI-1.5-A. This is understandable as in these combinations, CIS-DPI-50 and CIS-IV were administered the same day, increasing local concentration and therefore reaction induced by the addition of ET cisplatin-based treatment when compared to IV administration alone. The evaluation of NT-GRA levels one week later showed that the inflammation seemed to be reversible for DPI-0.5,

DPI-1 and COMBI-2-B_rec, but seemed to be maintained or even increased for the combination groups that were administered treatment the same day (COMBI-2-A_rec and COMBI-1.5-A_rec, respectively) **(Figure 62.A).**

As NT-GRA recruitment is partially controlled by CXCL1 and CXCL2 chemokines [264], these chemokines were therefore quantified in BALF. CXCL1 and CXCL2 were significantly higher for ET-LPS groups, when compared to their negative controls. Although non-significant, CXCL1 and CXCL2 increased dose-dependently for DPI-0.5 and DPI-1, as observed for the NT-GRA recruitment **(Figure 62.B and C)**. The evaluation of CXCL1 and CXCL2 levels for COMBI-2-A and COMBI-1.5-A did not seem to increase following the 2-week administration period when compared to their negative controls but were higher, but non-significant, 1 week later. In contrast, CXCL1 and CXCL2 levels for DPI-0.5 and DPI-1 seemed to be reversible within 1 week. Therefore, administering cisplatin using both routes on the same day, regardless of their doses, could compromise the reversibility of the NT-GRA recruitment as the delay of 24h between the administrations seemed favourable for COMBI-2-B in comparison with COMBI-2-A. This non-reversibility indicated a more intense local reaction for the combination groups administered the same day. These results are in line with the pro-inflammatory cytokine levels observed for COMBI-2-A and B, but not with the observations for COMBI-1.5-A **(Figure 59)**. As described above, pro-inflammatory cytokines levels may fluctuate depending on several factors (sampling day, mouse stress) leading to unexpected results [269]. Apart from inflammation, pulmonary tolerance should therefore be interpreted by considering cytotoxicity as well as lung damage.

3.2.2. Cytotoxicity evaluation

In the case of cell lysis, the protein content is released from cytosol, which makes it an interesting cytotoxicity biomarker. The protein content was higher for all groups administered treatment using the ET route (i.e. monotherapies and combinations) when compared to the IV groups. This may be correlated to a more prolonged exposure to cisplatin when administered in the lungs (controlled-release form) as no higher protein content was observed following the administration of CIS-IV. Although this increase was not significant for most groups, it was significant for DPI-0.5_rec ($p < 0.05$, **Figure 63.A**). The protein content for COMBI-2-A was also significant after the 2-week administration ($p < 0.01$) and maintained it even after the week of recovery ($p < 0.05$, **Figure 63.A**). COMBI-1.5-A protein levels were higher but not significant certainly due to the high variation observed within this group.

LDH is found in the cytoplasm of the cell of various tissue types (brain, lung, lymph nodes, etc.) and increases in the case of cell damage or death [265]. Consequently, LDH also seems to be an interesting biomarker for cytotoxicity. $LDH/LDH_{Negative\ control}$ showed no significant increase following the administration of monotherapies **(Figure 63.B)**. Nevertheless, DPI-1 and CIS-IV_2_rec were nearly 2-fold higher when compared to their negative controls. This was not observed for DPI-0.5 or CIS-IV_1.5. Moreover, the LDH ratio was more than 3-fold higher following the 2-week regimen of COMBI-2-A, and was even higher after the 1 week of recovery later ($p < 0.01$). LDH was significantly higher for COMBI-1.5-A ($p < 0.05$) but was reversible after 1 week of recovery **(Figure 63.B)**. This difference can be explained by the fact that a higher IV dose was administered for COMBI-2-A in comparison with COMBI-1.5-A (2.0 mg/kg *vs.* 1.5 mg/kg).
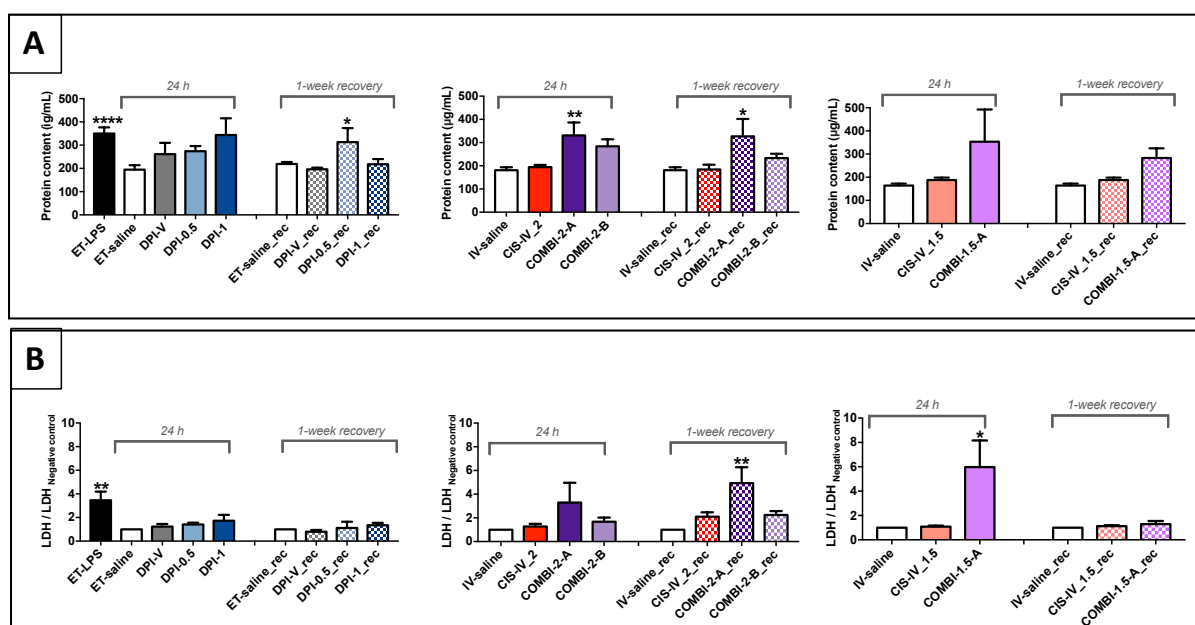

Figure 63: Evaluation of the total protein content (A) and the $LDH/LDH_{(Negative\ control)}$ (B) in BALF 24h after the treatment administration and after one week of recovery (_rec). The groups' abbreviations are described in **Figure 55 and Figure 56.** All results are expressed as means ± SEM (n=4-17). The statistical analyses were performed *vs.* the corresponded negative control group using one-way ANOVA and Bonferroni's post-test (**** for $p < 0.0001$, ** for $p < 0.01$ and * for $p < 0.05$).

Although the protein content evaluation included all the proteins that were retrieved in the cytosol following cell lysis and the LDH activity was specific to this unique protein, these cytotoxicity biomarkers tended to demonstrate similar trends. Indeed, no higher cytotoxicity was observed following the administration of monotherapies. However, once combined, a higher cytotoxicity was found in the groups that were administered the same day (COMBI-2-

A and COMBI-1.5-A), 24h after the last administration. This was also observed for the group administered with the highest dose after one week of recovery (COMBI-2-A_rec, **Figure 63**).

Lung inflammation resulting from an anti-cancer drug is often initiated by the phagocytosis of the inhaled particles or the epithelial cell debris by the AM [157,185]. As a result, these macrophages secrete pro-inflammatory cytokines and chemokines to recruit NT-GRA to phagocyte, degranulate or generate ROS [163]. Other cell types are also involved and play a crucial role in the induction of this inflammation such as NK cells, dendritic cells, LYM, mast cells and EOS, as discussed above [267]. Depending on the type of injury, these cells interact differently, produce various cytokines (pro-inflammatory and anti-inflammatory) and ultimately induce acute lung injury [267]. Once the phagocytosis is completed, the inflammatory cells undergo surface changes and the resolution of the inflammation starts [267]. In contrast, during chronic exposure, the resolution of the inflammation can take more time, leading to chronic inflammation [162].

ET and IV treatments seem to activate two different inflammation processes. Indeed, CIS-IV was characterized by increased TNF-α, IL-6 levels when compared to CIS-DPI-50. In contrast, CIS-IV showed no increase in terms of AM and NT-GRA recruitments (total and differential cell counts) nor did NT-GRA-related chemokines (CXCL1 and CXCL2). As the pulmonary tolerance impairment seemed to be related to higher concentration peaks in the lungs (whole cisplatin dose solubilized for CIS-IV *vs.* partial cisplatin release from CIS-DPI-50 particles), CIS-IV may have induced epithelial cell damage and injured the type II alveolar cells, which are involved in the airways' innate immunity [270]. This is the most well-described mechanism for cytotoxic injury [157,185]. As a consequence of this lung damage, pro-inflammatory cytokines (mainly TNF-α, IL-6 and IL-1β) were secreted to initiate local inflammation [270]. Other mediators may have been secreted but were not evaluated in this study, such as ROS and PLT-activating factors leading to the release of arachidonic acid from membrane lipids. This fatty acid is involved in the production of eicosanoids, which stimulates tissue inflammation [267].

For CIS-DPI-50 that was delivered repeatedly in the form of SLM, from which cisplatin is released slowly, local damage was therefore prevented. It should be noted that following the administration of DPI-1 using the DP4-M®Dry Powder Insufflator™, the cisplatin mass recovered in the lungs was 5.4 ± 0.7 μg (n=12), which corresponded to $26 \pm 3\%$ of the delivered dose, as exposed in *Experimental part I-section 3.2.4*. This was in the same range as previously published by Levet *et al.* [203]. As these microparticles were PEGylated, they were able to

escape AM recognition and uptake since AM identify hydrophobic surfaces more easily [203,271]. AM may have started to identify these particles in a time-delayed manner and secreted pro-inflammatory cytokines (mainly TNF-α, IL-6 and IL-1β) and chemokines, leading to AM and NT-GRA recruitment [133,185]. Moreover, as cisplatin was entrapped in lipid microparticles, its release from these particles took several hours as was shown from PK studies obtained previously. Following this release, the excipient was entrapped by the AM and its digestion started with its incorporation into the lysosomes. HCO is a triglyceride that can be potentially hydrolysed into glycerol and free fatty acids by the action of the lysosomal acid lipase A [272]. Low PEGylated and amphiphilic excipients such as TPGS can be solubilized and absorbed in the systemic circulation before being eliminated, mostly by urinary excretion [273]. Consequently, for a controlled-release formulation, AM seemed to control phagocytosis more efficiently by secreting pro-inflammatory cytokines smoothly, preventing any major peak in their levels in comparison with CIS-IV. Moreover, except for TNF-α and IL-6 fluctuations and considering the NT-GRA proportion, the combination groups seemed to induce higher toxicity effects than CIS-IV.

3.2.3. Histopathological analyses

Histopathological analyses showed no major damage for the monotherapy groups (DPI-V, DPI-0.5, CIS-IV_1.5 and CIS-IV_2) **(Figure 64).** Nevertheless, some rare interstitial NT-GRA were observed for the ET-LPS groups. However, BEV and AB were scored at 1/5 for 40% of the mice among the DPI-1 group. Both kinds of damage were reversible, as observed after the week of recovery. COMBI-2-A was characterized by an increased BEV and AB (score 1/5).

The BEV and AB observed for DPI-1 and COMBI-2-A were scored at 0.4/5 and 0.2/5, respectively. Cytoplasmic vacuolation is the creation of vacuoles in animal cells exposed to stressful stimuli, including chemotherapeutic drugs, affecting the cell cycle and migration [274,275]. This phenomenon has been observed for weak basic lipophilic compounds that contain amine groups such as cisplatin [274]. Indeed, in the extracellular medium, cisplatin can easily cross the membranes through passive diffusion. Once in the cytoplasm, where the pH is higher and the chloride concentration is lower, cisplatin loses its chloride ligands to hydroxyl groups and is transformed into positively-charged metabolites (monoaquacisplatin: $[Pt(NH_3)_2Cl(OH_2)]^+$, and diaquacisplatin: $[Pt(NH_3)_2(OH_2)_2]^{2+}$), which are no longer able to diffuse through the plasma membrane [274,276]. The accumulation of these charged metabolites increases the intraorganellar osmotic pressure. The equilibration of the osmotic

pressure is assured by water diffusion, leading to the formation of vacuoles [274]. Irreversible vacuolation can affect the endoplasmic reticulum as well as the endosomal-lysosomal system and Golgi apparatus, leading to cell death [274]. Histopathological analyses have already reported a vacuolation in the lungs related to amine-containing chemotherapeutics such as bleomycin [275]. Also, cisplatin has already been associated with vacuolation in liver injury [277].
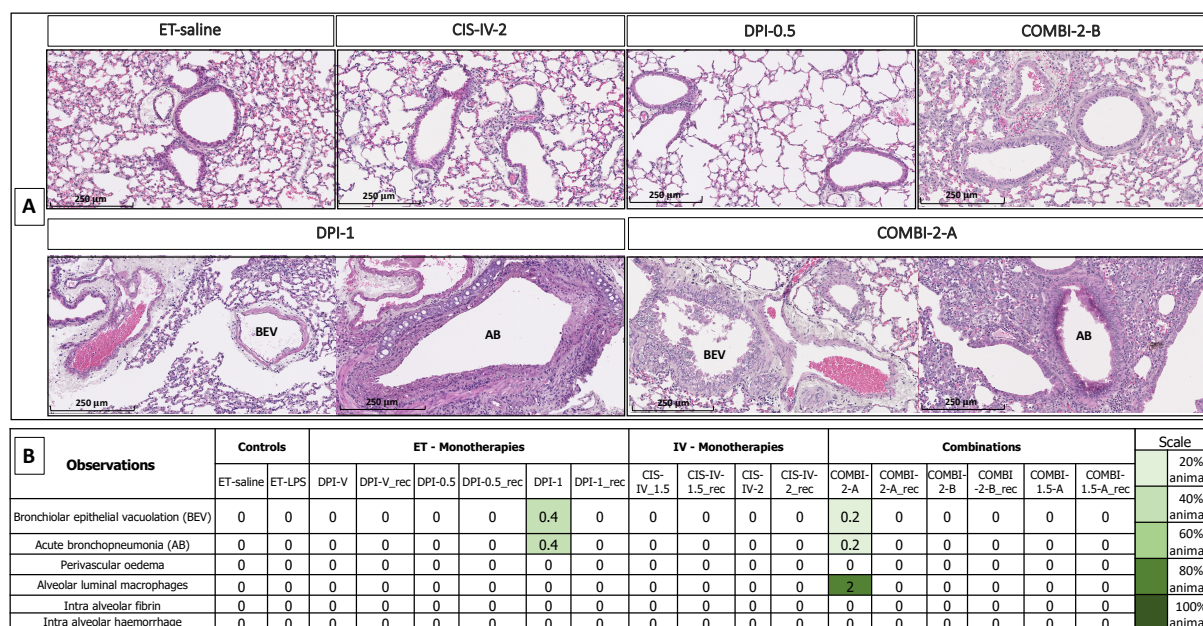

B Observations	Controls		ET - Monotherapies						IV - Monotherapies				Combinations						Scale
	ET-saline	ET-LPS	DPI-V	DPI-V_rec	DPI-0.5	DPI-0.5_rec	DPI-1	DPI-1_rec	CIS-IV_1.5	CIS-IV-1.5_rec	CIS-IV-2	CIS-IV-2_rec	COMBI-2-A	COMBI-2-A_rec	COMBI-2-B	COMBI-2-B_rec	COMBI-1.5-A	COMBI-1.5-A_rec	20% animals
Bronchiolar epithelial vacuolation (BEV)	0	0	0	0	0	0	0.4	0	0	0	0	0	0.2	0	0	0	0	0	40% animals
Acute bronchopneumonia (AB)	0	0	0	0	0	0	0.4	0	0	0	0	0	0.2	0	0	0	0	0	60% animals
Perivascular oedema	0	0	0	0	0	0	0	0	0	0	0	0	0	0	0	0	0	0	80% animals
Alveolar luminal macrophages	0	0	0	0	0	0	0	0	0	0	0	0	2	0	0	0	0	0	100% animals
Intra alveolar fibrin	0	0	0	0	0	0	0	0	0	0	0	0	0	0	0	0	0	0	
Intra alveolar haemorrhage	0	0	0	0	0	0	0	0	0	0	0	0	0	0	0	0	0	0	

Figure 64: Histopathology of lung tissue exposed to monotherapies and combinations. The groups' abbreviations are described in **Figure 55 and Figure 56.** Representative images of treated groups (A) and heat map of adverse observations and severity scores depending on lung tissue histopathology (B).

The slight and transient AB observed with DPI-1 and COMBI-2-A_rec has already been described for inhaled cisplatin delivered by nebulization in dogs [278]. Moreover, an increased number of alveolar luminal macrophages was also observed and scored from 1 to 4. Moreover, some perivascular oedema and NT-GRA were found for these groups. This was certainly related to a higher phagocytosis activity by the AM and an increased ingestion of the debris by the NT-GRA [267]. These observations seemed to be transient and more related to the ET treatment than IV, as no tissue damage was observed following CIS-IV administration, even at the highest dosage, CIS-IV MTD. Staggering these administrations for 24h (COMBI-2-B) prevented the development of all these observations, even at the highest dose. Moreover, combination groups at a lower dose (COMBI-1.5-A) did not show any tissue damage **(Figure 64)**.

As observed for biomarker quantification, and cell-count analysis, all these observations tended to describe an increased local inflammation for DPI-1 and for the highest and more frequent combination group (COMBI-2-A). It is important to mention that the difference in terms of histopathological analyses reported between DPI-1 and the 1 x 5 monotherapy regimen tested in *Experimental part II-section 3.2.2* (i.e. no histological side effects) could be attributed to the differences between mouse strains.

The quantitative techniques seemed to be more sensitive to dose and frequency of administration changes than histology, as no histological damage was observed for COMBI-2-B and COMBI-1.5-A. It is also important to note that since its first use and unlike other cytotoxic drugs (bleomycin, gemcitabine and mitomycin), cisplatin has not shown any major pulmonary toxicity when administered using the IV route, except some hypersensitivity reactions and in some rare cases, bronchospasm [77,156,157]. In one case report, cisplatin was reported to induce eosinophilic pneumonia but this seems to be very rare as it was only described for one patient [158,159]. These observations are therefore in line with what was observed for CIS-IV, as no major tissue damage was noticed during this study. These results confirmed that the increased TNF-α and IL-6 cytokines for IV groups were not related to any major lung damage. However, when administered by nebulization in the lungs, cisplatin induced bronchitis, dyspnoea, severe pneumonitis and mild to moderate fibrosis [178,278]. Delivering cisplatin as a controlled-release DPI could prevent the development of these side-effects and therefore improve its tolerance.

Overall, DPI-1 and COMBI-2-A were the less well-tolerated groups as a significant transient increase in terms of NT-GRA was observed as well as a reversible AB for DPI-1. For COMBI-2-A, a significant increase in terms of TNF-α, IL-6, NT-GRA and LDH/LDH$_{\text{Negative control}}$ was observed and maintained (except for IL-6) after the recovery period, as well as transient tissue damage such as BEV, AB and alveolar luminal macrophages, which were scored at 0.2/5, 0.2/5 and 2/5, respectively. Considering these pulmonary toxicities, these groups were discarded and will not be considered for the efficacy study. The overall pulmonary tolerance of DPI-0.5 seemed acceptable and its combination the same day with CIS-IV_1.5 was preferable to CIS-IV_2. However, the 24h delay between DPI-0.5 and CIS-IV_2 seemed to limit the pulmonary toxicity but with an irreversible and still higher TNF-α and a reversible NT-GRA increase. Interestingly, COMBI-1.5_A showed a significant increase in terms of NT-GRA that was maintained one week later as well as a reversible LDH/LDH$_{\text{Negative control}}$, but with no tissue damage.

3.3. Renal tolerance assessment of CIS-DPI-50, CIS-IV and their combinations

3.3.1. Preliminary study for the selection of AKI biomarkers

To assess early AKI, novel biomarkers have been intensively investigated, and have proven their sensitivity in both human and animal studies [136,137]. They are capable of detecting minor tubules and glomerular injuries, even when creatinine levels remain in normal ranges [140]. It is important to select optimal biomarkers not only based on their specificity and selectivity but also according to their kinetics. Therefore, NGAL, KIM-1, cystatin C and creatinine were chosen to be evaluated during a preliminary study with the aim of selecting the most pertinent biomarkers and a common collection timing.
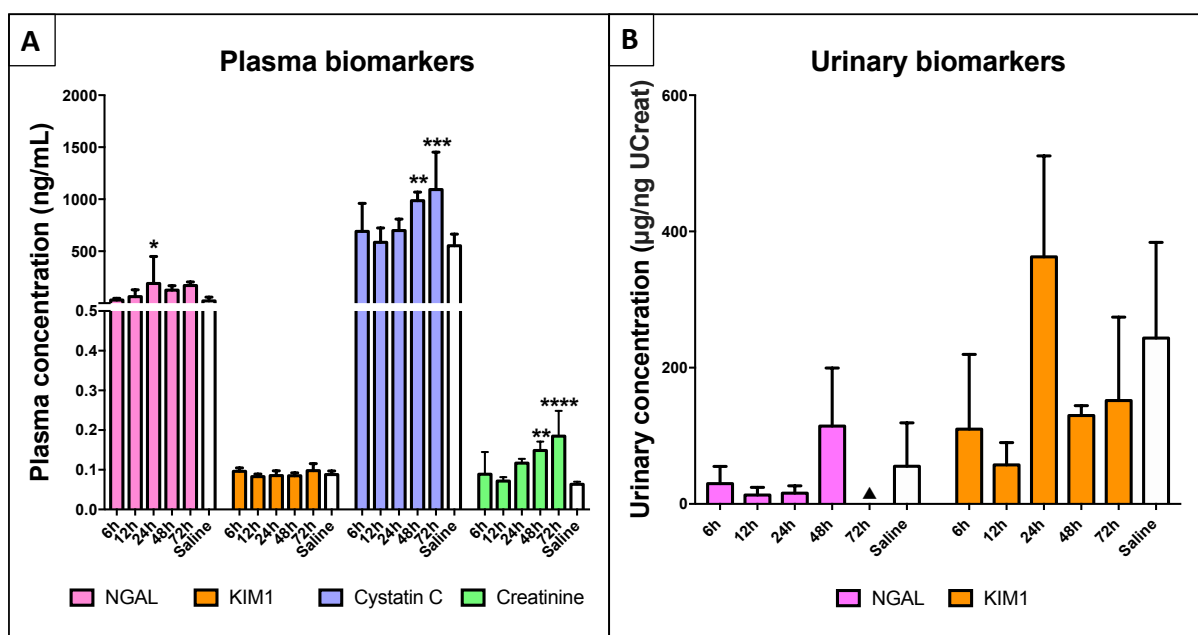
Figure 65: Evaluation of plasma (A) and urinary (B) NGAL, KIM-1, cystatin C and creatinine 6, 12, 24, 48 and 72h following the induction of an AKI model. All results are expressed as means ± SEM (N=5-6). The statistical analyses were performed *vs.* the control group using one-way ANOVA and Bonferroni's post-test (**** for $p < 0.0001$, *** for $p < 0.001$, ** for $p < 0.01$ and * for $p < 0.05$).

During this preliminary study, plasma creatinine, plasma cystatin C and both urine and plasma NGAL and KIM-1 were quantified. Plasma NGAL increased significantly 24h following the AKI-induced model. Both plasma cystatin C and creatinine also increased 24h following the induction and were significant only 48h and 72h later. Plasma KIM-1 levels remained low and no significant difference was observed when compared to the negative control **(Figure 65)**. KIM-1 is a transmembrane glycoprotein expressed at the apical membrane of proximal tubule

cells that increases in the case of ischemic or toxic injury [143,144]. In the literature, similar studies have shown that plasma KIM-1 increased up to 5 days after AKI, and was not as predictive as it was expected to be [279]. Urinary NGAL and KIM-1 showed a high variation between the time points **(Figure 65)**. Therefore, plasma NGAL, cystatin C and creatinine were selected for the renal tolerance evaluation. These biomarkers were collected 24h following the last administration as they were all higher than the negative control. It is important to note that this study aimed to evaluate the earliest phase in AKI for repeated (i.e. not single) administrations. Moreover, this timing also had to match the optimal kinetics timing (i.e. 24h following the last dose) of the pulmonary biomarkers as both pulmonary and renal tolerance were evaluated at the same time for the same mice. As described above, these AKI biomarkers were also evaluated 1 week later to assess the reversibility of cisplatin-induced nephrotoxicity.

3.3.2. MTD evaluation

For this evaluation, it was mandatory to include nephrotoxicity for the determination of CIS-IV MTD as it is a cisplatin DLT that imposes hours of hydration, massive side effects and separated cycles of administration. This was observed for CIS-IV at 2 mg/kg, as plasma NGAL, cystatin C and creatinine were higher when compared to their negative control ($p < 0.05$, $p < 0.01$, $p > 0.05$, respectively, **Figure 66**).
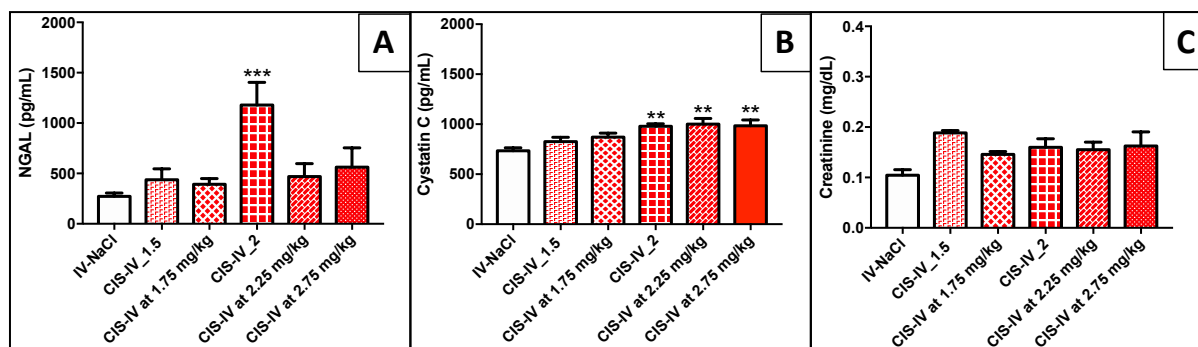
Figure 66: Evaluation of NGAL (A), cystatin C (B) and plasma creatinine (C) following the administration of CIS-IV at 1.5, 1.75, 2, 2.25 and 2.75 mg/kg. All results are expressed as means ± SEM (N=6). The statistical analyses were performed *vs.* the control groups using one-way ANOVA and Bonferroni's post-test (*** for $p < 0.001$ and ** for $p < 0.01$).

Moreover, bw profiles of all doses fluctuated following the administration days. The bw losses were limited and were observed at the lowest at -3 ± 2% for CIS-IV_1.5 (D5) and -2 ± 2% for CIS-IV at 2.75 mg/kg (D10) **(Figure 67)**.
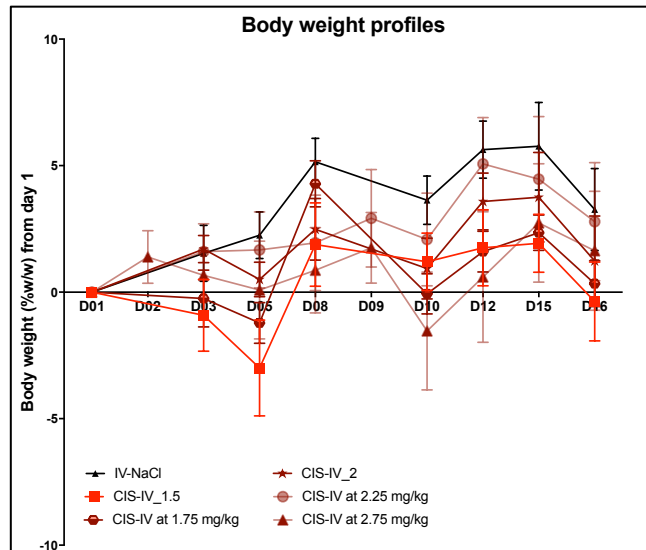
Figure 67: Evaluation of bw loss following three total CIS-IV administrations, each at the beginning of each cycle. All results are expressed as means ± SEM (N=6).

3.3.3. Monotherapies evaluation

CIS-IV administration increased the biomarkers to slightly higher than for CIS-DPI-50 (DPI-0.5 and DPI-1) **(Figure 68, Figure 69 and Figure 70)**.
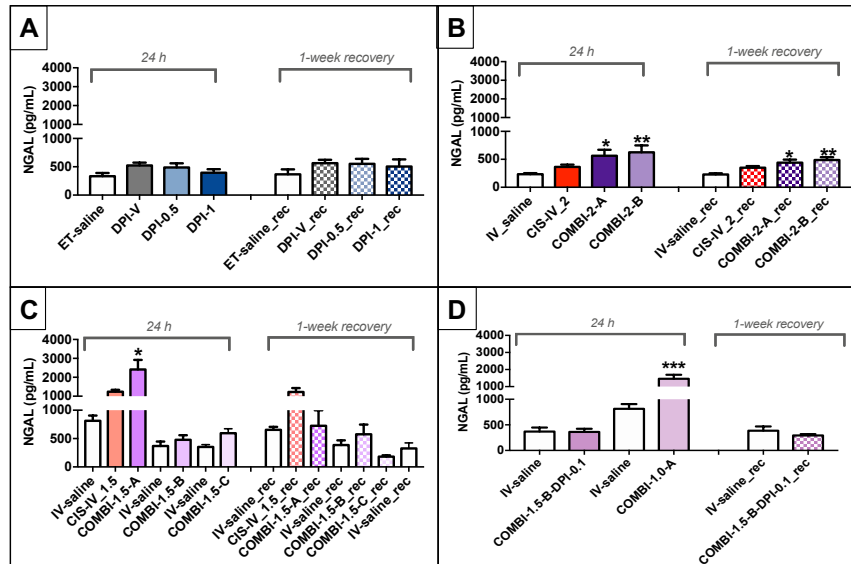
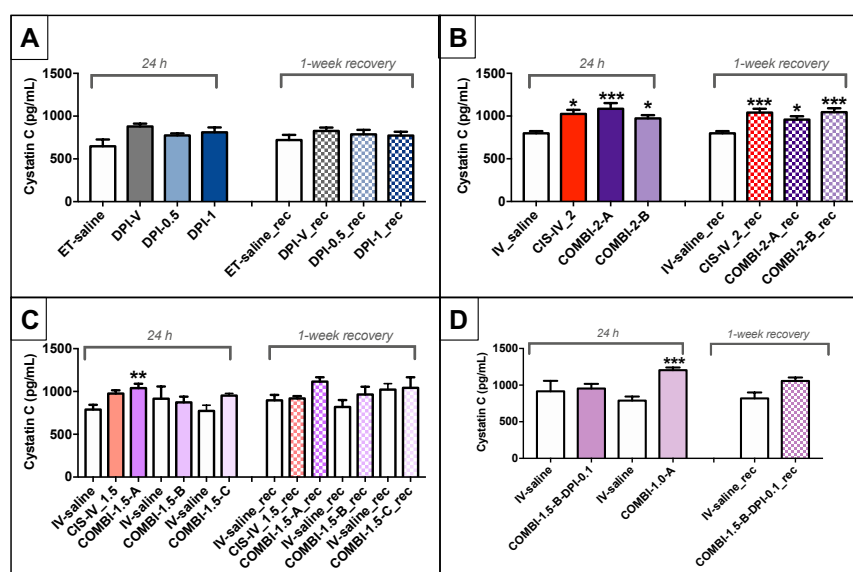

Figure 68: Evaluation of plasma NGAL 24h after the treatment administration and after one week of recovery (_rec). The groups' abbreviations are described in **Figure 55 and Figure 56.** All results are expressed as means ± SEM (n=4-17). The statistical analyses were performed *vs.* the corresponding negative control group using one-way ANOVA and Bonferroni's post-test (*** for $p < 0.001$,** for $p < 0.01$ and * for $p < 0.05$).

Indeed, CIS-IV_2 showed a significant increase in cystatin C and creatinine levels that was not reversible for cystatin C after the one week of recovery, whereas no significance was detected

for CIS-DPI-50 even at its highest dose (i.e. DPI-1). CIS-IV_2 and DPI-1 were compared to their respective negative controls. It is important to mention that high variability is predicted for *in vivo* experiments and that it is crucial to compare each group to its relative negative control. Considering this purpose, the negative control group followed the same scheme of administration and sampling. NGAL concentration was 366 ± 40 pg/mL for CIS-IV_2 and 396 ± 61 pg/mL for DPI-1 *vs.* their respective baselines, 233 ± 20 pg/mL for IV-saline and 335 ± 56 pg/mL for ET-saline.

Figure 69: Evaluation of plasma cystatin C 24h after the treatment administration and after one week of recovery (_rec). The groups' abbreviations are described in **Figure 55 and Figure 56.** All results are expressed as means ± SEM (n=4-17). The statistical analyses were performed *vs.* the corresponding negative control group using one-way ANOVA and Bonferroni's post-test (*** for $p < 0.001$, ** for $p < 0.01$ and * for $p < 0.05$).

Moreover, cystatin C concentration was $1\ 024 \pm 48$ pg/mL for CIS-IV_2 and 812 ± 56 pg/mL for DPI-1 *vs.* their respective baselines, 798 ± 26 pg/mL for IV-saline and 648 ± 79 pg/mL for ET-saline. Finally, creatinine concentration was 0.107 ± 0.005 mg/dL for CIS-IV_2 and 0.097 ± 0.005 mg/dL for DPI-1 *vs.* their respective baselines, 0.075 ± 0.005 pg/mL for IV-saline and 0.081 ± 0.004 pg/mL for ET-saline **(Figure 70)**. This was related to a higher systemic exposure following IV administration when compared to DPI. As plasma concentration peaks are related to renal injury [255], CIS-IV rapidly reached the kidneys. It showed a higher C_{max} than CIS-DPI-50, resulting in AKI. Interestingly, our PK results showed that the C_{max} in plasma for DPI-1 was 0.7 ± 0.6 pg/mL *vs.* 5 ± 2 pg/mL for CIS-IV, at 1.5 mg/kg **(Figure 39)**. Administering a lower dose of a prolonged-release cisplatin-based formulation using the ET route three times per cycle limited cisplatin peak concentration in the proximal tubule and improved its tolerance

by the kidneys. This was observed for a lower cumulative dose and also for a higher dose of CIS-DPI-50 (i.e. DPI-1, three times per cycle for two cycles) when compared to CIS-IV (i.e. CIS-IV_1.5, one time per cycle for a total of three administrations).
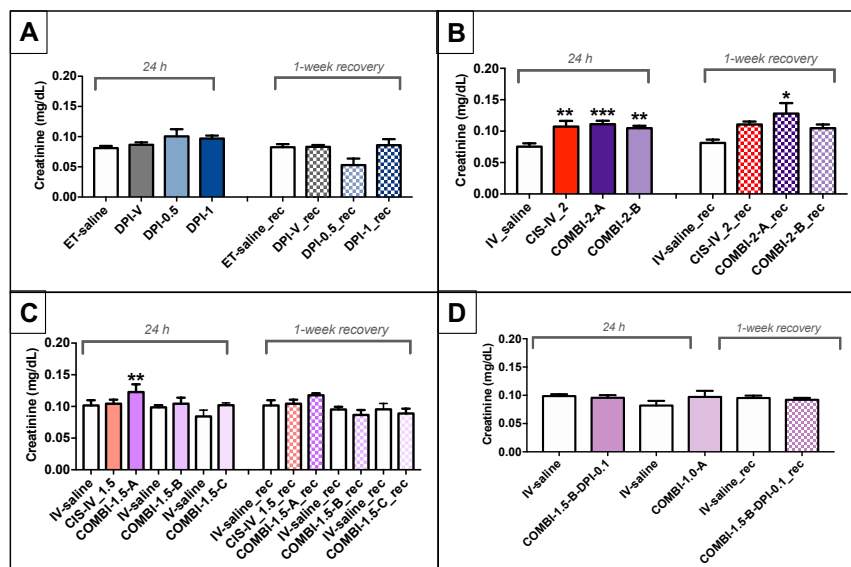

Figure 70: Evaluation of plasma creatinine 24h after the treatment administration and after one week of recovery (_rec). The groups' abbreviations are described in **Figure 55 and Figure 56.** All results are expressed as means ± SEM (n=4-17). The statistical analyses were performed *vs.* the corresponding negative control group using one-way ANOVA and Bonferroni's post-test (*** for $p < 0.001$,** for $p < 0.01$ and * for $p < 0.05$).

NGAL, cystatin C and creatinine showed no major increase following the administration of DPI-V, DPI-0.5 and DPI-1, whether this was done just after the 2-week treatment or after the 1-week recovery ($p > 0.05$). All these biomarkers tended to increase following the administration of CIS-IV_2 **(Figure 68, Figure 69 and Figure 70)**. This increase was significantly different for cystatin C ($p < 0.01$) and creatinine ($p < 0.001$) and was maintained at significant levels during the recovery week for cystatin C.

The 25%-fold reduction in the IV dose (i.e. CIS-IV_1.5) showed lower cystatin C and creatinine levels. CIS-IV_1.5 showed a slight but non-significant increase in NGAL and cystatin C ($p > 0.05$, **Figure 68 and Figure 70**) that was also maintained after 1 week of recovery. Plasma NGAL showed no significant difference when compared to the control groups. Therefore, CIS-IV_1.5 seemed to be better tolerated by the kidneys than CIS-IV_2 and seemed to be preferable to combine with CIS-DPI-50 at 0.5 mg/kg.

3.3.4. Combination evaluation

Levet *et al*. showed that the plasma C_{max} was reached immediately (~ 5 min) after the administration of CIS-IV_1.25 and was 7-fold lower 24h later. This result was correlated to the platinum concentration in the kidneys, which was 5-fold lower 24h following the administration of CIS-IV [203]. Therefore, it was considered that 24h were enough to consider cisplatin as being majorly eliminated. Consequently, mice received CIS-DPI-50 at 0.5 mg/kg either the same day (within 1 hour) or 24h following CIS-IV at 2 mg/kg or 1.5 mg/kg administration (COMBI-2A or B and COMBI-1.5A or B, respectively). In addition, as cisplatin concentration in plasma and kidneys was slightly lower 48h after the administration of CIS-IV_1.25, it was therefore interesting to evaluate a staggering of 48h between CIS-IV at 1.5 mg/kg and CIS-DPI-50 at 0.5 mg/kg (COMBI-1.5-C). Last but not least, a reduced dose of CIS-DPI-50 at 0.1 mg/kg was also selected to be combined with CIS-IV at 1.5 mg/kg with a delay of 24h (COMBI-1.5-B-DPI-0.1) to evaluate the impact of the ET treatment dose on the renal tolerance. Moreover, a reduced dose of CIS-IV at 1.0 mg/kg was also combined the same day to CIS-DPI-50 at 0.5 mg/kg (COMBI-1.0-A) to evaluate the impact of the IV treatment dose on the renal tolerance.

All biomarkers increased significantly when DPI-0.5 and CIS-IV_2 (COMBI-2) were administered the same day (COMBI-2-A; NGAL: $p < 0.05$, cystatin C: $p < 0.001$, creatinine: $p < 0.001$) or with a 24h gap (COMBI-2-B; NGAL: $p < 0.01$, cystatin C: $p < 0.05$, creatinine: $p < 0.01$, **Figure 68, Figure 69 and Figure 70**). These increases were not reversible even after 1 week of recovery. DPI-0.5 was administered when CIS-IV_2 had shown signs of AKI and its addition seemed to increase AKI.

Administering DPI-0.5 and CIS-IV_1.5 the same day (COMBI-1.5-A) increased significantly all the biomarkers (NGAL: $p < 0.05$, cystatin C and creatinine: $p < 0.01$). This increase seemed reversible within 1 week (COMBI-1.5-A_rec). When DPI-0.5 was delivered 24h (COMBI-1.5-B and _rec) or 48h (COMBI-1.5-C and _rec) after CIS-IV_1.5, no significant difference was observed between all the biomarker levels and their negative controls, whether immediately after the treatment or after the 1-week recovery ($p > 0.05$, **Figure 68, Figure 69 and Figure 70**). The similarity between COMBI-1.5-B and COMBI-1.5-C is attributed to the quite similar platinum concentration in plasma and kidneys as shown in the PK study using CIS-IV_1.25 [203].

The co-administration of this reduced dose of CIS-IV (i.e. 1.5 mg/kg) with a 5-fold reduced dose of CIS-DPI-50 at 0.1 mg/kg (i.e. COMBI-1.5-B-DPI-0.1) was considered in this study as

this dose ratio is more likely to be used in clinical studies. COMBI-1.5-B-DPI-0.1 did not induce any increase in any biomarker levels ($p > 0.05$, **Figure 68, Figure 69 and Figure 70**). This demonstrated that the most important parameter for avoiding cumulative nephrotoxicity was the modulation of the IV dose and the staggering of these administrations, as similar NGAL concentrations were reported between COMBI-1.5-B and COMBI-1.5-B-DPI-0.1.

Moreover, to evaluate whether a CIS-IV dose of 50% of the MTD (i.e 1 mg/kg) could have avoided the increase in biomarkers as observed for COMBI-1.5_A, DPI-0.5 was co-administered with CIS-IV at 1 mg/kg, the same day (within 1h). As observed for the groups co-administered within 1h (COMBI-2-A, COMBI-1.5-A), COMBI-1.0-A increased plasma NGAL and cystatin C significantly ($p < 0.001$, **Figure 68, Figure 69 and Figure 70**) and transiently, as no significance difference was observed after 1-week of recovery. This demonstrated that irrespective of the IV dose, the cumulative effect observed was related to the co-administration of CIS-DPI-50 and CIS-IV the same day.

In contrast to observations from the combination of the IV and ET respective MTDs (COMBI-2), the administration of DPI-0.5 the same day as CIS-IV_1.5 increased the C_{max}, resulting in reversible AKI. Therefore, decreasing the IV dose by 25% in the combination (COMBI-1.5) is preferred as the generated AKI seemed reversible after one week of recovery. Moreover, delaying the DPI-0.5 administration to CIS-IV (COMBI-1.5-B) by 24h was enough to prevent any AKI complication.

AKI biomarkers are divided into two categories, those that report on kidney or tubule function, and those that report on damage [137]. Creatinine and cystatin C are considered as functional biomarkers of AKI whereas NGAL is an upregulated protein that occurs during AKI [137]. Cystatin C is a small protein that is freely filtered by the glomerulus, and is almost completely reabsorbed and degraded in the proximal tubule [137,142]. Its increase in plasma reveals a filtration defect [137] as its filtration is performed inefficiently by the kidneys, as a consequence of AKI, and so cystatin C accumulates in plasma. NGAL, as its name indicates, is involved in NT-GRA maturation and renal tubular damage after its release by activated NT-GRA, epithelial cells and kidney tubular cells following cell damage or inflammation [138]. Nevertheless, during NT-GRA activation, its dimeric form prevails whereas in tubular cells the monomeric and heterodimeric forms are produced [137,139]. Many clinical studies have revealed that NGAL remains very low in biological fluids in the steady-state levels and is up-regulated in the case of AKI at an early stage [137,142,143]. In any case, urinary and plasma NGAL has shown similar sensitivity in many studies, which indicates NGAL specificity to kidneys [139].

Nevertheless, as NT-GRA were retrieved in BALF, it was mandatory to verify whether NGAL increases in plasma were attributed to pulmonary NT-GRA increase or to AKI. However, this investigation was a verification because following CIS-IV_2 and CIS-IV_1.5 administration, no significant NT-GRA increase in BALF was observed but NGAL in plasma was higher when compared to the negative groups.

To investigate NGAL increases, NGAL was quantified in BALF. It showed no significant increase in any group, except for ET_LPS ($p < 0.001$). However, NGAL in BALF increased slightly and dose-dependently for ET groups following NT-GRA increase. Moreover, NGAL also increased in some combination groups when compared to their respective IV monotherapies **(Figure 71)**. The differences observed in terms of NGAL levels between COMBI-2 and CIS-IV_2 and between COMBI-1.5-A and CIS-IV_1.5 are attributed to CIS-DPI-50 administration. Indeed, as NT-GRA also increased for the same combination groups, NGAL was therefore released in the lungs **(Figure 62 and Figure 71)**.
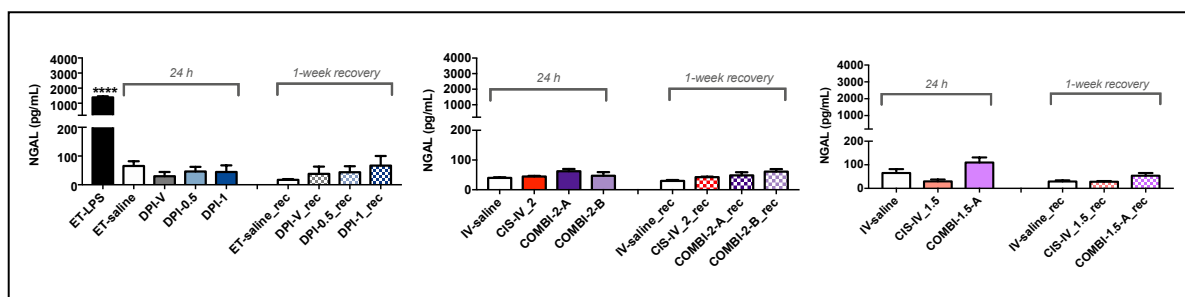
Figure 71: Evaluation of NGAL in BALF 24h after the treatment administration and after one week of recovery (_rec). The groups' abbreviations are described in **Figure 55 and Figure 56.** All results are expressed as means ± SEM (N=4-17). The statistical analyses were performed *vs.* the control groups using one-way ANOVA and Bonferroni's post-test (**** for $p < 0.0001$).

Nevertheless, NGAL levels were more than 40-fold higher in plasma than in BALF. Even if this necessitates further investigation, NGAL in BALF seemed to be correlated to NT-GRA recruitment and may represent an interesting novel marker to detect pulmonary inflammation. To complete the investigation of the specificity of NGAL, a qualitative IHC study was assessed to identify NGAL in the kidneys **(Figure 72)**. The negative control groups (ET-saline and IV-saline) showed no labelling, showing no NGAL in these sections. Following the administration of the IV monotherapies (CIS-IV_2 and CIS-IV_1.5), NGAL was retrieved in the renal cortex and more precisely in the proximal tubules, as described in the literature [137,139,144]. Brown staining was only detected in the tubule proximal area, and not in the glomeruli **(Figure 72)**.

All combination groups showed that NGAL was concentrated in proximal tubules and seemed to be more intense for the groups that were exposed to CIS-DPI-50 and CIS-IV on the same day (COMBI-2-A and COMBI-1.5-A). These results supported what was observed for NGAL quantification in plasma **(Figure 68)**. Consequently, plasma NGAL was a good biomarker of AKI, as widely described in the literature [136–138,144,279].
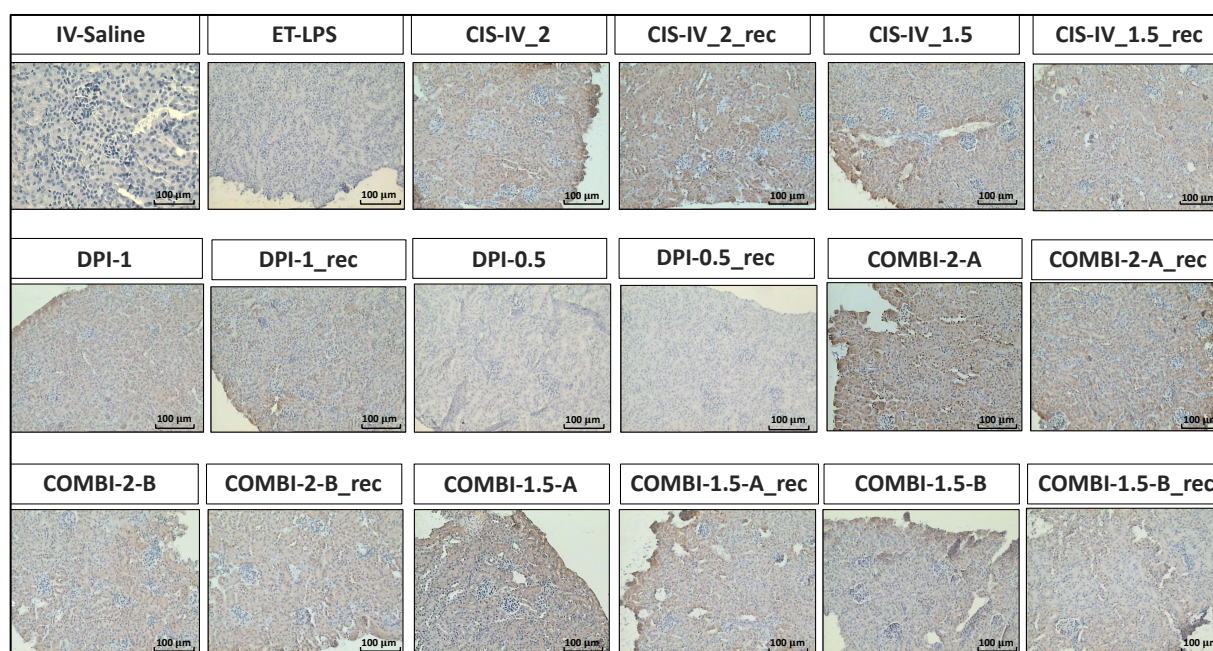

Figure 72: NGAL immuno-stained kidney sections of mice (magnification 100 x). The groups' abbreviations are described in **Figure 55 and Figure 56.**

Moreover, it is important to mention that the selected biomarkers tended to describe the same trends for all the groups, as no major difference between NGAL, cystatin C and creatinine was noticed. This increased the reliability of our mouse model in terms of selected biomarkers and suitable sampling timing. Plasma NGAL and cystatin C therefore seemed to be as reliable as plasma creatinine could be. Nevertheless, the novel biomarkers seem to be more sensitive to primitive injuries, as demonstrated for COMBI-1.0_A, CIS-IV_2_rec and COMBI-2-B_rec.
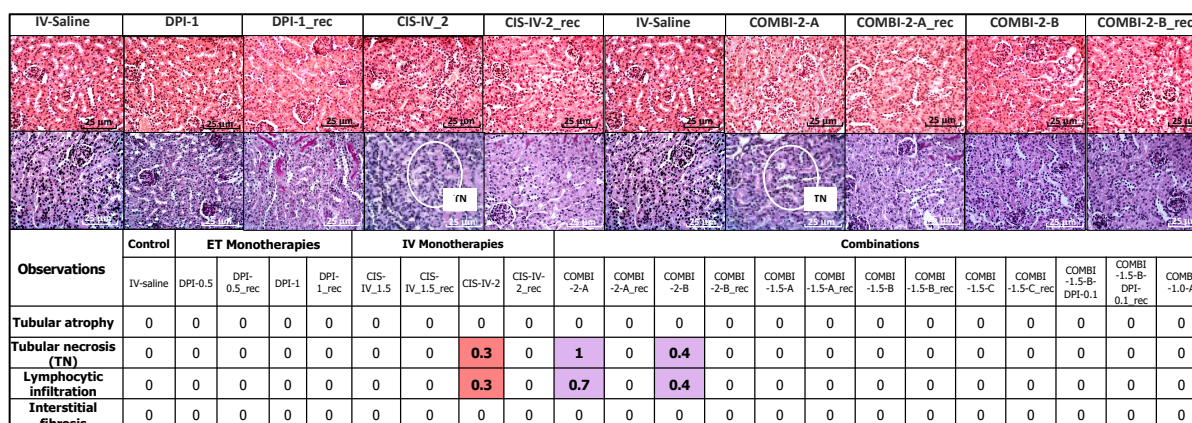
In these groups (CIS-IV_2, COMBI-2-A, COMBI-2-B, COMBI-1.5-A, COMBI-1.0_A), NGAL, cystatin C and creatinine levels significantly increased, suggesting a severe AKI complication compared to the other groups (ET groups, CIS-IV_1.5, COMBI-1.5-B, COMBI-1.5-C, COMBI-1.5-B-DPI-0.1). This result could be related to high concentrations of cisplatin and its metabolites (monoaquacisplatin: $[Pt(NH_3)_2Cl(OH_2)]^+$, and diaquacisplatin: $[Pt(NH_3)_2(OH_2)_2]^{2+}$) in the proximal tubular epithelium, as summarized in **Figure 13**. These metabolites are able to interact with the negatively charged DNA, leading to an increased ROS.

Moreover, they are also able to directly trigger ROS as they can react with GSH, with the mitochondrial respiratory chain and with cytochrome 450 microsome [125,128]. Moreover, they induce several chemokines and cytokines to promote: *(i)* inflammation driven by leukocytes leading to NGAL increase; and/or *(ii)* alteration of specific cytoplasmic structures [125,128,132]. An overall consequence of these observations is the apoptosis of proximal tubules cells leading to a dramatic filtration decrease, reflected by an increased plasma cystatin C level, confirming the occurrence of AKI [132].

3.3.5. Histopathological analyses

Following the analyses of HE and PAS staining of kidney sections, no major kidney injury was observed following the administration of the ET and IV monotherapies or the combination groups **(Figure 73)**. A light tubular necrosis and lymphocytic infiltration were scored at 0.3/5 for CIS-IV_2. Moreover, the administration of CIS-DPI-50 and CIS-IV at their MTD (COMBI-2) seemed to induce a transient tubular necrosis and lymphocytic infiltration, which were greater for COMBI-2-A than COMBI-2-B. These observations seemed to identify slight and transient tubular necrosis and inflammation for the highly dosed IV monotherapy as well as its combination with CIS-DPI-50. However, the tubular necrosis damage that was identified was described as "a rare single necrotic tubule", and the lymphocytic infiltration as "a few scattered cells" and did not seem significant. As already explained above for pulmonary histology, biomarker quantification seems to be more sensitive in detecting injury than histology can be.

Observations	Control	ET Monotherapies				IV Monotherapies				Combinations												
	IV-saline	DPI-0.5	DPI-0.5_rec	DPI-1	DPI-1_rec	CIS-IV_1.5	CIS-IV_1.5_rec	CIS-IV-2	CIS-IV-2_rec	COMBI-2-A	COMBI-2-A_rec	COMBI-2-B	COMBI-2-B_rec	COMBI-1.5-A	COMBI-1.5-A_rec	COMBI-1.5-B	COMBI-1.5-B_rec	COMBI-1.5-C	COMBI-1.5-C_rec	COMBI-1.5-B-DPI-0.1	COMBI-1.5-B-DPI-0.1_rec	COMBI-1.0-A
Tubular atrophy	0	0	0	0	0	0	0	0	0	0	0	0	0	0	0	0	0	0	0	0	0	0
Tubular necrosis (TN)	0	0	0	0	0	0	0	0.3	0	1	0	0.4	0	0	0	0	0	0	0	0	0	0
Lymphocytic infiltration	0	0	0	0	0	0	0	0.3	0	0.7	0	0.4	0	0	0	0	0	0	0	0	0	0
Interstitial fibrosis	0	0	0	0	0	0	0	0	0	0	0	0	0	0	0	0	0	0	0	0	0	0

Figure 73: Representative renal tissue histological analyses (magnification 400 x) from mice exposed to the most drastic conditions from monotherapies and combinations in terms of cisplatin nephrotoxicity and the corresponding negative control group IV-saline and summary of semi-quantitative score of tubulo-interstitial lesions. The groups' abbreviations are described in **Figure 55 and Figure 56.**

3.4. Conclusions for pulmonary and renal tolerance

In conclusion, DPI-V, DPI-0.5 and DPI-1 showed a good pulmonary and renal tolerance as they did not increase significantly any local or systemic biomarker. Nevertheless, DPI-0.5 and DPI-1 (3 times per cycle for two cycles) increased the NT-GRA proportion transiently, showing that a local inflammation was being initiated. However, DPI-0.5 remains the MTD to use in combination to IV as the bw does not decrease below 5%. CIS-IV_1.5 and CIS-IV_2 were less well-tolerated than DPI as they increased dose-dependently both pulmonary and AKI biomarkers. Adding DPI-0.5 to CIS-IV_2 decreased the pulmonary tolerance (i.e. cytokine levels, NT-GRA proportion and cytotoxicity) and increased AKI induced by CIS-IV_2 alone. Therefore, this combination cannot be used for further efficacy study. When the total IV dose was decreased to 25% in the combination therapy, pulmonary tolerance remained acceptable as no additional pulmonary damage was observed when compared to CIS-IV_1.5, except for a transient NT-GRA increase, as observed following DPI-0.5. However, the kidneys were still damaged under this regimen. Staggering the DPI administration to IV administration by 24h seemed to be enough to prevent renal damage. Therefore, COMBI-1.5-B seems to be the best regimen to be evaluated during efficacy studies.

3.5. Efficacy evaluation on the M109-HiFR-*Luc2* lung carcinoma orthotopic model in mice

To evaluate the added value of CIS-DPI-50 when combined with a conventional cisplatin based-chemotherapy, the conventional platinum doublet commonly used in clinics for NSCLC treatment was chosen. This doublet was based on cisplatin and paclitaxel. For this study, three groups were compared: the untreated negative control group, the IV platinum doublet used at the MTD (i.e. cisplatin at 1.5 mg/kg and paclitaxel at 10 mg/kg ([280])), and the combination of CIS-DPI-50 at 0.5 mg/kg with the platinum doublet IV solution at the MTD. The scheme of administration for each of them followed the rationale previously explained, with a delay of 24h between the IV doublet solution administration once a week and the ET CIS-DPI-50 three times a week, both for two consecutive cycles (i.e. COMBI-1.5-B) **(Figure 57)**. The efficacy investigation was performed in terms of tumour growth (according to the BLI values) and survival rates *vs.* time.

Tumour growth results indicated an exponential increase in untreated control mice **(Figure 74.A and B)** with a steep slope showing the aggressiveness of the M109-HiFR-*Luc2* lung

carcinoma model. Significant reduction in tumour growth was observed with the IV platinum doublet as from D21 ($p < 0.001$, two-way ANOVA), confirming the responsiveness of the M109-HiFR-*Luc2* to chemotherapy. The tumour growth tended to be lower in the CIS-DPI-50 combination group compared to the IV platinum doublet **(Figure 74)**, although no significant difference was found ($p > 0.05$). The antitumour response to the combination was more rapid than with the IV platinum doublet. Indeed, for the combination, the tumour growth slope become negative from D10 and was maintained up to D20 whereas this was only observed 7 days later (i.e. from D17 up to D20) for the IV platinum doublet **(Figure 74)**. Furthermore, according to the curve profiles, treatment with the combination group tended to demonstrate slower tumour re-growth than with the IV platinum doublet **(Figure 74.D)**.
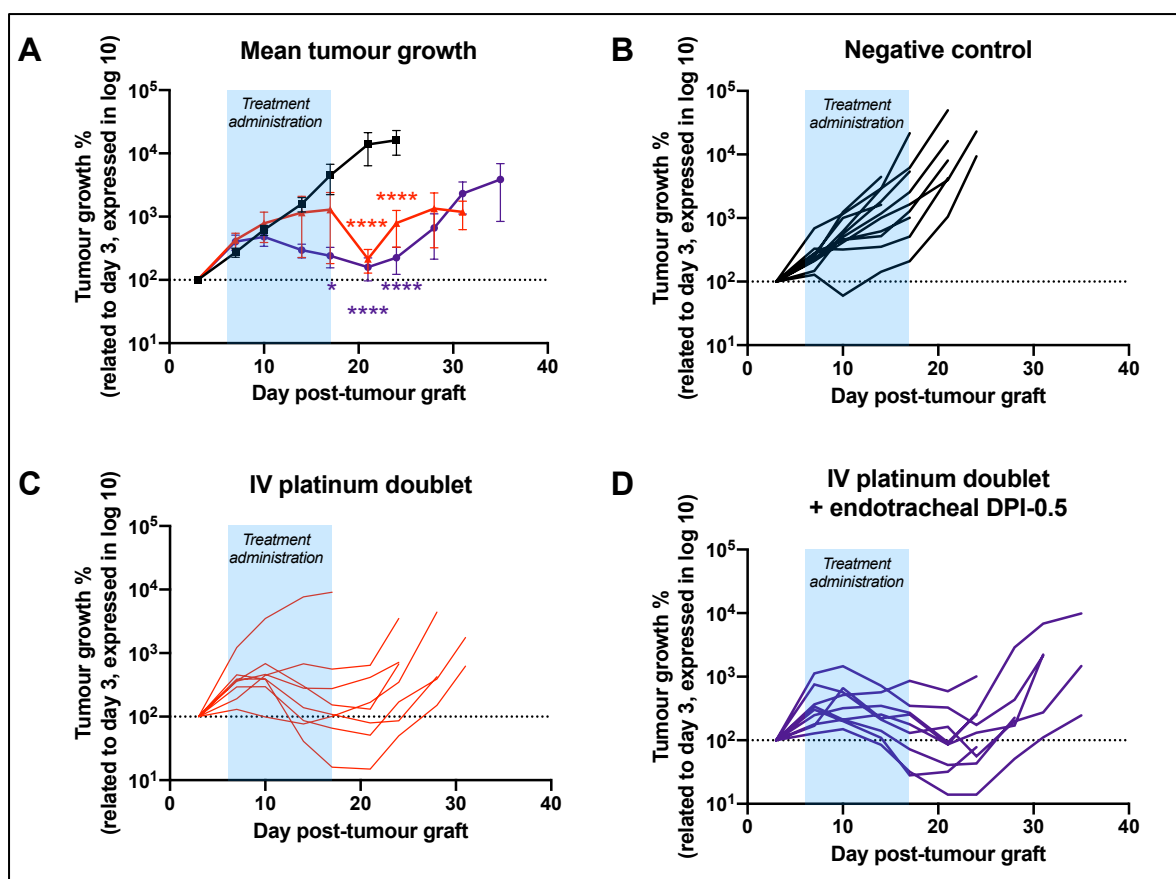
Figure 74: Tumour growth according to BLI and expressed as the mean ± SEM (A) and per subject of the negative control group (B, n=11), the group treated with IV platinum doublet (C, n=8), and the combination of DPI-0.5 and IV platinum doublet (D, n=9) following the regimen described in **Figure 57**. * $p < 0.05$, **** $p < 0.0001$ between the negative control and either the IV platinum group groups (red asterisks) or the combination group (purple asterisks). No significant difference was found between the IV platinum group groups and the combination group ($p > 0.05$, two-way ANOVA with Tukey-multiple comparison test).

A responder was defined as a mouse with tumour growth < 150% in comparison to the 100% value measured at D3. As reported in the previous efficacy study, the 10% of responders in the

negative control group corresponded to the mice for which the tumour mass had not yet achieved 150%, in the first days after graft. This was normalized after the treatment administration, as observed previously. As anticipated, mice treated with the IV platinum doublet controlled the tumour growth, as 50% of them (4/8) responded to the doublet **(Figure 75)**. The addition of CIS-DPI-50 to IV platinum doublet tended to increase the peak responder rate to 67% (6/9). As demonstrated in **Figure 75**, a peak in terms of the percentage of responders was observed for the combination group. Moreover, the response tended to be more sustained in the combination group *vs.* the IV platinum doublet, with a shift of the % responders curves to the right **(Figure 75)**.
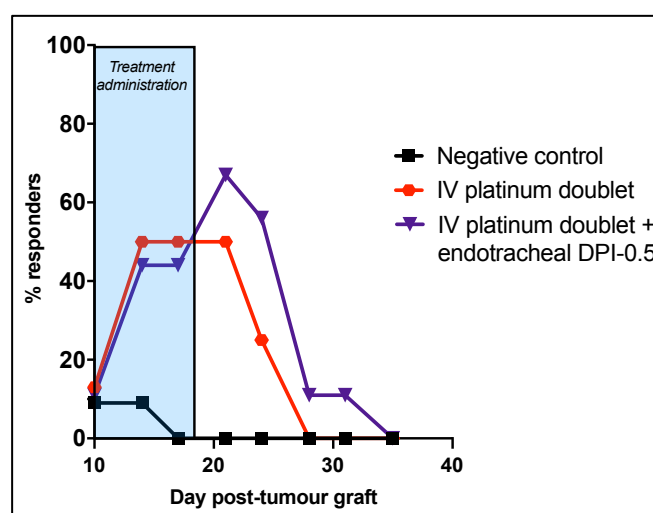
Figure 75: Response rate *vs.* time. A responder was defined as having tumour growth values < 150% in comparison to the 100% value measured at day 3. Mice were left untreated (negative control, n=11), treated with the IV platinum doublet (n=8), or with the combination of CIS-DPI-50 and the IV platinum doublet (n=9) following the regimen described in **Figure 57**.

In addition, a survival analysis was performed to assess the treatment effectiveness in terms of survival rates in days post-tumour engraftment. This analysis matched the tumour growth. It must be noted that six mice from the combination group died immediately following the ET administration and are not included in the survival analysis, as already observed for this type of procedure in animal studies [192,205]. Indeed, as previously mentioned, the ET technique of administration is cumbersome as it requires anaesthesia, ET intubation, and the delivery of repeated puffs of air tidal volume per administration to deliver the powder. Moreover, these mice are more weakened than healthy mice as they bear tumours and experience up to six repeated ET administrations.

The median survival times were significantly prolonged by 5 days following the IV platinum doublet when compared to the negative control (26 *vs.* 21 days, $p < 0.01$, log-rank test, **Figure 76**). The combination of CIS-DPI-50 and IV platinum doublet prolonged the median survival significantly by 10 days when compared to the negative control group ($p < 0.0001$). However, although the survival was increased by 5 more days (26 *vs.* 31 days) for the combination group in comparison with the IV platinum doublet, no significant difference was noticed between these two treated groups ($p = 0.1$, **Figure 76**). This could be explained by the rapid tumour re-growth once the treatment was stopped **(Figure 74)** leading to a limited differentiation of the two survival curves.
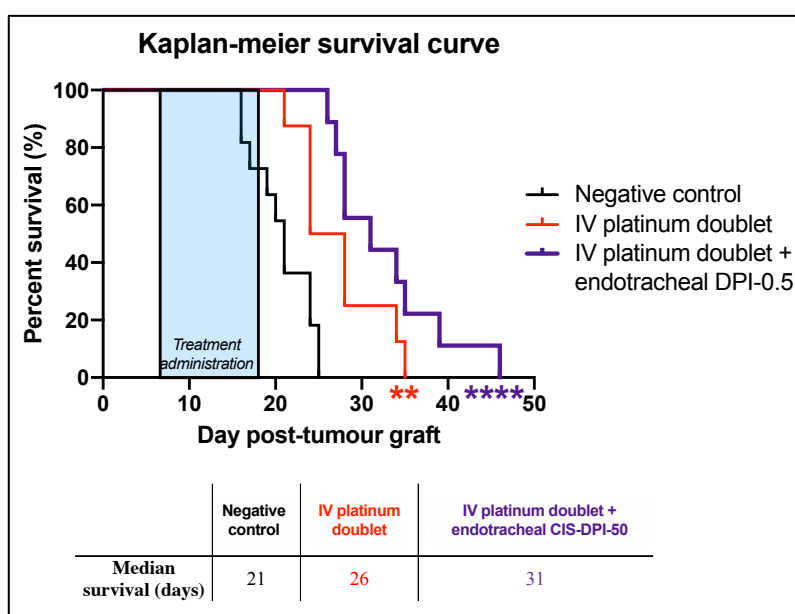
Figure 76: Kaplan-Meier survival curves and median survivals of M109-HiFR-*Luc2* mice. Mice were left untreated (negative control, n=11), treated with the IV platinum doublet (n=8), or with the combination of CIS-DPI-50 and the IV platinum doublet (n=9) following the regimen described in **Figure 57**. **** $p < 0.0001$ and **$p < 0.01$ between the group and the negative control (log-rank test).

It was therefore interesting to analyse the number of mice alive at specific days. At 24 days following the graft, all the negative control groups had died, whereas 62% (5/8) of mice among the IV platinum doublet group were alive and 100% (9/9) of the combination IV platinum doublet and CIS-DPI-50 group were still alive. On D28, 25% (2/8) of the mice were alive following the administration of the IV platinum doublet whereas 50% (4/8) were still alive among the mice treated with the combination. This led to a 20% increase in terms of the median survival rate when compared to the IV conventional treatment.

Taking all these results together, adding CIS-DPI-50 to the conventional platinum doublet chemotherapy tended to increase the response rate, helped to better control the tumour growth, and favoured a prolonged survival rate. These results were in line with results previously described for NSCLC patients, for whom an increased treatment effectiveness in terms of tumour size reduction, survival, and recurrence of the disease was correlated to higher platinum concentrations [204]. Moreover, the study conducted in NSCLC patients by Zarogoulidis *et al.* on inhaled carboplatin demonstrated a statistically significantly higher survival for the group that received inhaled carboplatin and the conventional IV doublet in comparison to the conventional IV doublet alone [79]. As previously described, this would be related to a higher concentration of the chemotherapeutic agent in the tumour site, lymph nodes, and systemic circulation [176]. This hypothesis was demonstrated in *Experimental part II-section 3.2.3*, as the platinum concentration in the tumour 2h following the single administration of a 4-fold lower dose of CIS-DPI-50 was more than 7-fold higher than CIS-IV_2 ($p < 0.05$, **Figure 50.B**). This difference was maintained following repeated administrations of CIS-DPI-50 over one cycle **(Figure 50.B)**. These trends confirmed that the promising strategy of adding a loco-regionalized treatment during the off-cycles to conventional IV chemotherapy favours a reduction in the increase of the tumour and improves the median survival rates. This was despite the limitations of the preclinical investigation in mice regarding the CIS-DPI-50 ET administration procedure and the model aggressiveness, which both made it not possible to investigate the real impact of the probable frequency of CIS-DPI-50 treatment administrations as it will be the in human patients (potential daily CIS-DPI-50 administration for 3-4 weeks *vs.* a single administration for CIS-IV per cycle).

4. <u>Conclusion</u>

Administering a cisplatin-based controlled-release DPI formulation following a 2-week regimen was overall well-tolerated by the lungs except for a transitory NT-GRA increase. None of the renal biomarkers increased significantly. Administering cisplatin using IV at its MTD increased both the pulmonary pro-inflammatory cytokines and the renal biomarkers, resulting in both renal and pulmonary damage. Therefore, flattening the pulmonary and plasmatic peaks by developing a controlled-release DPI to deliver cisplatin enhanced both pulmonary and renal tolerance compared to IV.

Regimens were optimized to find the highest drug dosage with least-spaced administrations while maintaining pulmonary and renal tolerance. The pulmonary and renal tolerance were

impaired as soon as CIS-DPI-50 and CIS-IV were administered at their respective MTDs. Fractionating the total dose between IV and DPI (i.e. decreasing the IV dose by 25%) was a good strategy to improve lung tolerance and to hinder any AKI complication. Staggering the DPI administration from IV administration by 24h was enough to prevent any signs of AKI, as no difference was observed with a staggering of 48h. This regimen (i.e. CIS-DPI-50 at 0.5 mg/kg administered 24h after CIS-IV_1.5) was therefore selected to assess efficacy in a mouse lung carcinoma model. Avoiding cumulative toxicities for this combination was challenging as the DLT of cisplatin is cumulative and irreversible nephrotoxicity due to saturable concentration mechanisms. This approach was taken to be able to evaluate the feasibility of its administration as a locoregional treatment during chemotherapy off-cycles, without decreasing systemic tolerance as these off-cycles are applied to allow normal tissue to recover. This combined regimen showed positive trends in the efficacy study on the aggressive M109-HiFR-*Luc2* lung carcinoma orthotopic model, with decreased tumour growth and recurrence of the disease resulting in an increased survival rate. Therefore, the selected cisplatin-based DPI formulation could be proposed as an add-on treatment to intensify the therapeutic response of cisplatin-based doublets in lung cancer therapy.

As the combination between CIS-DPI-50 and CIS-IV necessitated several adaptations to avoid nephrotoxicity (reduced CIS-IV dose, staggering between CIS-DPI-50 and CIS-IV administrations), which would have limited the potential of CIS-DPI-50, the next step was the evaluation of the feasibility of combining CIS-DPI-50 with a less nephrotoxic drug (i.e carboplatin). Indeed, it is anticipated that when using carboplatin, it is probable that fewer adaptations would be needed. Moreover, considering carboplatin-specific toxicities (i.e. haematological toxicity), and as carboplatin is intended to be combined to another cytotoxic drug (i.e. in platinum-based chemotherapy) characterized by the same DLT, it was interesting to further investigate both carboplatin and paclitaxel cumulative haematological toxicities in combination with CIS-DPI-50. This was done following different regimens in the last part of this experimental work.

Part IV: Evaluation of the tolerance of the combination of CIS-DPI-50 and IV carboplatin-based platinum doublet

These results are published in

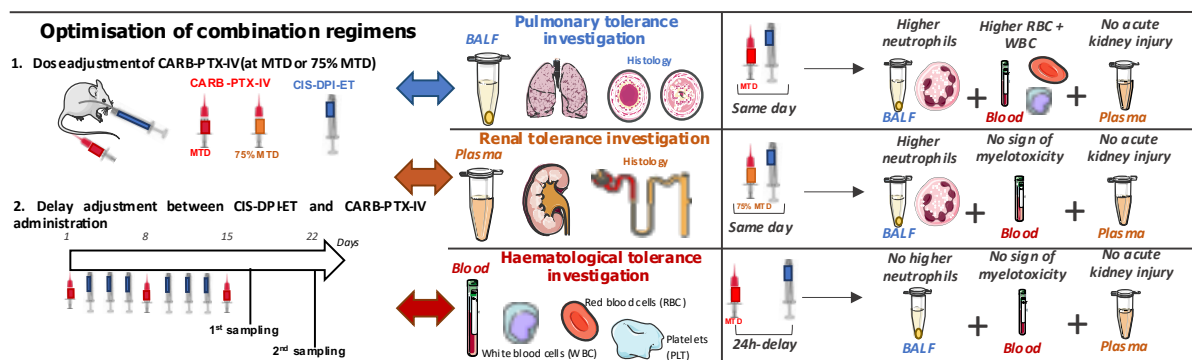the *Journal of Biomedicine and Pharmacotherapy*

Figure 77: Graphical abstract of the fourth experimental part.

1. <u>Introduction and aims</u>

CIS-DPI-50 was formulated to deliver cisplatin slowly and to expose the lungs (and therefore the tumour) to cytotoxic drug for several hours, as demonstrated in healthy and grafted mice in *Experimental parts I and II*. The tumour exposure to cisplatin was maintained following several administrations of CIS-DPI-50, demonstrating the added value of these repetitions. As described in *Experimental part III*, the main limitation related to the combination of both these routes of administration (ET and IV) was lung and renal tolerance. It was mandatory to decrease the CIS-IV MTD by 25% and to stagger ET from IV administrations by 24h to avoid additional pulmonary and renal injury. Nevertheless, even considering these adaptations (decreased IV dose and administration delay), the selected regimen tended to demonstrate a therapeutic intensification in the M109-HiFR-*Luc2* lung carcinoma orthotopic model in mice. However, these adaptations could have decreased the full therapeutic potential of this combination strategy.

As it is widely known that carboplatin is better tolerated by the kidneys than cisplatin [152], it was therefore interesting to evaluate the possibility of combining CIS-DPI-50 (ET route) with carboplatin-paclitaxel (CARB-PTX) (IV route), the same day at their MTDs. However, clinical studies have demonstrated increased leucopoenia and thrombocytopenia when cisplatin and carboplatin were administered together using the IV route [281,282].

Moreover, it is important to mention that as for carboplatin, a paclitaxel DLT is also myelosuppression and more precisely neutropenia, as represented in **Figure 12**. Moreover, pulmonary hypertensive reactions have been associated with both carboplatin (e.g. bronchospasm) and paclitaxel (e.g. pneumonia and hypersensitivity pneumonitis), when they were administered alone [77]. Consequently, it was crucial to consider the tolerance of the whole CARB-PTX IV doublet (i.e. not carboplatin alone) when combined with CIS-DPI-50.

Therefore the aim of this study was to *(i)* evaluate pulmonary, renal and haematological tolerance of the combination of CIS-DPI-50 and CARB-PTX and *(ii)* optimize their combinations in terms of doses and regimen. To the best of our knowledge, the combination of cisplatin using the ET route and carboplatin using the IV route has not yet been reported.

2. <u>Materials and methods</u>

2.1. Materials

Carboplatin was purchased from Umicore (Pilar, Argentina). All other materials used in this part are detailed in *Experimental part III-section 2.1*.

2.2. *In vivo* toxicity studies

Female 6-week-old BALB/cAnNRj mice (16-18 g) were purchased from Janvier Labs (Le Genest-Saint-Isle, France) and Charles River (Écully, France). All experiments and manipulations were approved by the CEBEA of the faculty of medicine (ULB) under approval number 585N (toxicity studies). During the MTD evaluation, mice were weighed up to five times per week. However, all housing conditions were identical to those described in *Experimental part I-section 2.3.3.1*.

2.3. Formulation and administration for *in vivo* experiments

2.3.1. CIS-DPI-50 blend

To deliver CIS-DPI-50 at 0.5 mg/kg to mice, CIS-DPI-50 was produced as described in *Experimental part I-section 2.4.1*. In this study, CIS-DPI-50 was weighed and diluted at 1% (w/w) in the spray-dried mannitol/leucine 10:1 diluent. The uniformity of cisplatin content was satisfactory, with a coefficient of variation below 5% (i.e. $1.12 \pm 0.03\%$ (CV% 3%), n=10). The *in vivo* administration of the CIS-DPI-50 blend by the ET route was performed as described in *Experimental part II-section 2.4*.

2.3.2. CARB-PTX solution

Carboplatin solution was prepared at 5 mg/mL in saline (0.9% NaCl) and diluted using the same vehicle at the appropriate concentration (i.e. 0.8 mg/mL for a dose of 8 mg/kg, 1.6 mg/mL for a dose of 17 mg/kg, 2.4 mg/mL for a dose of 25 mg/kg, 3.0 mg/mL for a dose of 34 mg/kg, 3.8 mg/mL for a dose of 42 mg/kg and 4.6 mg/mL for a dose of 51 mg/kg). This solution was kept protected from light, at 4°C, for maximum 3 days. Paclitaxel solution was prepared at 6 mg/mL using a mixture of Cremophor El® and absolute ethanol (50:50 v/v) and diluted in saline at the appropriate concentration (i.e. 0.5 mg/mL for a dose of 5 mg/kg, 1.0 mg/mL for a dose of 10 mg/kg, 1.4 mg/mL for a dose of 15 mg/kg, 1.8 mg/mL for a dose of 20 mg/kg, 2.2 mg/mL for a dose of 25 mg/kg and 2.7 mg/mL for a dose of 30 mg/kg). CARB-PTX solution was prepared immediately before use and renewed each day. The IV-vehicle group received the same

proportion of each excipient as in the MTD dose, which corresponded to 83.3% (v/v) saline, 8.3% (v/v) Cremophor EL® and 8.3% (v/v) ethanol absolute. The *in vivo* administration of CARB-PTX solution or vehicle was done by the IV route (tail vein).

2.4. Regimen administration

2.4.1. Carboplatin/paclitaxel ratio

To be closest to clinical practice, doses were based on the ratio of carboplatin and paclitaxel human doses recommended for lung cancer patients with no comorbidities (paclitaxel: 200 mg/m², carboplatin: AUC 6 mg/mL x min) [24]. For this purpose, the carboplatin dose was calculated using the Calvert formula, which involves different factors such as the patient sex, age, serum creatinine and weight [283]. In this study, it was interesting to determine this dose for a normal patient with no comorbidities as the study was conducted on healthy mice. Thus this corresponded to the maximum carboplatin dose that can be administered.

The patient's age was fixed at 71 years old as this is the median age for lung cancer patients [11]. The serum creatinine levels were considered to be in the normal ranges, 0.72-1.18 mg/dL for males and 0.55-1.02 mg/dL for females, as described by Ceriotti *et al.* [284]. The corresponding doses were calculated based on a bw of 60 kg. The carboplatin doses were expressed as mg/kg and their mean was calculated (9 mg/kg). The paclitaxel dose expressed in mg/m² (200 mg/m²) was converted to mg/kg as described by Reagan *et al.* [285], and was fixed at 5.4 mg/kg. The related CARB/PTX ratio was therefore calculated (9.1/5.4) and set at about 1.7. This ratio between the carboplatin and paclitaxel doses was maintained during the MTD investigation study on mice.

2.4.2. Maximum tolerated dose determination

The MTD of CARB-PTX IV was defined, as previously, as the highest dose at which mean bw loss did not exceed 5% w/w for any of the three tested animals for the whole of the applied regimen and for 28 days following the first dosing. This limit of 5% is a good threshold as *(i)* this treatment is intended to be combined to another treatment (i.e. DPI-0.5) and as, *(ii)* a bw decrease of less than 10% w/w was observed for combinations (i.e. CIS-DPI-ET and CIS IV) in which each monotherapy dose was selected with a threshold of 5% w/w, as demonstrated in *Experimental part III-section 3.1*. Six groups of three female 6-week old BALB/cAnNRj mice were administered CARB-PTX solution using the IV route the first day of each week for 3 consecutive weeks (days 1, 8 and 15) at 8-5 mg/kg (dose 1), 17-10 mg/kg (dose 2), 25-15 mg/kg (dose 3), 34-20 mg/kg (dose 4), 42-25 mg/kg (dose 5) and 51-30 mg/kg (dose 6) for carboplatin

and paclitaxel respectively. These groups were compared to the negative control group (IV-vehicle).

2.4.3. Administration of IV doublets, CIS-DPI-50 and control groups

CARB-PTX was administered as an IV doublet at its MTD (i.e. IV-CARB-PTX; 1.7 mg/mL for carboplatin and 1.0 mg/mL for paclitaxel) and at 75% of the MTD dose (i.e. CARB-PTX-0.75: 1.3 mg/mL for carboplatin and 0.75 mg/mL for paclitaxel) to healthy female 6-week old BALB/cAnNRj mice and was compared to the vehicle (i.e. IV-vehicle). IV-CARB-PTX (n=16), IV-CARB-PTX-0.75 (n=16) and IV-vehicle (n=24) were administered by IV following the regimen described for MTD determination (D1, D8 and D15) **(Figure 78.A)**.
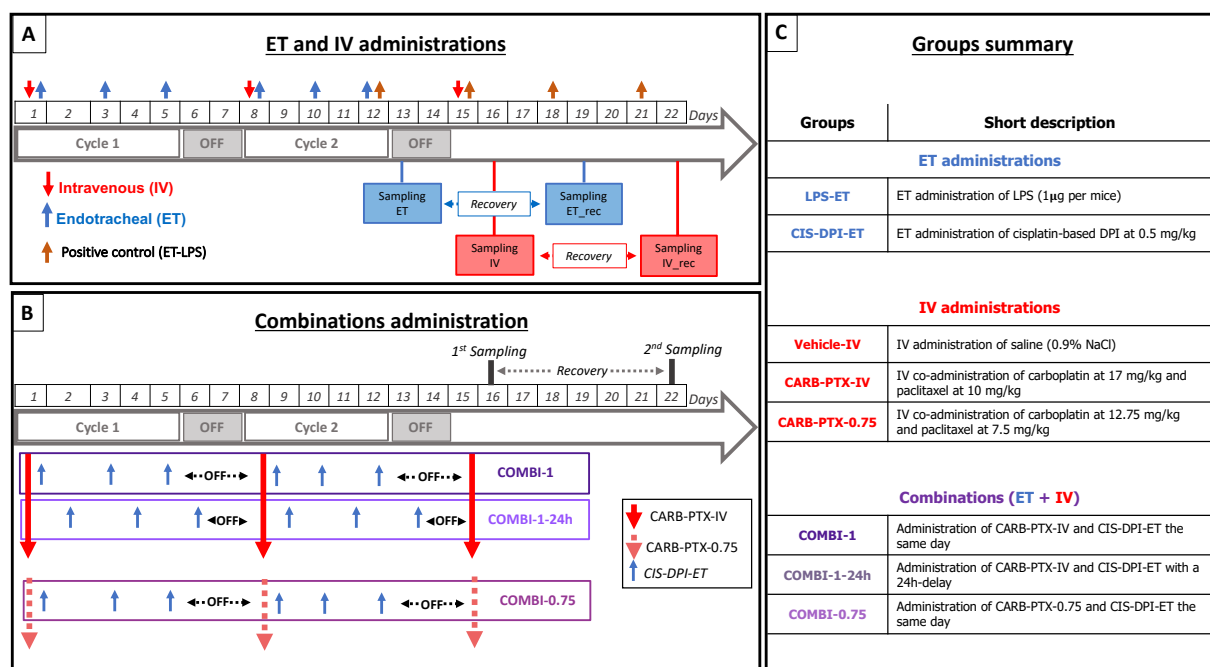
Figure 78: Scheme of administration of ET and IV doublets treatments (A) and their combinations (B) and sampling procedures 24h after the treatment administration and one week later (_rec) for all groups (C).

DPI-0.5 at its MTD, as determined in *Experimental part III-section 3.1* (i.e. 0.5 mg/kg) (n=30) was administered using the ET route three times per week for 2 consecutive weeks (D1, D3, D5, D8, D10, D12) **(Figure 78.A)**. The positive control group, ET-LPS (n=21), was administered as described in *Experimental part III-section 2.3.1.2*. Samples from both the positive (ET-LPS) and the negative control (IV-vehicle) groups were collected each sampling day (n=3). Samples from each type of control group were then pooled together and annotated with their group name, if sampled 24h after the last administration, or annotated with the suffix

'_rec' to their group name if sampled after one week of recovery, to evaluate myelotoxicity and pulmonary and renal toxicities and their reversibility.

2.4.4. Combination administration

Once IV-CARB-PTX, IV-CARB-PTX-0.75 and DPI-0.5 were evaluated separately, they were combined following three different regimens **(Figure 78.B)**. This was done to evaluate the input of a reduced IV dose or delayed days of administration, in case of cumulative toxicities. The first regimen (COMBI-1) (n=28) combined IV-CARB-PTX (i.e. administered on days 1, 8, 15) and DPI-0.5 administered three times a cycle, starting at D1 (i.e. days 1, 3, 5, 8, 10, 12). The second regimen (COMBI-1-24h) (n=29) combined IV-CARB-PTX (days 1, 8, 15) and DPI-0.5, administered 24h later than in the first regimen (i.e. on days 2, 4, 6, 9, 11, 13). The third regimen (COMBI-0.75) (n=26) combined the administration of CARB-PTX- 0.75 (i.e. on days 1, 8, 15) and DPI-0.5, three times a cycle starting the same day (i.e. days 1, 3, 5, 8, 10, 12). In COMBI-1 and COMBI-0.75, ET administrations on D1 and D8 were performed maximum one hour after the IV administrations. The myelotoxicity and pulmonary and renal toxicities were assessed 24h after the last administration (group name annotation) and after one week of recovery (group name with '_rec' suffix annotation).

2.5. Pulmonary tolerance evaluation

To evaluate the pulmonary tolerance, both inflammation and cytotoxicity were investigated as described in *Experimental part III-section 2.3.2.*

2.6. Renal tolerance evaluation

To evaluate the renal tolerance, blood sampling, kidney collection and AKI biomarkers analysis were assessed as described in *Experimental part III-section 2.3.3.*

2.7. Myelosuppression evaluation

Three to four drops of blood were collected by retro-orbital puncture in Minicollect® K3EDTA tubes (Greiner Bio-One, Vilvoorde, Belgium). Tubes were immediately gently inverted manually before being put in an automated rotary mixer to gently invert the tubes for 15 minutes. They were immediately placed at 4°C until analysis, which was performed a maximum of 4h following the sampling.

To evaluate myelotoxicity, the total count of RBC and white blood cell (WBC), including basophils and NT-GRA, EOS, LYM and MON, was evaluated, as well as each WBC type proportion among all WBC. Haemoglobin (Hb), haematocrit (Ht), mean corpuscular volume (MCV), mean cell haemoglobin (MCH), mean corpuscular haemoglobin concentration (MCHC), and red cell distribution width (RDW) were also determined. The total PLT count as well as the mean platelet volume (MPV) were investigated. All these parameters were determined using a haemocytometer (Scil Vet abc Plus+®, Altorf, France) [286].

2.8. Statistical analyses

All statistical tests were assessed using GraphPad PRISM® (7.0a) software. One-way ANOVA and the Bonferroni's post-hoc test were selected to compare myelotoxicity parameters (total and differential WBC count, Ht, Hb, MCV, MCH, MCHC, RDW, PLT and MPV), the toxicity biomarkers (NGAL, creatinine, cystatin C, IL-6, TNF-α, IL-1β, CXCL1, CXL2, protein content and LDH ratio) and the differential BALF cell counts (NT-GRA, AM and LYM) *vs.* their respective control groups. Moreover, to evaluate the effect of the addition of DPI-0.5 to IV-CARB-PTX, COMBI-1 and COMBI-1-24h were compared to IV-CARB-PTX and COMBI-0.75 was compared to IV-CARB-PTX-0.75. To evaluate the staggering effect on the different parameters, COMBI-1 and COMBI-1-24 were also compared. Results were considered as statistically significant (*) for $p < 0.05$, very significant (**) for $p < 0.01$, extremely significant for $p < 0.001$ (***) and extremely significant for $p < 0.0001$ (****).

3. <u>Results</u>

For more clarity and understanding, the results and the discussion of this part have been separated.

3.1. Determination of maximum tolerated dose for CIS-DPI-50 and IV-CARB-PTX

Pulmonary and renal toxicities as well as myelotoxicity (DLT of CARB-PTX) were investigated to select the safest but also least-spaced and most highly dosed regimen that can be applied to treat lung cancer. To do so, it was mandatory to identify the MTD, as defined previously, for both routes, following the ET and IV regimens as described in **Figure 79**. CIS-DPI-50 MTD was fixed at 0.5 mg/kg, as described in *Experimental part III-section 3.1*. CARB-PTX-IV-MTD was assessed to be the closest to clinical practice. To do so, the CARB/PTX

ratio (1.7) usually used in clinics was calculated and was applied during the MTD escalation as explained in *section 2.4.2*.

CARB-PTX was administered the first day of each cycle as illustrated in **Figure 78.A**. The highest dose (dose 6: carboplatin at 51 mg/kg and paclitaxel at 30 mg/kg) induced a major bw loss for one mouse of up to -14%, on D2, in comparison with the first day of administration, resulting in -10 ± 2%, for the whole group **(Figure 79)**. Dose 5 (carboplatin at 42 mg/kg and paclitaxel at 25 mg/kg) and dose 4 (carboplatin at 34 mg/kg and paclitaxel at 20 mg/kg) showed delayed toxicities as they both induced bw loss for one mouse up to -15% and -22%, respectively, on D5. Moreover, as major ulcerations in the tails of the mice were observed at the highest dose, these mouse groups were therefore euthanized as the humane endpoints were reached. This was certainly related to a higher CARB-PTX dose and to a higher solution viscosity (due to higher Cremophor EL® proportion) that prevented paclitaxel from diffusing in the whole mice body, resulting in an accumulation in the tail and therefore in local ulceration. This ulceration results from the accidental infiltration of chemotherapy into subcutaneous or sub-dermal tissue at the injection site, leading to tissue necrosis (i.e. extravasation) [287,288]. Paclitaxel has a poorly defined delineation between being vesicant (tissue necrosis and/or formation of blisters) and being irritant (inflammation, pain or irritation without blisters formation) [287]. However, considering the numerous reports showing that paclitaxel has led to tissue damage and blistering, it is probable that these tail ulcerations could be attributed to this cytotoxic drug. Moreover, this localized inflammation can also be triggered by the excipient as it is widely described that Cremophor EL® is involved in hypersensitive reactions [106].
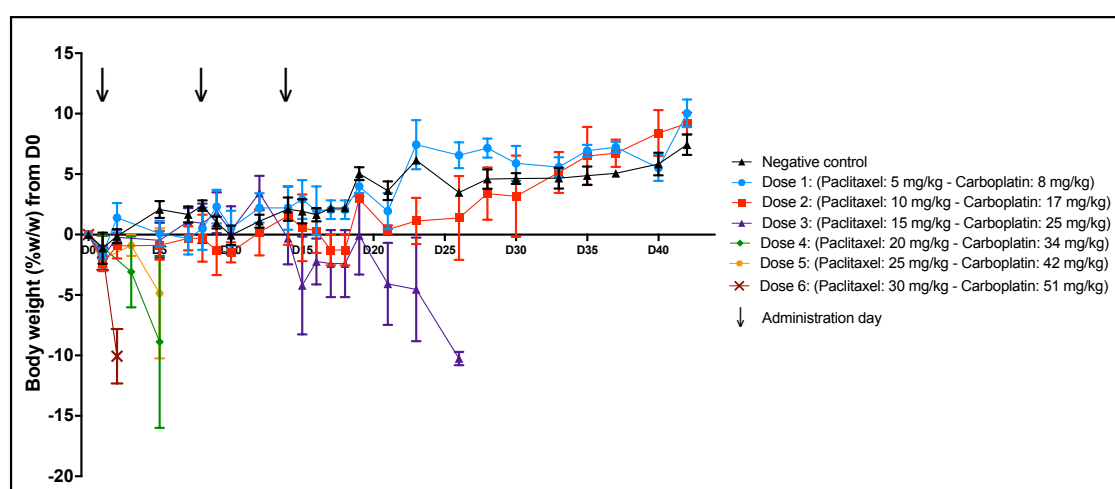

Figure 79: Bw profiles following carboplatin-paclitaxel administration using the IV route at different doses, *vs.* the vehicle group. All results are expressed as means ± SEM (n=3). The groups' abbreviations are described in **Figure 78.**

Dose 3 showed limited bw loss during the treatment administrations. However, the bw started to decrease on D21 until reaching -10.3 ± 0.5% on D26, leading to mice euthanasia **(Figure 79)**. The lower doses (doses 1 and 2) showed no major bw loss during the treatment administration, and a bw increase during the 28-day follow-up. Therefore, dose 2 with carboplatin at 17 mg/kg combined to paclitaxel at 10 mg/kg was fixed as the CARB-PTX-IV MTD.

3.2. Tolerance of DPI-0.5, IV-CARB-PTX and their combinations

Once the MTD was determined, DPI-0.5 and IV-CARB-PTX were administered starting the same day (COMBI-1) at their respective MTD. However, as the co-administration of DPI-0.5 and IV-CARB-PTX may induce cumulative toxicities, two strategies were developed. The first was the staggering of DPI-0.5 administration from IV-CARB-PTX administration by 24h (COMBI-1-24h); the second was the reduction of the IV dose by 25% as is commonly carried out in clinical practice to limit the risk of cumulative toxicity (COMBI-0.75) **(Figure 78)** [152]. To evaluate the pulmonary and renal tolerance due to the administration of CIS-DPI-50, it was mandatory to investigate histopathological damage (on lung and renal tissues) as well as specific biomarker levels following DPI-0.5, IV-CARB-PTX and their combinations [134]. Moreover, myelotoxicity was assessed to evaluate the DLT of CARB-PTX by counting WBC, RBC and PLT, as well as their related parameters.

3.3. Body weight profiles and general evaluation

The bw profiles of all the groups, illustrated in **Figure 80**, fluctuated during the treatment period but remained above -5%.
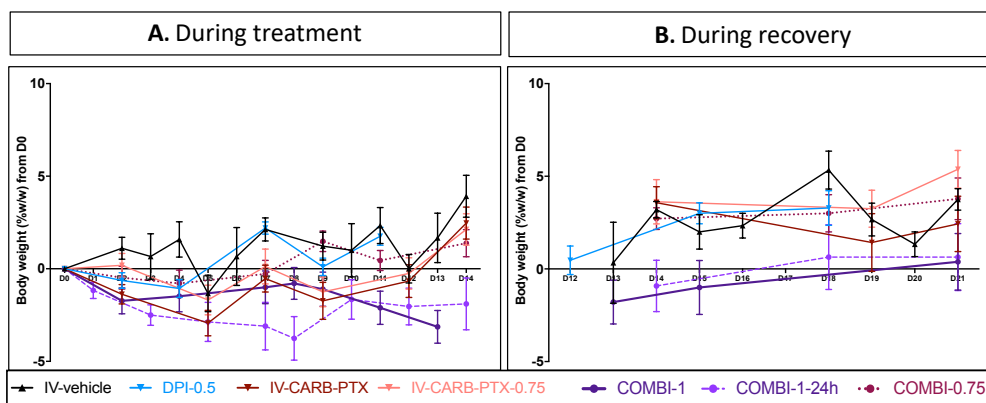

Figure 80: Bw profiles following carboplatin-paclitaxel administration using the IV route (IV doublets) at different doses, cisplatin-based DPI using the ET route (DPI-0.5) and their combinations *vs.* the IV-vehicle group. All results are expressed as means ± SEM (n=8-15). The groups' abbreviations are described in **Figure 78.**

IV-CARB-PTX and IV-CARB-PTX-0.75 bw profiles were similar and the bw losses decreased proportionally to the dose **(Figure 80.A)**. The highest bw losses for these groups were observed on D5 at -4 ± 1% and -2 ± 1%, respectively. Moreover, DPI-0.5 did not induce any major bw losses, with the highest bw loss observed on D4 at -1.0 ± 0.5% as already observed in *Experimental part III-section 3.1*. Combining DPI-0.5 with IV-CARB-PTX the same day (COMBI-1) or 24h later (COMBI-1-24h) was similarly well-tolerated by the mice. Their highest bw losses were observed on D13 at -3 ± 1% and on D8 at -4 ± 1%, respectively. However, decreasing the dose by 25%, as done by combining DPI-0.5 and IV-CARB-PTX-0.75 the same day (COMBI-0.75), seemed to be better tolerated than COMBI-1 and COMBI-1-24h. The highest bw loss for this group was observed on D8 at -1 ± 1%.

During the one-week recovery period, all bw increased and were positive at the end as mice were no longer exposed to any cytotoxic drug. This showed that bw losses were reversible.

3.4. Evaluation of pulmonary toxicity

Pulmonary inflammation and cytotoxicity were evaluated following the ET administrations of cisplatin (DPI-0.5), IV doublets and their combinations. As previously described, mouse groups were sampled 24h following the last administration and after one week of recovery. This was done to evaluate toxicity in its early acute phase and its possible reversibility within one week, as described in our previous preclinical study discussed in *Experimental part III-section 3.2.*

3.4.1. Inflammation

3.4.1.1. Total BALF cells

IV doublets and DPI-0.5

The repeated administration of DPI-0.5 following the selected regimen tended to increase total BALF cells, although this was non-significant in comparison with the IV-vehicle group at both sampling times ($p > 0.05$, **Figure 81.A**), as previously observed in our previous preclinical study. However, this increase was fully reversible after one week of recovery ($p > 0.05$, **Figure 81.B**). In contrast, the administration of IV-CARB-PTX at both doses did not induce any BALF cell recruitment at either sampling time ($p > 0.05$, **Figure 81**).
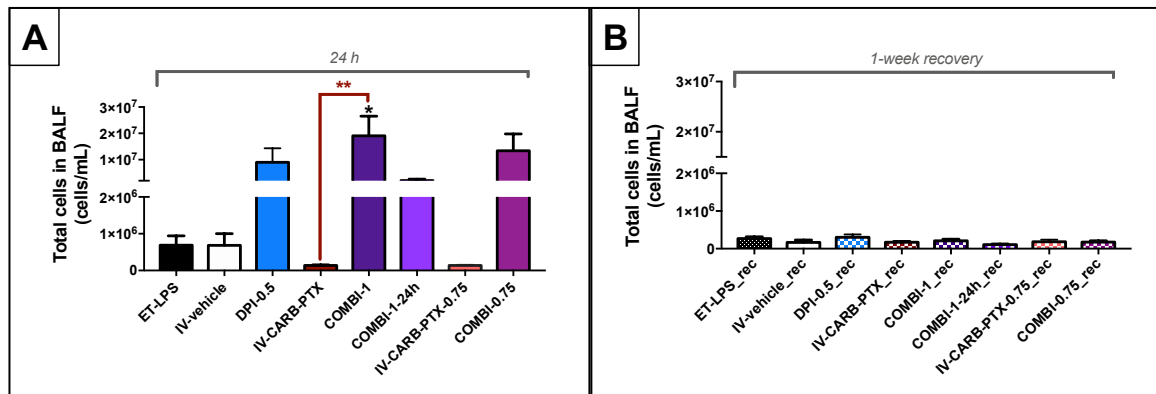
Figure 81: Evaluation of total BALF cells 24h following the last treatment administration, and one week of recovery later (_rec). The groups' abbreviations are described in **Figure 78.** All results are expressed as means ± SEM (n=8-15). The statistical analyses were performed *vs.* the IV-vehicle group (black) or *vs.* the selected groups as illustrated (red), using one-way ANOVA and Bonferroni's post-hoc test (** for $p < 0.01$ and * for $p < 0.05$).

Combinations

To evaluate the effect of the addition of DPI-0.5 to the IV chemotherapy, the combination groups were compared first to the IV-vehicle group and then to their respective IV doublets.

The co-administration of DPI-0.5 and IV-CARB-PTX, irrespective of the IV-dose and the scheme of administration, activated BALF-cell recruitment in comparison with the IV-vehicle control group 24h after the last treatment administration (COMBI-1: 1.9 ± 0.7 x 10^7 cells/mL, COMBI-1-24h: 2.1 ± 0.5 x 10^6 cells/mL and COMBI-0.75: 1.3 ± 0.6 x 10^7 cells/mL, *vs.* 7 ± 3 x 10^5 cells/mL, **Figure 81.A**) and were all reversible after one week of recovery ($p > 0.05$, **Figure 81.B**). This increase was only statistically higher for COMBI-1 in comparison with the IV-vehicle control group and in comparison with IV-CARB-PTX ($p < 0.05$ and $p < 0.01$, respectively, **Figure 81.A**). Moreover, this acute increase was not significant for COMBI-1-24h and COMBI-0.75 in comparison with their respective IV doublets ($p > 0.05$, **Figure 81.A**). Therefore, the administration of DPI-0.5 and IV-CARB-PTX at their MTD on the same day induced higher inflammatory-cell recruitment to trigger inflammation when compared to IV-CARB-PTX alone. However, this reaction seemed to be reduced when DPI-0.5 administration was staggered from IV-CARB-PTX administration by 24h or when the IV-CARB-PTX dose was reduced by 25% (IV-CARB-PTX-0.75).

3.4.1.2. Proportion of cells in BALF

IV doublets and DPI-0.5

Among the total BALF cell increase, the proportions of AM, NT-GRA and LYM were assessed. All ET-LPS positive control groups were administered 18h before the sampling and induced a

significant increase in NT-GRA compared to the IV-vehicle group ($p < 0.0001$, ET-LPS: $69 \pm 2\%$, ET-LPS_rec: $68 \pm 4\%$ *vs.* IV-vehicle: $0.1 \pm 0.1\%$, IV-vehicle_rec: $0.2 \pm 0.2\%$, **Figure 82.A**), as previously observed and discussed in *Experimental part III-section 3.2.1*.

The BALF cell count increase observed for DPI-0.5 **(Figure 81)** was related to higher NT-GRA in comparison with the IV-vehicle group ($p < 0.01$, $24 \pm 3\%$ *vs.* $0.1 \pm 0.1\%$, **Figure 82.A**) and was reversible within one week of recovery. However, the administration of IV doublets at both doses did not increase NT-GRA proportions at either sampling time **(Figure 82.A)**.
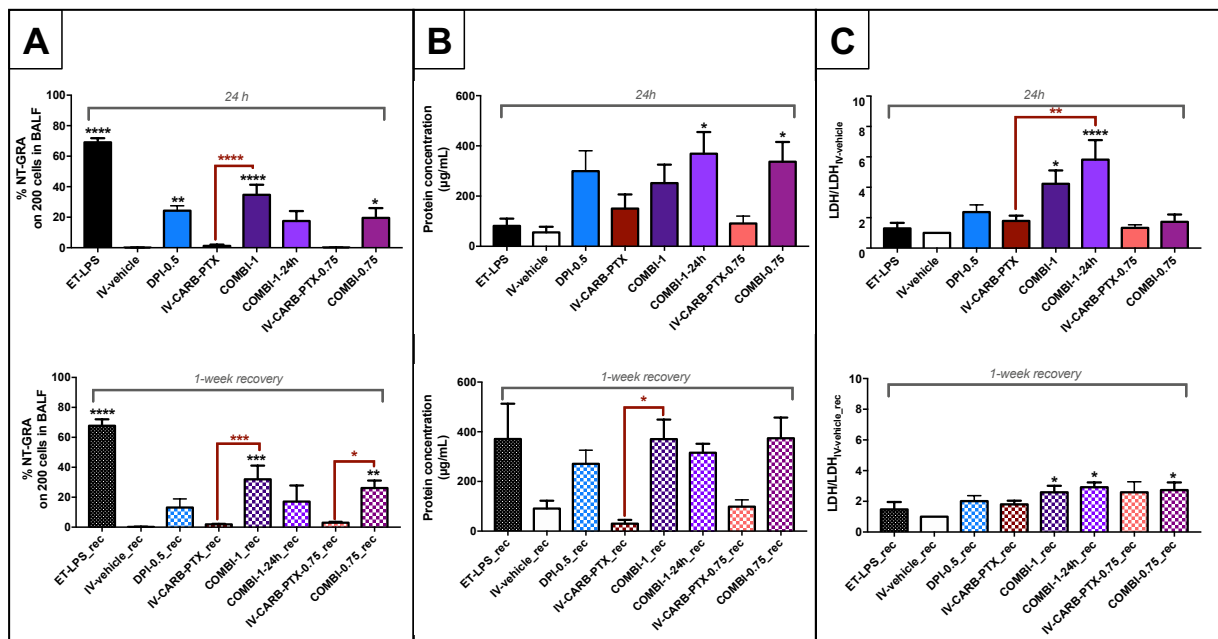
Figure 82: Evaluation of NT-GRA as a percentage of 200 BALF cells (A), total protein concentration (B), and the ratio of LDH activity reported on the LDH activity of the IV-vehicle or IV-vehicle_rec (C) in BALF 24h following the last treatment administration and after one week of recovery (_rec). The groups' abbreviations are described in **Figure 78.** All results are expressed as means $\pm$ SEM (n=8-15). Statistical analyses were performed *vs.* the IV-vehicle group (black) or *vs.* the selected groups as illustrated (red), using one-way ANOVA and Bonferroni's post-hoc test (**** for $p < 0.0001$, *** for $p < 0.001$, ** for $p < 0.01$ and * for $p < 0.05$).

Combinations

The combination of IV doublets and DPI-0.5 increased all NT-GRA proportions (COMBI-1: $35 \pm 7\%$, COMBI-1-24h: $18 \pm 7\%$, COMBI-0.75: $20 \pm 6\%$ *vs.* IV-vehicle: $0.1 \pm 0.1\%$, **Figure 82.A**). This increase was only significant for the groups that were administered DPI-0.5 and IV-CARB-PTX the same day (COMBI-1 and COMBI-0.75), in comparison with the IV-vehicle group ($p < 0.0001$ and $p < 0.05$), and was not reversible after one week of recovery ($p < 0.001$ and $p < 0.01$, **Figure 82.A**).

COMBI-1 increased significantly the NT-GRA proportion when compared to IV-CARB-PTX-MTD ($p < 0.0001$), which was not reversible after one week of recovery ($p < 0.001$). Moreover, COMBI-1-24h showed a lower increase in NT-GRA than COMBI-1 ($p < 0.05$, **Figure 82.A**). COMBI-1 and COMBI-0.75 showed that the pulmonary inflammation initiated 24h following the treatment administration was not reversible within one week. This demonstrated a more prolonged inflammation for these groups in comparison to COMBI-1-24h.

3.4.1.3. Inflammation biomarkers in BALF

CXCL1 and CXCL2

The mouse chemokines (CXCL1, CXCL2) involved in NT-GRA recruitment, were quantified in BALF supernatant **(Table 18)**. The ET-LPS positive control groups demonstrated significantly higher concentrations of both chemokines, when compared with the IV-vehicle group ($p < 0.0001$). For IV doublets and DPI-0.5, no major difference was observed when compared with the IV-vehicle group 24h after the last treatment administration ($p > 0.05$) or after one week of recovery ($p > 0.05$). Similarly, for the combinations, no significant difference was observed between them and the IV-vehicle group or their corresponding IV doublets, at both sampling times ($p > 0.05$, **Table 18**).

Table 18: Evaluation of chemokines (CXCL1 and CXCL2), pro-inflammatory cytokines (TNF-α, IL-6, and IL-1β) in BALF and biomarkers of AKI (cystatin C and creatinine) in plasma 24h following the last treatment administration and after one week of recovery (_rec). The groups' abbreviations are described in **Figure 78.** All results are expressed as means ± SEM (n=8-15). The statistical analyses were performed *vs.* the vehicle-IV group using one-way ANOVA and Bonferroni's post-hoc test (**** for $p < 0.0001$).

Biomarkers	Chemokines in BALF		Pro-inflammatory cytokines in BALF			AKI biomarkers in plasma	
	CXCL1 (pg/mL)	CXCL2 (pg/mL)	TNF-α (pg/mL)	IL-6 (pg/mL)	IL-1β (pg/mL)	Cystatin C (pg/mL)	Creatinine (pg/mL)
24h after treatment administration							
ET-LPS	330 ± 71****	49 ± 15****	150 ± 31****	54 ± 10****	87 ± 10****	-	-
IV-vehicle	30 ± 6	2.6 ± 0.6	57 ± 11	11 ± 2	18 ± 3	943 ± 37	0.13 ± 0.01
DPI-0.5	33 ± 6	5.9 ± 0.4	33 ± 4	16 ± 10	9 ± 3	989 ± 34	0.133 ± 0.006
IV-CARB-PTX	38 ± 13	1.8 ± 0.5	60 ± 12	12 ± 5	13 ± 4	974 ± 24	0.118 ± 0.006
COMBI-1	44 ± 6	3.1 ± 0.5	45 ± 8	9 ± 2	13 ± 4	949 ± 38	0.132 ± 0.008
COMBI-1-24h	38 ± 8	2.5 ± 0.5	71 ± 29	11 ± 5	23 ± 8	961 ± 35	0.137 ± 0.008
IV-CARB-PTX-0.75	22 ± 3	1.2 ± 0.5	47 ± 6	21 ± 7	8 ± 2	1020 ± 34	0.125 ± 0.003
COMBI-0.75	50 ± 5	1.2 ± 0.2	47 ± 6	8 ± 3	22 ± 5	911 ± 41	0.112 ± 0.006
One week of recovery after the treatment administration							
ET-LPS_rec	405 ± 98****	37 ± 9****	261 ± 153****	70 ± 16****	58 ± 11****	-	-
IV-vehicle_rec	42 ± 7	6.1 ± 0.7	51 ± 11	11 ± 3	20 ± 4	953 ± 31	0.119 ± 0.006
DPI-0.5_rec	48 ± 8	8 ± 2	30 ± 5	15 ± 3	15 ± 5	1039 ± 37	0.131 ± 0.006
IV-CARB-PTX_rec	67 ± 33	6.1 ± 0.5	46 ± 12	9 ± 4	9 ± 1	884 ± 43	0.12 ± 0.01
COMBI-1_rec	49 ± 7	7 ± 1	16 ± 4	3 ± 1	18 ± 6	907 ± 39	0.126 ± 0.005
COMBI-1-24h_rec	67 ± 21	6.7 ± 0.9	35 ± 7	3 ± 1	12 ± 2	923 ± 31	0.124 ± 0.005
IV-CARB-PTX-0.75_rec	22 ± 2	4.6 ± 0.2	26 ± 2	7 ± 4	7 ± 3	1013 ± 39	0.135 ± 0.007
COMBI-0.75_rec	53 ± 12	9 ± 2	26 ± 5	5 ± 2	21 ± 6	1005 ± 33	0.14 ± 0.01

TNF-α, IL-6 and IL-1β

TNF-α, IL-6 and IL-1β were quantified to evaluate pro-inflammatory responses following the treatment administration. As expected, all positive control groups (ET-LPS) were significantly higher than the IV-vehicle groups ($p < 0.0001$, **Table 18**). Following the administration of DPI-0.5, IV doublets and their combinations, at all doses and regimens, no significant increase was observed at either sampling time. Moreover, TNF-α, IL-6 and IL-1β levels were all lower one week later **(Table 18)**.

3.4.2. Cytotoxicity

3.4.2.1. Protein content

Following the administration of the IV doublets or DPI-0.5, protein concentration levels in BALF increased, dose-dependently. However, these were not significant in comparison with the IV-vehicle group 24h after the last treatment administration ($p > 0.05$, DPI-0.5: 300 ± 81 µg/mL, IV-CARB-PTX: 151 ± 56 µg/mL, IV-CARB-PTX-0.75: 91 ± 29 µg/mL *vs.* 56 ± 23 µg/mL), which remained high but still not significant after one week of recovery ($p > 0.05$, **Figure 82.B**). Although non-significant, DPI-0.5 protein concentration was more than 5-fold higher than in the IV-vehicle group and 2- and 3-fold higher than the IV-CARB-PTX and IV-CARB-PTX-0.75 groups, respectively, 24h after the last treatment administration.

The combination of both DPI-0.5 and IV-CARB-PTX irrespective of the dose or regimen showed higher protein concentrations than the IV-vehicle group (COMBI-1: 252 ± 74 µg/mL, COMBI-1-24: 369 ± 86 µg/mL, COMBI-0.75: 337 ± 78 µg/mL *vs.* 56 ± 23 µg/mL, **Figure 82.B**). However, this was only significant for COMBI-1-24h and COMBI-0.75 at 24h after the last treatment administration ($p < 0.05$) but not after one week of recovery ($p > 0.05$, **Figure 82.B**). None of the combination groups increased significantly the total protein concentration in comparison with their respective IV doublets, 24h after the treatment. However, after one week of recovery, only the COMBI-1 presented a total protein concentration significantly higher than the IV-CARB-PTX ($p < 0.05$, **Figure 82.B**). This was due to the addition of DPI-0.5 the same day as its co-administration with CARB-PTX-IV would have led to a cumulative cytotoxicity from both CARB-PTX-IV and CIS-DPI-ET leading to potentially higher protein content for this group.

3.4.2.2. Lactate dehydrogenase activity

As observed for the protein concentration evaluation, the LDH activity was higher following the administration of IV doublets and DPI-0.5 than for the IV-vehicle group but without

significant difference ($p > 0.05$, **Figure 82.C**), at both sampling times. However, all combination groups increased significantly the LDH ratios 24h after the last treatment administration (COMBI-1: 4.2 ± 0.9, COMBI-1-24h: 6 ± 1, COMBI-0.75: 1.8 ± 0.5, *vs.* IV-vehicle group: 1) except for COMBI-0.75 ($p > 0.05$). These groups were all significantly higher after one week of recovery ($p < 0.05$, **Figure 82.C**) when compared to the IV-vehicle group. Moreover, a significant increase in LDH activity was shown for COMBI-1-24h when compared to IV-CARB-PTX 24h after the last treatment administration ($p < 0.01$). However, this increase was not maintained after one week of recovery ($p > 0.05$, **Figure 82.C**).

3.4.3. Histopathological analysis

As previously observed during the evaluation of the pro-inflammatory cytokines and chemokines as well as during the cytotoxicity evaluation **(Table 18)**, no major lung damage was observed for IV doublets and DPI-0.5 administered alone or in combinations. The scores of all the adverse observations were less than 1 on a severity score scale of 0-5 and occurred in a maximum of 45% of the mice **(Figure 83.B)**.

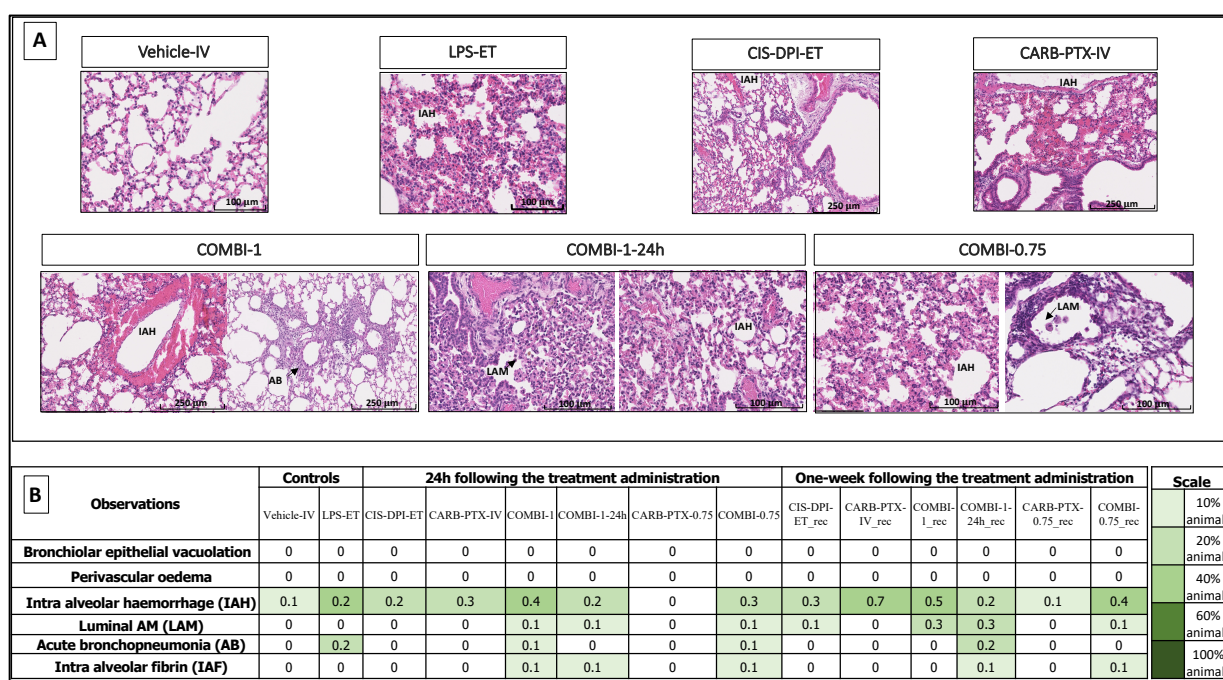| B Observations	Controls		24h following the treatment administration						One-week following the treatment administration						Scale
	Vehicle-IV	LPS-ET	CIS-DPI-ET	CARB-PTX-IV	COMBI-1	COMBI-1-24h	CARB-PTX-0.75	COMBI-0.75	CIS-DPI-ET_rec	CARB-PTX-IV_rec	COMBI-1_rec	COMBI-1-24h_rec	CARB-PTX-0.75_rec	COMBI-0.75_rec	10% animals
Bronchiolar epithelial vacuolation	0	0	0	0	0	0	0	0	0	0	0	0	0	0	20% animals
Perivascular oedema	0	0	0	0	0	0	0	0	0	0	0	0	0	0	40% animals
Intra alveolar haemorrhage (IAH)	0.1	0.2	0.2	0.3	0.4	0.2	0	0.3	0.3	0.7	0.5	0.2	0.1	0.4	60% animals
Luminal AM (LAM)	0	0	0	0	0.1	0.1	0	0.1	0.1	0	0.3	0.3	0	0.1	
Acute bronchopneumonia (AB)	0	0.2	0	0	0.1	0	0	0.1	0	0	0	0.2	0	0	100% animals
Intra alveolar fibrin (IAF)	0	0	0	0	0.1	0.1	0	0.1	0	0	0	0.1	0	0.1	

Figure 83: Histopathology of lung tissue exposed to IV doublets, ET monotherapy and their combinations. Representative images of treated groups (A) and heat map of adverse observations (in scale of proportion of mice concerned) and severity scores (from 0 to 5) depending on lung tissue histopathology (B) (Optical microscopy, 400 x). The groups' abbreviations are described in **Figure 78.**

3.4.4. Vacuolation and perivascular oedema

None of the groups displayed BEV or perivascular oedema.

3.4.5. Intra-alveolar haemorrhage

All the groups except CARB-PTX-0.75, even the IV-vehicle groups, displayed intra-alveolar haemorrhage. This was certainly related to the technique of sampling as blood may have not been completely removed before the paraffin-embedding. This could be also attributed to the BALF collection procedure. However, intra-alveolar haemorrhage seemed to be more intensely and frequently encountered for some groups such as COMBI-1, CARB-PTX-IV_rec, COMBI-1-rec and COMBI-0.75_rec than for the IV-vehicle **(Figure 83.B)**.

3.4.6. Luminal alveolar macrophage

In terms of luminal AM, which can be a sign of ongoing acute inflammation, DPI-0.5 and IV doublet groups showed a score of 0/5 24h after the last administration **(Figure 83)**. They also showed this after one week of recovery except for DPI-0.5_rec, which had a score of 0.1/5. However, once results for each combination were combined, a score of 0.1/5 was observed for all combinations for 7% of mice (COMBI-1, COMBI-1-24h and COMBI-1-0.75) 24h after the last treatment administration **(Figure 83.B)**. This increased to 0.3/5 for COMBI-1_rec and COMBI-1-24h_rec for 27% and 23% of mice, respectively. However, for COMBI-0.75, the initial score of 0.1/5 was maintained after one week of recovery for 7% of mice **(Figure 83.B)**.

3.4.7. Acute bronchopneumonia

AB was scored at 0/5 for DPI-0.5 and IV doublets at both doses and sampling times. This was also scored at 0.1/5 for COMBI-1, 0/5 for COMBI-1-24h and 0.1/5 for COMBI-0.75 24h after the last treatment administration **(Figure 83.B)**. This was observed for 13% of mice, for both groups and was already reported following cisplatin nebulization [77]. However, this observation was reversible within one week for the lower-dosed regimen of both groups (COMBI-1 and COMBI-0.75) and was not reversible for the highest dosed group (0.2/5 for COMBI-1-24h) **(Figure 83.B)**.

3.4.8. Intra-alveolar fibrin

Intra-alveolar fibrin was scored at 0/5 for DPI-0.5 IV doublets at both sampling times **(Figure 83.B)**. For the combination groups (COMBI-1, COMBI-1-24h and COMBI-0.75), this showed

a low score of 0.1/5 and was observed for only for 7% of the mice and was maintained after one week of recovery except for COMBI-1 **(Figure 83.B)**.

3.5. Evaluation of nephrotoxicity

The DLT of cisplatin is cumulative nephrotoxicity. It is therefore important that DPI-0.5 does not induce nephrotoxicity as this treatment is designed to be administered during off-cycles as a complement to IV doublets. Moreover, it is important to verify that there is no accumulation of toxicity on the kidneys using the combinations as carboplatin can also impact their function [88].

3.5.1. Plasma biomarkers

3.5.1.1. Neutrophil-gelatinase associated lipocalin

IV doublets and DPI-0.5

The repeated administration of DPI-0.5 did not induce any major significant NGAL difference in comparison with the IV-vehicle group ($p > 0.05$), both 24h after the last administration (107 ± 32 pg/mL *vs.* 300 ± 35 pg/mL) and after one week of recovery **(Figure 84.A)**. IV doublets showed a dose-dependent but non-significant increase in NGAL when compared to the IV-vehicle group 24h after the last treatment administration (IV-CARB-PTX: 602 ± 108 pg/mL, IV-CARB-PTX-0.75: 539 ± 43 pg/mL *vs.* 300 ± 35 pg/mL). The NGAL concentrations decreased for all groups and were all non-significant after one week of recovery ($p > 0.05$, **Figure 84.A**).

Combinations

The co-administration of DPI-0.5 and IV-CARB-PTX, at both doses and regimens, increased NGAL concentrations to higher concentrations than with the vehicle group-IV (COMBI-1: 939 ± 287 pg/mL, COMBI-1-24h: 575 ± 45 pg/mL, COMBI-0.75: 715 ± 72 pg/mL *vs.* 300 ± 35 pg/mL). The increase was significant only for COMBI-1 ($p < 0.01$, **Figure 84.A**), 24h after the last treatment administration. These increases were all reversible after one week of recovery **(Figure 84.A)**. This result was expected, as COMBI-1 was the most highly dosed regimen in which DPI-0.5 and IV doublets administrations were less spaced. In comparison with their relative IV groups, all combinations showed a non-significant increase in NGAL concentration at both sampling times **(Figure 84.A)**.
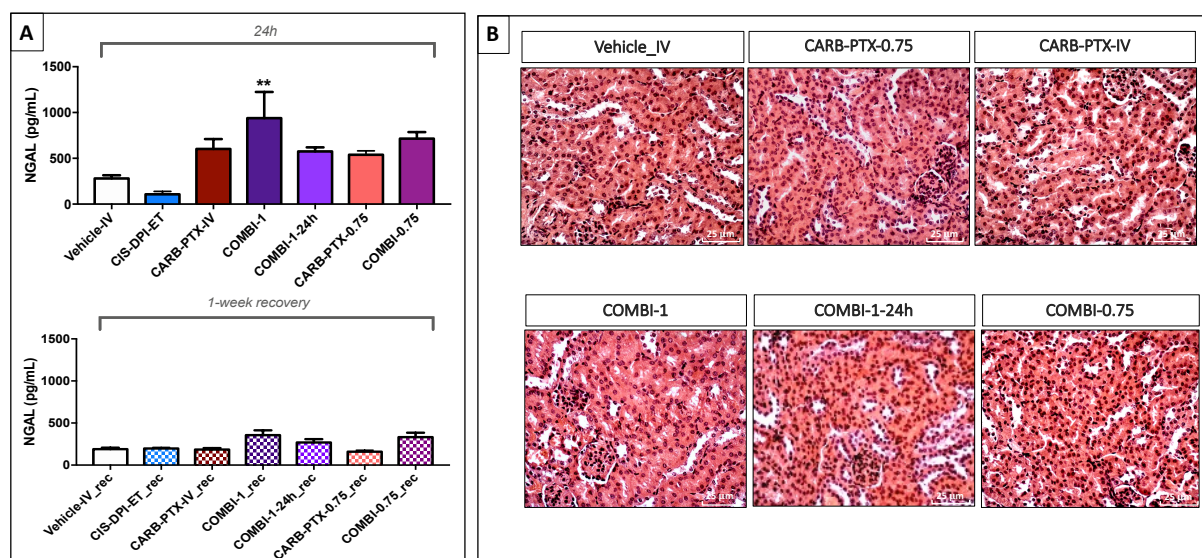
Figure 84: Evaluation of plasma NGAL (A) 24h following the last treatment administration and after one week of recovery (_rec). The groups' abbreviations are described in **Figure 78.** All results are expressed as means ± SEM (n=8-15). The statistical analyses were performed *vs.* the IV-vehicle group (black) or *vs.* the selected groups as illustrated (red), using one-way ANOVA and Bonferroni's post-hoc test (** for *p* < 0.01). Representative renal tissue histological analyses (HE, magnification 400 x) in selected mice groups (B).

3.5.1.2. Cystatin C and creatinine

The repeated administration of DPI-0.5, IV doublets and their combinations did not induce higher cystatin C or creatinine levels when compared to the IV-vehicle group, at either sampling time (*p* > 0.05, **Table 18**).

3.5.2. Histopathological analysis

Following the analysis of PAS and HE staining, no AKI was noticed for all groups of all doses and regimens at both sampling times **(Figure 84.A)**. These results confirmed observations during the plasma biomarker evaluation.

3.6. Evaluation of myelotoxicity

Myelosuppression is an adverse effect often responsible for the interruption of the treatment by 3 weeks, which it is the time necessary to renew bone-marrow stem cells [289]. Therefore, it is crucial that the CIS-DPI-50 does not induce cumulative myelosuppression if it is administered during the off-cycles of IV chemotherapy. To verify this, the total numbers of WBC, RBC and PLT, and their related parameters, were determined 24h after the treatment administration regimen and after one week of recovery.

To improve the clarity of the figures, WBC results are represented in **Figure 85.A** without the statistical analyses specified hereunder.
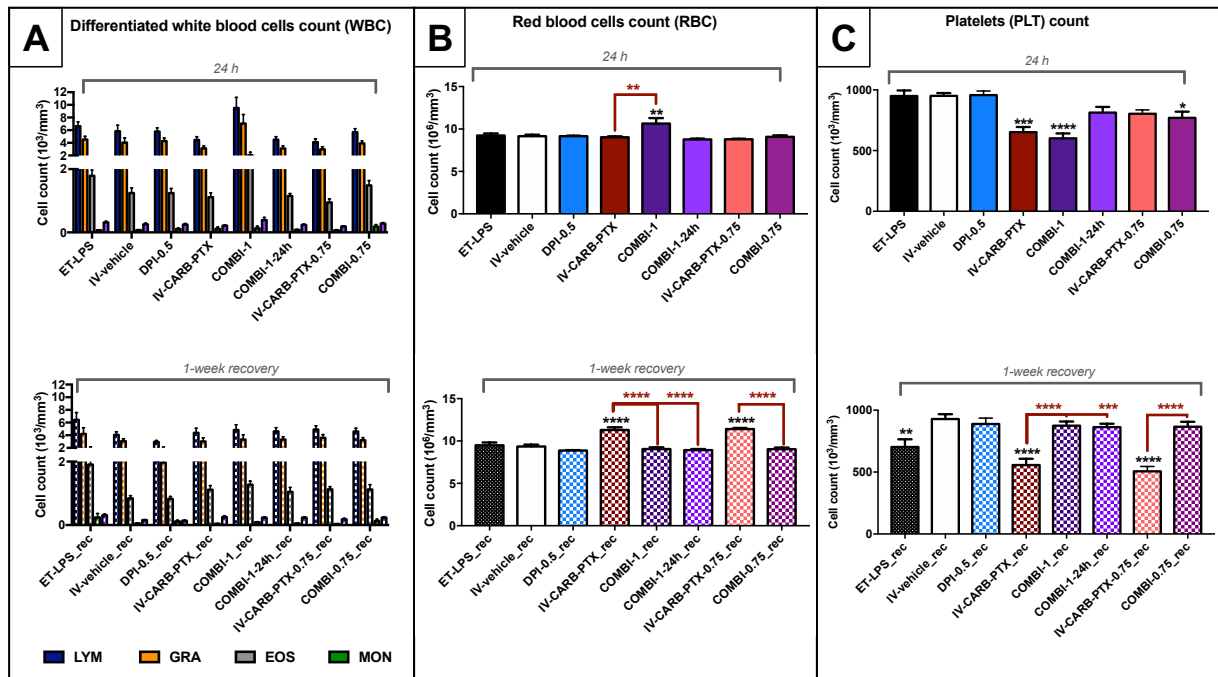
Figure 85: Evaluation of the differentiated WBC count of LYM, GRA, EOS and MON (A), the total RBC (B) and the total PLT (C) in blood, 24h following the last treatment administration and after one week of recovery (_rec). The groups' abbreviations are described in **Figure 78.** All results are expressed as means ± SEM (n=8-15). The statistical analyses were performed *vs.* the IV-vehicle group (black) or *vs.* the selected groups as illustrated (red), using one-way ANOVA and Bonferroni's post-hoc test (**** for $p < 0.0001$, *** for $p < 0.001$, ** for $p < 0.01$ and * for $p < 0.05$).

3.6.1. White blood cells

3.6.1.1. IV doublets and DPI-0.5

The administration of DPI-0.5 did not induce any leukopenia or WBC increase in comparison with the IV-vehicle group ($p > 0.05$, **Figure 85.A**). The administration of the IV doublets induced a non-significant slight decrease in the total WBC *vs.* the IV-vehicle group (IV-CARB-PTX: 4.5 ± 0.5 x 10^3 cells/mm^3 and IV-CARB-PTX-0.75: 4.1 ± 0.5 x 10^3 cells/mm^3, respectively *vs.* 5.8 ± 0.9 x 10^3 cells/mm^3). These differences were all reversible after the recovery week ($p > 0.05$). However, it should be noted that for the positive ET-LPS_rec groups, the proportions of GRA and LYM were significantly higher in comparison to the IV-vehicle group ($p < 0.001$, **Figure 85.A**).

3.6.1.2. Combinations

The administration of COMBI-1 increased significantly the total WBC count *vs.* the IV-vehicle group: 10 ± 2 x 10^3 cells/mm^3 *vs.* 5.8 ± 0.9 x 10^3 cells/mm^3 ($p < 0.05$, **Figure 85.A**) 24h after the last treatment administration. This was observed for all the different WBC but was only significant for the total number of LYM ($p < 0.05$) 24h after the last treatment administration. This increase was reversible after one week of recovery as no significant difference was observed between this group and the IV-vehicle group (4.8 ± 0.8 x 10^3 cells/mm^3 *vs.* 4.0 ± 0.5 x 10^3 cells/mm^3) ($p > 0.05$, **Figure 85.A**). Moreover, after one week of recovery, the proportion of LYM remained significant and the proportion of GRA became significant for COMBI-1 in comparison to the IV-vehicle group ($p < 0.05$ and $p < 0.01$, respectively). The total WBC count of COMBI-1 was very significant when compared to IV-CARB-PTX ($p < 0.01$, **Figure 85.A**) 24 h after the last treatment administration. This was related to higher LYM ($p < 0.01$), GRA ($p < 0.05$) and MON ($p < 0.05$) for COMBI-1 in comparison with IV-CARB-PTX. In contrast, this was not the case for COMBI-1-24h or COMBI-0.75 24h after the last treatment administration as no significant difference was observed *vs.* the IV-vehicle group or their respective IV doublets ($p > 0.05$, **Figure 85.A**).

Moreover, the difference in terms of WBC counts 24h after the last treatment administration between COMBI-1-24h and COMBI-1 or between COMBI-0.75 and COMBI-1 was significant, in both cases ($p < 0.001$, $p < 0.01$, respectively, **Figure 85.A**). This was related to the increase in LYM ($p < 0.001$) and GRA ($p < 0.05$) for COMBI-1 and to the increase in LYM ($p < 0.01$) for COMBI-0.75 when compared to COMBI-1-24h. All differences observed between COMBI-1-24h and COMBI-1 or between COMBI-0.75 and COMBI-1 were reversible one week later ($p > 0.05$, **Figure 85.A**). The 24h delay and the dose reduction therefore both seemed useful to limit the inflammation.

3.6.2. Red blood cells

3.6.2.1. IV doublets and DPI-0.5

The administration of DPI-0.5 or IV doublets did not show any significant difference in terms of total RBC count, Hb and Ht 24h after the last treatment administration with the IV-vehicle group. However, after one week of recovery, total RBC count, Hb and Ht were significantly higher for the IV doublets at both doses (IV-CARB-PTX and IV-CARB-PTX-0.75) ($p < 0.0001$, **Figure 85.A and Table 19**).

Moreover, both IV doublets were also characterized by significantly higher MCV (i.e. macrocytosis) after one week of recovery in comparison with the IV-vehicle group ($p < 0.001$ for IV-CARB-PTX and $p < 0.01$ for IV-CARB-PTX-0.75). In addition, the RDW of IV doublets was significantly different ($p < 0.01$, **Table 19**).

Table 19: Evaluation of RBC, WBC and PLT parameters in plasma 24h following the last treatment administration and after one week of recovery (_rec). The groups' abbreviations are described in **Figure 78.** All results are expressed as means ± SEM (n=8-15). The statistical analyses were performed *vs.* the IV-vehicle-IV group using one-way ANOVA and Bonferroni's post-hoc test (**** for $p < 0.0001$, *** for $p < 0.001$, ** for $p < 0.01$ and * for $p < 0.05$).

Parameters	MCHC (g/dL)	Hb (g/dL)	Ht (%)	MCV (%)	RDW (µm³)	MCH (pg)	MPV (µm³)
24h after the treatment administration							
ET-LPS	34.8 ± 0.4	15.6 ± 0.2	44.9 ± 0.9	49.1 ± 0.2	12.7 ± 0.1	17.1 ± 0.2	6.1 ± 0.1
IV-vehicle	34.3 ± 0.2	15.5 ± 0.3	45.2 ± 0.8	49.3 ± 0.2	12.75 ± 0.07	16.87 ± 0.08	6.0 ± 0.1
DPI-0.5	34.4 ± 0.2	15.4 ± 0.2	44.8 ± 0.6	48.8 ± 0.1	12.80 ± 0.06	16.85 ± 0.08	6.18 ± 0.07
IV-CARB-PTX	34.5 ± 0.2	15.5 ± 0.2	44.9 ± 0.7	49.8 ± 0.3	13.00 ± 0.08	17.15 ± 0.08	6.1 ± 0.1
COMBI-1	34.3 ± 0.1	18 ± 1****	54 ± 4 ***	50.2 ± 0.2**	13.0 ± 0.1	17.2 ± 0.1	6.2 ± 0.1
COMBI-1-24h	33.8 ± 0.2	14.8 ± 0.2	43.9 ± 0.5	50.2 ± 0.1**	12.96 ± 0.06	16.93 ± 0.09	6.3 ± 0.1
IV-CARB-PTX-0.75	34.3 ± 0.2	15.1 ± 0.2	44 ± 2	50.0 ± 0.2	13.2 ± 0.1**	17.2 ± 0.1	6.00 ± 0.08
COMBI-0.75	34.1 ± 0.1	15.4 ± 0.3	45.2 ± 0.9	49.9 ± 0.2	12.92 ± 0.08	16.95 ± 0.08	6.4 ± 0.1
One-week recovery after the treatment administration							
ET-LPS_rec	34.5 ± 0.4	16.1 ± 0.5	47 ± 2	49.0 ± 0.2	12.90 ± 0.07	17.0 ± 0.2	6.5 ± 0.2**
IV-vehicle_rec	34.4 ± 0.2	15.8 ± 0.3	46 ± 1	49.3 ± 0.2	12.95 ± 0.08	16.9 ± 0.1	6.03 ± 0.06
DPI-0.5_rec	34.7 ± 0.2	15.3 ± 0.1	44.0 ± 0.5	49.5 ± 0.1	12.89 ± 0.05	17.2 ± 0.1	5.86 ± 0.06
IV-CARB-PTX_rec	33.8 ± 0.2	19.4 ± 0.6****	57 ± 2****	50.8 ± 0.3***	14.1 ± 0.2****	17.2 ± 0.1	6.3 ± 0.2
COMBI-1_rec	34.6 ± 0.3	15.7 ± 0.3	46 ± 1	50.2 ± 0.2	13.6 ± 0.1*	17.4 ± 0.2	6.00 ± 0.06
COMBI-1-24h_rec	33.8 ± 0.3	15.2 ± 0.2	45.1 ± 0.6	50.5 ± 0.2**	13.5 ± 0.1	17.1 ± 0.1	6.07 ± 0.07
IV-CARB-PTX-0.75_rec	33.8 ± 0.2	19.5 ± 0.3****	58 ± 1****	50.6 ± 0.2**	13.3 ± 0.08	17.10 ± 0.09	6.03 ± 0.08
COMBI-0.75_rec	34.2 ± 0.2	15.4 ± 0.3	44.9 ± 0.9	49.7 ± 0.4	13.34 ± 0.08	17.0 ± 0.2	6.09 ± 0.07

3.6.2.2. Combinations

COMBI-1 induced significantly higher numbers of RBC ($10.6 \pm 0.7 \times 10^6$ cells/mm³ *vs.* $9.1 \pm 0.2 \times 10^6$ cells/mm³, $p < 0.01$, **Figure 85.B**), Hb (18 ± 1 g/dL *vs.* 15.5 ± 0.8 g/dL, $p < 0.0001$) and Ht ($54 \pm 11\%$ *vs.* $45.2 \pm 0.8\%$, $p < 0.001$) than IV-vehicle group, 24h after the last treatment administration. This increase was reversible after one week of recovery as no significance difference was observed with the IV-vehicle group **(Table 19)**. However, the RDW was significantly higher for COMBI-1 in comparison with the IV-vehicle group ($p < 0.05$, **Table 19**).

Total RBC count, Hb and Ht of COMBI-1 were also significantly higher than for IV-CARB-PTX ($p < 0.01$, $p < 0.0001$ and $p < 0.001$, respectively) and COMBI-1-24h ($p < 0.0001$, for all), 24h after the last treatment administration **(Figure 85.B and Table 19)**.

Consequently, the administration of COMBI-1 seemed to induce an increased number of RBC (polycythaemia) 24h after the last treatment administration. This was much earlier than with both IV doublets (IV-CARB-PTX and IV-CARB-PTX-0.75).

COMBI-1-24h did not increase significantly RBC, MCHC, Hb, Ht or RDW in comparison with the IV-vehicle group or IV-CARB-PTX at either sampling time ($p > 0.05$, **Figure 85.B and Table 19**). However, both COMBI-1 and COMBI-1-24h were characterized by a significant increase in the MCV, in comparison with the IV-vehicle group ($p < 0.01$) although not with the IV-CARB-PTX group ($p > 0.05$), 24h after the last treatment administration. On the other hand, the MCV increase was maintained for COMBI-1-24h after one week of recovery in comparison to the IV-vehicle group ($p < 0.01$, **Table 19**). COMBI-0.75 did not induce any increase in terms of RBC count or their related parameters **(Figure 85.B and Table 19)**, for either sampling time. It should be noted that for all groups, MCH and MHCH were similar to those for the IV-vehicle group.

3.6.3. Platelets

Thrombocytopenia is one of the most common cumulative side effects of CARB-PTX doublet chemotherapy [152–154,290]. It was therefore mandatory to investigate total PLT count and MPV for all the tested groups.

3.6.3.1. DPI-0.5 and IV doublets

DPI-0.5 did not decrease the total PLT count as no significant difference with the IV-vehicle group was observed at either sampling time ($p > 0.05$, **Figure 85.C**). On the other hand, the administration of IV-CARB-PTX induced a significant decrease in total PLT count, in comparison with the IV-vehicle group ($p < 0.001$), which remained one week after administration ($p < 0.0001$, **Figure 85.C**). In contrast, this was not the case for IV-CARB-PTX-0.75, as no significant difference was observed with the IV-vehicle group ($p > 0.05$) 24h after the last treatment administration, although this was the case after one week of recovery ($p < 0.0001$, **Figure 85.C**).

None of the DPI-0.5 or IV doublets increased MPV in comparison with the IV-vehicle group at either sampling time ($p > 0.05$, **Table 19**).

3.6.3.2. Combinations

The administration of COMBI-1 or COMBI-0.75 led to a significantly lower PLT count than for the IV-vehicle group 24h after the last administration and was proportional to the administered dose ($p < 0.0001$ and $p < 0.05$, respectively). However, these lower PLT counts

were reversible after one week of recovery with no significant difference with the IV-vehicle group ($p > 0.05$, **Figure 85.C**).

COMBI-1-24h showed no significant difference in total PLT count compared with the IV-vehicle group at either sampling time ($p > 0.05$). Moreover, COMBI-1-24h had a significantly higher total PLT count than COMBI-1, 24h after the last administration ($p < 0.001$, **Figure 85.C**). No significant difference was observed between the combination groups and their respective IV doublets 24h after the treatment. However, a significant difference was observed for all the combination groups one week later, as the decreases observed with IV doublets were significantly higher than with their respective combination groups (COMBI-1 ($p < 0.0001$), COMBI-1-24h ($p < 0.001$) *vs.* IV-CARB-PTX, and COMBI-0.75 *vs.* IV-CARB-PTX-0.75 ($p < 0.0001$, **Figure 85.C**).

None of the combination groups increased MPV in comparison with the IV-vehicle group at either sampling time ($p > 0.05$, **Table 19**).

4. <u>Discussion</u>

It was fundamental to verify that the addition of DPI-0.5 during IV doublet off-cycles did not impair general tolerance (i.e. bw losses) or pulmonary, renal and haematological tolerance. Indeed, these resting cycles are crucial for recovery before the administration of the following treatment cycle. The bw profiles demonstrated limited bw losses during the treatment administration and increased bw during recovery. This matched the general tolerance cited above.

The investigation of the pulmonary tolerance of DPI-0.5 and IV doublets separately and in combination was necessary as platinum-based agents and taxanes have been reported to induce hypersensitive reactions in lungs. This occurred with acute onset of bronchospasm, dyspnoea, cough and hypotension, leading to treatment discontinuation [77]. Indeed, 30% of patients treated with paclitaxel have developed, within the first 10 minutes of infusion, acute pneumonia and hypersensitivity pneumonitis in addition to the reactions described above [77].

In our study, pulmonary inflammation and cytotoxicity were evaluated directly in BALF to increase the specificity of the lung-related tolerance. As inflammatory cells are involved in the earliest phase of inflammation, BALF-packed cells were evaluated in terms of differential and total cell counts [151,163]. A higher total cell recruitment (total BALF cell analysis) was detected for the groups exposed to DPI-0.5 locally (DPI-0.5, COMBI-1, COMBI-1-24h and

COMBI-0.75). This recruitment was related to higher NT-GRA cell proportions in comparison to their respective IV doublets **(Figure 81 and Figure 82)**. This demonstrated a more intense inflammation for these groups related to the prolonged exposure to cisplatin following DPI-0.5 administration. Indeed, NT-GRA are the most common cells among GRA and are recruited at the site of inflammation to help remove phagocytosis debris by releasing ROS, antimicrobial proteins and degradative enzymes [267].

It should be noted that in *Experimental part III-section 3.2*, we demonstrated that the administration of the vehicle (used for the preparation of CIS-DPI-50 blend) following the scheme described in **Figure 55** did not induce any inflammation in mice. Indeed, the administration of the diluent did not lead to any bw loss, lung inflammatory reaction (i.e. no increase in pro-inflammatory cytokines, chemokines, or proportion of NT-GRA in BALF), lung cytotoxicity (i.e. no increase in protein content) or AKI (i.e. no increase in NGAL, cystatin-c, creatinine). Consequently, the adverse effects observed in lungs and kidneys following DPI-0.5 administration were only attributed to cisplatin, not to the excipients or to the technique of administration. The mechanism for the generation of pulmonary injury following the administration of cytotoxic drug was already discussed in *Experimental part III-section 3.2*.

As cell recruitment occurs using specific mouse chemokines, CXCL1 and CXCL2 were also quantified in BALF [264]. However, the observed lung inflammatory reactions did not seem to be related to higher CXCL1 and/or CXCL2 levels **(Table 18)**. This might have been related to the fact that NT-GRA had already been retrieved in BALF and needed no further recruitment. Moreover, these chemokines may have increased gradually during the treatment administration and may have normalized once NT-GRA were recruited in BALF. Indeed, these chemokines increase in the early phase of inflammation and also seem to have an active role in the regulation and homeostasis of NT-GRA recruitment [291,292]. As pro-inflammatory cytokines are well-known to take an active part in the generation of acute inflammation, TNF-α, IL-6 and IL-1β were quantified in BALF supernatant. Indeed, these cytokines are the most involved in inflammation in both human and mouse models [133,163]. In our study, except for the positive control (ET-LPS), none of the treated groups demonstrated a higher lung inflammation **(Table 18)**. However, in *Experimental part III*, in which DPI-0.5 and CIS-IV were combined, a higher pulmonary inflammation was reported following their administration on the same day at their MTD (i.e. 0.5 mg/kg for DPI-0.5 and 2 mg/kg for CIS-IV_2) in terms of NT-GRA recruitment, TNF-α and IL-6 levels. It has been reported that the administration of cisplatin using

nebulization through the ET route was responsible for severe pneumonitis and mild to moderate fibrosis during a preclinical study on dogs [278]. Moreover, its administration in a phase I study was correlated to dyspnoea, bronchitis and hoarseness, which were scored 1-2 above 4 [178]. This may have been avoided in our study by developing cisplatin as a controlled-release formulation.

Lung cytotoxicity was evaluated by quantifying the LDH activity and total protein content. Cytotoxicity leads to cell rupture, leading to the release of their contents into the extracellular compartment. The determination of the total protein content is therefore correlated to cell lysis and to cytotoxicity. By the same logic, LDH is an enzyme that is retrieved in the cytoplasm of different tissues and increases in the case of cell rupture or death. As its concentration is up to 500-fold higher in lung tissue than in plasma, it was therefore interesting to quantify LDH in BALF [265]. Results tended to show that DPI-0.5 administered using the ET route seemed to induce higher cytotoxicity in BALF than the IV doublets **(Figure 82)**. These results were similar to those obtained for DPI-0.5 and CIS-IV during our previous preclinical study. This can be explained by a more prolonged and more frequent exposure to the cytotoxic drug following DPI-0.5 in comparison with IV doublets. Considering both these biomarkers, the combination groups seemed to be characterized by higher protein content when compared to their relative IV doublets. This was predictable as cytotoxicity is related to the total cytotoxic drug dose (higher dose for combinations *vs.* IV doublets or DPI-0.5).

The histopathological analyses did not demonstrate any major lung damage for any of the groups and confirmed the results obtained with the pulmonary biomarkers. Indeed, BEV (score 0/5), perivascular oedema (score 0/5), major intra-alveolar haemorrhage (score 0.7/5), AB (score 0.2/5) and intra-alveolar fibrin (0.1/5) were the maximum observed scores and were all less than 1 **(Figure 83)**. Luminal AM investigation in lung sections demonstrated a slight transient increase for the combination groups. The recruitment of AM related to the administration of DPI-0.5, as observed during BALF cell counts, was to ensure phagocytosis as this is the main innate defence mechanism **(Figure 81)** [163]. Moreover, an increased blood congestion and a higher blood flow are observed in inflammation to ensure inflammatory cell recruitment and extravasation [293], which may explain the intensified intra-alveolar haemorrhage and luminal AM observations in lung sections. Furthermore, "tissue factor" is an integral plasma membrane protein expressed by AM, lung epithelium and fibroblasts, which increases in lung or pleural injuries to initiate the extrinsic pathway of coagulation [294]. In the sites of injury, this pro-coagulation factor activates thrombin leading to localized fibrin sections

[294]. This is a well-known reaction to inflammation [294] and may explain the slight intra-alveolar fibrin observations.

These results seemed to demonstrate a good pulmonary tolerance of all combinations. Indeed, except for total BALF cell and NT-GRA proportion increases, DPI-0.5, IV doublets and their combinations at their MTD, administered on the same day, did not seem to induce acute pulmonary inflammation. However, these combination groups seemed to induce a higher cytotoxicity than their respective IV doublets (COMBI-1-24h *vs.* IV-CARB-PTX), which would be favourable for treatment efficacy. This tended to be associated to higher but still light lung damage for these groups in comparison to IV doublets. It is important to report that higher lung inflammation was observed following the administration of CIS-IV_2 at its MTD (i.e. 2.0 mg/kg) when combined with DPI-0.5, the same day or 24h later in *Experimental part III*. All lung-related inflammatory reactions were reversible within one week of recovery, except for NT-GRA recruitment. The reported inflammation was avoided only when the CIS-IV_2 dose was reduced by 25% (i.e. CIS-IV_1.5). The combination of CARB-PTX IV doublets and DPI-0.5 seemed to be overall better tolerated by the lungs than the previous CIS-IV and DPI-0.5 combinations. Indeed, while the combination of IV-CARB-PTX and DPI-0.5 did not induce higher pro-inflammatory cytokines, the combination of CIS-IV and DPI-0.5 induced an irreversible increase in TNF-α levels and a reversible increase in IL-6 levels. Moreover, luminal AM observation was scored higher for the combination of CIS-IV and DPI-0.5 than IV-CARB-PTX and DPI-0.5 (2/5 *vs.* 0.1/5, respectively), demonstrating a more intense phagocytotic reaction for this combination. These differences may be related to the fact that carboplatin has a slower rate of aquation and therefore a lower cytotoxic activity than cisplatin, leading to a better overall toxicity profile [87,93,295]. Therefore, considering only lung-related inflammatory reactions, the co-administration of IV-CARB-PTX and DPI-0.5 the same day should be considered while the combination of CIS-IV_2 at its MTD and DPI-0.5 on the same day should be avoided.

As described previously, the investigation of AKI is mandatory to assess the safety of the combination groups as platinum compounds are reported to be highly nephrotoxic [88]. To evaluate early AKI, novel biomarkers that have already proven their specificity and sensitivity in both preclinical and clinical studies were selected [137]. In *Experimental part III* of this work, AKI was detected 24h after its induction using NGAL, cystatin C and creatinine in plasma. As previously discussed, AKI biomarkers are divided into tubule-function biomarkers (cystatin C, creatinine) and kidney-damage biomarkers (NGAL) [137] and should be both

considered for AKI assessment [136]. On the one hand, the functional biomarker cystatin C is freely filtered and almost completely reabsorbed and degraded in the proximal tubule. Therefore, it increases if there is a filtration defect [137,142]. On the other hand, NGAL is secreted by NT-GRA and kidney tubular cells in the early stages of renal damage or inflammation [137,142,143].

The administration of DPI-0.5 following three administrations a cycle for two consecutive cycles was well-tolerated by the kidneys as no early or delayed AKI was notified **(Figure 84 and Table 18)**, as already demonstrated in *Experimental part III-section 3.3.3*. Indeed, no significant increase in NGAL, cystatin C, or creatinine was identified following the administration of DPI-0.5 at 0.5 mg/kg or even at 1 mg/kg. Moreover, the administration of IV-CARB-PTX at its MTD did not seem to induce AKI, whereas this was observed following the administration of CIS-IV_2 at its MTD. It is widely known that, unlike cisplatin, carboplatin does not interact with the OCT2. This results in a lower concentration of carboplatin in the proximal tubule cells than cisplatin, leading to less renal damage [87].

The combination of DPI-0.5 and CARX-PTX IV the same day induced higher NGAL levels, but with similar and non-significant cystatin C and creatinine levels, resulting in significantly higher damage and/or inflammation than with the IV-vehicle group. However, this increase was reversible within one week, and was not significantly different from IV-CARB-PTX. In addition, no renal injury or higher plasma AKI biomarkers were observed for the other groups **(Figure 84 and Table 18)**. This showed that the strategies of dose reduction by 25% or a delay in administrations were promising to avoid any major biomarker increase when compared to groups treated with IV doublets. In contrast, the combination of DPI-0.5 and CIS-IV_2 at their respective MTD, the same day or 24h later, induced non-reversible AKI, with increases in NGAL, cystatin C and creatinine levels, as demonstrated in *Experimental part II-section 3.3.4*. It was mandatory to reduce the IV dose by 25% and stagger the administrations by 24h to avoid AKI. As expected, the combinations with CIS-IV seemed to induce higher AKI than those with IV-CARB-PTX as no dose or regimen adaptations were required. These last results validated our preclinical AKI model and confirmed its appropriateness, as carboplatin is widely described to be less nephrotoxic than cisplatin [152].

Last but not least, haematological tolerance was assessed to ensure that the addition of DPI-0.5 did not impair the regeneration of bone-marrow stem cells that normally occurs during the off-cycles [289]. Indeed, paclitaxel causes myelosuppression by preventing depolymerization as it binds strongly with bone marrow cells microtubules leading to inhibition of mitosis and to

apoptosis [147]. In contrast, platinum drugs binds to bone marrow cells' DNA leading to DNA damage during replication [147]. This leads to leukopenia (reduced levels of WBC), neutropenia, thrombocytopenia (reduced levels of PLT) and anaemia (reduced levels of RBC) [115] and remains one of the primary causes of morbidity and mortality during cancer treatment [146]. To evaluate myelotoxicity, which is the CARB-PTX DLT, total cell counts of WBC, RBC and PLT as well as their related parameters were investigated.

Except for ET-LPS and COMBI-1, no significant difference in terms of WBC counts in any group with IV-vehicle was reported 24h after the last administration or after one week of recovery **(Figure 85.A)**. The significantly higher MON, GRA and LYM retrieved in the blood for COMBI-1 in comparison with IV-CARB-PTX seemed to be related to the AM and NT-GRA recruitments detected in BALF following DPI-0.5 administrations, 24h after the last administration **(Figure 81, Figure 82.A and Figure 83.A)**. This increase was intensified when combined on the same day with IV-CARB-PTX, as discussed previously and with regard to the result obtained with ET-LPS groups (higher MON, GRA and LYM than in the IV-vehicle group). Indeed, MON, the principal immune effector cells, are retrieved in circulating blood (40%) and in all tissues in a steady state (60%) [151]. They are capable of differentiating into macrophages or dendritic cells as soon as they cross the endothelium [296]. In the case of inflammation, their number is increased to ensure phagocytosis [163]. Following this innate response, dendritic cells can migrate to lymph nodes and induce an immune reaction by stimulating LYM. In parallel, GRA basophils release histamine and serotonin to maintain the acute-phase response [163]. This explains how MON, GRA (mainly NT-GRA and basophils) and LYM were recruited in the early phase of pulmonary inflammation following DPI-0.5 administration and how they were retrieved in both blood and BALF **(Figure 81, Figure 82.A and Figure 83.A)**.

One week later, both total BALF cells and WBC counts for COMBI-1 were reversible and similar to those of the IV-vehicle group. However, the proportion of GRA and LYM in blood remained significantly higher than the baseline and for IV doublets, as observed for the NT-GRA proportion in BALF **(Figure 81.A and Figure 82.A)**. The similarity between these trends confirmed that the WBC count increases seemed related to pulmonary inflammation.

The evaluation of anaemia demonstrated a higher RBC count (polycythaemia), MCHC, Hb, Ht and RDW for COMBI-1 one week earlier than for the IV doublets, while no significant difference was reported with the other combination groups **(Figure 85.B and Table 19)**. In addition, as described above, COMBI-1 also induced an increased plasma GRA proportion in the blood **(Figure 85.A)**. It has been reported that both of these observations are increased as a

response to anaemia, as erythropoietin production is raised and may be detected from a higher RBC count, Hb and Ht, describing polycythaemia [151]. Indeed, it has been described that an increase in RBC count (polycythaemia) is observed 7-14 days after an acute drop due to bone-marrow erythrocyte production, depending on the species [149]. This may explain why the RBC counts of IV doublets were higher after one week of recovery. The last IV administration could have led to a drop in RBC and to their generation 7 days later, which corresponded to the results from the second sampling time **(Figure 85.B)**.

The observed anaemia might be attributed to carboplatin as it is was reported that carboplatin was able to destroy mature RBC (haemolysis) through three different mechanisms [149]. Moreover, higher MCV (macrocytosis) was found in the mice treated with COMBI-1 and COMBI-1-24 **(Table 19)** and is described as often associated with polycythaemia in mice undergoing exuberant regenerative responses to anaemia [151]. Reports of macrocytosis for patients undergoing chemotherapy remain rare but it is has been associated with patients undergoing antimetabolite-based chemotherapy treatment [297]. However, a recent study reported that macrocytosis was also associated with CARB-PTX doublet in ovarian cancer patients [298].

Thrombocytopenia was investigated by means of PLT count. The results from IV-CARB-PTX and IV-CARB-PTX-0.75 24h after the last treatment demonstrated that the strategy of dose reduction of 25%, as in clinical practice, was successful to prevent a PLT count drop **(Figure 85.C)**. Moreover, the strategy of delaying the administrations by 24h was also promising as no significant difference in PLT counts was observed for COMBI-1-24h in comparison with the IV-vehicle group, at either sampling time. However, PLT count decrease was observed and/or worsened one week later for the IV doublet groups. This has already been observed 24h after the last administration for IV-CARB-PTX, COMBI-1 and COMBI-0.75. For the RBC count, our hypothesis is that the addition of DPI-0.5 may have led to earlier thrombocytopenia for the combination groups, which was reversible within one week. Moreover, no significance difference in MPV was observed for any group at either sampling time. This showed that no higher PLT production due to hypoxia-induced thrombocytopenia was observed [151], which was consistent with our previous observations.

Furthermore, it was interesting to observe that total PLT counts for ET-LPS_rec were significantly lower than for the IV-vehicle group ($p < 0.01$, 703 ± 62 x 10^3 cells/mm^3 *vs.* 930 ± 39 x 10^3 cells/mm^3, **Figure 85.C**). PLT are known to be recruited at the site of inflammation as

they have important roles in the inflammation initiation by *(i)* secreting adhesion molecules to aggregate with WBC and *(ii)* stimulating NT-GRA, MON and LYM using chemotactic chemokines for WBC to form aggregates and launch inflammation [299]. Consequently, a reduced number of circulating PLT could be available for cell count if there is local inflammation [299]. This is also a hypothesis for the reduction in PLT for COMBI-1 and COMBI-0.75 24h after the last administration **(Figure 85.C)**.

The comparison between COMBI-1 and COMBI-1-24h in terms of pulmonary and haematological tolerance was interesting for the evaluation of the added value of the 24h delay between IV doublets and DPI-0.5 administration in the design of the regimens. A significantly lower proportion of NT-GRA in BALF ($p < 0.05$) together with lower WBC ($p < 0.001$) and PLT counts ($p < 0.01$) in blood were detected for COMBI-1-24h in comparison with COMBI-1. This demonstrated that staggering the administrations by 24h seemed to avoid *(i)* the recruitment of pro-inflammatory cells in BALF (especially NT-GRA) and consequently in blood (WBC count) as well as *(ii)* the sequestration of PLT in the lungs leading to higher PLT in blood available for count.

Considering all these results, even if the combination groups (COMBI-1, COMBI-0.75) induced thrombocytopenia, the addition of DPI-0.5 to IV chemotherapy did not induce higher thrombocytopenia than was observed with IV doublets. Therefore thrombocytopenia induced by COMBI-1 and COMBI-0.75 was considered as light. This result was not surprising as DPI-0.5 alone did not induce any form of thrombocytopenia. Moreover, considering all the mouse groups and all the blood parameters, total WBC counts ranged between 2.9 ± 0.2 x 10^3 and 10 ± 2 x 10^3 cells/mm^3 and PLT counts between 507 ± 38 x 10^3 and 958 ± 33 x 10^3 cells/mm^3. These values are still considered as normal for BALB/c mice, as described in the literature (WBC: $\sim$ 3-13 x 10^3 cells/mm^3 and PLT: $\sim$ 400-1600 x 10^3 cells /mm^3) [300,301]. This showed that the significant fluctuations from the treated groups in comparison with the IV-vehicle group do not describe major toxicities for these combinations. These combinations can therefore be considered as potential therapeutic options.

Overall, the co-administration of DPI-0.5 and IV doublets, regardless of the regimen and doses, did not induce any major bw losses or pulmonary, renal or haematological toxicities. Therefore these groups should be considered as possible therapeutic options as they were all associated with higher pulmonary cytotoxicity. It is probable that the strategies of dose reduction by 25%

or a delay in administrations would hinder the full potential of CIS-DPI-ET and CARB-PTX-IV combinations. Indeed, a 24h-delay would further give to the tumour the opportunity to grow (i.e. as it is not exposed to cisplatin locally) than if both administrations (CIS-PDI-ET and CARB-PTX-IV) were performed the same day. In a similar way, a 25%-reduced IV dose would lead to a lower efficacy than a total IV dose, as there is a clear established dose-response relationship for cytotoxic drugs. However, even considering both of these strategies, a therapeutic intensification is expected, in comparison to the well-spaced conventional chemotherapy cycles [24].

However, these groups demonstrated several differences. Indeed, COMBI-1 induced significantly higher BALF cell counts, in part due to the recruitment of the NT-GRA proportion in BALF in comparison with IV-CARB-PTX. This was related to higher MON, LYM and GRA in blood than IV-CARB-PTX. Moreover, regenerative anaemia (polycythaemia and macrocytosis) was observed one week earlier than with IV-CARB-PTX. Although thrombocytopenia was detected for this group (COMBI-1), this was not significantly different from its occurrence with IV-CARB-PTX. Consequently, except for a recruitment of pro-inflammatory cells in BALF and inducement of regenerative anaemia earlier than the IV chemotherapy, COMBI-1 did not induce any other toxicity than with IV-CARB-PTX.

Furthermore, the strategy of reducing the CARB-PTX dose by 25% (IV-CARB-PTX-0.75) also increased the proportion of NT-GRA in BALF in comparison with IV doublets, in a lower proportion than COMBI-1, with no major WBC, RBC or PLT count differences with IV-CARB-PTX-0.75. However, the strategy of delaying the administrations by 24h (COMBI-1-24h) seemed to avoid pro-inflammatory cell (mostly NT-GRA) recruitment in BALF as well as WBC, RBC and PLT differences in comparison with IV-CARB-PTX. Moreover, none of these groups demonstrated higher AKI in comparison to IV doublets. Consequently, all these combination groups seemed interesting to be investigated in future efficacy studies.

5. <u>Conclusion</u>

The administration of a controlled-release cisplatin-based DPI formulation (CIS-DPI-50) in the lungs three times a week for 2 consecutive weeks, did not lead to any sign of myelotoxicity, AKI or pulmonary inflammation except for a transient NT-GRA increase. The addition of DPI-0.5 to IV-CARB-PTX on the same day at their MTD induced a higher WBC and BALF cell counts, a higher NT-GRA proportion in BALF and earlier regenerative anaemia than with IV-

CARB-PTX alone. The strategy of IV dose reduction by 25% and the separation of DPI-0.5 and IV-CARB-PTX administration by 24h avoided regenerative anaemia and/or BALF and WBC increase when compared to their respective IV doublets. Interestingly, all the combination groups induced non-reversible higher cytotoxicity (total protein concentration and LDH activity) than the non-treated groups. These combination strategies were well-tolerated overall and should be considered for the evaluation of their efficacy on preclinical lung carcinoma models. Indeed, it could be interesting to identify their potential in comparison with the combinations with IV-cisplatin based chemotherapy.

GENERAL CONCLUSIONS AND PERSPECTIVES

This work has demonstrated the feasibility of optimizing and administering a cisplatin-based DPI (CIS-DPI-50) with controlled-release and lung-retention properties during the off-cycles encountered with the conventional IV chemotherapy, in terms of tolerance and efficacy in mice. Regarding the *in vivo* results generated so far, this treatment intensification should be considered for lung cancer therapy, as its added value in terms of efficacy tended to be demonstrated in a preclinical model with no higher toxicities than the conventional treatment alone. These general conclusions were supported by the results generated in the four parts of this work.

In the first experimental part of this work, we optimized the cisplatin-based DPI formulation developed by Vincent Levet during his thesis. This optimization consisted of the replacement of TS by HCO, a more hydrophilic lipid than TS. Thanks to its higher hydrophilicity, HCO allowed us to produce the powder with an initial concentration 2-fold higher than that developed so far by Levet *et al.* [187], thus reducing the manufacturing time. In addition, unlike TS, this pharmaceutical-grade excipient is already used for other delivery routes and considered as GRAS by the FDA, and so should necessitate fewer experiments to be accepted for inhalation than non-recognized excipients. However, the safety and tolerability of this excipient should be investigated following ICH guidelines prior to the clinical stage. Moreover, as expected, this higher hydrophilicity led to a quicker cisplatin burst effect during the *in vitro* release, which had an impact on the PK parameters. This impact led to a higher clearance *in vivo* from mouse lungs into the blood than with the formulation developed with Levet *et al.*, which demonstrated a lower release fraction from the particles. However, even with this higher burst effect, the controlled-release and the lung-retention properties were maintained with a lung T_a comprised between the immediate- and controlled-release DPI developed by Levet *et al.* Indeed, as the previous formulation administered at its MTD in the M109-HiFR lung carcinoma orthotopic mouse model showed a level of significance lower than those obtained with CIS-IV, we aimed to increase the cisplatin release from the microparticles to boost its efficacy while maintaining a good tolerance.

In addition, CIS-DPI-50 was produced using scalable processes over three batches and showed low variations among them, with interesting *in vitro* characteristics. CIS-DPI-50 was characterized by good aerodynamic performance with low dependency on air flow using a single-dose low-resistance RS.01 inhaler, selected from four devices. Indeed, CIS-DPI-50 showed good aerosolization and aerodynamic performance even at 40 L/min. This is crucial as lung cancer patients often have impaired lung function, leading to lower inspiratory peak

airflow. Moreover, the stability data generated over 6 months at normal conditions (25°C, 60% RH) showed limited variations over time, mainly due to the stabilisation of the *β*-form of HCO as well as the crystalline state of cisplatin, and to the limited residual solvent content. However, the stability of this formulation over drastic conditions (40°C, 75% RH), as recommended by the FDA, should be further investigated. The PK study conducted on healthy mice showed interesting lung retention with limited systemic and renal exposure, in comparison to CIS-IV. This confirmed the lung targeting of this formulation administered using the ET route.

An important perspective from the formulation side would be the scale-up of the process to produce clinical batches, as well as the evaluation of the effect of industrial capsule-filling on the *in vitro* characteristics prior to the clinical stage.

The second part of this work aimed to characterize the biodistribution of CIS-DPI-50 on LLC1-*Luc*-grafted mice and to investigate whether the potential of CIS-DPI-50 in tumour targeting would be demonstrated. A single administration of CIS-DPI-50 at 0.5 mg/kg in LLC1-*Luc*-grafted mice showed a prolonged tumour exposure, with limited exposure in tumour-free lungs and plasma, in contrast to that was observed for CIS-IV even at a 4-fold higher dose. Moreover, this part also aimed to select the regimen of administration of CIS-DPI-50 as a monotherapy that can be combined to the conventional chemotherapy IV treatment. This was achievable by finding the best balance between tolerance and efficacy.

The repeated administrations of CIS-DPI-50 in LLC1-*Luc*-grafted mice following different doses and schemes of administration were well tolerated overall with limited bw losses and good pulmonary tolerance of tumour-free lungs. These regimens did not show any significant difference in terms of cisplatin activity, or tumour size in comparison to untreated groups, due to the lack of sensitivity of LLC1-*Luc* to cisplatin. Moreover, they showed similar concentrations in the tumour, tumour-free lungs, kidneys and plasma than a single administration of CIS-DPI-50. This was observed for all the regimen over a one-cycle treatment. Following the second cycle, the platinum accumulation was more intense in tumour-free lungs, kidneys and plasma and lower in tumours. This was correlated to limited penetration in the increased tumour mass, but also, and more importantly, to the moribund overall condition of the animals, mostly due to the lack of sensitivity of LLC1-*Luc* to cisplatin. Therefore, the regimens with the lowest cumulative dose (0.5 mg/kg administered three times/cycle and 0.3 mg/kg administered five times/cycle) were selected to be combined with IV chemotherapy as this treatment can on its own induce DLT. These regimens were evaluated in terms of efficacy on the M109-HiFR-*Luc2* model, which is more sensitive to cisplatin than LLC1-*Luc*. Results

showed no difference in terms of tumour size, proportion of responders and survival but with higher platinum in kidneys for the groups treated every day. Therefore, the regimen with the more spaced administrations was selected to avoid cumulative toxicities, as it is intended to be combined to the conventional treatment, which is already highly nephrotoxic.

Consequently, following the results generated, it was essential to investigate the tolerance in tumour-free lungs and in kidneys of repeated administration of CIS-DPI-50 at the selected regimen. Therefore, the third part of this work focused on the evaluation of the pulmonary and renal tolerance using early biomarkers (chemokines, cytokines) of inflammation and cytotoxicity in BALF (lung tolerance), and in plasma (renal tolerance), along with a lung and renal tissue histological investigation.

Except for NT-GRA recruitment, results from this first investigation regarding the use of monotherapies showed a better pulmonary and renal tolerance profile of repeated CIS-DPI-50 at 1 mg/kg than with CIS-IV at 2 mg/mL. This was certainly attributed to the controlled release of cisplatin from CIS-DPI-50 particles in comparison with the total solubilized fraction of cisplatin following CIS-IV_2 injection. However, the next step of the development is a preclinical toxicity programme following ICH guidelines on the formulation prior to a first-in-human study.

As we aim to combine a CIS-DPI-50 monotherapy regimen to CIS-IV, it was useful to evaluate both pulmonary and renal tolerance of these combined regimens to select the one with the lowest tolerance impairment. Results from that study showed pulmonary and renal tolerance impairment for the group treated with CIS-DPI-50 and CIS-IV at their respective MTDs. Fractionating the total dose between IV and DPI (i.e. decreasing the IV dose by 25%) was a good strategy to improve lung tolerance and to allow AKI be reversible within one week. Staggering CIS-DPI-50 from IV administrations by 24h was enough to prevent any signs of AKI, as no difference was observed with the longer staggering of 48h. Considering the results provided in the second part, in terms of platinum accumulation in grafted mice, the evaluation of pulmonary and renal tolerance on grafted mice should be investigated in future studies. Indeed, following repeated administrations of CIS-DPI-50, higher platinum concentrations were retrieved in plasma and kidneys, which could be attributed to the effect of repeated treatment administration, to an impaired clearance function due to the presence of tumours, and/or to the degradation of the overall condition. The tolerance results that we obtained in healthy mice could be interesting to compare to those obtained in grafted mice. Moreover, it

could be interesting to investigate AKI using urinary biomarkers during the preclinical toxicity programme following ICH guidelines. Indeed, they can provide complementary indications on the initiation, progression and reversibility of AKI. This could be evaluated in rats to overcome the limitations encountered with mice in terms of urine volumes and availability.

The combined regimen selected during the tolerance study (CIS-IV dose reduced by 25%, with a staggering of 24h from CIS-IV administration) was therefore selected to assess its efficacy in the M109-HiFR-*Luc2* lung carcinoma model. Results from this study tended to show an improvement in terms of tumour growth, percentage of responders and survival. This was encouraging and demonstrated that the selected CIS-DPI-50 could be a good strategy to be proposed as an add-on treatment to intensify the therapeutic response of cisplatin-based doublets in lung cancer therapy. This perspective also involves the addition of CIS-DPI-50 during the off-cycles encountered with pemetrexed-cisplatin for SCLC patients. Indeed, as mentioned in the introductory part of this work, conventional chemotherapy remains the most recommended therapeutic option for these patients.

It should be taken into account that the M109-HiFR lung carcinoma model is very aggressive and the potential of CIS-DPI-50 could have been hindered. Indeed, it should be interesting to evaluate the efficacy of the combination between CIS-DPI-50 and the conventional chemotherapy treatment in a model that offers the possibility to administer several cycles of administration (i.e. slower tumour progression). In this case, the doses could be adapted to limit the accumulation of toxicities. Moreover, it could be interesting to monitor biomarker levels repeatedly by sampling blood during the treatment cycle (i.e., not just at the end of each cycle). This was not achievable in mice, but may be considered during preclinical studies on healthy rats, for example. Moreover, it could be interesting to consider the administration of CIS-DPI-50 every day as this tended to demonstrate a higher platinum accumulation in the tumour and would therefore be related to an increased efficacy. However, this can be achievable only if both pulmonary and renal tolerance are maintained. Last but not least, it is important to mention that it was not possible to monitor mouse hydration before, during and after the treatment administration, which is performed for humans following the administration of IV cisplatin. Therefore, it is probable that with an appropriate hydration protocol in humans, the adaptations in terms of dose reductions and delays needed in mice will not be required. However, the optimization of the hydration protocol should be closely managed in clinics.

Moreover, considering the adaptations that were needed to avoid cumulative toxicities and were reported in our previous study, it is possible that the potential of the combination of CIS-DPI-50 with the conventional chemotherapy treatment would have been limited. Therefore, it was interesting to evaluate the combination of CIS-DPI-50 with a less nephrotoxic drug such as carboplatin, which would necessitate fewer adjustments (i.e. dose adjustment and administration delays).

As carboplatin is intended to be combined to paclitaxel in the conventional chemotherapy doublet, and as they have both the same DLT (i.e. myelosuppression), it was mandatory to investigate the myelosuppression in addition to the pulmonary and renal tolerance. The overall results from this tolerance study showed that the combinations composed of CIS-DPI-50 and carboplatin-paclitaxel IV doublet were better tolerated in general (bw), as well as in terms of pulmonary and renal tolerance, than those obtained in combination with IV cisplatin. The addition of CIS-DPI-50 to the carboplatin-paclitaxel doublet the same day at their respective MTD showed higher WBC counts in plasma and BALF with a higher neutrophil (mainly granulocytes) proportion in BALF and earlier regenerative anaemia than with the IV doublet alone. However, all these observations were reversible in one week. The reduction of the IV dose by 25% and the staggering of CIS-DPI-50 administration from the IV-doublet by 24h avoided regenerative anaemia and/or BALF and WBC increase when compared to their respective IV doublets. Above all, all the combination groups induced non-reversible higher cytotoxicity (total protein concentration and LDH activity) than the non-treated groups, demonstrating their potential in terms of efficacy for lung cancer therapy.

An overall perspective for these regimens is the evaluation of their efficacy once combined with immunotherapy, and more specifically with immune checkpoint inhibitors. Indeed, as this carboplatin-paclitaxel IV doublet remains a first-line therapy for advanced or metastatic disease in combination with immunotherapy (in the case of PD-L1, tumour proportion score < 50%) [24], it could be interesting to evaluate the added value of a localized treatment in grafted mice. This is interesting as increased CD3 staining was observed for the groups treated with CIS-DPI-50 in comparison to untreated grafted mice. The quantification of CD3, as a positive fraction area as performed for caspase 3, could be done to evaluate the involvement of the immune system following the administration of CIS-DPI-50. This can also be assessed for CD8 marker to specifically identify cytotoxic T LYM, that play a crucial role in killing tumour cells [53]. This is particularly interesting considering that cisplatin has immunomodulatory properties and can contribute to transforming cold tumours (i.e. lacking pre-existing tumour T

LYM) to hot and immunologically active tumours [302]. This can be done through the recruitment of antigen-presenting cells (e.g. dendritic cells) as well as the stimulation of TLR4 receptors, thus inducing a pro-inflammatory state [101].

Moreover, this perspective is promising as preliminary results from the combination of repeated CIS-DPI-50 with anti-PD-1 showed a significantly faster response to the treatment in terms of tumour size, along with a reduced tumour growth, than reported for anti-PD-1 monotherapy alone. This was confirmed by the proportion of responders, which was higher for the combination group in comparison to anti-PD-1 alone. Moreover, reports from the KEYNOTE-042 study showed that the anti-tumour response to immunotherapy is often delayed by more than 6 months, leading to a higher efficacy in groups treated with conventional chemotherapy than those treated with immunotherapy alone [303]. Therefore, the combination of CIS-DPI-50-carboplatin/paclitaxel regimen and immunotherapy could lead to an earlier anti-tumour response, preventing tumour growth in NSCLC patients with a PD-L1 tumour proportion score of < 50% thus increasing its efficacy. Another possible combination is of CIS-DPI-50 and anti-PD-L1 for lung cancer patients with a tumour proportion score of > 50%.

This work showed the feasibility of combining a localized cisplatin-based DPI treatment with conventional IV chemotherapy (cisplatin and with carboplatin-paclitaxel doublets) in terms of tolerance. Efficacy results tended to demonstrate its potential in combination with IV chemotherapy (cisplatin-paclitaxel doublet) in an aggressive lung carcinoma model on mice. However, this work opens the door to a wide range of combinations with other therapies to select the indications for which cisplatin-based inhaled chemotherapy would be the most effective and most suitable option considering the different lung cancer stages.

BIBLIOGRAPHY

[1]   H. Sung, J. Ferlay, R.L. Siegel, M. Laversanne, I. Soerjomataram, A. Jemal, F. Bray, Global cancer statistics 2020: GLOBOCAN estimates of incidence and mortality worldwide for 36 cancers in 185 countries, CA. *Cancer J. Clin*. 71 (2021) 209–249. https://doi.org/10.3322/caac.21660.

[2]   Globocan 2020, Belgium cancer fact sheet, 2021. https://gco.iarc.fr/today/data/factsheets/populations/56-belgium-fact-sheets.pdf.

[3]   Belgium Cancer Registry, Cancer Fact Sheet Lung cancer, (2017).

[4]   B.C. Bade, C.S. Dela Cruz, Lung cancer 2020: Epidemiology, etiology, and prevention, *Clin. Chest Med*. 41 (2020) 1–24. https://doi.org/10.1016/j.ccm.2019.10.001.

[5]   C.R. MacRosty, M.P. Rivera, Lung cancer in women: A modern epidemic, *Clin. Chest Med*. 41 (2020) 53–65. https://doi.org/10.1016/j.ccm.2019.10.005.

[6]   J. Jeon, T.R. Holford, D.T. Levy, E.J. Feuer, P. Cao, J. Tam, L. Clarke, J. Clarke, C.Y. Kong, R. Meza, Smoking and lung cancer mortality in the United States from 2015 to 2065: A comparative modeling approach, *Ann. Intern. Med*. 169 (2018) 684–693. https://doi.org/10.7326/M18-1250.

[7]   J. Ferlay, M. Ervik, F. Lam, M. Colombet, L. Meryl, M. Piñeros, A. Znaor, I. Soerjomataram, F. Bray, Global cancer observatory: cancer today, *Int. Agency Res. Cancer*. (2020). https://gco.iarc.fr/today (accessed May 19, 2021).

[8]   G. Tegin, H.M. Mekala, S.K. Sarai, S. Lippmann, E-cigarette toxicity?, *South. Med. J.* 111 (2018) 35–38. https://doi.org/10.14423/SMJ.0000000000000749.

[9]   L.G. Collins, C. Haines, R. Perkel, R.E. Enck, Lung cancer: Diagnosis and management, *Am. Fam. Physician*. 75 (2007) 56–63.

[10]   T. Lu, X. Yang, Y. Huang, M. Zhao, M. Li, K. Ma, J. Yin, C. Zhan, Q. Wang, Trends in the incidence, treatment, and survival of patients with lung cancer in the last four decades, *Cancer Manag. Res*. 11 (2019) 943–953. https://doi.org/10.2147/CMAR.S187317.

[11]   National Cancer Institute, SEER Cancer Stat Facts: Lung and bronchus cancer., (2020). https://seer.cancer.gov/statfacts/html/lungb.html (accessed May 19, 2021).

[12]   N. Duma, R. Santana-Davila, J.R. Molina, Non–small cell lung cancer: Epidemiology, screening, diagnosis, and treatment, *Mayo Clin. Proc*. 94 (2019) 1623–1640. https://doi.org/10.1016/j.mayocp.2019.01.013.

[13]   W. D.Travis, E. Brambilla, H.K. Muller-Hermelink, C. C.Harris, Pathology & Genetics-Tumours of the lung, pleura, thymus and heart, WHO Classif. Tumours. (2004) 344.

[14]   C. Zappa, S.A. Mousa, Non-small cell lung cancer: Current treatment and future advances, *Transl. Lung Cancer Res*. 5 (2016) 288–300. https://doi.org/10.21037/tlcr.2016.06.07.

[15]   G.S. Shroff, N. Kalhor, R.J. Mehran, P.M. De Groot, B.W. Carter, Staging of small-cell lung cancer, *Diagnostic Imaging Thorac. Surg*. (2018) 175–188. https://doi.org/10.1007/978-3-319-89893-3.

[16]   W.D. Travis, E. Brambilla, A.G. Nicholson, Y. Yatabe, J. Austin, M.B. Beasley, L. Chirieac, S. Dacic, E. Duhig, D.B. Flieder, K. Geisinger, F. Hirsch, Y. Ishikawa, K. Kerr, M. Noguchi, G. Pelosi, C. Powell, M.S. Tsao, I. Wistuba, The 2015 WHO classification of lung tumors-impact of genetic, clinical and radiologic advances since the 2004 classification, *J. Thorac. Oncol*. 10 (2015) 1243–1260. https://doi.org/DOI: 10.1097/JTO.0000000000000630.

[17]   H.J. De Koning, C.M. Van Der Aalst, P.A. De Jong, E.T. Scholten, K. Nackaerts, M.A. Heuvelmans, J.W.J. Lammers, C. Weenink, U. Yousaf-Khan, N. Horeweg, S. Van'T Westeinde, M. Prokop, W.P. Mali, F.A.A. Mohamed Hoesein, P.M.A. Van Ooijen, J.G.J.V. Aerts, M.A. Den Bakker, E. Thunnissen, J. Verschakelen, R. Vliegenthart, J.E. Walter, K. Ten Haaf, H.J.M. Groen, M. Oudkerk, Reduced lung-cancer mortality with volume CT screening in a randomized trial, *N. Engl. J. Med*. 382 (2020) 503–513. https://doi.org/10.1056/NEJMoa1911793.

[18]   The national lung screening trial research team, Reduced lung-cancer mortality with low-dose computed tomographic screening, *N Engl J Med*. 365 (2011) 395–409. https://doi.org/10.1056/NEJMoa1102873.Reduced.

[19]   P.C. Prorok, G.L. Andriole, R.S. Bresalier, S.S. Buys, D. Chia, E.D. Crawford, R. Fogel, E.P. Gelmann, F. Gilbert, M.A. Hasson, R.B. Hayes, C.C. Johnson, J.S. Mandel, A. Oberman, B. O'Brien, M.M. Oken, S. Rafla, D. Reding, W. Rutt, J.L. Weissfeld, L. Yokochi, J.K. Gohagan, Design of the prostate, lung, colorectal and ovarian (PLCO) cancer screening trial, *Control. Clin. Trials*. 21 (2000) 273–309. https://doi.org/10.1016/s0197-2456(00)00098-2.

[20]   H. Soda, S. Kohno, M. Oka, H. Tomita, Limitation of annual screening chest radiography for the diagnosis of lung cancer. A retrospective study, *Cancer*. 72 (1993) 2341–2346.

[21]   P.B. Bach, J.N. Mirkin, T. Oliver, C. Azzoli, D. Berry, O. Brawley, T. Byers, G. Colditz, M. Gould, J. Jett, A. Sabichi, R. Smidth-Bindman, D. Wood, A. Qaseem, F. Detterbeck, Benefits and harms of CT screening for lung cancer: a systematic review, *JAMA*. 307 (2012) 2418–2429. https://doi.org/10.1001/jama.2012.5521.

[22]   V.A. Moyer, Screening for lung cancer: U.S. preventive services task force recommendation statement, *Ann. Intern. Med*. 160 (2014) 330–338. https://doi.org/10.7326/m13-2771.

[23]   H.U. Kauczor, A.M. Baird, T.G. Blum, L. Bonomo, C. Bostantzoglou, O. Burghuber, B. Čepická, A. Comanescu, S. Couraud, A. Devaraj, V. Jespersen, S. Morozov, I.N. Agmon, N. Peled, P. Powell, H. Prosch, S. Ravara, J. Rawlinson, M.P. Revel, M. Silva, A. Snoeckx, B. van Ginneken, J.P. van Meerbeeck, C. Vardavas, O. von Stackelberg, M. Gaga, ESR/ERS statement paper on lung cancer screening, *Eur. Respir. J.* 55 (2020) 1–18. https://doi.org/10.1183/13993003.00506-2019.

[24]   NCCN Guidelines - NSCLC- Version 3.2020, 2020.

[25]   P.E. Postmus, K.M. Kerr, M. Oudkerk, S. Senan, D.A. Waller, J. Vansteenkiste, C. Escriu, S. Peters, Early and locally advanced non-small-cell lung cancer (NSCLC): ESMO clinical practice guidelines for diagnosis, treatment and follow-up, *Ann. Oncol.* 28 (2017). https://doi.org/10.1093/annonc/mdx222.

[26]   P. Villalobos, I. Wistuba, Lung cancer biomarkers, *Hematol Oncol Clin North Am*. 31 (2017) 13–29. https://doi.org/10.1016/j.hoc.2016.08.006.

[27]   D. Planchard, S. Popat, K. Kerr, S. Novello, E.F. Smit, C. Faivre-Finn, T.S. Mok, M. Reck, P.E. Van Schil, M.D. Hellmann, S. Peters, Metastatic non-small cell lung cancer: ESMO Clinical Practice Guidelines for diagnosis, treatment and follow-up, *Ann. Oncol.* 29 (2020). https://doi.org/10.1093/annonc/mdy275.

[28]   F.C. Detterbeck, D.J. Boffa, A.W. Kim, L.T. Tanoue, The Eighth edition lung cancer stage classification, *Chest*. 151 (2017) 193–203. https://doi.org/10.1016/j.chest.2016.10.010.

[29]   W. Lim, C.A. Ridge, A.G. Nicholson, S. Mirsadraee, The 8th lung cancer TNM classification and clinical staging system: Review of the changes and clinical implications, *Quant. Imaging Med. Surg*. 8 (2018) 709–718. https://doi.org/10.21037/qims.2018.08.02.

[30]   F.R. Hirsch, G. V. Scagliotti, J.L. Mulshine, R. Kwon, W.J. Curran, Y.L. Wu, L. Paz-Ares, Lung cancer: current therapies and new targeted treatments, *Lancet*. 389 (2017) 299–311. https://doi.org/10.1016/S0140-6736(16)30958-8.

[31]   J. Galon, F. Pagès, F.M. Marincola, M. Thurin, G. Trinchieri, B.A. Fox, T.F. Gajewski, P.A. Ascierto, The immune score as a new possible approach for the classification of cancer, *J. Transl. Med*. 10 (2012) 1. https://doi.org/10.1186/1479-5876-10-1.

[32]   D.S. Zander, C.F. Farver, Molecular basis of pulmonary disease, in: *Mol. Pathol.,* 2018: pp. 347–381. https://doi.org/10.1016/B978-0-12-802761-5.00018-3.

[33]   H. Iwata, Adenocarcinoma containing lepidic growth, *J. Thorac. Dis*. 8 (2016) E1050–E1052. https://doi.org/10.21037/jtd.2016.08.78.

[34]   K.J. Butnor, Controversies and challenges in the histologic subtyping of lung adenocarcinoma, *Transl. Lung Cancer Res*. 9 (2020) 839–846. https://doi.org/10.21037/tlcr.2019.12.30.

[35]   B.Y. Wang, J.Y. Huang, H.C. Chen, C.H. Lin, S.H. Lin, W.H. Hung, Y.F. Cheng, The comparison between adenocarcinoma and squamous cell carcinoma in lung cancer patients, *J. Cancer Res. Clin. Oncol.* 146 (2020) 43–52. https://doi.org/10.1007/s00432-019-03079-8.

[36]   M. Majem, O. Juan, A. Insa, N. Reguart, J.M. Trigo, E. Carcereny, R. García-Campelo, Y. García, M. Guirado, M. Provencio, SEOM clinical guidelines for the treatment of non-small cell lung cancer, *Clin. Transl. Oncol.* 21 (2019) 3–17. https://doi.org/10.1007/s12094-018-1978-1.

[37]   P.M. Forde, D.S. Ettinger, Targeted therapy for non-small-cell lung cancer: past, present and future, *Expert Rev Anticancer Ther*. 13 (2013) 745–758. https://doi.org/doi:10.1586/era.13.47.

[38]   L. Falzone, S. Salomone, M. Libra, Evolution of cancer pharmacological treatments at the turn of the third millennium, *Front. Pharmacol*. 9 (2018). https://doi.org/10.3389/fphar.2018.01300.

[39]   J. Dong, B. Li, D. Lin, Q. Zhou, D. Huang, Advances in targeted therapy and immunotherapy for non-small cell lung cancer based on accurate molecular typing, *Front. Pharmacol*. 10 (2019) 1–10. https://doi.org/10.3389/fphar.2019.00230.

[40] R. G. Salloum, T. J.Smith, G. A.Jensen, J. Elston Lafata, Survival among non-small cell lung cancer patients with poor performance status after first line chemotherapy, *Lung Cancer*. 77 (2008) 545–549. https://doi.org/doi:10.1016/j.lungcan.2012.04.019.

[41] D. Planchard, S. Popat, K. Kerr, S. Novello, E.F. Smit, C. Faivre-Finn, T.S. Mok, M. Reck, P.E. Van Schil, M.D. Hellmann, S. Peters, Metastatic non-small cell lung cancer: ESMO clinical practice guidelines for diagnosis, treatment and follow-up, *Ann. Oncol*. 29 (2018). https://doi.org/10.1093/annonc/mdy275.

[42] J.H. Schiller, D. Harrington, C.P. Belani, C. Langer, A. Sandler, J. Krook, J. Zhu, D.H. Johnson, Comparison of four chemotherapy regimens for advanced non-small-cell lung cancer, *N. Engl. J. Med*. 346 (2002) 92–98. https://doi.org/10.1056/NEJMoa011954.

[43] M.A. Socinski, Update on taxanes in the first-line treatment of advanced non-small-cell lung cancer, *Curr. Oncol*. 21 (2014) 691–703. https://doi.org/10.3747/co.21.1997.

[44] E. Quoix, G. Zalcman, J.P. Oster, V. Westeel, E. Pichon, A. Lavolé, J. Dauba, D. Debieuvre, P.J. Souquet, L. Bigay-Game, E. Dansin, M. Poudenx, O. Molinier, F. Vaylet, D. Moro-Sibilot, D. Herman, J. Bennouna, J. Tredaniel, A. Ducoloné, M.P. Lebitasy, L. Baudrin, S. Laporte, B. Milleron, Carboplatin and weekly paclitaxel doublet chemotherapy compared with monotherapy in elderly patients with advanced non-small-cell lung cancer: IFCT-0501 randomised, phase 3 trial, *Lancet*. 378 (2011) 1079–1088. https://doi.org/10.1016/S0140-6736(11)60780-0.

[45] M. Zukin, C.H. Barrios, J.R. Pereira, R.D.A. Ribeiro, C.A.D.M. Beato, Y.N. Do Nascimento, A. Murad, F.A. Franke, M. Precivale, L.H.D.L. Araujo, C.S.D.R. Baldotto, F.M. Vieira, I.A. Small, C.G. Ferreira, R.C. Lilenbaum, Randomized phase III trial of single-agent pemetrexed versus carboplatin and pemetrexed in patients with advanced non-small-cell lung cancer and Eastern Cooperative Oncology Group performance status of 2, *J. Clin. Oncol*. 31 (2013) 2849–2853. https://doi.org/10.1200/JCO.2012.48.1911.

[46] Palliative Care, 2020. http://www.ninr.nih.gov/sites/www.ninr.nih.gov/files/palliative-care-brochure.pdf.

[47] M.G. Kris, R.B. Natale, R.S. Herbst, T.J. Lynch, D. Prager, C.P. Belani, J.H. Schiller, K. Kelly, H. Spiridonidis, A. Sandler, D. Cella, M.K. Wolf, S.D. Averbuch, J.J. Ochs, A.C. Kay, Efficacy of gefitinib, an inhibitor of tyrosine kinase, in symptomatic patients with non-small cell lung cancer- a randomized trial, *J. Am. Med. Assoc*. 290 (2003) 2149–2158.

[48] T.S. Mok, Y. Wu, S. Thongprasert, C. Yang, N. Saijo, P. Sunpaweravong, B. Han, B. Margono, Y. Ichinose, Y. Nishiwaki, Y. Ohe, J. Yang, B. Chewaskulyong, H. Jiang, E.L. Duffield, C.L. Watkins, A.A. Armour, M. Fukuoka, Gefitinib or carboplatin–paclitaxel in pulmonary adenocarcinoma, *N. Engl. J. Med*. 361 (2009) 947–957. https://doi.org/10.1056/NEJMoa0810699.

[49] Y. Cheng, Y. He, W. Li, H. long Zhang, Q. Zhou, B. Wang, C. Liu, A. Walding, M. Saggese, X. Huang, M. Fan, J. Wang, S.S. Ramalingam, Osimertinib Versus Comparator EGFR TKI as First-Line Treatment for EGFR-Mutated Advanced NSCLC: FLAURA China, A Randomized Study, *Target. Oncol*. 16 (2021) 165–176. https://doi.org/10.1007/s11523-021-00794-6.

[50] FDA approves lorlatinib for metastatic ALK-positive NSCLC, (2021). https://www.fda.gov/drugs/drug-approvals-and-databases/fda-approves-lorlatinib-metastatic-alk-positive-nsclc (accessed May 4, 2021).

[51] FDA approves first targeted therapy to treat aggressive form of lung cancer, (2021). https://www.fda.gov/news-events/press-announcements/fda-approves-first-targeted-therapy-treat-aggressive-form-lung-cancer (accessed May 4, 2021).

[52] FDA grants accelerated approval to tepotinib for metastatic non-small cell lung cancer, (2021). https://www.fda.gov/drugs/drug-approvals-and-databases/fda-grants-accelerated-approval-tepotinib-metastatic-non-small-cell-lung-cancer (accessed May 4, 2021).

[53] D.W. Siemann, Tumor Microenvironment, *Medicina (B. Aires)*. 56 (2020) 1–21. https://doi.org/10.1002/9780470669891.

[54] M.Z. Jin, W.L. Jin, The updated landscape of tumor microenvironment and drug repurposing, *Signal Transduct. Target. Ther*. 5 (2020). https://doi.org/10.1038/s41392-020-00280-x.

[55] FDA approves cemiplimab-rwlc for non-small cell lung cancer with high PD-L1 expression, (2021). https://www.fda.gov/drugs/resources-information-approved-drugs/fda-approves-cemiplimab-rwlc-non-small-cell-lung-cancer-high-pd-l1-expression.

[56]   T.A. Chan, M. Yarchoan, E. Jaffee, C. Swanton, S.A. Quezada, A. Stenzinger, S. Peters, Development of tumor mutation burden as an immunotherapy biomarker: Utility for the oncology clinic, *Ann. Oncol.* 30 (2019) 44–56. https://doi.org/10.1093/annonc/mdy495.

[57]   FDA approves atezolizumab for first-line treatment of metastatic NSCLC with high PD-L1 expression, (2020). https://ascopost.com/issues/june-10-2020/fda-approves-atezolizumab-for-the-first-line-treatment-of-patients-with-metastatic-nsclc-and-high-pd-l1-expression/ (accessed May 4, 2021).

[58]   EMA, Summary of product characteristics - Atezolizumab, (2021). https://doi.org/10.1163/ej.9789004166523.i-402.43.

[59]   EMA, Summary of product characteristics - Pembrolizumab, (2021). https://doi.org/10.1163/ej.9789004166523.i-402.43.

[60]   G. Mountzios, J. Remon, S. Novello, N. Blais, R. Califano, T. Cufer, A.M. Dingemans, S. V. Liu, N. Peled, N.A. Pennell, M. Reck, C. Rolfo, D. Tan, J. Vansteenkiste, H. West, B. Besse, Position of an international panel of lung cancer experts on the decision for expansion of approval for pembrolizumab in advanced non-small-cell lung cancer with a PD-L1 expression level of ≥1% by the USA Food and Drug Administration, *Ann. Oncol.* 30 (2019) 1686–1688. https://doi.org/10.1093/annonc/mdz295.

[61]   T. Berghmans, A.M. Dingemans, L.E.L. Hendriks, J. Cadranel, Immunotherapy for nonsmall cell lung cancer: A new therapeutic algorithm, *Eur. Respir. J.* 55 (2020) 1–5. https://doi.org/10.1183/13993003.01907-2019.

[62]   N.A. Rizvi, B.C. Cho, N. Reinmuth, K.H. Lee, A. Luft, M.J. Ahn, M.M. Van Den Heuvel, M. Cobo, D. Vicente, A. Smolin, V. Moiseyenko, S.J. Antonia, S. Le Moulec, G. Robinet, R. Natale, J. Schneider, F.A. Shepherd, S.L. Geater, E.B. Garon, E.S. Kim, S.B. Goldberg, K. Nakagawa, R. Raja, B.W. Higgs, A.M. Boothman, L. Zhao, U. Scheuring, P.K. Stockman, V.K. Chand, S. Peters, Durvalumab with or Without Tremelimumab vs Standard Chemotherapy in First-line Treatment of Metastatic Non-Small Cell Lung Cancer: The MYSTIC Phase 3 Randomized Clinical Trial, *JAMA Oncol.* 6 (2020) 661–674. https://doi.org/10.1001/jamaoncol.2020.0237.

[63]   FDA approves nivolumab plus ipilimumab and chemotherapy for first-line treatment of metastatic NSCLC, (2020). https://www.fda.gov/drugs/drug-approvals-and-databases/fda-approves-nivolumab-plus-ipilimumab-and-chemotherapy-first-line-treatment-metastatic-nsclc (accessed May 4, 2021).

[64]   N.H. Hanna, B.J. Schneider, S. Temin, S.B. Jr, J. Brahmer, Therapy for stage IV Non–small-cell lung cancer without driver alterations : ASCO and OH (CCO) joint guideline update, *J. Clin. Oncol.* (2020) 1–25. https://doi.org/10.1200/JCO.19.03022.

[65]   NCCN Clinical Practice Guidelines in Oncology, Small cell lung cancer- version1.2021, 2016. https://doi.org/10.1007/978-3-319-40389-2_14.

[66]   A. Rossi, M. Di Maio, P. Chiodini, R.M. Rudd, H. Okamoto, D.V. Skarlos, M. Früh, W. Qian, T. Tamura, E. Samantas, T. Shibata, F. Perrone, C. Gallo, C. Gridelli, O. Martelli, S.M. Lee, Carboplatin- or cisplatin-based chemotherapy in first-line treatment of small-cell lung cancer: The COCIS meta-analysis of individual patient data, *J. Clin. Oncol.* 30 (2012) 1692–1698. https://doi.org/10.1200/JCO.2011.40.4905.

[67]   FDA approves durvalumab for extensive-stage small cell lung cancer, 2020. (n.d.). https://www.fda.gov/drugs/resources-information-approved-drugs/fda-approves-durvalumab-extensive-stage-small-cell-lung-cancer.

[68]   R. Rosière, J. Hureaux, V. Levet, K. Amighi, N. Wauthoz, Inhaled chemotherapy – Part 1: General concept and current technological challenges, *Rev. Mal. Respir.* 35 (2018) 357–377. https://doi.org/10.1016/j.rmr.2018.02.001.

[69]   L. Zitvogel, L. Apetoh, F. Ghiringhelli, G. Kroemer, Immunological aspects of cancer chemotherapy, *Nat. Rev. Immunol.* 8 (2008) 59–73. https://doi.org/10.1038/nri2216.

[70]   A.I. Minchinton, I.F. Tannock, Drug penetration in solid tumours., *Nat. Rev. Cancer.* 6 (2006) 583–592.

[71]   J. Zugazagoitia, C. Guedes, S. Ponce, I. Ferrer, S. Molina-Pinelo, L. Paz-Ares, Current challenges in cancer treatment, *Clin. Ther.* 38 (2016) 1551–1566. https://doi.org/10.1016/j.clinthera.2016.03.026.

[72]   H. Maeda, M. Khatami, Analyses of repeated failures in cancer therapy for solid tumors: poor

tumor-selective drug delivery, low therapeutic efficacy and unsustainable costs, *Clin. Transl. Med.* 7 (2018) 1–20. https://doi.org/10.1186/s40169-018-0185-6.

[73]   W.C.M. Dempke, T. Suto, M. Reck, Targeted therapies for non-small cell lung cancer, *Lung Cancer.* 67 (2010) 257–274. https://doi.org/10.1016/j.lungcan.2009.10.012.

[74]   D.Y. Wang, J.E. Salem, J. V. Cohen, S. Chandra, C. Menzer, F. Ye, S. Zhao, S. Das, K.E. Beckermann, L. Ha, W.K. Rathmell, K.K. Ancell, J.M. Balko, C. Bowman, E.J. Davis, D.D. Chism, L. Horn, G. V. Long, M.S. Carlino, B. Lebrun-Vignes, Z. Eroglu, J.C. Hassel, A.M. Menzies, J.A. Sosman, R.J. Sullivan, J.J. Moslehi, D.B. Johnson, Fatal toxic effects associated with immune checkpoint inhibitors: A systematic review and meta-analysis, *JAMA Oncol.* 4 (2018) E1–E8. https://doi.org/10.1001/jamaoncol.2018.3923.

[75]   D.A. Yardley, Nab-Paclitaxel mechanisms of action and delivery, *J. Control. Release.* 170 (2013) 365–372. https://doi.org/10.1016/j.jconrel.2013.05.041.

[76]   N.I. Marupudi, J.E. Han, K.W. Li, V.M. Renard, B.M. Tyler, H. Brem, Paclitaxel: A review of adverse toxicities and novel delivery strategies, *Expert Opin. Drug Saf.* 6 (2007) 609–621. https://doi.org/10.1517/14740338.6.5.609.

[77]   A. De Sanctis, L. Taillade, S. Vignot, S. Novello, R. Conforti, J.P. Spano, G.V. Scagliotti, D. Khayat, Pulmonary toxicity related to systemic treatment of nonsmall cell lung cancer, *Cancer.* 117 (2011) 3069–3080. https://doi.org/10.1002/cncr.25894.

[78]   K. Abhinav, L.A. Dailey, F. Ben, Lost in translation: what is stopping inhaled nanomedicines from realizing their potential?, *Ther. Deliv.* 5 (2014) 757–761. https://doi.org/10.1002/9781118903681.

[79]   P. Zarogoulidis, E. Eleftheriadou, I. Sapardanis, V. Zarogoulidou, H. Lithoxopoulou, T. Kontakiotis, N. Karamanos, G. Zachariadis, M. Mabroudi, A. Zisimopoulos, K. Zarogoulidis, Feasibility and effectiveness of inhaled carboplatin in NSCLC patients, *Invest. New Drugs.* 30 (2012) 1628–1640. https://doi.org/10.1007/s10637-011-9714-5.

[80]   P. Zarogoulidis, E. Chatzaki, K. Porpodis, K. Domvri, W. Hohenforst-Schmidt, E.P. Goldberg, N. Karamanos, K. Zarogoulidis, Inhaled chemotherapy in lung cancer: future concept of nanomedicine, *Int. J. Nanomedicine.* 7 (2012) 1551–1572. https://doi.org/10.2147/IJN.S29997.

[81]   S. Dasari, P. Bernard Tchounwou, Cisplatin in cancer therapy: molecular mechanisms of action, *Eur. J. Pharmacol.* 740 (2014) 1–33. https://doi.org/10.1016/j.ejphar.2014.07.025.

[82]   G. Ciarimboli, Membrane transporters as mediators of cisplatin effects and side effects., *Scientifica (Cairo).* 2012 (2012) 473829. https://doi.org/10.6064/2012/473829.

[83]   S.A. Aldossary, Review on pharmacology of cisplatin: Clinical use, toxicity and mechanism of resistance of cisplatin, *Biomed. Pharmacol. J.* 12 (2019) 7–15. https://doi.org/10.13005/bpj/1608.

[84]   S. Spreckelmeyer, C. Orvig, A. Casini, Cellular transport mechanisms of cytotoxic metallodrugs: An overview beyond cisplatin, *Molecules.* 19 (2014) 15584–15610. https://doi.org/10.3390/molecules191015584.

[85]   T. Alcindor, N. Beauger, Oxaliplatin: A review in the era of molecularly targeted therapy, *Curr. Oncol.* 18 (2011) 18–25. https://doi.org/10.3747/co.v18i1.708.

[86]   S. Ghosh, Cisplatin: The first metal based anticancer drug, *Bioorg. Chem.* 88 (2019) 1–20. https://doi.org/10.1016/j.bioorg.2019.102925.

[87]   G. Ciarimboli, T. Ludwig, D. Lang, H. Pavenstädt, H. Koepsell, H.J. Piechota, J. Haier, U. Jaehde, J. Zisowsky, E. Schlatter, Cisplatin nephrotoxicity is critically mediated via the human organic cation transporter 2, *Am. J. Pathol.* 167 (2005) 1477–1484. https://doi.org/10.1016/S0002-9440(10)61234-5.

[88]   V.F. Vasconcellos, G.N. Marta, E.M. da Silva, A.F. Gois, T.B. de Castria, R. Riera, Cisplatin versus carboplatin in combination with third-generation drugs for advanced non-small cell lung cancer, *Cochrane Database Syst. Rev.* (2020) 1–52. https://doi.org/10.1002/14651858.CD009256.pub3.

[89]   A.F. Westendorf, L. Zerzankova, L. Salassa, P.J. Sadler, V. Brabec, P.J. Bednarski, Influence of pyridine versus piperidine ligands on the chemical, DNA binding and cytotoxic properties of light activated trans,trans,trans-[Pt(N 3)2(OH)2(NH3)(L)], *J. Inorg. Biochem.* 105 (2011) 652–662. https://doi.org/10.1016/j.jinorgbio.2011.01.003.

[90]   I. V. Tetko, I. Jaroszewicz, J.A. Platts, J. Kuduk-Jaworska, Calculation of lipophilicity for Pt(II)

complexes: Experimental comparison of several methods, *J. Inorg. Biochem.* 102 (2008) 1424–1437. https://doi.org/10.1016/j.jinorgbio.2007.12.029.

[91]   N. Martinho, T.C.B. Santos, H.F. Florindo, L.C. Silva, Cisplatin-membrane interactions and their influence on platinum complexes activity and toxicity, *Front. Physiol.* 9 (2019) 1–15. https://doi.org/10.3389/fphys.2018.01898.

[92]   G.F. de Sousa, S.R. Wlodarczyk, G. Monteiro, Carboplatin: Molecular mechanisms of action associated with chemoresistance, *Brazilian J. Pharm. Sci.* 50 (2014) 693–702. https://doi.org/10.1590/S1984-82502014000400004.

[93]   S. Harrach, G. Ciarimboli, Role of transporters in the distribution of platinum-based drugs, *Front. Pharmacol.* 6 (2015) 1–7. https://doi.org/10.3389/fphar.2015.00085.

[94]   M.A. Perazella, Pharmacology behind common drug nephrotoxicities, *Clin. J. Am. Soc. Nephrol.* 13 (2018) 1897–1908. https://doi.org/10.2215/CJN.00150118.

[95]   T. Makovec, Cisplatin and beyond: molecular mechanisms of action and drug resistance development in cancer chemotherapy, *Radiol. Oncol.* 53 (2019) 148–158. https://doi.org/10.2478/raon-2019-0018.

[96]   E.R. Jamieson, S.J. Lippard, Structure, recognition, and processing of cisplatin-DNA adducts, *Chem. Rev.* 99 (1999) 2467–2498. https://doi.org/10.1021/cr980421n.

[97]   V.M.L. De Sousa, L. Carvalho, Heterogeneity in lung cancer, *Pathobiology*. 85 (2018) 96–107. https://doi.org/10.1159/000487440.

[98]   S.-H. Chen, J.-Y. Chang, New insights into mechanisms of cisplatin resistance: From tumor cell to microenvionement, *Int. J. Mol. Sci.* 20 (2019) 1–21. https://doi.org/doi:10.3390/ijms20174136.

[99]   C. Rébé, L. Demontoux, T. Pilot, F. Ghiringhelli, Platinum derivatives effects on anticancer immune response, Biomolecules. 10 (2020) 1–22. https://doi.org/10.3390/biom10010013.

[100]   L. Oliveira, J.M. Caquito, M.S. Rocha, Carboplatin as an alternative to Cisplatin in chemotherapies: New insights at single molecule level, *Biophys. Chem.* 241 (2018) 8–14. https://doi.org/10.1016/j.bpc.2018.07.004.

[101]   S. V. Hato, A. Khong, I.J.M. De Vries, W.J. Lesterhuis, Molecular pathways: The immunogenic effects of platinum-based chemotherapeutics, *Clin. Cancer Res.* 20 (2014) 2831–2837. https://doi.org/10.1158/1078-0432.CCR-13-3141.

[102]   Y. Xiang, L. Chen, L. Li, Y. Huang, Restoration and Enhancement of Immunogenic Cell Death of Cisplatin by Coadministration with Digoxin and Conjugation to HPMA Copolymer, *ACS Appl. Mater. Interfaces*. 12 (2020) 1606–1616. https://doi.org/10.1021/acsami.9b19323.

[103]   G. Giaccone, Clinical perspectives on platinum resistance, *Drugs*. 59 (2000) 9–17. https://doi.org/10.2165/00003495-200059004-00002.

[104]   V.A. De Weger, J.H. Beijnenb, J.H.M. Schellensa, Cellular and clinical pharmacology of the taxanes docetaxel and paclitaxel -A review, *Anticancer. Drugs*. 25 (2014) 488–494. https://doi.org/10.1097/CAD.0000000000000093.

[105]   H. Parekh, H. Simpkins, The transport and binding of taxol, *Gen. Pharmacol.* 29 (1997) 167–172. https://doi.org/10.1016/S0306-3623(97)89716-9.

[106]   C.D. Scripture, W.D. Figg, A. Sparreboom, Paclitaxel chemotherapy: from empiricism to a mechanism-based formulation strategy, *Ther. Clin. Risk Manag.* 1 (2005) 107–114. https://doi.org/10.2147/tcrm.1.2.107.62910.

[107]   H.J. Kuh, S.H. Jang, M.G. Wientjes, J.L.S. Au, Computational model of intracellular pharmacokinetics of paclitaxel, *J. Pharmacol. Exp. Ther*. 293 (2000) 761–770.

[108]   S. Bandara, M. Diehl, G. Fricker, A mathematical model for the transport of paclitaxel (Taxol) across the blood-brain barrier, *Chem. Eng. Res. Des*. 85 (2007) 1065–1071. https://doi.org/10.1205/cherd06238.

[109]   G.A. Orr, P. Verdier-Pinard, H. McDaid, S.B. Horwitz, Mechanisms of Taxol resistance related to microtubules, *Oncogene*. 22 (2003) 7280–7295. https://doi.org/10.1038/sj.onc.1206934.

[110]   J. Crawford, N. Denduluri, D. Patt, X. Jiao, P.K. Morrow, J. Garcia, R. Barron, G.H. Lyman, Relative dose intensity of first-line chemotherapy and overall survival in patients with advanced non-small-cell lung cancer, *Support. Care Cancer*. 28 (2020) 925–932. https://doi.org/10.1007/s00520-019-04875-1.

[111]   A. Luciani, C. Bertuzzi, G. Ascione, E. Di Gennaro, S. Bozzoni, S. Zonato, D. Ferrari, P. Foa,

Dose intensity correlate with survival in elderly patients treated with chemotherapy for advanced non-small cell lung cancer, *Lung Cancer*. 66 (2009) 94–96. https://doi.org/10.1016/j.lungcan.2008.12.019.

[112] T. Berghmans, A. Scherpereel, A.P. Meert, V. Giner, J. Lecomte, J.J. Lafitte, N. Leclercq, M. Paesmans, J.P. Sculier, P. Van Houtte, M. Roelandts, J. Thiriaux, C.G. Alexopoulos, M. Vaslamatzis, S. Holbrechts, P. Wackenier, P. Recloux, Y. Bonduelle, J.L. Corhay, O. Van Cutsem, M. Mairesse, A. Efremidis, G. Koumakis, M.C. Florin, E. Maetz, A. Strecker, M. Richez, X. Ficheroulle, B. Colinet, T. Collon, C. Zacharias, S. Bensliman, A. Drowart, T. Prigogine, D. Brohée, B. Stach, P. Ravez, M.C. Berchier, J. Amourette, A. Tagnon, F. Kroll, F. Steenhouwer, A Phase III randomized study comparing a chemotherapy with cisplatin and etoposide to a etoposide regimen without cisplatin for patients with extensive small-cell lung cancer, *Front. Oncol.* 7 (2017). https://doi.org/10.3389/fonc.2017.00217.

[113] E. Nusseibeh, L. Weber, K. Won, S. Reidt, Chart review of predisposing factors to cisplatin-induced nephrotoxicity in patients with cancer, *JHOP*. 9 (2019) 11–19.

[114] M. Adams, I.J. Kerby, I. Rocker, A. Evans, K. Johansen, C.R. Franks, A comparison of the toxicity and efficacy of cisplatin and carboplatin in advanced ovarian cancer, *Acta Oncol. (Madr)*. 28 (1989) 57–60. https://doi.org/10.3109/02841868909111182.

[115] R. Oun, Y.E. Moussa, N.J. Wheate, The side effects of platinum-based chemotherapy drugs: A review for chemists, *Dalt. Trans*. 47 (2018) 6645–6653. https://doi.org/10.1039/c8dt00838h.

[116] F. Shahid, Z. Farooqui, F. Khan, Cisplatin-induced gastrointestinal toxicity: An update on possible mechanisms and on available gastroprotective strategies, *Eur. J. Pharmacol*. 827 (2018) 49–57. https://doi.org/10.1016/j.ejphar.2018.03.009.

[117] W.J. Gradishar, S. Tjulandin, N. Davidson, H. Shaw, N. Desai, P. Bhar, M. Hawkins, J. O'Shaughnessy, Phase III trial of nanoparticle albumin-bound paclitaxel compared with polyethylated castor oil-based paclitaxel in women with breast cancer, *J. Clin. Oncol*. 23 (2005) 7794–7803. https://doi.org/10.1200/JCO.2005.04.937.

[118] R. Velasco, J. Bruna, Taxane-induced peripheral neurotoxicity, *Toxics*. 3 (2015) 152–169. https://doi.org/10.3390/toxics3020152.

[119] J.P. Guastalla, V. Diéras, The taxanes: Toxicity and quality of life considerations in advanced ovarian cancer, *Br. J. Cancer*. 89 (2003) 16–22. https://doi.org/10.1038/sj.bjc.6601496.

[120] S. Boussios, G. Pentheroudakis, K. Katsanos, N. Pavlidis, Systemic treatment-induced gastrointestinal toxicity: Incidence, clinical presentation and management, *Ann. Gastroenterol*. 25 (2012) 106–118.

[121] C. Colby, S. Koziol, S.L. McAfee, B. Yeap, T.R. Spitzer, High-dose carboplatin and regimen-related toxicity following autologous bone marrow transplant, *Bone Marrow Transplant*. 29 (2002) 467–472. https://doi.org/10.1038/sj.bmt.1703417.

[122] P. Mazzanti, C. Massacesi, M.B.L. Rocchi, R. Mattioli, P. Lippe, R. Trivisonne, F. Buzzi, G. De Signoribus, G. Tuveri, G. Rossi, L. Di Lullo, F. Sturba, D. Morale, S. Catanzani, A. Pilone, M. Bonsignori, T. Battelli, Randomized, multicenter, phase II study of gemcitabine plus cisplatin versus gemcitabine plus carboplatin in patients with advanced non-small cell lung cancer, *Lung Cancer*. 41 (2003) 81–89. https://doi.org/10.1016/S0169-5002(03)00140-5.

[123] O. Kanat, H. Ertas, B. Caner, Platinum-induced neurotoxicity: A review of possible mechanisms, *World J. Clin. Oncol*. 8 (2017) 329–333. https://doi.org/10.5306/wjco.v8.i4.329.

[124] Y. Bennis, A. Savry, M. Rocca, L. Gauthier-Villano, P. Pisano, B. Pourroy, Cisplatin dose adjustment in patients with renal impairment, which recommendations should we follow?, *Int. J. Clin. Pharm*. 36 (2014) 420–429. https://doi.org/10.1007/s11096-013-9912-7.

[125] S. Manohar, N. Leung, Cisplatin nephrotoxicity: a review of the literature, *J. Nephrol*. 31 (2017) 15–25. https://doi.org/10.1007/s40620-017-0392-z.

[126] X. Yao, K. Panichpisal, N. Kurtzman, K. Nugent, Cisplatin Nephrotoxicity: A Review, *Am. J. Med. Sci*. 334 (2007) 115–124.

[127] F. Hayati, M. Hossainzadeh, S. Shayanpour, Z. Abedi-Gheshlaghi, S. Seifollah, B. Mousavi, Prevention of cisplatin nephrotoxicity, *J. Nephropharmacology*. 5 (2016) 57–60. https://doi.org/10.1016/0277-5379(86)90001-5.

[128] T. Karasawa, P.S. Steyger, An integrated view of cisplatin-induced nephrotoxicity and ototoxicity, *Toxicol. Lett*. 237 (2015) 219–227. https://doi.org/10.1016/j.toxlet.2015.06.012.

[129] M. Hanigan, P. Devarajan, Cisplatin nephrotoxicity: molecular mechanisms, *Cancer Ther.* 1 (2003) 47–61.

[130] T.A. Wynn, Fibrosis under arrest, *Nat. Med.* 16 (2010) 523–525. https://doi.org/10.1038/nm0510-523.

[131] W. LV, G. W. Booz, Y. Wang, F. Fan, R. J. Roman, Inflammation and renal fibrosis: recent developments on key signaling molecules as potential therapeutic targets, *Eur. J. Pharmacol.* (2018) 1–31. https://doi.org/10.1016/j.ejphar.2017.12.016.

[132] V. Bunel, Y. Tournay, T. Baudoux, E. De Prez, M. Marchand, Z. Mekinda, R. Maréchal, T. Roumeguère, M.H. Antoine, J.L. Nortier, Early detection of acute cisplatin nephrotoxicity: Interest of urinary monitoring of proximal tubular biomarkers, *Clin. Kidney J.* 10 (2017) 1–9. https://doi.org/10.1093/ckj/sfx007.

[133] M. Bhargava, C. Wendt, Biomarkers in acute lung injury, *Transl. Res.* 159 (2012) 205–217. https://doi.org/10.1016/j.trsl.2012.01.007.

[134] C.G. Kilty, J. Keenan, M. Shaw, Histologically defined biomarkers in toxicology, *Expert Opin. Drug Saf.* 6 (2007) 207–215. https://doi.org/10.1517/14740338.6.2.207.

[135] M.S. Rizvi, K.B. Kashani, Biomarkers for early detection of acute kidney injury, *J. Appl. Lab. Med.* 2 (2017) 386–399. https://doi.org/10.1373/jalm.2017.023325.

[136] M. Ostermann, A. Zarbock, S. Goldstein, K. Kashani, E. Macedo, R. Murugan, M. Bell, L. Forni, L. Guzzi, M. Joannidis, S.L. Kane-Gill, M. Legrand, R. Mehta, P.T. Murray, P. Pickkers, M. Plebani, J. Prowle, Z. Ricci, T. Rimmelé, M. Rosner, A.D. Shaw, J.A. Kellum, C. Ronco, Recommendations on acute kidney injury biomarkers from the acute disease quality initiative consensus conference: A consensus statement, *JAMA Netw. Open.* 3 (2020) 1–17. https://doi.org/10.1001/jamanetworkopen.2020.19209.

[137] J.R. Charlton, D. Portilla, M.D. Okusa, A basic science view of acute kidney injury biomarkers, *Nephrol. Dial. Transplant.* 29 (2014) 1301–1311. https://doi.org/10.1093/ndt/gft510.

[138] M. Ning, X. Mao, Y. Niu, B. Tang, H. Shen, Usefulness and limitations of neutrophil gelatinase-associated lipocalin in the assessment of kidney diseases, *J. Lab. Precis. Med.* 3 (2018) 1–10. https://doi.org/10.21037/jlpm.2017.12.09.

[139] T. Kaucsár, M. Godó, C. Révész, M. Kovács, A. Mócsai, N. Kiss, M. Albert, T. Krenács, G. Szénási, P. Hamar, Urine/plasma neutrophil gelatinase associated lipocalin ratio is a sensitive and specific marker of subclinical acute kidney injury in mice, *PLoS One.* 11 (2016) 1–16. https://doi.org/10.1371/journal.pone.0148043.

[140] G. Schley, C. Köberle, E. Manuilova, S. Rutz, C. Forster, M. Weyand, I. Formentini, R. Kientsch-Engel, K.U. Eckardt, C. Willam, Comparison of plasma and urine biomarker performance in acute kidney injury, *PLoS One.* 10 (2015) 1–23. https://doi.org/10.1371/journal.pone.0145042.

[141] D.J. Van Veldhuisen, L.M. Ruilope, A.S. Maisel, K. Damman, Biomarkers of renal injury and function: Diagnostic, prognostic and therapeutic implications in heart failure, *Eur. Heart J.* 37 (2016) 2577–2585. https://doi.org/10.1093/eurheartj/ehv588.

[142] V.S. Vaidya, M.A. Ferguson, J. V Bonventre, Biomarkers of acute kidney injury, Annu. Rev. *Pharmacol. Toxicol.* 48 (2008) 462–493. https://doi.org/10.1146/annurev.pharmtox.48.113006.094615.Biomarkers.

[143] M.E. Wasung, L.S. Chawla, M. Madero, Biomarkers of renal function, which and when?, *Clin. Chim. Acta.* 438 (2015) 350–357. https://doi.org/10.1016/j.cca.2014.08.039.

[144] Q. hui Luo, M. lu Chen, F. jiao Sun, Z. li Chen, M. yang Li, W. Zeng, L. Gong, A. chun Cheng, X. Peng, J. Fang, L. Tang, Y. Geng, KIM-1 and NGAL as biomarkers of nephrotoxicity induced by gentamicin in rats, *Mol. Cell. Biochem.* 397 (2014) 53–60. https://doi.org/10.1007/s11010-014-2171-7.

[145] P. Devarajan, Emerging urinary biomarkers in the diagnosis of acute kidney injury, *Expert Opin. Med. Diagn.* 2 (2008) 387–398. https://doi.org/10.1517/17530059.2.4.387.

[146] J.N. Barreto, K.B. McCullough, L.L. Ice, J.A. Smith, Antineoplastic agents and the associated myelosuppressive effects: A review, *J. Pharm. Pract.* 27 (2014) 440–446. https://doi.org/10.1177/0897190014546108.

[147] R. Noviyani, P.A. Indrayathi, I.N.G. Budiana, R. Niruri, K. Tunas, N.M.D.D. Adnyani, Effect of paclitaxel-cisplatin chemotherapy towards hemoglobin, platelet, and leukocyte levels in

epithelial ovarian cancer patients, *J. Appl. Pharm. Sci.* 9 (2019) 104–107. https://doi.org/10.7324/JAPS.2019.90115.

[148] T.M. Marani, M.B. Trich, K.S. Armstrong, P.M. Ness, J. Smith, C. Minniti, S.G. Sandler, Carboplatin-induced immune hemolytic anemia, *Transfusion*. 36 (1996) 1016–1018. https://doi.org/10.1046/j.1537-2995.1996.36111297091748.x.

[149] C.M. Carter, Alterations in blood components, in: *Compr. Toxicol.* Third Ed., 2018: pp. 249–293. https://doi.org/10.1016/B978-0-12-801238-3.64251-4.

[150] J.-F. Lambert, P. Beris, Pathophysiology and differential diagnosis of anaemia, 2009.

[151] K.E. O'Connell, A.M. Mikkola, A.M. Stepanek, A. Vernet, C.D. Hall, C.C. Sun, E. Yildirim, J.F. Staropoli, J.T. Lee, D.E. Brown, Practical murine hematopathology: A comparative review and implications for research, *Comp. Med.* 65 (2015) 96–113.

[152] Y.J. Cheng, R. Wu, M.L. Cheng, J. Du, X.W. Hu, L. Yu, X.K. Zhao, Y.M. Yao, Q.Z. Long, L.L. Zhu, J.J. Zhu, N.W. Huang, H.J. Liu, Y.X. Hu, F. Wan, Carboplatin-induced hematotoxicity among patients with nonsmall cell lung cancer: Analysis on clinical adverse events and drug-gene interactions, *Oncotarget*. 8 (2017) 32228–32236. https://doi.org/10.18632/oncotarget.12951.

[153] G.M. Strauss, J.E. Herndon, M.A. Maddaus, D.W. Johnstone, E.A. Johnson, D.H. Harpole, H.H. Gillenwater, D.M. Watson, D.J. Sugarbaker, R.L. Schilsky, E.E. Vokes, M.R. Green, Adjuvant paclitaxel plus carboplatin compared with observation in stage IB non-small-cell lung cancer: CALGB 9633 with the cancer and leukemia group B, radiation therapy oncology group, and North Central cancer treatment group study groups, *J. Clin. Oncol.* 26 (2008) 5043–5051. https://doi.org/10.1200/JCO.2008.16.4855.

[154] C. Langer, L. John, C. Robert, O. Peter, M. Cecilia, B. Colleen, E. Paul, L. Samuel, O. Robert, Paclitaxel and carboplatin in combination in the treatment of advanced non-small-cell lung cancer: A phase II toxity, response, and survival analysis, *J. Med. Assoc. Thail.* 13 (1995) 1860–1870.

[155] J.P. Sculier, M. Paesmans, J. Thiriaux, J. Lecomte, G. Bureau, V. Giner, G. Koumakis, J.J. Lafitte, M.C. Berchier, C.G. Alexopoulos, C. Zacharias, P. Mommen, V. Ninane, J. Klastersky, A comparison of methods of calculation for estimating carboplatin AUC with a retrospective pharmacokinetic-pharmacodynamic analysis in patients with advanced non-small cell lung cancer, *Eur. J. Cancer*. 35 (1999) 1314–1319. https://doi.org/10.1016/S0959-8049(99)00029-5.

[156] C.H. Collis, Lung damage from cytotoxic drugs, Cancer Chemother. *Pharmacol*. 4 (1980) 17–27.

[157] I.Y.R. Adamson, Drug-induced pulmonary fibrosis, *Envionmental Heal. Perspect*. 55 (1984) 25–36.

[158] F. De Giacomi, R. Vassallo, E.S. Yi, J.H. Ryu, Acute eosinophilic pneumonia: causes, diagnosis, and management, *Am. J. Respir. Crit. Care Med*. 197 (2018) 728–736. https://doi.org/10.1164/rccm.201710-1967CI.

[159] H. Ideguchi, K. Kojima, S. Hirosako, H. Ichiyasu, K. Fujii, H. Kohrogi, Cisplatin-induced eosinophilic pneumonia, *Case Rep. Pulmonol*. 2014 (2014) 1–3. https://doi.org/10.1155/2014/209732.

[160] C. Hsia, D. Hyde, E. Weibel, Lung structure and the intrinsic challenges of gas exchange, Compr. Physiol. 6 (2016) 827–895. https://doi.org/doi:10.1002/cphy.c150028.

[161] V.C. Broaddus, R. J.Mason, J. D.Ernst, T. E.King, S. C.Lazarus, J. F.Murray, J. A.Nadel, A. S.Slutsky, M. B.Gotway, Murray & Nadel 's Textbook of Respiratory Medicine, 6th ed., Elsevier Saunders, 2016.

[162] C.T. Robb, K.H. Regan, D.A. Dorward, A.G. Rossi, Key mechanisms governing resolution of lung inflammation, *Semin. Immunopathol*. 38 (2016) 425–448. https://doi.org/10.1007/s00281-016-0560-6.

[163] L.A. Abdulkhaleq, M.A. Assi, R. Abdullah, M. Zamri-Saad, Y.H. Taufiq-Yap, M.N.M. Hezmee, The crucial roles of inflammatory mediators in inflammation: A review, *Vet. World*. 11 (2018) 627–635. https://doi.org/10.14202/vetworld.2018.627-635.

[164] F. Lavorini, F. Buttini, O.S. Usmani, 100 Years of drug delivery to the lungs, 2019. https://doi.org/10.1007/164_2019_335.

[165] L.Y. Yeo, J.R. Friend, M.P. Mcintosh, E.N. Meeusen, D.A. Morton, Ultrasonic nebulization

platforms for pulmonary drug delivery, *Expert Opin. Drug Deliv*. 7 (2010) 663–679. https://doi.org/10.1517/17425247.2010.485608.

[166] F. Lavorini, The challenge of delivering therapeutic aerosols to asthma patients, *ISRN Allergy*. 2013 (2013) 1–17. https://doi.org/10.1155/2013/102418.

[167] M.R. Elkins, P. Robinson, S.D. Anderson, C.P. Perry, E. Daviskas, B. Charlton, Inspiratory flows and volumes in subjects with cystic fibrosis using a new dry powder inhaler device, *Open Respir. Med. J*. 8 (2014) 1–7. https://doi.org/10.2174/1874306401408010001.

[168] G. Pilcer, N. Wauthoz, K. Amighi, Lactose characteristics and the generation of the aerosol, *Adv. Drug Deliv. Rev*. 64 (2012) 233–256. https://doi.org/10.1016/j.addr.2011.05.003.

[169] G. Pilcer, K. Amighi, Formulation strategy and use of excipients in pulmonary drug delivery, *Int. J. Pharm*. 392 (2010) 1–19. https://doi.org/doi:10.1016/j.ijpharm.2010.03.017.

[170] A.K. Singh, Structure, synthesis, and application of nanoparticles, 2016. https://doi.org/10.1016/b978-0-12-801406-6.00002-9.

[171] N. Wauthoz, K. Amighi, Formulation strategies for pulmonary delivery of poorly soluble drugs, in: Pulm. Drug Deliv., 2015: pp. 87–122. https://doi.org/10.1002/9781118799536.ch5.

[172] C. Kosmidis, K. Sapalidis, P. Zarogoulidis, Inhaled cisplatin for NSCLC: Facts and results, *Int. J. Mol. Sci*. 20 (2019) 1–12.

[173] N. Wauthoz, R. Rosière, K. Amighi, Expert Opinion on drug delivery inhaled cytotoxic chemotherapy : clinical challenges , recent developments, and future prospects future prospects, *Expert Opin. Drug Deliv*. (2020) 1–22. https://doi.org/10.1080/17425247.2021.1829590.

[174] S.P. Newman, Delivering drugs to the lungs: The history of repurposing in the treatment of respiratory diseases, *Adv. Drug Deliv. Rev*. 133 (2018) 5–18. https://doi.org/10.1016/j.addr.2018.04.010.

[175] F. Gagnadoux, J. Hureaux, L. Vecellio, T. Urban, A. Le Pape, I. Valo, J. Montharu, V. Leblond, M. Boisdron-Celle, S. Lerondel, C. Majoral, P. Diot, J.L. Racineux, E. Lemarie, Aerosolized chemotherapy., *J. Aerosol Med. Pulm. Drug Deliv*. 21 (2008) 61–69. https://doi.org/10.1089/jamp.2007.0656.

[176] P. Zarogoulidis, K. Darwiche, L. Krauss, H. Huang, G.A. Zachariadis, A. Katsavou, W. Hohenforst-Schmidt, A. Papaiwannou, T.J. Vogl, L. Freitag, G. Stamatis, K. Zarogoulidis, Inhaled cisplatin deposition and distribution in lymph nodes in stage II lung cancer patients, *Futur. Oncol*. 9 (2013) 1307–1313. https://doi.org/10.2217/fon.13.111.

[177] A.. Chou, R. Gupta, M.. Bell, K.. Riewe, P.. Meyers, R. Gorlick, Inhaled lipid cisplatin (ILC) in the treatment of patients with relapsed/progressive osteosarcoma metastatic to the lung, *J. Clin. Oncol*. 60 (2013) 580–586. https://doi.org/10.1002/pbc.

[178] B.P.H. Wittgen, P.W.A. Kunst, K. Van Der Born, A.W. Van Wijk, W. Perkins, F.G. Pilkiewicz, R. Perez-Soler, S. Nicholson, G.J. Peters, P.E. Postmus, Phase I study of aerosolized SLIT cisplatin in the treatment of patients with carcinoma of the lung, *Clin. Cancer Res*. 13 (2007) 2414–2421. https://doi.org/10.1158/1078-0432.CCR-06-1480.

[179] G.A. Otterson, M.A. Villalona-calero, W. Hicks, C.L. Cancer, Phase I / II study of inhaled doxorubicin combined with platinum-based therapy for advanced non−small cell lung cancer, *Clin. Cancer Res*. 16 (2010) 2466–2473. https://doi.org/10.1158/1078-0432.CCR-09-3015.

[180] G.A. Otterson, M.A. Villalona-Calero, S. Sharma, M.G. Kris, A. Imondi, M. Gerber, D.A. White, M.J. Ratain, J.H. Schiller, A. Sandler, M. Kraut, S. Mani, J.R. Murren, Phase I study of inhaled doxorubicin for patients with metastatic tumors to the lungs, *Cancer Ther. Clin*. 13 (2007) 1246–1252. https://doi.org/10.1158/1078-0432.CCR-06-1096.

[181] T. Tatsumura, S. Koyama, M. Tsujimoto, M. Kitagawa, S. Kagamimori, Further study of nebulisation chemotherapy, a new chemotherapeutic method in the treatment of lung carcinomas: fundamental and clinical, *Br. J. Cancer*. 68 (1993) 1146–1149. https://doi.org/10.1038/bjc.1993.495.

[182] C.F. Verschraegen, B.E. Gilbert, E. Loyer, A. Huaringa, G. Walsh, R.A. Newman, V. Knight, Clinical Evaluation of the Delivery and Safety of Aerosolized Liposomal 9-Nitro-20 (S) - Camptothecin in Patients with Advanced Pulmonary Malignancies Clinical Evaluation of the Delivery and Safety of Aerosolized Liposomal 9-Nitro-20 (S) -Camptothecin, *Clin. Cancer Res*. 20 (2004) 2319–2326.

[183] E. Lemarie, L. Vecellio, J. Hureaux, C. Prunier, C. Valat, D. Grimbert, M. Boidron-Celle, B.

Giraudeau, A. Le Pape, E. Pichon, P. Diot, A. El Houfia, F. Gagnadoux, Aerosolized gemcitabine in patients with carcinoma of the lung: Feasibility and safety study, *J. Aerosol Med. Pulm. Drug Deliv*. 24 (2011) 261–270. https://doi.org/10.1089/jamp.2010.0872.

[184] C. Sardeli, P. Zarogoulidis, C. Kosmidis, A. Amaniti, A. Katsaounis, D. Giannakidis, C. Koulouris, W. Hohenforst-Schmidt, H. Huang, C. Bai, N. Michalopoulos, K. Tsakiridis, K. Romanidis, P. Oikonomou, K. Mponiou, A. Vagionas, A.M. Goganau, I. Kesisoglou, K. Sapalidis, Inhaled chemotherapy adverse effects: mechanisms and protection methods, *Lung Cancer Manag*. 8 (2019). https://doi.org/10.2217/lmt-2019-0007.

[185] K. Darwiche, P. Zarogoulidis, N.K. Karamanos, K. Domvri, E. Chatzaki, T.C. Constantinidis, S. Kakolyris, K. Zarogoulidis, Efficacy versus safety concerns for aerosol chemotherapy in non-small-cell lung cancer: A future dilemma for micro-oncology, *Futur. Oncol*. 9 (2013) 505–525. https://doi.org/10.2217/fon.12.205.

[186] R. Rosière, T. Berghmans, P. de Vuyst, K. Amighi, N. Wauthoz, The position of inhaled chemotherapy in the care of patients with lung tumors: Clinical feasibility and indications according to recent pharmaceutical progresses, *Cancers (Basel)*. 11 (2019) 1–13. https://doi.org/10.3390/cancers11030329.

[187] V. Levet, R. Rosière, R. Merlos, L. Fusaro, G. Berger, K. Amighi, N. Wauthoz, Development of controlled-release cisplatin dry powders for inhalation against lung cancers, *Int. J. Pharm*. 515 (2016) 209–220. https://doi.org/10.1016/j.ijpharm.2016.10.019.

[188] S.A. Meenach, K.W. Anderson, J.Z. Hilt, R.C. McGarry, H.M. Mansour, High-performing dry powder inhalers of paclitaxel DPPC/DPPG lung surfactant-mimic multifunctional particles in lung cancer: physicochemical characterization, in vitro aerosol dispersion, and cellular studies., *AAPS PharmSciTech*. 15 (2014) 1574–1587. https://doi.org/10.1208/s12249-014-0182-z.

[189] N. Wauthoz, P. Deleuze, A. Saumet, C. Duret, R. Kiss, K. Amighi, Temozolomide-based dry powder formulations for lung tumor-related inhalation treatment, *Pharm. Res*. 28 (2010) 762–775. https://doi.org/DOI 10.1007/s11095-010-0329-x.

[190] M.T. Newhouse, P.H. Hirst, S.P. Duddu, Y.H. Walter, T.E. Tarara, A.R. Clark, J.G. Weers, Inhalation of a dry powder tobramycin pulmosphere formulation in healthy volunteers, *Chest*. 124 (2003) 360–366. https://doi.org/10.1378/chest.124.1.360.

[191] H.M. Abdelaziz, M. Gaber, M.M. Abd-Elwakil, M.T. Mabrouk, M.M. Elgohary, N.M. Kamel, D.M. Kabary, M.S. Freag, M.W. Samaha, S.M. Mortada, K.A. Elkhodairy, J.Y. Fang, A.O. Elzoghby, Inhalable particulate drug delivery systems for lung cancer therapy: Nanoparticles, microparticles, nanocomposites and nanoaggregates, *J. Control. Release*. 269 (2018) 374–392. https://doi.org/10.1016/j.jconrel.2017.11.036.

[192] N. Wauthoz, P. Deleuze, J. Hecq, I. Roland, S. Saussez, I. Adanja, O. Debeir, C. Decaestecker, V. Mathieu, R. Kiss, K. Amighi, In vivo assessment of temozolomide local delivery for lung cancer inhalation therapy, *Eur. J. Pharm. Sci*. 39 (2010) 402–411. https://doi.org/10.1016/j.ejps.2010.01.010.

[193] A. Dabbagh, N.H. Abu Kasim, C.H. Yeong, T.W. Wong, N. Abdul Rahman, Critical parameters for particle-bsed pulmonary delivery of chemotherapeutics, *J. Aerosol Med. Pulm. Drug Deliv*. 30 (2017) 1–16. https://doi.org/10.1089/jamp.2017.1382.

[194] G. Garrastazu Pereira, A.J. Lawson, F. Buttini, F. Sonvico, Loco-regional administration of nanomedicines for the treatment of lung cancer, *Drug Deliv*. (2015) 1–16. https://doi.org/10.3109/10717544.2015.1114047.

[195] W.H. Roa, S. Azarmi, M.H.D.K. Al-Hallak, W.H. Finlay, A.M. Magliocco, R. Löbenberg, Inhalable nanoparticles, a non-invasive approach to treat lung cancer in a mouse model, *J. Control. Release*. 150 (2011) 49–55. https://doi.org/10.1016/j.jconrel.2010.10.035.

[196] O. Taratula, A. Kuzmov, M. Shah, O.B. Garbuzenko, T. Minko, Nanostructured lipid carriers as multifunctional nanomedicine platform for pulmonary co-delivery of anticancer drugs and siRNA, *J. Control. Release*. 171 (2013) 349–357. https://doi.org/10.1016/j.jconrel.2013.04.018.

[197] A. Gautam, N. Koshkina, Paclitaxel (Taxol) and taxoid derivates for lung cancer treatment: Potential for aerosol delivery, *Curr. Cancer Drug Targets*. 3 (2003) 287–296. https://doi.org/10.2174/1568009033481912.

[198] A.E. Hershey, I.D. Kurzman, L.J. Forrest, C.A. Bohling, M. Stonerook, M.E. Placke, A.R. Imondi, D.M. Vail, Inhalation chemotherapy for macroscopic primary or metastatic lung tumors:

Proof of principle using dogs with spontaneously occurring tumors as a model, *Clin. Cancer Res.* 5 (1999) 2653–2659.

[199] R. Rosière, M. Van Woensel, M. Gelbcke, V. Mathieu, J. Hecq, T. Mathivet, M. Vermeersch, P. Van Antwerpen, K. Amighi, N. Wauthoz, New folate-grafted chitosan derivative to improve delivery of paclitaxel-loaded solid lipid nanoparticles for lung tumor therapy by inhalation, *Mol. Pharm.* 15 (2018) 899–910. https://doi.org/10.1021/acs.molpharmaceut.7b00846.

[200] Q.T. Zhou, P. Tang, S.S.Y. Leung, J.G.Y. Chan, H.K. Chan, Emerging inhalation aerosol devices and strategies: Where are we headed?, *Adv. Drug Deliv. Rev.* 75 (2014) 3–17. https://doi.org/10.1016/j.addr.2014.03.006.

[201] C. Kleinstreuer, Z. Zhang, Targeted drug aerosol deposition analysis for a four-generation lung airway model with hemispherical tumors, *J. Biomech. Eng.* 125 (2003) 197–206. https://doi.org/10.1115/1.1543548.

[202] S. Mangal, W. Gao, T. Li, Q.T. Zhou, Pulmonary delivery of nanoparticle chemotherapy for the treatment of lung cancers: Challenges and opportunities, *Acta Pharmacol.* Sin. 38 (2017) 782–797. https://doi.org/10.1038/aps.2017.34.

[203] V. Levet, R. Merlos, R. Rosière, K. Amighi, N. Wauthoz, Platinum pharmacokinetics in mice following inhalation of cisplatin dry powders with different release and lung retention properties, *Int. J. Pharm.* 517 (2017) 359–372. https://doi.org/10.1016/j.ijpharm.2016.12.037.

[204] E.S. Kim, J.J. Lee, G. He, C.W. Chow, J. Fujimoto, N. Kalhor, S.G. Swisher, I.I. Wistuba, D.J. Stewart, Z.H. Siddik, Tissue platinum concentration and tumor response in non-small-cell lung cancer, *J. Clin. Oncol.* 30 (2012) 3345–3352. https://doi.org/10.1200/JCO.2011.40.8120.

[205] V. Levet, R. Rosiere, J. Hecq, I. Langer, K. Amighi, N. Wauthoz, Tolerance of cisplatin dry powders for inhalation and efficacy on an orthotopic grafted lung tumor preclinical model, in: RDD Eur. 2017, 2017: pp. 335–340. http://www.rddonline.com/publications/articles/article.php?ArticleID=2333&return=1.

[206] M.G. Ghi, A. Paccagnella, Therapeutic intensification and induction chemotherapy for high-risk locally advanced squamous cell carcinoma, *Curr. Treat. Options Oncol.* 20 (2019) 1–15. https://doi.org/10.1007/s11864-019-0599-4.

[207] N.S. Kalman, E. Weiss, P.R. Walker, J.G. Rosenman, Local radiotherapy intensification for locally advanced non–small-cell lung cancer – A call to arms, *Clin. Lung Cancer.* 19 (2017) 17–26. https://doi.org/10.1016/j.cllc.2017.05.024.

[208] A.C. Easty, N. Coakley, R. Cheng, M. Cividino, P. Savage, R. Tozer, R.E. White, Safe handling of cytotoxics: Guideline recommendations, *Curr. Oncol.* 22 (2015) e27–e37. https://doi.org/10.3747/co.21.2151.

[209] Y.-J. Son, J.T. McConville, Development of a standardized dissolution test method for inhaled pharmaceutical formulations, *Int. J. Pharm.* 382 (2009) 15–22. https://doi.org/doi:10.1016/j.ijpharm.2009.07.034.

[210] M.R.C. Marques, R. Loebenberg, M. Almukainzi, Simulated biologic fluids with possible application in dissolution testing, *Dissolution Technol.* (2011) 15–28. https://doi.org/10.1002/jps.23029.

[211] R. Rosière, M. Van Woensel, V. Mathieu, I. Langer, T. Mathivet, M. Vermeersch, K. Amighi, N. Wauthoz, Development and evaluation of well-tolerated and tumor-penetrating polymeric micelle-based dry powders for inhaled anti-cancer chemotherapy, *Int. J. Pharm.* 501 (2016) 148–159. https://doi.org/10.1016/j.ijpharm.2016.01.073.

[212] M.D. Duque, D.A. Silva, M.G. Issa, V. Porta, R. Löbenberg, H.G. Ferraz, In silico prediction of plasma concentrations of fluconazole capsules with different dissolution profiles and bioequivalence study using population simulation, *Pharmaceutics.* 11 (2019) 1–12. https://doi.org/10.3390/pharmaceutics11050215.

[213] M.. O'Neil, The Merck Index: An Encyclopedia of Chemicals, Drugs, and Biologicals, 14th editi, 2006.

[214] C. Duret, N. Wauthoz, R. Merlos, J. Goole, C. Maris, I. Roland, T. Sebti, F. Vanderbist, K. Amighi, In vitro and in vivo evaluation of a dry powder endotracheal insufflator device for use in dose-dependent preclinical studies in mice, *Eur. J. Pharm. Biopharm.* 81 (2012) 627–634. https://doi.org/10.1016/j.ejpb.2012.04.004.

[215] S.W.S. Yapa, J. Li, K. Patel, J.W. Wilson, M.J. Dooley, J. George, D. Clark, S. Poole, E.

Williams, C.J.H. Porter, R.L. Nation, M.P. McIntosh, Pulmonary and systemic pharmacokinetics of inhaled and intravenous colistin methanesulfonate in cystic fibrosis patients: Targeting advantage of inhalational administration, *Antimicrob. Agents Chemother*. 58 (2014) 2570–2579. https://doi.org/10.1128/AAC.01705-13.

[216] S. Vouillamoz-Lorenz, J. Bauer, F. Lejeune, L.A. Decosterd, Validation of an AAS method for the determination of platinum in biological fluids from patients receiving the oral platinum derivative JM216, *J. Pharm. Biomed. Anal*. 25 (2001) 465–475. https://doi.org/10.1016/S0731-7085(00)00508-2.

[217] P. Selvam, D. McNair, R. Truman, H.D.C. Smyth, A novel dry powder inhaler: Effect of device design on dispersion performance, *Int. J. Pharm*. 401 (2010) 1–6.

[218] A.C. Fisher, S.L. Lee, D.P. Harris, L. Buhse, S. Kozlowski, L. Yu, M. Kopcha, J. Woodcock, Advancing pharmaceutical quality: An overview of science and research in the U.S. FDA's office of pharmaceutical quality, *Int. J. Pharm*. 515 (2016) 390–402. https://doi.org/10.1016/j.ijpharm.2016.10.038.

[219] S. Salar-Behzadi, S. Wu, A. Mercuri, C. Meindl, S. Stranzinger, E. Fröhlich, Effect of the pulmonary deposition and in vitro permeability on the prediction of plasma levels of inhaled budesonide formulation, *Int. J. Pharm*. 532 (2017) 337–344. https://doi.org/10.1016/j.ijpharm.2017.08.124.

[220] N.D. Eljack, H.-Y.M. Maa, J. Drucker, C. Shen, T.W. Hambley, E.J. New, R.J. Clarke, T. Friedrich, Mechanisms of cell uptake and toxicity of the anticancer drug cisplatin, *Metallomics*. 6 (2014) 1–17.

[221] FDA-Center for Drug Evaluation and Research, Inactive Ingredient Search for Approved Drug Products, (2021). https://www.accessdata.fda.gov/scripts/cder/iig/index.cfm?event=BasicSearch.page (accessed October 29, 2020).

[222] C. Loira-Pastoriza, J. Todoroff, R. Vanbever, Delivery strategies for sustained drug release in the lungs, Adv. Drug Deliv. Rev. 75 (2014) 81–91. https://doi.org/10.1016/j.addr.2014.05.017.

[223] T. Riley, D. Christopher, A. Jan, A. Casazza, A. Colombani, A. Cooper, M. Dey, J. Maas, J. Mitchell, M. Reiners, N. Sigari, T. Tougas, S. Lyapustina, Challenges with developing in vitro dissolution tests for orally inhaled products (OIPs), *Am. Assoc. Pharm. Sci*. 13 (2012) 978–989. https://doi.org/10.1208/s12249-012-9822-3.

[224] S.P. Velaga, J. Djuris, S. Cvijic, S. Rozou, P. Russo, G. Colombo, A. Rossi, Dry powder inhalers: An overview of the in vitro dissolution methodologies and their correlation with the biopharmaceutical aspects of the drug products, *Eur. J. Pharm. Sci*. 113 (2017) 18–28. https://doi.org/10.1016/j.ejps.2017.09.002.

[225] G.S. Zijlstra, Dry powder inhalation of biopharmaceuticals: from formulation to proof-of-concept, *Groningen*:sn, 2009.

[226] M.K. Hatipoglu, A.J. Hickey, L. Garcia-Contreras, Pharmacokinetics and pharmacodynamics of high doses of inhaled dry powder drugs, *Int. J. Pharm*. 549 (2018) 306–316. https://doi.org/https://doi.org/10.1016/j.ijpharm.2018.07.050.

[227] S. Urien, E. Brain, R. Bugat, X. Pivot, I. Lochon, M.L. Vo Van, F. Vauzelle, F. Lokiec, Pharmacokinetics of platinum after oral or intravenous cisplatin: A phase 1 study in 32 adult patients, *Cancer Chemother. Pharmacol*. 55 (2005) 55–60. https://doi.org/10.1007/s00280-004-0852-8.

[228] E.M. Abdou, S.M. Kandil, A. Morsi, M.W. Sleem, In-vitro and in-vivo respiratory deposition of a developed metered dose inhaler formulation of an anti-migraine drug, *Drug Deliv*. 26 (2019) 689–699. https://doi.org/10.1080/10717544.2019.1618419.

[229] N. Wauthoz, I. Hennia, B. Dejaeger, S. Ecenarro, K. Amighi, Proposed algorithm for healthcare professionals based on product characteristics and in vitro performances in different use conditions using formoterol-based marketed products for inhalation, *Int. J. Pharm*. 530 (2017) 415–429. https://doi.org/10.1016/j.ijpharm.2017.07.021.

[230] W. Azouz, P. Chetcuti, H.S.R. Hosker, D. Saralaya, J. Stephenson, H. Chrystyn, The inhalation characteristics of patients when they use different dry powder inhalers, *J. Aerosol Med. Pulm. Drug Deliv*. 28 (2015) 35–42. https://doi.org/10.1089/jamp.2013.1119.

[231] EMA, ICH topic Q 1 A (R2)- Stability testing of new drug substances and products, 2003.

https://doi.org/10.32388/yokp53.

[232] E.E.M. Brouwers, A.D.R. Huitema, J.H. Beijnen, J.H.M. Schellens, Long-term platinum retention after treatment with cisplatin and oxaliplatin, *BMC Clin. Pharmacol.* 8 (2008) 1–10. https://doi.org/10.1186/1472-6904-8-7.

[233] R. Rosière, R. Bischof, S. Chraibi, P. Gérard, I. Hennia, E. Meeusen, K. Amighi, N. Wauthoz, Pharmacokinetic and preliminary toxicity investigation of an innovative controlled-release cisplatin dry powder inhalation formulation in sheep, in: RDD Eur. 2020, 2020: pp. 521–526.

[234] V. Sharma, J.H. McNeill, To scale or not to scale: The principles of dose extrapolation, *Br. J. Pharmacol.* 157 (2009) 907–921. https://doi.org/10.1111/j.1476-5381.2009.00267.x.

[235] F. Janker, W. Weder, J.H. Jang, W. Jungraithmayr, Preclinical, non-genetic models of lung adenocarcinoma: A comparative survey, *Oncotarget.* 9 (2018) 30527–30538. https://doi.org/10.18632/oncotarget.25668.

[236] B.L. Bullock, A.K. Kimball, J.M. Poczobutt, A.J. Neuwelt, H.Y. Li, A.M. Johnson, J.W. Kwak, E.K. Kleczko, R.E. Kaspar, E.K. Wagner, K. Hopp, E.L. Schenk, M.C.M. Weiser-Evans, E.T. Clambey, R.A. Nemenoff, Tumor-intrinsic response to IFNγ shapes the tumor microenvironment and anti-PD-1 response in NSCLC, *Life Sci. Alliance.* 2 (2019) 1–17. https://doi.org/10.26508/lsa.201900328.

[237] I. Bar, A. Merhi, L. Larbanoix, M. Constant, S. Haussy, S. Laurent, J.L. Canon, P. Delrée, Silencing of casein kinase 1 delta reduces migration and metastasis of triple negative breast cancer cells, *Oncotarget.* 9 (2018) 30821–30836. https://doi.org/10.18632/oncotarget.25738.

[238] M.C. Jones, S.A. Jones, Y. Riffo-Vasquez, D. Spina, E. Hoffman, A. Morgan, A. Patel, C. Page, B. Forbes, L.A. Dailey, Quantitative assessment of nanoparticle surface hydrophobicity and its influence on pulmonary biocompatibility, *J. Control. Release.* 183 (2014) 94–104. https://doi.org/10.1016/j.jconrel.2014.03.022.

[239] W.D. Travis, S. Dacic, I. Wistuba, L. Sholl, P. Adusumilli, L. Bubendorf, P. Bunn, T. Cascone, J. Chaft, G. Chen, T.Y. Chou, W. Cooper, J.J. Erasmus, C.G. Ferreira, J.M. Goo, J. Heymach, F.R. Hirsch, H. Horinouchi, K. Kerr, M. Kris, D. Jain, Y.T. Kim, F. Lopez-Rios, S. Lu, T. Mitsudomi, A. Moreira, N. Motoi, A.G. Nicholson, R. Oliveira, M. Papotti, U. Pastorino, L. Paz-Ares, G. Pelosi, C. Poleri, M. Provencio, A.C. Roden, G. Scagliotti, S.G. Swisher, E. Thunnissen, M.S. Tsao, J. Vansteenkiste, W. Weder, Y. Yatabe, IASLC multidisciplinary recommendations for pathologic assessment of lung cancer resection specimens after neoadjuvant therapy, *J. Thorac. Oncol.* 15 (2020) 709–740. https://doi.org/10.1016/j.jtho.2020.01.005.

[240] A. Bressenot, S. Marchal, L. Bezdetnaya, J. Garrier, F. Guillemin, F. Plénat, Assessment of apoptosis by immunohistochemistry to active caspase-3, active caspase-7, or cleaved PARP in monolayer cells and spheroid and subcutaneous xenografts of human carcinoma, *J. Histochem. Cytochem.* 57 (2009) 289–300. https://doi.org/10.1369/jhc.2008.952044.

[241] A. Yu, J.J. Mansure, S. Solanki, D.R. Siemens, M. Koti, A.B.T. Dias, M.M. Burnier, F. Brimo, W. Kassouf, Presence of lymphocytic infiltrate cytotoxic T lymphocyte CD3+, CD8+, and immunoscore as prognostic marker in patients after radical cystectomy, *PLoS One.* 13 (2018) 1–13. https://doi.org/10.1371/journal.pone.0205746.

[242] J. Fan, J. Du, J. Wu, S. Fu, D. Hu, Q. Wan, Antitumor effects of different administration sequences of cisplatin and endostar on lewis lung carcinoma, *Oncol. Lett.* 9 (2015) 822–828. https://doi.org/10.3892/ol.2014.2783.

[243] D.N. Price, N.K. Kunda, P. Muttil, Challenges associated with the pulmonary delivery of therapeutic dry powders for preclinical testing, *KONA Powder Part. J.* 36 (2019) 129–144. https://doi.org/10.14356/kona.2019008.

[244] A. Kellar, C. Egan, D. Morris, Preclinical murine models for lung cancer: clinical trial applications, Biomed Res. Int. 2015 (2015) 1–18. https://doi.org/10.1155/2015/621324.

[245] J.T. Barr, T.B. Tran, B.M. Rock, J.L. Wahlstrom, U.P. Dahal, Strain-dependent variability of early discovery small molecule pharmacokinetics in mice: Does strain matter?, *Drug Metab. Dispos.* 48 (2020) 613–621. https://doi.org/10.1124/DMD.120.090621.

[246] T.S. Tracy, A.S. Chaudhry, B. Prasad, K.E. Thummel, E.G. Schuetz, X.B. Zhong, Y.C. Tien, H. Jeong, X. Pan, L.M. Shireman, J. Tay-Sontheimer, Y.S. Lin, Interindividual variability in cytochrome P450–mediated drug metabolism, *Drug Metab. Dispos.* 44 (2016) 343–351. https://doi.org/https://doi.org/10.1124/dmd.115.067900.

[247] E.C.K. Siu, R.F. Tyndale, Characterization and comparison of nicotine and cotinine metabolism in vitro and in vivo in DBA/2 and C57BL/6 mice, *Mol. Pharmacol.* 71 (2007) 826–834. https://doi.org/10.1124/mol.106.032086.

[248] T.M. Allen, P.R. Cullis, Drug delivery systems: Entering the mainstream, *Science* (80-.). 303 (2004) 1818–1822. https://doi.org/10.1126/science.1095833.

[249] A. Shemi, E.Z. Khvalevsky, R.M. Gabai, A. Domb, Y. Barenholz, Multistep, effective drug distribution within solid tumors, *Oncotarget.* 6 (2015) 39564–39577. https://doi.org/10.18632/oncotarget.5051.

[250] H. Gonzalez, C. Hagerling, Z. Werb, Roles of the immune system in cancer: From tumor initiation to metastatic progression, *Genes Dev.* 32 (2018) 1267–1284. https://doi.org/10.1101/GAD.314617.118.

[251] L.J. Zhang, Y.Z. Hao, C.S. Hu, Y. Ye, Q.P. Xie, R.F. Thorne, P. Hersey, X.D. Zhang, Inhibition of apoptosis facilitates necrosis induced by cisplatin in gastric cancer cells, *Anticancer. Drugs.* 19 (2008) 159–166. https://doi.org/10.1097/CAD.0b013e3282f30d05.

[252] R.S.Y. Wong, Apoptosis in cancer: From pathogenesis to treatment, *J. Exp. Clin. Cancer Res.* 30 (2011) 1–14. https://doi.org/10.1186/1756-9966-30-87.

[253] D.D. Yu, C.T. Wang, H.S. Shi, Z.Y. Li, L. Pan, Q.Z. Yuan, F. Leng, Y. Wen, X. Chen, Y.Q. Wei, Enhancement of cisplatin sensitivity in lewis lung carcinoma by liposome-mediated delivery of a survivin mutant, *J. Exp. Clin. Cancer Res.* 29 (2010) 1–7. https://doi.org/10.1186/1756-9966-29-46.

[254] L. Fournel, Z. Wu, N. Stadler, D. Damotte, F. Lococo, G. Boulle, E. Ségal-Bendirdjian, A. Bobbio, P. Icard, J. Trédaniel, M. Alifano, P. Forgez, Cisplatin increases PD-L1 expression and optimizes immune check-point blockade in non-small cell lung cancer, *Cancer Lett.* 464 (2019) 5–14. https://doi.org/10.1016/j.canlet.2019.08.005.

[255] N. Nagai, M. Kinoshita, H. Ogata, D. Tsujino, Y. Wada, K. Someya, T. Ohno, K. Masuhara, Y. Tanaka, K. Kato, H. Nagai, A. Yokoyama, Y. Kurita, Relationship between pharmacokinetics of unchanged cisplatin and nephrotoxicity after intravenous infusions of cisplatin to cancer patients, *Cancer Chemother. Pharmacol.* 39 (1996) 131–137. https://doi.org/10.1007/s002800050548.

[256] G.W. Boswell, I. Bekersky, D. Buell, R. Hiles, T.J. Walsh, Toxicological profile and pharmacokinetics of a unilamellar liposomal vesicle formulation of amphotericin B in rats, Antimicrob. Agents Chemother. 42 (1998) 263–268. https://doi.org/10.1128/aac.42.2.263.

[257] University of Maryland-School of medicine, Endpoint guidelines for animal use protocols, Maryland, 2018.

[258] T. Burkholder, C.J. Foltz, E. Karlsson, G.C. Linton, J.M. Smith, Health evaluation of experimental laboratory mice, *Curr Protoc Mouse Biol.* 2 (2012) 145–165. https://doi.org/10.1002/9780470942390.mo110217.

[259] J. Domagala-Kulawik, The role of the immune system in non-small cell lung carcinoma and potential for therapeutic intervention, *Transl. Lung Cancer Res.* 4 (2015) 177–190. https://doi.org/10.3978/j.issn.2218-6751.2015.01.11.

[260] A.E. Tilley, M.S. Walters, R. Shaykhiev, R.G. Crystal, Cilia dysfunction in lung disease, *Annu. Rev. Physiol.* 77 (2015) 379–406. https://doi.org/10.1146/annurev-physiol-021014-071931.

[261] B. Bondue, O. de Henau, S. Luangsay, T. Devosse, P. de Nadaï, J.Y. Springael, M. Parmentier, O. Vosters, The Chemerin/ChemR23 system does not affect the pro-inflammatory response of mouse and human macrophages ex vivo, *PLoS One.* 7 (2012) 1–10. https://doi.org/10.1371/journal.pone.0040043.

[262] S.J. Holditch, C.N. Brown, A.M. Lombardi, K.N. Nguyen, C.L. Edelstein, Recent advances in models, mechanisms, biomarkers, and interventions in cisplatin-induced acute kidney injury, *Int. J. Mol. Sci.* 20 (2019) 1–25. https://doi.org/10.3390/ijms20123011.

[263] F. Debelle, J. Nortier, V.M. Arlt, E. De Prez, A. Vienne, I. Salmon, D.H. Phillips, M. Deschodt-Lanckman, J.L. Vanherweghem, Effects of dexfenfluramine on aristolochic acid nephrotoxicity in a rat model for Chinese-herb nephropathy, *Arch. Toxicol.* 77 (2003) 218–226. https://doi.org/10.1007/s00204-003-0438-y.

[264] K. De Filippo, A. Dudeck, M. Hasenberg, E. Nye, N. van Rooijen, K. Hartmann, M. Gunzer, A. Roers, N. Hogg, Mast cell and macrophage chemokines CXCL1/CXCL2 control the early stage of neutrophil recruitment during tissue inflammation., *Blood.* 121 (2013) 4930–4937.

https://doi.org/10.1182/blood-2013-02-486217.

[265] M. Drent, N.A.M. Cobben, R.F. Henderson, E.F.M. Wouters, M. Van Dieijen-Visser, Usefulness of lactate dehydrogenase and its isoenzymes as indicators of lung damage or inflammation, *Eur. Respir. J.* 9 (1996) 1736–1742. https://doi.org/10.1183/09031936.96.09081736.

[266] Y. Cheng, R.S. Jope, E. Beurel, A pre-conditioning stress accelerates increases in mouse plasma inflammatory cytokines induced by stress, *BMC Neurosci.* 16 (2015) 1–8. https://doi.org/10.1186/s12868-015-0169-z.

[267] B. Moldoveanu, P. Otmishi, P. Jani, J. Walker, X. Sarmiento, J. Guardiola, M. Saad, J. Yu, Inflammatory mechanisms in the lung, *J. Inflamm. Res.* 2 (2009) 1–12.

[268] N.R. Aggarwal, L.S. King, F.R.D. Alessio, Diverse macrophage populations mediate acute lung inflammation and resolution, *Am J Physiol Lung Cell Mol Physiol.* 306 (2014) 1709–1720. https://doi.org/10.1152/ajplung.00341.2013.

[269] M. Nassimi, C. Schleh, H.D. Lauenstein, R. Hussein, H.G. Hoymann, W. Koch, G. Pohlmann, N. Krug, K. Sewald, S. Rittinghausen, A. Braun, C. Müller-Goymann, A toxicological evaluation of inhaled solid lipid nanoparticles used as a potential drug delivery system for the lung, *Eur. J. Pharm. Biopharm.* 75 (2010) 107–116. https://doi.org/10.1016/j.ejpb.2010.02.014.

[270] T. Hussell, T.J. Bell, Alveolar macrophages: Plasticity in a tissue-specific context, *Nat. Rev. Immunol.* 14 (2014) 81–93. https://doi.org/10.1038/nri3600.

[271] K. Amighi, N. Wauthoz, R. Rosière, Dry powder inhalation formulation and its use for the therapeutic treatment of lungs - Patent WO2020/136276A1, 2020.

[272] F. Li, H. Zhang, Lysosomal acid lipase in lipid metabolism and beyond, *Arterioscler. Thromb. Vasc. Biol.* 39 (2019) 850–856. https://doi.org/10.1161/ATVBAHA.119.312136.

[273] A. Baumann, D. Tuerck, S. Prabhu, L. Dickmann, J. Sims, Pharmacokinetics, metabolism and distribution of PEGs and PEGylated proteins: Quo vadis?, *Drug Discov. Today.* 19 (2014) 1623–1631. https://doi.org/10.1016/j.drudis.2014.06.002.

[274] A. V. Shubin, I. V. Demidyuk, A.A. Komissarov, L.M. Rafieva, S. V. Kostrov, Cytoplasmic vacuolization in cell death and survival, *Oncotarget.* 7 (2016) 55863–55889. https://doi.org/10.18632/oncotarget.10150.

[275] D. Zong, P. Hååg, I. Yakymovych, R. Lewensohn, K. Viktorsson, Chemosensitization by phenothiazines in human lung cancer cells: Impaired resolution of γh2AX and increased oxidative stress elicit apoptosis associated with lysosomal expansion and intense vacuolation, *Cell Death Dis.* 2 (2011). https://doi.org/10.1038/cddis.2011.62.

[276] D. Corinti, C. Coletti, N. Re, S. Piccirillo, M. Giampà, M.E. Crestoni, S. Fornarini, Hydrolysis of cis- and transplatin: structure and reactivity of the aqua complexes in a solvent free environment, *RSC Adv.* 7 (2017) 15877–15884. https://doi.org/10.1039/C7RA01182B.

[277] T.H. Huang, Y.H. Chiu, Y.L. Chan, W. Wang, T.L. Li, C.Y. Liu, C.T. Yang, T.Y. Lee, J.S. You, K.H. Hsu, C.J. Wu, Antrodia cinnamomea alleviates cisplatin-induced hepatotoxicity and enhances chemo-sensitivity of line-1 lung carcinoma xenografted in BALB/cByJ mice, *Oncotarget.* 6 (2015) 25741–25754. https://doi.org/10.18632/oncotarget.4348.

[278] K. Selting, J.C. Waldrep, C. Reinero, K. Branson, D. Gustafson, D.Y. Kim, C. Henry, N. Owen, R. Madsen, R. Dhand, Feasibility and safety of targeted cisplatin delivery to a select lung lobe in dogs via the AeroProbe® intracorporeal nebulization catheter, *J. Aerosol Med. Pulm. Drug Deliv.* 21 (2008) 255–268. https://doi.org/10.1089/jamp.2008.0684.

[279] Y. Togashi, Y. Sakaguchi, M. Miyamoto, Y. Miyamoto, Urinary cystatin C as a biomarker for acute kidney injury and its immunohistochemical localization in kidney in the CDDP-treated rats, *Exp. Toxicol. Pathol.* 64 (2012) 797–805. https://doi.org/10.1016/j.etp.2011.01.018.

[280] R. Rosière, Development of dry powder formulations for inhalation based on nanomedicine for targeted lung cancer therapy, Université libre de Bruxelles, 2016.

[281] H. Kreisman, M. Goutsou, C. Modeas, S.L. Graziano, M.E. Costanza, M.R. Green, Cisplatin-carboplatin therapy in extensive non-small cell lung cancer: a cancer and leukemia group B study, *Eur. J. Cancer Clin. Oncol.* 26 (1990) 1057–1060. https://doi.org/10.1016/0277-5379(90)90051-T.

[282] J.P. Sculier, J. Klastersky, V. Giner, G. Bureau, J. Thiriaux, G. Dabouis, A. Efremidis, F. Ries, M.C. Berchier, R. Sergysels, P. Mommen, M. Paesmans, Phase II randomized trial comparing high-dose cisplatin with moderate- dose cisplatin and carboplatin in patients with advanced non-

small-cell lung cancer, *J. Clin. Oncol.* 12 (1994) 353–359. https://doi.org/10.1016/0169-5002(94)90641-6.

[283] Medscape, Carboplatin AUC dose calculation-Calvert formula, (2020). https://reference.medscape.com/calculator/carboplatin-auc-dose-calvert (accessed May 5, 2020).

[284] F. Ceriotti, J.C. Boyd, G. Klein, J. Henny, J. Queraltó, V. Kairisto, M. Panteghini, Reference intervals for serum creatinine concentrations: Assessment of available data for global application, *Gen. Clin. Chem.* 54 (2008) 559–566. https://doi.org/10.1373/clinchem.2007.099648.

[285] S. Reagan-Shaw, M. Nihal, N. Ahmad, Dose translation from animal to human studies revisited, *FASEB J.* 22 (2007) 659–661. https://doi.org/10.1096/fj.07-9574lsf.

[286] S. Bellier, N. Cordonnier, Les valeurs usuelles en hématologie vétérinaire, *Rev. Francoph. Des Lab.* 420 (2010) 27–29. https://doi.org/10.1111/cjag.12228.

[287] F.Y. Kreidieh, H.A. Moukadem, N.S. El Saghir, Overview, prevention and management of chemotherapy extravasation, *World J. Clin. Oncol.* 7 (2016) 87–97. https://doi.org/10.5306/wjco.v7.i1.87.

[288] M.S. Barbee, T.K. Owonikoko, R.D. Harvey, Taxanes: Vesicants, irritants, or just irritating?, *Ther. Adv. Med. Oncol.* 6 (2014) 16–20. https://doi.org/10.1177/1758834013510546.

[289] J.J. Kim, I.F. Tannock, Repopulation of cancer cells during therapy: An important cause of treatment failure, *Nat. Rev. Cancer.* 5 (2005) 516–525. https://doi.org/10.1038/nrc1650.

[290] Y. Ohe, Y. Ohashi, K. Kubota, T. Tamura, K. Nakagawa, S. Negoro, Y. Nishiwaki, N. Saijo, Y. Ariyoshi, M. Fukuoka, Randomized phase III study of cisplatin plus irinotecan versus carboplatin plus paclitaxel, cisplatin plus gemcitabine, and cisplatin plus vinorelbine for advanced non-small-cell lung cancer: Four-arm cooperative study in Japan, *Ann. Oncol.* 18 (2007) 317–323. https://doi.org/10.1093/annonc/mdl377.

[291] C. Tecchio, M. Cassatella, Neutrophil-derived chemokines on the road to immunity, *Semin. Immunol.* 28 (2016) 119–128.

[292] S. Paudel, P. Baral, L. Ghimire, S. Bergeron, L. Jin, J.A. DeCorte, J.T. Le, S. Cai, S. Jeyaseelan, CXCL1 regulates neutrophil homeostasis in pneumonia-derived sepsis caused by Streptococcus pneumoniae serotype 3, *Blood.* 133 (2019) 1335–1345. https://doi.org/10.1182/blood-2018-10-878082.

[293] J.S. Pober, W.C. Sessa, Inflammation and the bloodmicrovascular system, *Cold Springs Harb Perspect Biol.* 7 (2015) 1–11.

[294] S. Idell, A.P. Mazar, P. Bitterman, S. Mohla, A.L. Harabin, Fibrin turnover in lung inflammation and neoplasia, *Am. J. Respir. Crit. Care Med.* 163 (2001) 578–584. https://doi.org/10.1164/ajrccm.163.2.2005135.

[295] M.J. McKeage, Comparative adverse effect profiles of platinum drugs, *Drug Saf.* 13 (1995) 228–244. https://doi.org/10.2165/00002018-199513040-00003.

[296] P. Chomarat, J. Banchereau, J. Davoust, A.K. Palucka, IL-6 switches the differentiation of monocytes from dendritic cells to macrophages, *Nat. Immunol.* 1 (2000) 510–514. https://doi.org/10.1038/82763.

[297] F. Aslinia, J.J. Mazza, S.H. Yale, Megaloblastic anemia and other causes of macrocytosis outpatient practice tips management, *Clin. Med. Res.* 4 (2006) 236–241. http://www.clinmedres.org.

[298] T. Boraska Jelavić, T. Boban, L. Brčić, E. Vrdoljak, Is macrocytosis a potential biomarker of the efficacy of dose-dense paclitaxel-carboplatin combination therapy in patients with epithelial ovarian cancer?, *Anticancer. Drugs.* 28 (2017) 922–927. https://doi.org/10.1097/CAD.0000000000000538.

[299] O. Sonmez, M. Sonmez, Role of platelets in immune system and inflammation, *Porto Biomed. J.* 2 (2017) 311–314. https://doi.org/10.1016/j.pbj.2017.05.005.

[300] M. Jirouskova, A.S. Shet, G.J. Johnson, A guide to murine coagulation factor structure, function, assays, and genetic alterations, *J. Thromb. Haemost.* 5 (2007) 661–669. https://doi.org/10.1111/j.1538-7836.2007.02408.x.

[301] M. Barrios, A. Rodríguez-Acosta, A. Gil, A.M. Salazar, P. Taylor, E.E. Sánchez, C.L. Arocha-Piñango, B. Guerrero, Comparative hemostatic parameters in BALB/c, C57BL/6 and C3H/He

mice, *Thromb. Res*. 124 (2009) 338–343. https://doi.org/10.1016/j.thromres.2008.11.001.

[302] A. Kalbasi, A. Ribas, Tumour-intrinsic resistance to immune checkpoint blockade, *Nat. Rev. Immunol*. 20 (2020) 25–39. https://doi.org/10.1038/s41577-019-0218-4.

[303] T.S.K. Mok, Y.L. Wu, I. Kudaba, D.M. Kowalski, B.C. Cho, H.Z. Turna, G. Castro, V. Srimuninnimit, K.K. Laktionov, I. Bondarenko, K. Kubota, G.M. Lubiniecki, J. Zhang, D. Kush, G. Lopes, Pembrolizumab versus chemotherapy for previously untreated, PD-L1-expressing, locally advanced or metastatic non-small-cell lung cancer (KEYNOTE-042): a randomised, open-label, controlled, phase 3 trial, *Lancet*. 393 (2019) 1819–1830. https://doi.org/10.1016/S0140-6736(18)32409-7.

APPENDIX

1. <u>Abstract and Poster at Drug Delivery to the Lungs (DDL, 29) Conference, Edinburgh, Scotland, UK. December 12-14, 2018</u>

"In silico Prediction of Pharmacokinetic Parameters after Cisplatin Intravenous and Endotracheal Administration Using GastroPlus™ Software"

Selma Chraibi[1], Jessica Spires[2], Karim Amighi[1] & Nathalie Wauthoz[1]

[1]Laboratory of Pharmaceutics and Biopharmaceutics, Faculty of Pharmacy, Université libre de Bruxelles (ULB), Boulevard du Triomphe, B-1050 Brussels, Belgium, schraibi@ulb.ac.be

[2]Simulation Plus, Inc., 42505 10th Street West, Lancaster 93534, United States of America (USA)

This abstract was peer-reviewed and is published in the Journal of Aerosol Medicine and Pulmonary Drug Delivery. The poster was presented at DDL29 conference. It contains the preliminary part of the work presented in the preliminary section in the first experimental part.

ULB UNIVERSITÉ LIBRE DE BRUXELLES

S+ SimulationsPlus
SCIENCE + SOFTWARE = SUCCESS

In silico Prediction of Pharmacokinetic Parameters after Cisplatin Intravenous and Endotracheal Administration Using GastroPlus[TM] Software

Selma Chraibi[1], Jessica Spires[2], Karim Amighi[1] & Nathalie Wauthoz[1]

[1] Unit of Pharmaceutics and Biopharmaceutics, Faculty of Pharmacy, Université libre de Bruxelles (ULB)
[2] Simulation Plus, Inc., 42505 10th Street West, Lancaster, 93534, USA

* Email : selma.chraibi@ulb.ac.be

INTRODUCTION

GastroPlus[TM] (SimulationPlus, Lancaster, USA) is a software that helps in optimizing the drug formulation by predicting its likely *in vivo* behavior relying on only *in vitro* data. This software has an **Additional Dosage Routes Module** (ADRM[TM]) and more specifically the Nasal pulmonary module that can simulate solution and powder biodistribution after pulmonary administration. The model considers four pulmonary compartments (extra-thoracic, thoracic, bronchiolar, alveolar-interstitial) that are connected to the stomach, to the systemic compartment and/or to the lymph. This module takes into account the specifications of the compound (i.e. pulmonary permeability, PP and systemic/lymph absorption rate, SAR) but also the specific physiology of each compartment, along with its enzymes and transporters.

Cisplatin (CIS) is one of the most widely used drugs in **lung cancer** chemotherapy[1]. However, this drug is nephrotoxic which imposes massive hydration of patients before, during and after intravenous administration[1]. To benefit from its efficacy and to reduce its toxicity, new inhalable treatments are developed[2]. These treatments aim to develop CIS solution (SOL) and CIS for dry powder inhaler (DPI) that can be administered directly into the lungs. The **pulmonary route** delivers CIS in the tumour environment directly, which reduces the amount that goes to the systemic compartment and causes nephrotoxicity.

The **aim of our work** was to develop a **pulmonary model** in mice that is able to predict **CIS pharmacokinetic (PK) parameters** considering only *in vitro* data (i.e. CIS physico-chemical parameters, DPI release profile). This simulation could help us develop more quickly advanced CIS formulations presenting a suitable PK profile to treat lung cancer more efficiently.

MATERIALS AND METHODS

1. Converting plasmatic concentration *vs* time profiles into PK parameters
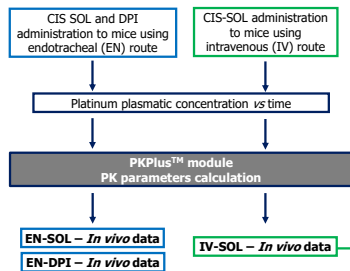
2. Establishment of IV and EN simulations
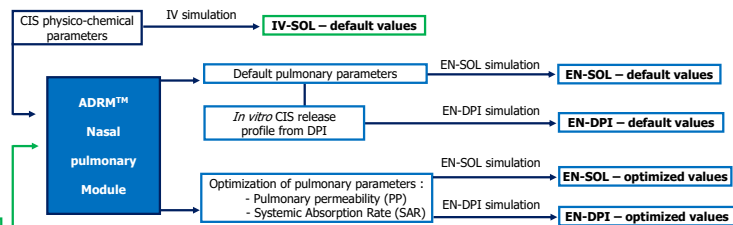
RESULTS AND DISCUSSION

Intravenous model

- The IV-SOL default values obtained match the IV-SOL – *In vivo* data **(Fig.1.A)** using only CIS physico-chemical parameters.

- The 5-minutes shift (T_{max} : 0.08 h *vs* 0.00 h) observed corresponded to the time required to take the blood samples from the mice during the *in vivo* experiment.

Endotracheal model

- The default pulmonary parameters are not adequate to reach the *in vivo* data after EN administration for both SOL and DPI formulations **(Fig.1.B and Fig.1.C)**.

- The optimization of the pulmonary parameters showed that the PP and the SAR were 10 and 100-fold higher than the default parameters **(Table 1)**.

- The optimized values obtained using optimized pulmonary parameters are closer to the EN-SOL and EN-DPI- *In vivo* data than the default values **(Fig.1.B and Fig.1.C)**.

- The GastroPlus[TM] predicted results show that CIS from the EN-DPI takes more time to reach the bloodstream than from the EN-SOL (T_{max} : 0.16 h *vs* 0.10 h) due to the dissolution step of the powder. This is something that can barely be observed *in vivo*.
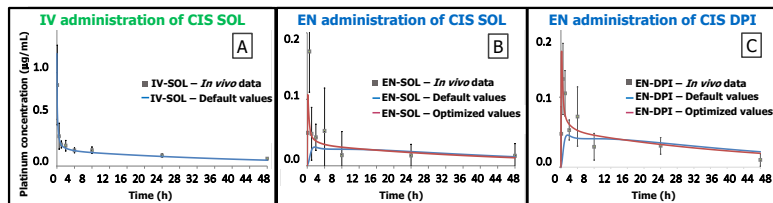
PK parameters	IV-SOL administration values		EN-SOL administration values			EN-DPI administration values		
	In vivo	Default	*In vivo*	Default	Optimized	*In vivo*	Default	Optimized
C_{max} (µg/mL)	0.9 ± 0.4*	1.20	0.17 ± 0.06*	0.03	0.11	0.13 ± 0.05*	0.05	0.17
T_{max} (h)	0.08	0.00	0.50	1.70	0.10	0.50	1.60	0.16
AUC (µg.h/mL)	6.31	5.42	0.99	0.98	1.05	1.47	1.60	1.71

Figure 1. *Plasma concentration vs time profile simulated by GastroPlus[TM] using default (blue) and optimized (red) parameters after IV (A) and EN administration of a CIS solution (B) and EN administration of CIS-DPI (C) compared to the in vivo data (grey dots). The table shows the default and optimized PK parameters compared to the in vivo data observed after IV, EN or DPI administrations. *Mean ± SD*

Table 1. *Pulmonary permeability (PP) and systemic absorption rate (SAR) values used for the default and optimized simulations.*

Pulmonary compartment	Default values		Optimized values	
	PP (cm/s)	SAR (1/s)	PP (cm/s)	SAR (1/s)
Extra-thoracic	$1.38.10^{-6}$	$4.82.10^{-5}$	$1.38.10^{-5}$	$4.82.10^{-3}$
Thoracic	$7.38.10^{-6}$	$4.82.10^{-5}$	$7.38.10^{-5}$	$4.82.10^{-3}$
Bronchiolar	$5.57.10^{-6}$	$4.82.10^{-5}$	$5.57.10^{-5}$	$4.82.10^{-3}$
Alveolar-interstitial	$3.05.10^{-4}$	$4.82.10^{-5}$	$3.05.10^{-2}$	$4.82.10^{-3}$

CONCLUSION

The cisplatin PK parameters were successfully predicted by the GastroPlus[TM] after an IV administration. The adjustment of the pulmonary permeability and the systemic absorption rate was mandatory to reach the *in vivo* data for both solution and immediate-release DPI administered by the EN route. The pulmonary permeability can be verified, as a complement, using *in vitro* tests on Calu-3 monolayers. We are aiming now to develop a model that can predict the PK parameters after an EN administration of a controlled-release DPI formulation by implementing the software.

References: [1] Sakaida E et al, Jpn J Clin Oncol 2016 - [2] Levet V et al, Int J Pharm 2016.

29th Drug Delivery to the Lungs, Edinburgh, Scotland, December 12-14, 2018

2. <u>Abstract and Poster at 12th World Meeting on Pharmaceutics, Biopharmaceutics and Pharmaceutical Technology</u>

" Evaluation of pulmonary and renal tolerance of a cisplatin- based dry powder for inhalation to treat lung cancer "

S. Chraibi[1], R. Rosière[1], E. De Prez[2], I. Langer[3], J. Nortier[2], K. Amighi[1], N. Wauthoz[1]

[1] Unit of Pharmaceutics and Biopharmaceutics, Faculty of Pharmacy, Université libre de Bruxelles (ULB), Boulevard du Triomphe, B-1050 Brussels, Belgium, selma.chraibi@ulb.be
[2] Laboratory of Experimental Nephrology, Faculty of Medicine, ULB,
[3] Institut de Recherche Interdisciplinaire en Biologie Humaine et Moléculaire (IRIBHM), ULB.

This abstract was peer-reviewed It contains a section of the work presented in third experimental part.

Evaluation of pulmonary and renal tolerance on mice of a cisplatin-based dry powder for inhalation to treat lung cancer

ULB

Selma Chraibi[1], R. Rosière[1], E. De Prez[2], I. Langer[3], J. Nortier[2], K. Amighi[1] & N. Wauthoz[1]

[1] Unit of Pharmaceutics and Biopharmaceutics, Faculty of Pharmacy, Université libre de Bruxelles (ULB)
[2] Laboratory of Experimental Nephrology, Faculty of Medicine, ULB,
[3] Institut de Recherche Interdisciplinaire en Biologie Humaine et Moléculaire (IRIBHM), ULB

* Email : selma.chraibi@ulb.be

INTRODUCTION

Despite the recent advances in targeted therapies and immunotherapy, **lung cancer** is still the most frequent and deadliest cancer worldwide[1].

Cisplatin (CIS) remains one of the most widely used drug in conventional chemotherapy[2]. As it is a cytotoxic drug, its toxicity is directly related to its efficacy: it induces **acute kidney injury (AKI)** and its administration imposes several hours of hydration and extensive resting cycles[2]. Administrating into the lungs to treat lung cancer can be a promising strategy to deliver CIS directly to its site of action while limiting its systemic adverse effects. Clinical studies have shown that delivering CIS by nebulization was well-tolerated but the maximum tolerated dose (MTD) was never reached, mainly due to poor delivery performance of nebulizers[2]. Therefore, these approaches were insufficient to combat lung tumors[2]. **A controlled-released cisplatin-based dry powder inhaler (CIS-DPI)** formulation can be an encouraging strategy to treat lung cancer as high amounts of CIS can be delivered locally for several hours to expose the tumour to CIS while reducing the local but also the renal toxicity.

Therefore, the **aim of this work** is to evaluate the **pulmonary and renal tolerance** of CIS-DPI. Pulmonary tolerance was evaluated using pro-inflammatory cytokines (TNF-α, IL-6, IL-1-ß), total and differential cell count, and polymorphonuclear neutrophils (PMN) recruitment chemokines (CXCL1, CXCL2). Lung cytotoxicity was evaluated using the total protein content assay and the lactate dehydrogenase (LDH) activity in bronchoalveolar lavage fluids (BALF). CIS-DPI AKI was assessed using plasma biomarkers NGAL, cystatin-c and creatinine and was compared to CIS that was administered using the IV route (CIS-IV).

RESULTS AND DISCUSSION
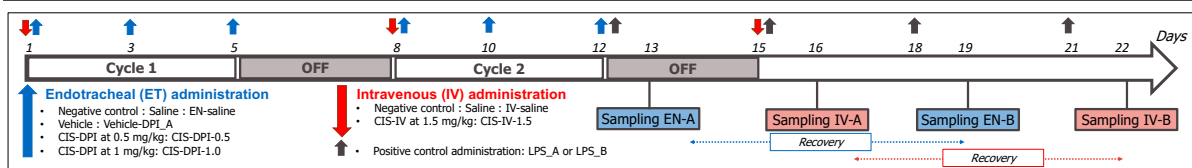
Figure 1. Scheme of administration and follow-up

Pulmonary tolerance evaluation

Inflammation

Cytotoxicity

Renal tolerance evaluation
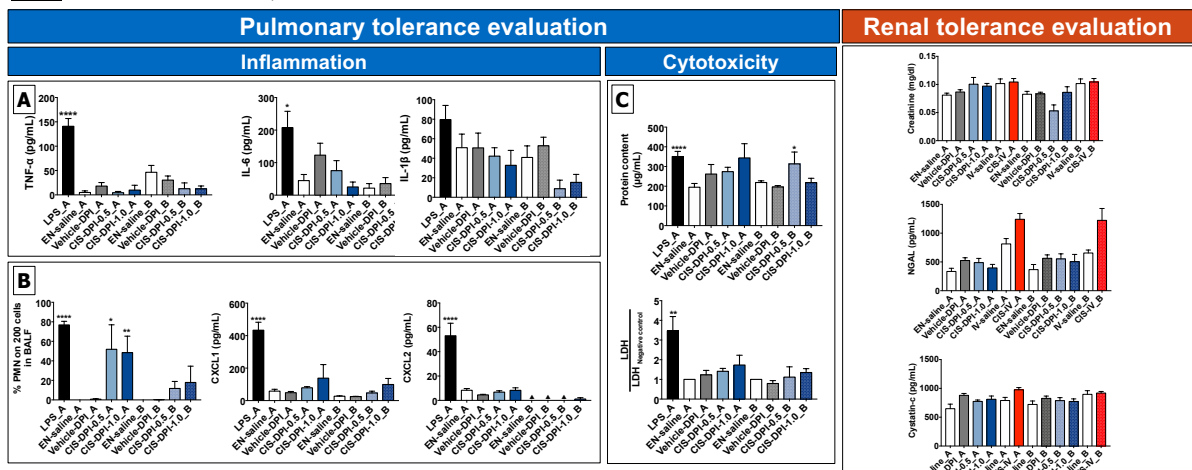
Figure 2. (A) Evaluation of pro-inflammatory cytokines (TNF- α, IL-6 and IL-1-ß), (B) polymorphonuclear neutrophils (PMN) determined as a proportion on 200 counted cells, chemokines (CXCL1 and CXCL2), (C) Protein content and the LDH activity as a proportion of LDH/LDH $_{Negative\ control}$, in BALF. All the results are expressed as means ± SEM (N=4-7). The statistical analysis was performed vs the control groups using one-way ANOVA and Bonferroni's post-test (*** for p < 0.001, ** for p < 0.01 and * for p < 0.05). Limit of quantification (LOQ) for CXCL2: 7.6 pg/mL, CXCL1, IL-1ß and IL-6: 15.6 pg/mL, TNF-α: 31.3 pg/mL from the manufacturer's kit.

Figure 3. Evaluation of Creatinine, NGAL and Cystatin-C in plasma. All the results are expressed as means ± SEM (N=4-7)

- Repeated ET and IV schemes were well-tolerated with body weight loss below 5%, except for CIS-DPI-1.0 (-7 ± 3%). All the body weights increased during the recovery week.

- CIS-DPI tended to increase transiently the total number of BALF cells, 24h after the last dose.
- No significative increase was observed for the pro-inflammatory cytokines when compared to the negative control (TNF- α, IL-6, IL-1-ß)(**Fig.2A**).
- **CIS-DPI-0.5** and **CIS-DPI-1.0** induced a significative but transient recruitment of PMN in BALF (**Fig.2B**). This increase was related to a non-significative dose-dependent increase of CXCL1 and CXCL2 (**Fig.2B**).
- In terms of cytotoxicity, both LDH/LDH $_{Negative\ control}$ and protein content seemed to increase dose-dependently and normalized one-week later for all the groups except for CIS-DPI-0.5-B (i.e. protein content after recovery) (**Fig.2C**) .

- In terms of AKI, no significant increases of plasma creatinine, cystatin-c nor NGAL were observed for all the groups (**Fig.3**).
- NGAL concentrations showed that the administration of CIS by IV seemed to have a higher but non-significative impact on AKI than by ET, for the same cumulative dose, when compared to their respective negative controls (CIS-DPI-0.5_A: 46% *vs* CIS-IV_A: 53%) (**Fig.3**). This difference was even higher one week later (CIS-DPI-0.5_A: 51% *vs* CIS-IV_A: 87%) (**Fig.3**).
- No difference between the NGAL concentrations was observed among the ET groups (Vehicle-DPI_A: 545 ± 46 pg/mL, CIS-DPI-0.5: 488 ± 74 pg/mL and CIS-DPI-1.0 : 396 ± 61 pg/mL).

CONCLUSION

Despite a transient increase in PMN, the repeated ET administration of CIS-DPI at 0.5 mg/kg and 1.0 mg/kg during 2 weeks was well-tolerated. CIS-IV at 1.5 mg/kg started to show an early sign of AKI. Nevertheless CIS was better tolerated by the kidneys when administered using the ET route than by IV. As the body weight loss and the PMN increase were reversible within one-week, separating ET treatment cycles can still be a promising approach to enhance local chemotherapy tolerance.
Future studies will evaluate the feasibility of combining the administration of CIS by ET and IV in terms of local and systemic tolerance as well as their efficacy on a murine lung carcinoma model.

References: [1] Bray F et al, Cancer J. Clin 2018 - [2] Levet V et al, Int J Pharm 2017.

12th World Meeting on Pharmaceutics, Biopharmaceutics and Pharmaceutical Technology, LIVE event from 11-14 May 2021

3. <u>Abstract and Poster at Respiratory Drug Delivery (RDD, 20) Conference, DIGITAL, 2020</u>

"Optimization of Cisplatin-based Regimens Combining Pulmonary and Intravenous Routes for Lung Cancer Therapy "

Selma Chraibi,[1] Rémi Rosière,[1] Lionel Larbanoix,[2] Sophie Laurent,[2] Eric De Prez,[3] Joelle Nortier,[3] Karim Amighi[1] and Nathalie Wauthoz[1]

[1] Unit of Pharmaceutics and Biopharmaceutics, (ULB), Brussels, Belgium
[2] Center for Microscopy and Molecular Imaging (CMMI), Charleroi, Belgium
[3] Laboratory of Experimental Nephrology, ULB, Brussels, Belgium

This abstract was peer-reviewed and is published in RDD online and in the conference book. The poster was presented at DDL29 conference. It contains a section of the work presented in third experimental part.

Optimization of Cisplatin-based Regimens Combining Pulmonary and Intravenous Routes for Lung Cancer Therapy

ULB

Selma Chraibi[1], R. Rosière[1], L. Larbanoix[2], S. Laurent[2], E. De Prez[3],
J. Nortier[3], K. Amighi[1] & N. Wauthoz[1]

[1] Unit of Pharmaceutics and Biopharmaceutics, Faculty of Pharmacy, Université libre de Bruxelles (ULB)
[2] Center for Microscopy and Molecular Imaging (CMMI), Charleroi, Belgium
[3] Laboratory of Experimental Nephrology, Faculty of Medicine, ULB

INTRODUCTION

Lung cancer is the most frequent and deadliest cancer worldwide with a five-year relative survival rate of 20.6% [1]. This is related to a late diagnosis as approximately 57% of new patients are distant stage [1]. Intravenous (IV) chemotherapy doublet remains the backbone of the care combining a platinum compound (e.g. **cisplatin (CIS)**) with another anticancer drug (e.g. **paclitaxel (PTX)**), which can also be combined with immune checkpoint inhibitors [2].

Because of its cumulative and dose-dependent **nephrotoxicity**, CIS must be administered in well-spaced cycles (usually every 3–4 weeks) and requires six to eight hours of massive hydration before, during and after administration [3]. These **off-cycles** help the patient recover but permits to the tumor to regenerate and spread.

Our **strategy** is to deliver a **controlled-release dry powder inhaler CIS-based formulation (CIS-DPI)** to the lungs **during these resting cycles** to continuously expose the tumor to CIS. This can be promising as long as the combination of these two routes of administration does not increase the nephrotoxicity.

The **aim** of our work is to evaluate the **renal tolerance** of different chemotherapy regimens and to assess the **antitumor efficacy** of the most frequent and best tolerated one.

RESULTS AND DISCUSSION

Renal tolerance evaluation on healthy mice
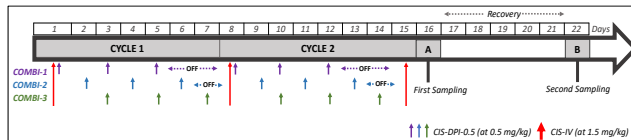
Figure 1. Toxicity study scheme of administration and sampling.

- During the toxicity study, **body weight** decreased transiently for all groups, reached 10% maximum at the end of the administration cycles, and increased during the recovery week.

- **CIS-IV** and **COMBI-1** both increased all the nephrotoxicity biomarkers when compared to the negative control group. This increase was significant for COMBI-1 but not for CIS-IV ($p > 0.05$, one-way ANOVA, **Figure 2**).
  → COMBI-1 therefore demonstrates that **administering CIS-DPI while CIS-IV was not completely cleared** (within 4 h) increased the Cmax resulting in **kidney injury** [5].

- In contrast, **no biomarkers have shown significant increase** when the administration of CIS-IV and CIS-DPI was **delayed by 24 h or 48 h** (COMBI-2 and COMBI-3, respectively). Interestingly, Levet *et al.* showed that the platinum concentration in the kidneys after 24 h was very low and similar to the concentration in the kidneys retrieved after 48 h following IV [4].

- **All biomarkers levels in all groups decreased within the one-week recovery**.

  → **COMBI-2** was preferred over COMBI-3 for the efficacy study assessment to treat the tumor more often and to limit off-period.
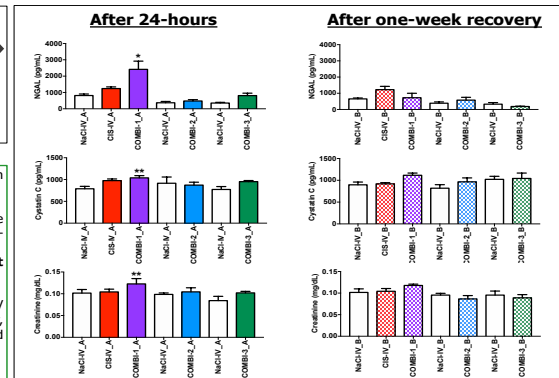
Figure 2. Evaluation of NGAL, cystatin-C and creatinine in plasma 24 h (A-groups) following the two-week treatment and after one-week recovery (B-groups). All the results are expressed as means ± SEM (N=4-6). The statistical analyses were performed vs the negative control groups using one-way ANOVA and Bonferroni's post-test (*** for $p < 0.001$, ** for $p < 0.01$ and * for $p < 0.5$).

Antitumor efficacy evaluation on M109 HiFr lung carcinoma model
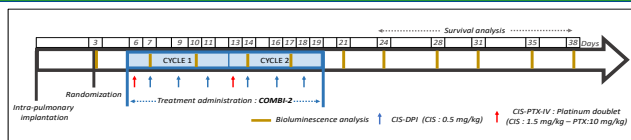
Figure 3. Efficacy study scheme of administration and follow-up.

- Tumor signal intensity of all the **negative control** mice increased continuously, leading to **death between day 17 and 21 (Figure 4A)**.

- **CIS-PTX-IV** temporarily reduced the tumor growth for **most mice** (7/8 mice) but had a **tumor regrowth** beginning on **day 21**. Adding **CIS-DPI** to **CIS-PTX-IV** (i.e. applying the COMBI-2 regimen) increased the response rate to **100% (8/8 responders)** and **reduced the tumor size** (6/8 vs 4/8 for CIS-PTX-IV), from the size at randomization. The **tumor regrowth** was observed on **day 24** for the group treated with the combination.

  → Adding **CIS-DPI** to the conventional treatment **helped inhibit tumor growth** (Figure 4D).

- Survival analysis showed that **CIS-PTX-IV increased the median survivals by 10 days** when compared to the negative control (26 vs 16) and the **addition of CIS-DPI prolonged the median survival for another 5 days** (26 vs 31, p=0.10, log-rank test, Figure 4E).
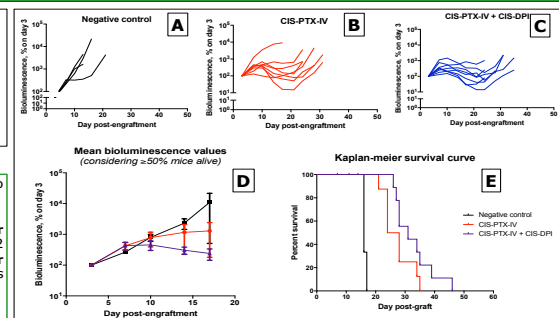
Figure 4. Evaluation of tumors' bioluminescence signal intensities for (A) the negative control group (vehicle, n=4), (B) the group treated with platinum doublet (CIS-PTX-IV, n=8) and (C) the COMBI-2 combination group (n=8) and the corresponded Kaplan-Meier survival curves (D). Each curve represents either a mice (A,B,C) or a group (D) (mean ± SEM) vs the randomization at day 3 (N=4–8).

CONCLUSION

The administration of CIS the same day by inhalation and IV tended to increase nephrotoxicity biomarkers. However, delaying pulmonary administration by 24 h reduced biomarker levels associated with kidney injury. Efficacy model results showed reduced tumor growth using the combination of CIS-IV and CIS-DPI when compared to CIS-IV alone.

Future studies will evaluate the tolerance and efficacy of CIS-DPI when combined to other conventional therapies and in other models of cancer.

References: [1] SEER Cancer Statistics 1975-2016 - [2] Hirsch et al, The Lancet 2017 - [3] Sakaida et al, Jpn J Clin Oncol 2016. - [4] Levet et al, Int J Pharm 2017. - [5] Nagai et al, Cancer Chemother Pharmacol 1996.

RDD 2020 DIGITAL
Respiratory Drug Delivery

4. <u>Abstract for an oral presentation at Congrès de la Société Francophone de Néphrologie, Dialyse et Transplantation (SFNDT), DIGITAL, October 7-8 2020</u>

"Évaluation préclinique de la tolérance rénale suite à l'administration par voie systémique et par inhalation de cisplatine dans un modèle murin de cancer pulmonaire "

S. Chraibi[1], *E. De Prez[2], R. Rosière[1], F. Touzani[2], M.H. Antoine[2], N. Wauthoz[1], K. Amighi[1], J. Nortier[2].

[1] Unit of Pharmaceutics and Biopharmaceutics, (ULB), Brussels, Belgium
[2] Laboratory of Experimental Nephrology, ULB, Brussels, Belgium

Évaluation préclinique de la tolérance rénale suite à l'administration par voie systémique et par inhalation de cisplatine dans un modèle murin de cancer pulmonaire

S. Chraibi[1], E. De Prez[2], R. Rosière[1], F. Touzani[2], M.H. Antoine[2], N. Wauthoz[1], K. Amighi[1], J. Nortier[2].

[1]*Laboratoire De Pharmacie Galénique Et Biopharmacie - Bruxelles (Belgique),*
[2]*Laboratoire De Néphrologie Expérimentale - Bruxelles (Belgique)*

Introduction

Malgré les progrès en immunothérapie et en thérapies ciblées, la chimiothérapie intraveineuse à base de cisplatine (CIS-IV) demeure le pilier central dans le traitement du cancer pulmonaire. Son administration est limitée par la néphrotoxicité dose-dépendante et cumulative, imposant des phases d'interruption de traitement durant lesquelles la fonction rénale se rétablit mais qui favorise la repopulation tumorale.

Description claire et complète de l'expérience

Une formulation à libération contrôlée et soutenue de cisplatine sous forme de poudre sèche pour inhalation (CIS-PSI) a été élaborée afin d'être administrée pendant les phases d'interruption et augmenter l'exposition de la tumeur au traitement. Cette stratégie a démontré son efficacité sur un modèle murin de cancer du poumon (XXX) mais n'est envisageable que si elle n'entraîne pas une néphrotoxicité accrue.

Le but de notre travail a été (i) d'évaluer l'atteinte rénale aiguë (ARA) chez la souris suite à l'administration répétée des monothérapies (CIS-PSI, CIS-IV) et (ii) d'optimiser leurs combinaisons (doses et jours d'administration).

Méthodes (explication détaillée de votre analyse)

Un modèle d'ARA a été généré chez la souris et documenté à l'aide d'une cinétique de biomarqueurs sériques précoces (NGAL, Cystatine C *vs.* créatinine) (Fig. 1). Ensuite, les monothérapies ainsi que les combinaisons ont été évaluées en phase aiguë et après 1 semaine pour estimer l'intensité de l'ARA et sa réversibilité aux niveaux sérique et histologique.

Résultats obtenus

Contrairement au CIS-IV, l'administration répétée du CIS-PSI n'a pas induit d'ARA, une libération prolongée du CIS ayant permis d'éviter toute augmentation du C_{MAX} plasmatique. Des signes d'ARA ont été observés dès que CIS-IV et CIS-PSI étaient combinés à leurs doses maximales tolérées. En réduisant la dose du CIS-IV de 25% et en séparant les administrations de CIS-PSI de 24h, la survenue d'ARA a pu être évitée.

Conclusion

Une approche rigoureuse de toxicologie préclinique a permis d'optimiser une chimiothérapie originale combinant le CIS-PSI au CIS-IV conventionnel, évitant ainsi la survenue d'une ARA délétère.
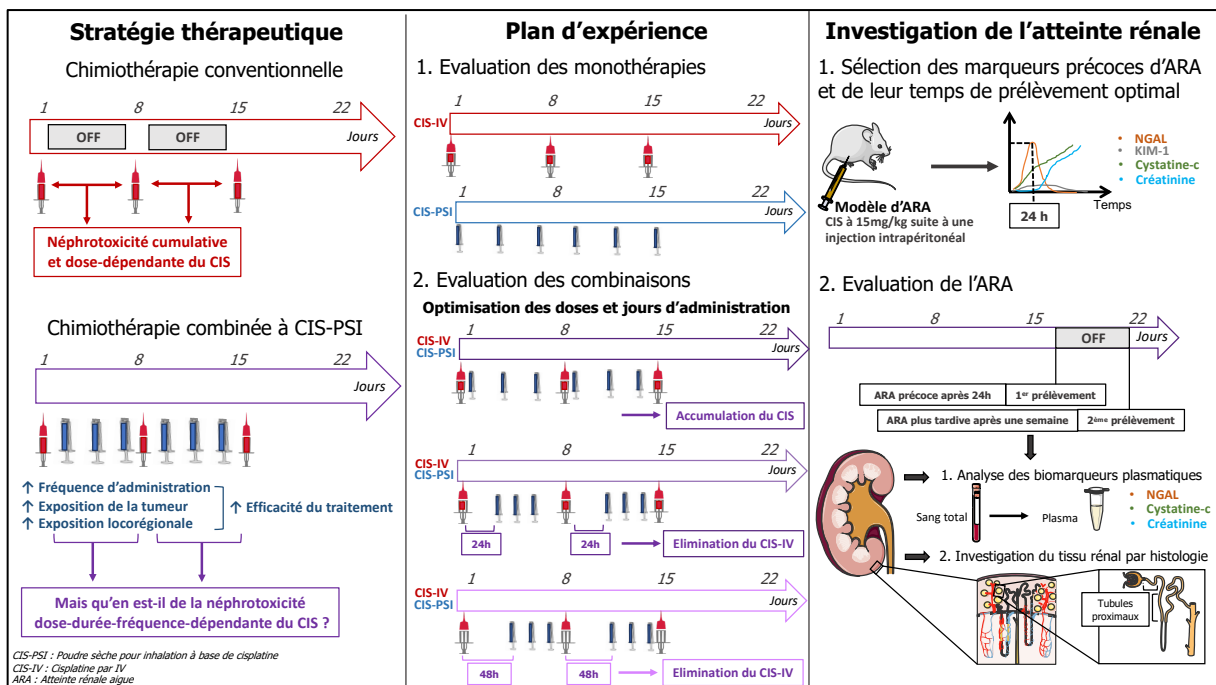
5. Article 1: Pulmonary and renal tolerance of cisplatin-based regimens combining intravenous and endotracheal routes for lung cancer treatment in mice

Pulmonary and renal tolerance of cisplatin-based regimens combining intravenous and endotracheal routes for lung cancer treatment in mice

S. Chraibi [a,*], R. Rosière [a,b], E. De Prez [c], M.H. Antoine [c], M. Remmelink [d], I. Langer [e], J. Nortier [c], K. Amighi [a], N. Wauthoz [a]

[a] *Unit of Pharmaceutics and Biopharmaceutics, Faculty of Pharmacy, Université libre de Bruxelles (ULB), Brussels, Belgium*
[b] *InhaTarget Therapeutics, Rue Auguste Piccard 37, Gosselies, Belgium*
[c] *Laboratory of Experimental Nephrology, Faculty of Medicine, ULB, Brussels, Belgium*
[d] *Department of Pathology, ULB, Hôpital Erasme, Brussels, Belgium*
[e] *Institut de Recherche Interdisciplinaire en Biologie Humaine et Moléculaire (IRIBHM), ULB, Brussels, Belgium*

ARTICLE INFO

ABSTRACT

Despite recent advances, platinum-based chemotherapy (partially composed of cisplatin, CIS) remains the backbone of non-small-cell lung cancer treatment. As CIS presents a cumulative and dose-limiting nephrotoxicity, it is currently administered with an interruption phase of 3–4 weeks between treatment cycles. During these periods, the patient recovers from the treatment side effects but so does the tumour. Our strategy is to increase the treatment frequency by delivering a cisplatin controlled-release dry powder for inhalation (CIS-DPI) formulation during these off-cycles to expose the tumour environment for longer to CIS, increasing its effectiveness. This is promising as long as the pulmonary and renal toxicities remain acceptable. The aim of the present investigation was to evaluate the pulmonary and renal tolerance of CIS-DPI (three times per cycle) and CIS using the intravenous (IV) route (CIS-IV) (one time per cycle) as monotherapies and to optimize their combination in terms of dose and schedule. At the maximum tolerated dose (MTD), combining CIS-DPI and CIS-IV impaired the pulmonary and the renal tolerance. Therefore, pulmonary tolerance was improved when the CIS-IV dose was decreased by 25% (to 1.5 mg/kg) while maintaining the MTD for CIS-DPI. In addition to this dose adjustment, a delay of 24 h between CIS-DPI and CIS-IV administrations limited the acute kidney injury.

1. Introduction

Despite recent advances in new therapies (i.e. targeted therapy and immunotherapy), lung cancer remains the most frequent and deadliest cancer worldwide (18.4% of all cancer deaths in 2018) (Bray et al., 2018). The 5-year relative survival rate is strongly related to the stage at diagnosis and varies from 57.4% for localized stages to 5.2% for distant stages in the USA (2009–2015) (National Cancer Institute, 2020). As 57% of newly diagnosed patients already have distant metastasis, the overall 5-year relative survival remains low at 19.4% (USA, 2009–2015) (National Cancer Institute, 2020).

To treat non-small cell lung cancer (NSCLC, 85% of lung cancers), platinum-based chemotherapy remains the backbone of care. It combines a platinum compound (mostly cisplatin (CIS) or carboplatin) with another anti-cancer drug (e.g. paclitaxel, gemcitabine or pemetrexed). Platinum-based chemotherapy is highly recommended as an adjuvant therapy after surgery for resectable stage II and III cancers, and in combination with radiotherapy (and more recently also with immunotherapy) for unresectable stage III cancers (Duma et al., 2019; Passiglia et al., 2020). For patients with advanced diseases and with no specific genomic alterations at the tumour level, immunotherapy is the first-line therapy as monotherapy or in association with platinum-based chemotherapy (Hanna et al., 2020; Majem et al., 2019).

Although platinum-based chemotherapy drugs are highly effective, they lack selectivity for tumour cells. Systemic distribution of the drugs through the intravenous (IV) route leads to heavy side effects (e.g. hair loss, digestive disorders) (American Cancer Society, 2020). Among them, some are dose-limiting such as the dose-dependent and cumulative nephrotoxicity for CIS (Sakaida et al., 2016). This leads to administering CIS in well-spaced cycles (every 3–4 weeks, for a maximum of 4–6 cycles) with massive hydration (at least 2 h before and 6 h after the 6 h-8 h treatment administration) (Hayati et al., 2016; "NCCN Guidelines - NSCLC- Version 3.2020," 2020; Sakaida et al., 2016). A significant

---

6. Article 2: The combination of an innovative dry powder for inhalation and a standard cisplatin-based chemotherapy in view of therapeutics intensification against lung tumours

The combination of an innovative dry powder for inhalation and a standard cisplatin-based chemotherapy in view of therapeutic intensification against lung tumours

Selma Chraibi [a], Rémi Rosière [a,b,1,*], Lionel Larbanoix [c], Pierre Gérard [b], Ismael Hennia [b], Sophie Laurent [c], Marjorie Vermeersch [c], Karim Amighi [a], Nathalie Wauthoz [a]

[a] *Unit of Pharmaceutics and Biopharmaceutics, Faculty of Pharmacy, Université libre de Bruxelles (ULB), Brussels, Belgium*
[b] *InhaTarget Therapeutics, Rue Auguste Piccard 37, Gosselies, Belgium*
[c] *Center for Microscopy and Molecular Imaging (CMMI), Université de Mons, Gosselies, Belgium*

ARTICLE INFO

ABSTRACT

Cisplatin is one of the most commonly used chemotherapy in lung cancer despite its high nephrotoxicity leading to an administration only every 3–4 weeks. This study is the first report of a preclinical investigation of therapeutic intensification combining a cisplatin dry powder for inhalation (CIS-DPI) with an intravenous (iv) cisplatin-based treatment. CIS-DPI with 50% cisplatin content (CIS-DPI-50) was developed using lipid excipients through scalable processes (high-speed and high-pressure homogenization and spray-drying). CIS-DPI-50 showed good aerodynamic performance (fine particle fraction of ~ 55% and a mass median aerodynamic particle size of ~ 2 μm) and a seven-fold increase and decrease in C_{max} in the lungs and in plasma, respectively, in comparison with an iv cisplatin solution (CIS-iv) in healthy mice. Finally, the addition of CIS-DPI-50 to the standard cisplatin/paclitaxel iv doublet increased the response rate (67% *vs* 50%), decreased the tumour growth and prolonged the median survival (31 *vs* 21 days), compared to the iv doublet in the M109 lung carcinoma model tending to demonstrate a therapeutic intensification of cisplatin.

1. Introduction

The survival rates of patients with lung cancer have significantly improved with platinum-based doublet chemotherapy and, more recently, with targeted therapies and immunotherapies. Despite therapeutic advances, lung cancer remains the world-leading cause of cancer-related deaths (approximately 2 million per year), due to innate or acquired tumour resistance to treatments [1].

Conventional chemotherapy combines a platinum salt, i.e. cisplatin or carboplatin, with another antineoplastic agent, which is most often paclitaxel or pemetrexed [2]. It remains very useful for treating non-small cell lung cancer (NSCLC, 85% of total cases [3]). These so-called platinum doublets are the first-line treatment, and are often in combination with other therapies, i.e., surgery, radiotherapy, and immunotherapy. It is used at nearly all stages of the disease (i.e. resectable stage II, resectable and unresectable stage III, and non-specifically altered stage IV) [3–6]. This is despite severe systemic toxicities that are due to chemotherapy's poor selectivity for tumour cells compared to normal cells and to the use of systemic routes of administration, i.e., mainly the intravenous (iv) route. The iv route results in a distribution of

7. Article 3: Preclinical tolerance evaluation of the addition of a cisplatin-based dry powder for inhalation to the conventional carboplatin-paclitaxel doublet for the treatment of non-small cell lung cancer

Preclinical tolerance evaluation of the addition of a cisplatin-based dry powder for inhalation to the conventional carboplatin-paclitaxel doublet for treatment of non-small cell lung cancer

S. Chraibi [a,*], R. Rosière [a,b], E. De Prez [c], P. Gérard [b], MH. Antoine [c], I. Langer [d], J. Nortier [c], M. Remmelink [e], K. Amighi [a], N. Wauthoz [a]

[a] *Unit of Pharmaceutics and Biopharmaceutics, Faculty of Pharmacy, Université libre de Bruxelles (ULB), Brussels, Belgium*
[b] *InhaTarget Therapeutics, Rue Auguste Piccard 37, 6041 Gosselies, Belgium*
[c] *Laboratory of Experimental Nephrology, Faculty of Medicine, ULB, Brussels, Belgium*
[d] *Institut de Recherche Interdisciplinaire en Biologie Humaine et Moléculaire (IRIBHM), ULB, Brussels, Belgium*
[e] *Department of Pathology, ULB, Hôpital Erasme, Brussels, Belgium*

ABSTRACT

Despite the advances in targeted therapies and immunotherapy for non-small cell lung cancer (NSCLC) patients, the intravenous administration of carboplatin (CARB) and paclitaxel (PTX) in well-spaced cycles is widely indicated for the treatment of NSCLC from stage II to stage IV. Our strategy was to add a controlled-release cisplatin-based dry-powder for inhalation (CIS-DPI-ET) to the conventional CARB-PTX-IV doublet, administered during the treatment off-cycles to intensify the therapeutic response while avoiding the impairment of pulmonary, renal and haematological tolerance of these combinations. The co-administration of CIS-DPI-ET (0.5 mg/kg) and CARB-PTX-IV (17–10 mg/kg) the same day showed a higher proportion of neutrophils in BALF (35 ± 7% *vs* 1.3 ± 0.8%), with earlier regenerative anaemia than with CARB-PTX-IV alone. A first strategy of CARB-PTX-IV dose reduction by 25% also induced neutrophil recruitment, but in a lower proportion than with the first combination (20 ± 6% *vs* 0.3 ± 0.3%) and avoiding regenerative anaemia. A second strategy of delaying CIS-DPI-ET and CARB-PTX-IV administrations by 24 h avoided both the recruitment of neutrophils in BALF and regenerative anaemia. Moreover, all these groups showed higher cytotoxicity (LDH activity, protein content) with no higher renal toxicities. These two strategies seem interesting to be assessed in terms of antitumor efficacy in mice.

1. Introduction

The improvement in terms of screening as well as the development of new personalized medicines (targeted therapies, immunotherapy), along with a reduction in incidence (USA, 2013–2016), has led to a reduced death rate related to lung cancer [1,2]. Worldwide, lung cancer remains a major public health problem. It is still the most frequent and deadliest among all cancers, for both sexes combined, with 11.6% of total cases and 18.4% of total cancer deaths in 2018 [3]. Therefore there is still an urgent need to increase treatment effectiveness by developing new treatment strategies and drug combinations or by repurposing current therapies.

Conventional platinum-based chemotherapy combining a platinum compound (*i.e.* cisplatin (CIS) or carboplatin (CARB)) to another antineoplastic agent such as paclitaxel (PTX) or pemetrexed (recommended for non-squamous histology) is still widely recommended for the